thesis titled:

"Gas Phase Synthesis of Interstellar Cumulenes. Mass Spectrometric and Theoretical Studies."

submitted for the Degree of Doctor of Philosophy (Ph.D.)

by

Stephen J. Blanksby

B.Sc.(Hons.)

from the

Department of Chemistry
The University of Adelaide

SUB CRUCE LUMEN

April 1999

i

Contents

Abstract

Astrophysics has identified a range of fascinating molecular species residing in the large gas clouds which are present in regions of interstellar and circumstellar space. Some of the more interesting of these are hydrocarbon cumulenes of the form C_nH and C_nH_2. We present here methodologies for the synthesis of charged analogues of a number of these species in the gas phase. These ions have been subjected to neutralisation reionisation mass spectrometry to establish the stability of the corresponding neutrals on the mass spectrometric timescale. These studies represent some of the first terrestrial observations of such cumulenes and further investigation has yielded novel homologues and structural isomers. Quantum chemical calculations have been employed in this study to provide further insight into the structure and energetics of these unusual molecules.

Statement of Originality

This work contains no material which has been accepted for the award of any other degree or diploma in any university or other tertiary institution and, to the best of my knowledge and belief, contains no material previously published or written by another person except where due reference has been made in the text.

I give consent to this copy of my thesis, when deposited in the University Library, being available for loan and photocopying.

Stephen J. Blanksby

7/4/99

Date

Acknowledgments

A thesis such as this cannot be produced in isolation. Many other people and organisations have been involved with providing assistance and support for the work presented here. It is necessary, and also appropriate to acknowledge their contributions.

Firstly, I would like to sincerely thank my PhD supervisor Professor John H. Bowie. Professor Bowie has provided the opportunity for me to work in a fascinating and exciting area of chemistry. His knowledge of, and enthusiasm for, gas phase ion-chemistry is infectious and his strong work ethic has been highly motivating to me during my candidature. I am also grateful to Professor Bowie for creating opportunities for me to participate in the larger scientific community. He has made it possible for me to attend conferences and collaborate in research with colleagues, both in Australia and overseas. The time I have spent under Professor Bowie's supervision has been inspiring and I certainly hope to carry many of his attitudes into my future career.

I would also like to thank Dr Suresh Dua for his contributions to the research presented in this thesis as well as for his continued wisdom and encouragement throughout my studies. Suresh guided much of the condensed phase synthetic work which I carried out and prepared some of the less stable precursors. He was also responsible for teaching me a great deal about the ZAB 2HF mass spectrometer. In this regard, I would also like to acknowledge the contributions of Tom Blumenthal and Rob Pearce who have both taught me a great deal about mass spectrometry. My knowledge of computational techniques has been ably assisted by Mark Taylor and Dr Mark Buntine who have both given generously of their time to help me with theoretical calculations.

In a general sense, I would like to acknowledge past and present members of the Bowie research group. In my four years with the group I have always found other members willing

to help with large or small problems as well as providing a relaxed but focussed working environment. In particular I would like to thank, Dr Simon Steinborner, Dr John Hevko, Paul Wabnitz, C.S. Brian Chia, Tom Rozek and Mark Taylor. I am also thankful to Professor Helmut Schwarz and members of his research group at the Technical University of Berlin. My four month sabbatical there advanced my knowledge of chemistry substantially and motivated much of my subsequent research. I would like to mention in particular, Dr Detlef Schröder, Dr Georg Hornung, Dr Christoph Schalley and Dr Jeremy Harvey who have all contributed to the science presented in this thesis.

I would like to express my appreciation to those people who have spent many hours proof reading parts or the whole of this thesis. These patient individuals were Professor Bowie, Dr Suresh Dua, Sam Peppe, Dr Mark Buntine and Peter Turner.

Thanks must also go to the Department of Chemistry at the University of Adelaide. The academic, research and technical staff as well as my fellow students have readily provided their time, advice and assistance for all range of matters. I have enjoyed the working and social environment within the Department in my time here as a postgraduate student. I also acknowledge the University of Adelaide for providing administrative and financial assistance, particularly for the award of an Overseas Travel Grant and a George Murray Scholarship to support my visit to the Berlin laboratories in 1997. On further financial matters, I am appreciative of the support Australian Postgraduate Awards for awarding me a postgraduate stipend for the years 1996-1999.

List of Figures

Figure 4.2 *The reaction coordinate diagram for rearrangement processes occurring on the neutral radical C_5H potential surface. The geometries of all stationary points were calculated at the B3LYP/6-31G level of theory: structures of the transition states and reactive intermediates appear as appendices to this Chapter (Table 4.7). The relative energies were calculated using the same theory with the larger, aug-cc-pVDZ basis set and are given in kcal mol^{-1}, with zero-point energy contributions included.*

Figure 4.3 *Optimised geometry for the $^1A_1$ ground state of $HC_2C_3^-$ (2$^-$). The geometry was calculated at the B3LYP/aug-cc-pVDZ level of theory. All bond lengths are given in angstroms and all angles in degrees.*

Figure 4.4 *Optimised geometry for the $^1A'$ ground state of $C_2C_3H^-$ (3$^-$). The geometry was calculated at the B3LYP/aug-cc-pVDZ level of theory. All bond lengths are given in angstroms and all angles in degrees.*

Figure 4.5 *Optimised geometry for the $^1A_1$ ground state of $C_2CHC_2^-$ (4$^-$). The geometry was calculated at the B3LYP/aug-cc-pVDZ level of theory. All bond lengths are given in angstroms and all angles in degrees.*

Figure 4.6 $^-CR^+$ *(O_2, 80% T; O_2, 80% T) spectra of m/z 61 from (a) $TMSC{\equiv}CC{\equiv}CCH_2OCH_3$, giving C_4CH^- and (b) $HC{\equiv}CCH(OCOCH_2CH_3)C{\equiv}CH$ giving $C_2CHC_2^-$. These spectra both show fragments of the forms C_nH^+ and $C_n{\cdot}^+$.*

Figure 4.7 $^-NR^+$ *(O_2, 80% T; O_2, 80% T) spectra of m/z 61 from (a) $TMSC{\equiv}CC{\equiv}CCH_2OCH_3$, giving C_4CH^- and (b) $HC{\equiv}CCH(OCOCH_2CH_3)C{\equiv}CH$ giving $C_2CHC_2^-$. These spectra both show fragments of the forms C_nH^+ and $C_n{\cdot}^+$.*

Figure 5.1 $^-NR^+$ *(O_2, 80% T; O_2, 80% T) spectra of m/z 64 from (a) $DC{\equiv}CCH(OH)C{\equiv}CD$, giving $DC_5D^{\cdot-}$ and (b) $TMSC{\equiv}CC{\equiv}CCD_2OH$, giving $C_4CD_2^{\cdot-}$. These spectra both show fragment ions of the forms, $C_nD_2{\cdot}^+$, $C_nD{\cdot}^+$ and $C_n{\cdot}^+$ (where n = 1-5).*

Figure 5.2 $^-CR^+$ *(O_2, 80% T; O_2, 80% T) spectra of m/z 62 from (a) $HC{\equiv}CCD(OH)C{\equiv}CH$, giving $HC_5H^{\cdot-}$ (b) $TMSC{\equiv}CC{\equiv}CCH_2OCH_3$, giving $C_4CH_2^{\cdot-}$ and (c) $TMSC{\equiv}CCH(OH)C{\equiv}CH$, giving $C_2CHC_2H^{\cdot-}$. These spectra each show fragment ions of the forms, $C_nH_2{\cdot}^+$, $C_nH{\cdot}^+$ and $C_n{\cdot}^+$ (where n = 1-5).*

Figure 5.3 *Optimised geometry for the C_5H_2 radical anion isomer 4$^{\cdot-}$ (C_{2v}). Optimisation was carried out at the B3LYP/6-31G level of theory, with bond lengths given in angstroms and angles in degrees.*

Figure 5.4 *Optimised geometry for the C_5H_2 radical anion isomer 5$^{\cdot-}$ (C_{2v}). Optimisation was carried out at the B3LYP/6-31G level of theory, with bond lengths given in angstroms and angles in degrees.*

Chapter 1: The Generation and Characterisation of Ions in the Gas Phase

(I) ABSTRACT

Astrophysics has provided a challenge to the laboratory chemist with a vast range of seemingly unstable molecules detected in interstellar and circumstellar gas clouds. One of the fundamental problems facing the chemist is the ability to generate and observe such transient neutrals in the terrestrial laboratory. The formation and analysis of unusual ionic species has long been the domain of mass spectrometry. If ionic analogues of these unstable neutrals can be generated in the gas phase utilising mass spectrometry, then their structures and reactivities can be studied. The most difficult part of the mass spectrometric approach to the formation of transient molecules comes in finding suitable precursors and ionisation techniques to generate the ions of interest. The theory behind a number of important ion generation methodologies will be discussed in this Chapter along with a description of the techniques for ion characterisation employed in this thesis. Methods for the generation of transient neutrals and assessment of their stability will also be discussed.

(II) GENERATING IONS

A. Positive Ions

1. Electron impact ionisation

All positive ions discussed in this thesis have been generated by electron impact (EI) ionisation. This is the oldest and still the most widely used form of ion generation in mass spectrometry.[1] Electrons are generated by the heating *in vacuo* of a filament generally consisting of tungsten wire or rhenium ribbon. A small accelerating voltage is applied (most typically 70 V)# generating a beam of electrons whilst a weak magnetic field (ca. 300 gauss) confines the beam to a narrow helical path. When an electron in the beam interacts with a volatilised compound (M) the electron may impart some of its energy to the neutral substrate. Providing there is sufficient energy transfer in this interaction (i.e. an energy greater than the ionisation energy of M) then a molecular cation $M^{\cdot+}$ can be produced (Scheme 1.1).

Scheme 1.1

$$M + e^- \rightarrow M^{\cdot+} + 2e^-$$
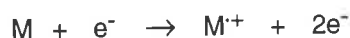
It is estimated that only 1 in 1000 gas molecules are actually ionised. Ions thus formed are extracted from the ion source by a small perpendicular voltage.[2] Ionisation of the neutral substrate by the accelerated electrons is a vertical process: that is, electron removal occurs to yield a product ion with an intial structure similar to that of the progenitor molecule. Thus EI ionisation may produce either (i), a stable radical cation as suggested in Scheme 1.1 or (ii), an unstable cationic species leading directly to dissociation products. The latter process is often referred to as dissociative ionisation and is illustrated by the Morse potential curves shown in Figure 1.1.[3]

Most standard reference mass spectra are recorded with electrons accelerated to 70 eV.
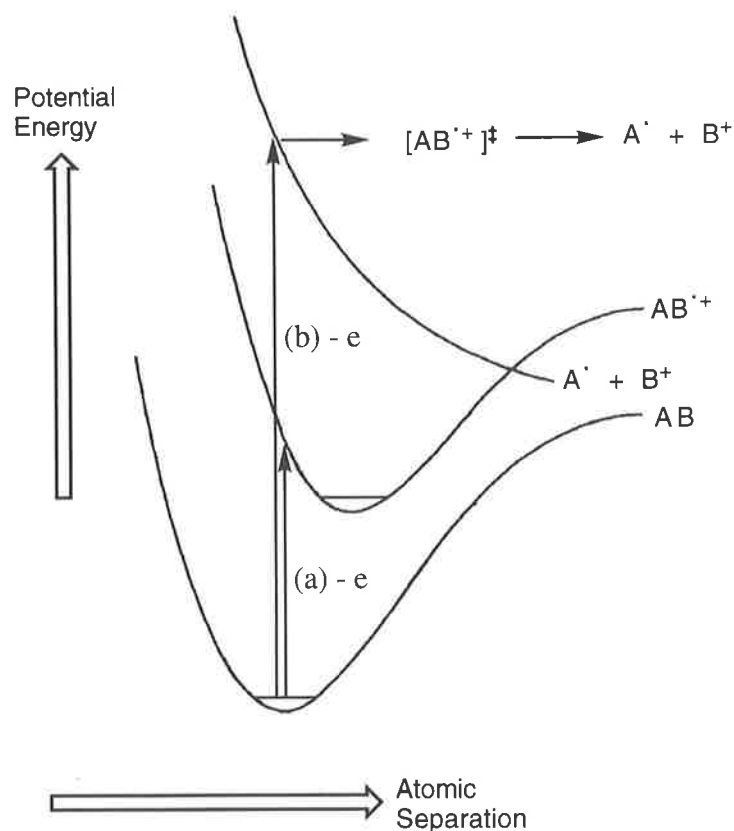
Figure 1.1 *Stylised Morse potential curves for some diatomic AB. Vertical ionisation of the neutral by electron impact (EI) results in access of (a), a stable (bound) radical cation* $AB^{\cdot+}$ *and (b), an unbound potential surface resulting in dissociation to a neutral radical A˙ and the even electron cation* B^+ *(dissociative ionisation).*

B. Even Electron Negative Ions

1. *Resonance capture*

Negative ions may also be formed under EI conditions by a process known as resonance capture. This involves a molecule of substrate gas M, of positive electron affinity, capturing an electron from the ionisation beam to form a radical anion (Scheme 1.2).

Scheme 1.2

$$M + e^- \rightarrow M^{\cdot-}$$
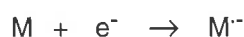
Resonance capture is less probable than electron removal (Scheme 1.1) by a factor of about 100.[3] The actual probability of electron capture depends on the nature of M and can vary widely between substrates. For example, formation of the carbon tetrachloride radical anion

by resonance capture is more favourable than the analogous process for hexane by a factor of about 10^6.[4] Electron attachment is a vertical transition and necessarily provides an excess energy to the nascent ion.# Consequently, fragmentation and ion-pair formation may occur (Scheme 1.3, e and d) in a manner analogous to the dissociative ionisation processes discussed for EI ionisation (Figure 1.1). Such ionisation is described as dissociative electron attachment. However, if the neutral substrate has a high electron affinity and a large number of internal degrees of freedom through which to dissipate the excess energy gained from electron attachment, it will be much more likely to survive on the mass spectrometric timescale (ca. 10^{-6} s).[5]

Excited radical anions formed by electron capture may dissipate excess internal energy by radiative emissions or through collisions with other gas molecules (Scheme 1.3, a and b). Alternatively they may undergo (i) electron ejection (ii) fragmentation or (iii) ion pair formation in order to lower their internal energy (Scheme 1.3, c, d and e respectively). The latter three processes form low energy electrons and/or even electron anions which may then particpate in secondary reactions in the source of the mass spectrometer.[6] These secondary processes can be utilised in negative ion chemical ionisation which is discussed in the next section.

Scheme 1.3

$$AB + e^- \rightarrow [AB^{-}]^{\ddagger}$$

$$[AB^{-}]^{\ddagger} \rightarrow AB^{-} + h\upsilon \qquad (a)$$

$$[AB^{-}]^{\ddagger} + X \rightarrow AB^{-} + [X]^{\ddagger} \qquad (b)$$

$$[AB^{-}]^{\ddagger} \rightarrow AB + e^- \qquad (c)$$

$$[AB^{-}]^{\ddagger} \rightarrow A^+ + B^- + e^- \qquad (d)$$

$$[AB^{-}]^{\ddagger} \rightarrow A^- + B^{\cdot} \qquad (e)$$
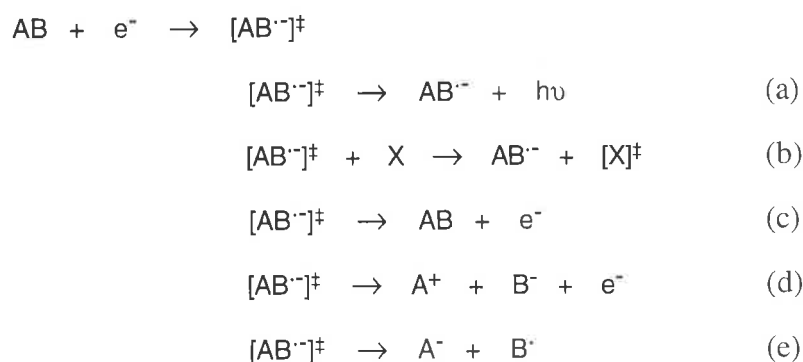
The excess energy must be greater than, or equal to, the electron affinity of the neutral substrate.

2. *Negative Ion Chemical Ionisation*

At higher source pressures (often ca. 0.1 Torr) than those used for EI ionisation a greater number of interactions occur between the electron beam and the substrate molecules. Under such conditions the processes resulting from resonance capture are favoured. The consequent production of low energy electrons (Scheme 1.3, c and d) facilitates further electron capture and thus an overall increase in the production of negative ions. In addition, at these higher pressures, ion-molecule reactions may occur between the nascent anions and neutral gas molecules. This forms the basis of negative ion chemical ionisation (NICI).[7] This technique often involves introducing a small amount of the substrate of interest with a reasonably high pressure of reagent gas into the ion source. The reagent gas, typically water (although ammonia and methanol are also commonly used), undergoes dissociative resonance capture to give a hydride anion and a hydroxyl radical (Scheme 1.4, a). Under the high pressure conditions of the source the hydride anion then rapidly deprotonates a further water molecule producing hydroxide ions (Scheme 1.4, b). Hydroxide ions are produced in high concentrations by this process and they react further to deprotonate substrate molecules (M) and produce even electron [M-H]$^-$ anions (Scheme 1.4, c).

Scheme 1.4

$$H_2O \ + \ e^- \ \rightarrow \ [H_2O^{-}]^{\ddagger} \ \rightarrow \ HO^{\cdot} \ + \ H^- \qquad (a)$$

$$H_2O \ + \ H^- \ \rightarrow \ HO^- \ + \ H_2 \qquad (b)$$

$$HO^- \ + \ MH_n \ \rightarrow \ [MH_{n-1}]^- \ + \ H_2O \qquad (c)$$
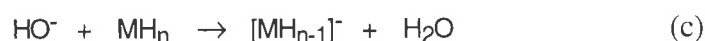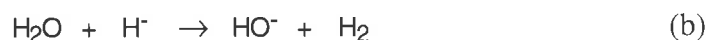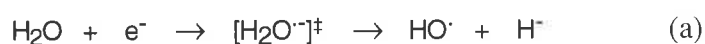
3. *Decarboxylation and Desilylation*

A problem with deprotonation in NICI (as described above) is that it is not necessarily site specific. When a substrate molecule (M) has more than one acidic proton then in principle a number of isomeric [M-H]$^-$ anions may be formed. Another problem arises for molecules which bear no suitable acidic protons (for example alkenes and alkanes) since they will not deprotonate by traditional methods. In the latter case, alternative methods have been developed to overcome the problem. The first involves decarboxylation of a carboxylate

anion. Decarboxylation involves selection of a precursor molecule with a carboxylic acid moiety at the site which should bear the negative charge.[8] Deprotonation will lead to formation of carboxylate anions and some of these may have sufficient internal energy to undergo decarboxylation (Scheme 1.5).* This method has been used to generate alkenyl and alkyl anions [for example $H_2C=CH^-$ and $(CH_3)_2CH^-$].[9]

Scheme 1.5

$$RCO_2H + HO^- \rightarrow RCO_2^- + H_2O$$

$$RCO_2^- \rightarrow R^- + CO_2$$
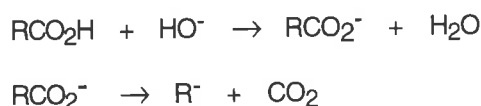
The second method of generating elusive R^- ions involves an $S_N2(Si)$ reaction between $RSiMe_3$ and Nu^- (where $Nu = F$, OH, etc.). Precursor molecules substituted with a trimethyl silyl (TMS) function have been shown to react with a gas phase nucleophile as shown in Scheme 1.6. The anion is formed at the site previously substituted with the silicon. The fluoride anion has been most commonly used nucleophile for this technique because of its well known affinity for silicon.[10] It has been shown however that other gas phase anions such as hydroxide can also displace TMS.[11] This technique has been used to synthesise the two isomeric C_3H_3 anions, $^-C\equiv CCH_3$ and $^-CH_2C\equiv CH$ in the gas phase.[10] It has also been utilised in the preparation of unusual species such as the acetyl anion (CH_3CO^-).[12]

Scheme 1.6

$$R\text{-}SiMe_3 + Nu^- \rightarrow R^- + Nu\text{-}SiMe_3$$
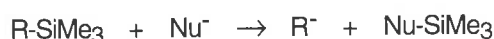
C. Radical Anions

1. *Resonance capture*

Radical anions are also of interest and a number of methodologies have been established specifically for the generation of these species in the gas phase: these have recently been

---

* Collisional activation of the carboxylate anion may be required in some cases.

reviewed.[13] As previously discussed (pp 3), some substrates will simply capture an electron under EI or CI conditions, but this is highly dependent on the nature of the compound.

2. *Radical loss from even electron anions*

The fragmentation of even electron anions under collisional activation has been well documented and reviewed.[14,15] The more common of these will be discussed later, but it is pertinent to note here that a number of even electron anions decompose *via* homolytic cleavage of covalent bonds resulting in the loss of a radical and the generation of a radical anion. For example, deprotonated benzyl ethers of the form [PhCHOR]⁻, on collisional activation readily lose R as a radical resulting in the formation of the PhCHO radical anion.[16] Similar fragmentations may also occur in the source of the mass spectrometer. For example, the C_5O radical anion may be formed in the source by loss of the *tert*-butyl radical from the even electron precursor, $^-C{\equiv}CC{\equiv}CC(O)C(CH_3)_3$.[17]

3. *Ion-molecule reactions of the oxygen radical anion*

The oxygen radical anion is readily formed from the dissociative resonance capture of nitrous oxide (Scheme 1.7, a). This dissociative electron attachment has been used extensively to generate $O^{\cdot-}$.[18,19] The utility of this ion as a chemical ionisation reagent was realised by Dawson and Jennings who showed the formation of a range of radical anions from the reactions between organic substrates and $O^{\cdot-}$.[20] It was found that for many organic substrates, the loss of a proton and a hydrogen radical (the elements of $H_2^{\cdot+}$) could compete favourably with simple deprotonation (Scheme 1.7, b and c respectively).

Scheme 1.7

$$N_2O + e^- \rightarrow N_2 + O^{\cdot-} \qquad\qquad (a)$$

$$RH_2 + O^{\cdot-} \rightarrow R^{\cdot-} + H_2O \qquad\qquad (b)$$

$$RH_2 + O^{\cdot-} \rightarrow RH^- + HO^{\cdot} \qquad\qquad (c)$$
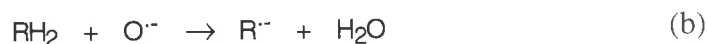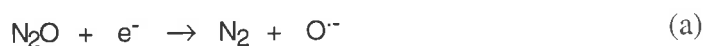
This methodology has proved extremely useful for producing a great many radical anions.[21] It has been used to synthesise the radical anion of vinylidene, an important organic intermediate. It was found that reaction of $H_2C=CD_2$ with the oxygen radical anion lead to formation of $H_2C=C^{\cdot-}$ and $D_2C=C^{\cdot-}$ by loss of D_2O and H_2O respectively with no observation of $[DC=CH]^{\cdot-}$.[22] Subsequent analysis of the available thermochemical data for this reaction reveals that it probably proceeds *via* initial H-atom abstraction followed by proton abstraction (Scheme 1.8). This is largely a thermodynamic argument, as initial $H^{\cdot}$ abstraction from ethylene is endothermic by < 1 kcal mol^{-1} whilst H^+ abstraction is endothermic by almost 25 kcal mol^{-1}.[5,21,23] This is the generally accepted mechanism for the ion-molecule reactions of $O^{\cdot-}$ with organic substrates which result in the elimination of the elements of $H_2^{\cdot+}$.

Scheme 1.8

$$H_2C=CH_2 \ + \ O^{\cdot-} \ \rightarrow \ [(H_2C=CH^{\cdot}) \ HO^-] \ \rightarrow \ H_2C=C^{\cdot-} \ + \ H_2O$$

4. *Diazo compounds*

Dissociative resonance capture of diazo-substituted organic substrates generates the corresponding radical anion in good abundance (Scheme 1.9). The loss of dinitrogen from such a precursor molecule is generally quite facile.[24]

Scheme 1.9

$$RC(N_2)R' \ + \ e^- \ \rightarrow \ [RCR']^{\cdot-} \ + \ N_2$$
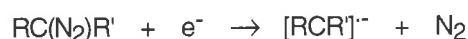
This method has been used to successfully synthesise the radical anion of the reactive intermediate, acetyl carbene (CH_3COCH).[25]

5. *Double-Desilylation*

A relatively recent methodology for the generation of radical anions has been termed double desilylation.[26,27] It follows on from the single desilylation previously discussed which

gives rise to an even electron anion. In this case a substrate molecule substituted with two trimethylsilyl (TMS) moieties is reacted with an ion flux containing fluoride ions and molecular fluorine. The result is the loss of both TMS groups and the formation of a radical anion. The big advantage of this method is that it allows for the selective generation of distonic[28] radical anions, i.e. where the charge and the unpaired electron reside on different atoms within the molecule. This is illustrated by some of the successful applications of this technique: $(TMSCH_2)_2C=CH_2$ when reacted with F^-/F_2 in the gas phase produces the trimethylene methane radical anion.[26] The proposed mechanism for this type of chemical ionisation is outlined in Scheme 1.10 using trimethylene methane as the prototypical example. The formation of *para* -benzyne[27] and oxyallyl[25] radical anions are two further examples of the utility of this methodology.

Scheme 1.10
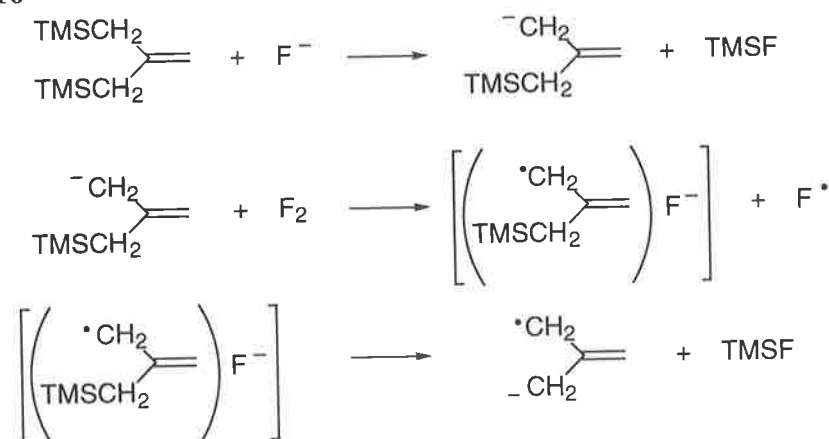
(III) THE MASS SPECTROMETER

A. The VG ZAB 2HF instrument

All ions discussed in this thesis were generated and analysed using the VG ZAB 2HF mass spectrometer (ZAB) at the University of Adelaide (Figure 1.2). The ZAB is a two sector reverse geometry instrument.[29] This refers to the arrangement of the sectors with the magnetic (B) preceding the electric (E) sector. This is sometimes denoted BE and has several advantages over the conventional or Nier-Johnson geometry (EB).[30] By far the major advantage is the ability of a BE instrument to mass select a parent ion and record the spectrum of its fragment ions by scanning the voltage across the electric sector. This is known as mass-analysed ion kinetic energy (MIKE) spectrometry.[31]
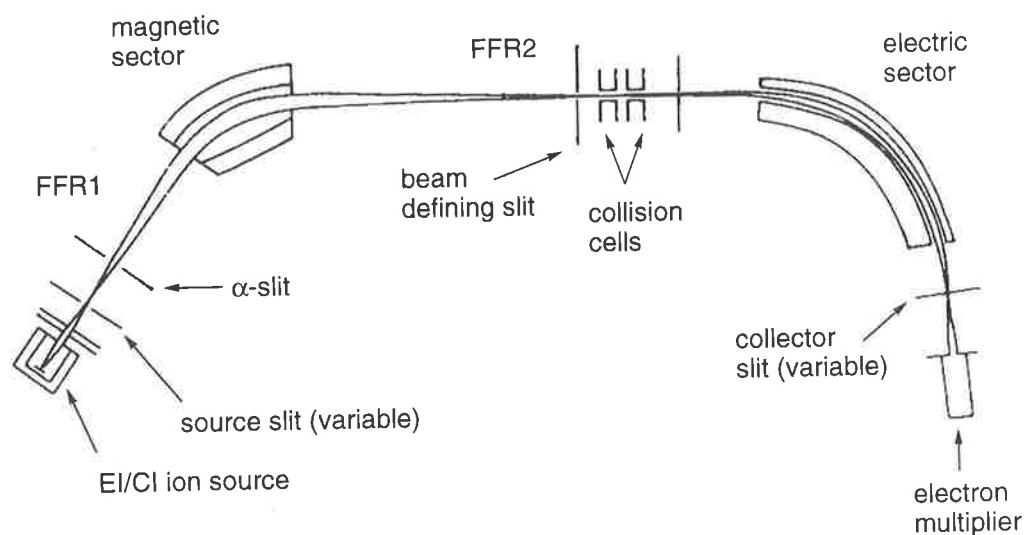
Figure 1.2 *A simplified schematic representation of the VG ZAB 2HF (FFR refers to field-free region).*

B. Mass-Analysed Ion Kinetic Energy Spectrometry

Once formed in the EI/CI source of the ZAB instrument, ions are accelerated to 7 kV before being mass selected using the magnetic sector. This is achieved by adjusting the magnetic field strength (B) such that the ion of interest will traverse the circular radius of the sector (r) and is thus transmitted through the instrument (see Equation 1.1). In this way, an ion of mass to charge ratio m/z accelerated to voltage V will be transmitted exclusively (e = 1.6 x 10^{-19} C).

Equation 1.1

$$m/z = B^2 r^2 e/2V$$

The mass selected, or parent ion, is transmitted through the second field free region to the electric sector. The electric sector is then scanned from the maximum voltage V (typically 7 kV for the ZAB) to 0 V. Ions are transmitted through the electric sector to the detector when the ratio of their kinetic energy (V) and the electric field strength (E) matches the fixed sector radius (r) according to Equation 1.2.

Equation 1.2

$$r = 2V/E$$

The spectrum achieved from a mass selected parent ion shows the parent ion and any fragment ions which may form from it in the second field free region. When a parent ion AB^- decomposes in this region, the kinetic energy (V) of AB^- is divided between the charged and neutral fragments A^- and B in the ratio of their masses. Consequently the fragment (or daughter) ions A^- will appear in the spectrum at a voltage (V_A) which is related to its mass (M_A) according to Equation 1.3. As all ions are detected on the basis of their kinetic energy, this technique is termed mass-analysed ion kinetic energy (MIKE) spectrometry.[31]

Equation 1.3

$$M_A/M_{AB} = V_A/V_{AB}$$

(IV) CHARACTERISATION OF IONS

A. Collisional Activation

Decomposition of the parent ion in the second field free region (i) may occur spontaneously due to internal energy already located in the ion: this is called a metastable decomposition,[32] or (ii) it may be induced by a glancing collision between the ion and a neutral gas.[33] The latter process is known as either collisional activation (CA) or collisionally induced decomposition (CID).

Collision between a translationally energetic ion (AB^-) and a neutral gas (N) can lead to either vibrational or electronic excitation, depending on the energy of the collision.* At high translational energies such as those utilised in the ZAB mass spectrometer (typically 7 kV) it is generally accepted that a collision with a neutral gas will lead to vertical electronic excitation.[32,34] The excited ion may then undergo fragmentation in order to lower its internal energy (Scheme 1.11).

Scheme 1.11

$$AB^- + N \rightarrow [AB^-]^\ddagger + N \rightarrow A^- + B + N$$

The distribution of energies imparted in a high energy, kilovolt collision is thought to be predominantly less than 10 eV.[32,34] The distribution does possess a high energy tail with processes requiring almost 16 eV observed in some CA spectra.[35]

In the ZAB mass spectrometer, CA occurs in one of the two collision cells which are located in the second field free region (Figure 1.2). The nature and the pressure of the gas used has significance on the efficiency of the CA process. Collisionally induced decomposition (Scheme 1.11) is not the only process which may occur upon collision between an accelerated ion and a neutral gas. For example, neutralisation and ion scattering must also be considered (Scheme 1.12). Whilst the former process may in fact be useful in some

---

* This discussion is equally pertinent to positive ions.

instances,# for a typical CA experiment, conditions which suppress both these alternate pathways will increase the efficiency of decomposition proccesses.[36]

Scheme 1.12

$$AB^- + N \rightarrow AB + N + e^- \qquad \text{(a)}$$

$$AB^- + N \rightarrow AB^-_{(scattered)} + N \qquad \text{(b)}$$
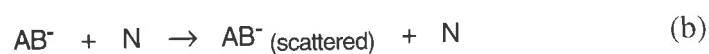
Inert atomic gases such as helium and argon are amongst the most efficient collision gases for CA processes. This is because of the low propensity of these gases to induce neutralisation and scattering processes (compared with other gases investigated).[37] The pressure of gas in the collision cell is also important. An increase in pressure results in an increase in the probability of collision between a translationally energetic ion and a neutral molecule. The optimal scenario is for the maximum number of ions to undergo a single collision, while the minimum number of ions undergo multiple collisions. The attenuation of the parent ion beam (i.e. the reduction in intensity) with the introduction of collision gas into the cells is an indication of the collision conditions. It has been demonstrated that for attenuation between 10-20% about 1 in 5 ions will undergo collision with the neutral gas. Of these, more than 90% will undergo a single collision, while less than 10% will be involved in double or multiple collisions.[38] Thus, if the gas pressure in a collision cell is adjusted to achieve 10-20% attenuation of the parent ion beam, then these may be considered single collision conditions.

Fragment ions formed in the second field free region (either by metastable decomposition or CA) in a MIKE experiment may gain some energy released in the decomposition of the parent. This energy could be kinetic and the process may be detected by an alteration of peak shape in a MIKE spectrum. This phenomena is known as kinetic energy release and can be extremely useful in the elucidation of unimolecular reactions of ions.[32]

\# See later discussion on charge reversal and neutralisation reionisation mass spectrometry.

B. Charge Reversal

It has been observed that many ions, particularly negative ions, do not fragment under CA conditions. This creates a problem with assigning structure in the gas phase. In the mid-1970's Bowie and Blumenthal reported the detection of charge reversed negative ions under CA conditions.[39,40] This procedure has become known as charge reversal (CR) and it involves the charge stripping of incident negative ions (AB⁻) in a high energy collision with a neutral gas (N). This process forms the corresponding positive ions following loss of two electrons (Scheme 1.13, a).[41] The energy (E) imparted in the collision is at least the sum of the electron affinity (EA) and the ionisation energy (IE) of AB (Equation 1.4). The energy loss in conversion of the anion to the cation can actually be measured in a MIKE experiment.[42,43] Like all collision induced processes, it is generally accepted that CR is vertical, with the nascent cation initially formed with the same structure as the progenitor anion. CR is also most commonly a single step stripping of two electrons[43] as depicted in Scheme 1.13 although some examples do exist for a sequential two step electron loss.[44] The nature of the collision gas can be of paramount importance for charge inversion experiments. Oxygen is commonly used for CR because it has been demonstrated to readily capture electrons in collision events and, in addition, causes less fragmentation of the charge inverted ions than a hard target gas such as helium.*

Scheme 1.13

$$AB^- + N \rightarrow AB^+ + N + 2e^- \qquad (a)$$

$$AB^- + N \rightarrow A^+ + B + N + 2e^- \qquad (b)$$

Equation 1.4

$$E = EA(AB^-) + IE(AB)$$

Cation fragmentations are also commonly observed (Scheme 1.13, b)[42] and these sometimes prove to be structurally characteristic such that CR has become a useful technique for

---

* See also later discussion on selection of target gases for neutralisation reionisation mass spectrometry.

distinguishing isomeric anions.# For example, the three isomeric carbanions $CH_2=C=CH^-$, $CH_3C\equiv C^-$ and *cyc* -$CH_2CH=C^-$ show distinct charge reversal spectra.[46] In addition, the CR technique has enabled the generation of some ionic species not readily accessible by traditional ionisation methods (*cf.* CH_3O^+).[47]

It should be mentioned that the other permutation of charge reversal has also been observed, where the high energy collision of a positive ion and a neutral gas results in the production of a negative ion signal.[48] This method has not found broad application because of the difficulty of attaching two electrons in a collision process. Nevertheless, to differentiate the two charge reversal permutations the charge states sometimes appear in the nomenclature for the experiment. For example, the charge reversal of an incident anion to the corresponding cation is denoted $^-CR^+$.

C. Neutralisation Reionisation

It may sound paradoxical to indicate that mass spectrometry is a technique for the generation and investigation of neutrals, but in fact this has become an important application of mass spectrometry in recent years. Earlier discussions mentioned that neutralisation of an incident ion (positive or negative) is a process which can co-occur with collisionally induced decomposition of an ion (Scheme 1.12, pp 13). In a two-sector reverse geometry instrument (or the equivalent) such as the ZAB (Figure 1.2) a parent ion can be mass selected, and then neutralised in a collision occurring in the first of the two collision cells in the second field free region. A voltage applied perpendicular to the flight path after the first collision cell deflects all ionic species resulting in the transmission of a pure beam of neutrals. The neutrals themselves cannot, of course, be detected and so a second collision in the second cell is required, resulting in reionisation. The reionised particles can then be detected along with fragment ions by scanning the electric sector as occurs in a traditional MIKE spectrum.

Some care must be exercised here given the proclivity of some cations to scramble and rearrange. For example the CR spectrum of the 2,4,6-d$_3$-methyl benzoate anion demonstrates that scrambling of the ring hydrogens precedes decomposition of the parent cation.[45]

This is the basis of neutralisation reionisation mass spectrometry[49-52] (NRMS, Figure 1.3) which was pioneered by McLafferty *et. al.* in the early 1980's.[53]
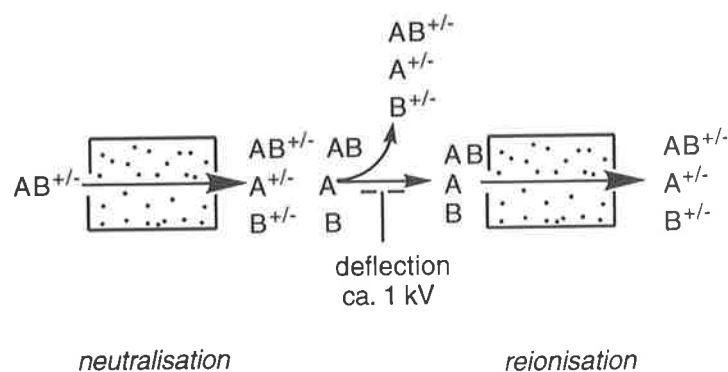
Figure 1.3 *A simplified schematic depicting the neutralisation reionisation process.*

All charge permutations are possible for NRMS. The most common are (i) neutralisation of an incident positive ion and reionisation to an ion of the same charge ($^+NR^+$) and (ii) the stepwise stripping of two electrons from an incident negative ion to form a positively charged species ($^-NR^+$). Successful $^+NR^-$ and $^-NR^-$ have also been reported but are limited by the difficulty in inducing electron attachment to a neutral species in a binary collision.[54] Careful selection of collision gases can maximise the observed NRMS signal, as was seen in the case of CR. For $^+NR^+$ a typical configuration uses xenon[55] or benzene[48] for neutralisation* of the cation in the first cell and oxygen for reionisation in the second. Whilst for $^-NR^+$ oxygen is typically used in both collision cells. Oxygen has found favour as a reionisation gas (and neutralisation for $^-NR^+$) because (i) it has been demonstrated to readily undergo electron capture in a collision and (ii) it is known as a soft target gas because it minimises fragmentation of the reionised (or neutralised) species.[57] The use of soft target gases is important when examining the stability or otherwise of some neutral AB by NRMS. Neutralisation with a soft target gas ensures maximum yield of AB. This is because minimal energy is deposited into the nascent neutral during the neutralisation event and consequently potential fragmentation and rearrangement pathways of AB are suppressed.# In addition to

---

* Vapourised metals such as mercury or sodium have also been utilised.[56]
# The possibility of fragmentation and/or rearrangement of transient neutrals will be discussed in the following section.

soft neutralisation, optimal NRMS may require soft reionisation so that the signal corresponding to reionised AB$^{+/-}$ is maximised (this is often referred to as the recovery signal). Use of a soft reionisation target gas such as oxygen ensures that the abundance of the recovery signal is optimal relative to fragmentation of the ion.

Most commonly, NRMS experiments have been aimed at demonstrating the stability or otherwise of a transient neutral in the gas phase. If a recovery signal is observed then it can generally be inferred that the neutral species is stable for the time taken to traverse the distance between the two collision cells.# This is dependent on the configuration of the instrument. In most instruments the distance (d) between the two collision cells is of the order of ca. 50 mm. For an ion accelerated to voltage, V (typically 7 keV) the flight time of the neutral is of the order of microseconds (10^{-6} s, Equation 1.5) depending on its mass (m, in kilograms).

Equation 1.5

$$t = d/(2eV/m)^{1/2}$$

It is estimated that for a keV collision, the electron transfer proceeds in ca. 10^{-15} s and may therefore be regarded as vertical (this is equally applicable to any of the processes described: CA, CR or NR). As a consequence, geometry changes during neutralisation and reionisation steps of a NRMS experiment are considered to be negligible.[58] Franck-Condon factors therefore dictate the efficiency of both steps, and accordingly, determine the internal energies of the species and the observed fragmentation patterns.[58,59] This is best illustrated by the simplified Franck-Condon representation depicted in Figure 1.4. The figure focusses specifically on the efficiency of a $^{+}$NR^{+} experiment, however the concepts are applicable to all charge permutations. The first scenario (Figure 1.4, a) shows a situation where both the neutral and cationic charge states of AB are stable with respect to dissociation, have similar geometries and hence a favourable Franck-Condon overlap. Consequently, neutralisation of

---

The possibility of reactive behaviour of transient neutrals cannot be excluded and will be discussed in the following section.

AB$^+$ produces energetically cold AB and similarly, reionisation regenerates AB$^+$ without significant excitation. Therefore, this scenario results in minimal fragmentation and a large recovery signal. In the second example, AB and AB$^+$ have quite different geometries. The poor Franck-Condon overlap between cation and neutral potential surfaces results in excitation occurring in both neutralisation and reionisation events. Consequently, fragmentation of AB and/or AB$^+$ may occur producing a decrease in the recovery signal and a concomitant increase in fragment ions.[60]
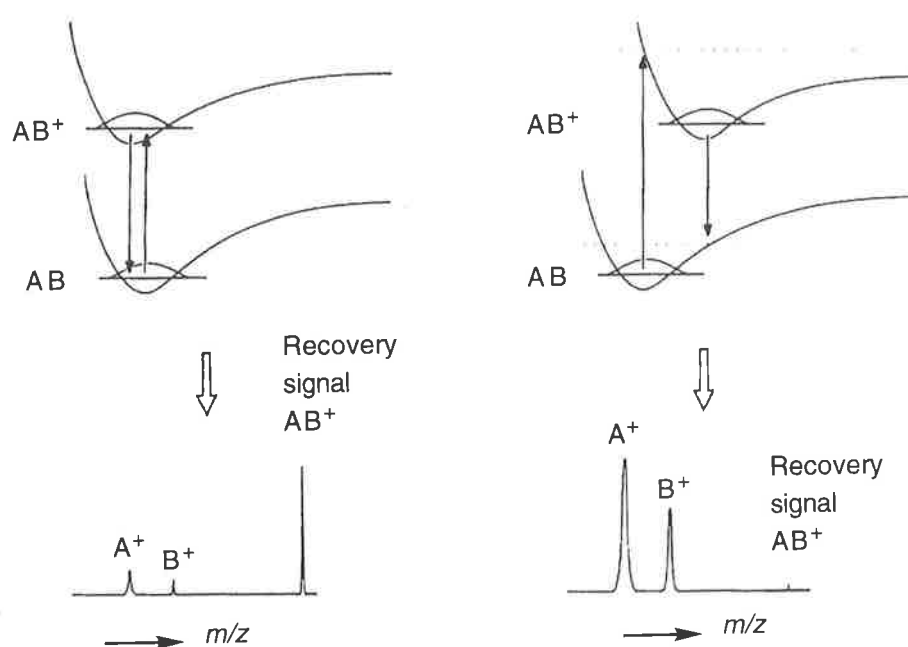
Figure 1.4 *Franck-Condon diagrams illustrating the effects of the vertical electron transitions in a $^+NR^+$ experiment: (a) represents the situation where the geometries of AB and AB$^+$ are similar whilst in (b) the structures are different.*[60]

Since its inception, NRMS has been used to pursue many and varied reactive neutral intermediates. Formation of (i), neutral diradicals such as CO_3[54] and CH_2OCH_2[61] and (ii), hypervalent species such as $HCNCH_2$[62] are examples of the utility of this technique. Recently, a comprehensive effort has been focussed toward observation of the elusive molecule C_2O_2. Whilst unsuccessful, this study is a good example of the breadth of NRMS methodology which can be invoked, utilising all four NR permutations.[63] Further examples with particular relevance to the work in this thesis will be discussed later in Chapter 3.

D. Neutral Reactivity

While NRMS has been most often concerned with the generation and detection of transient neutrals, recent efforts have demonstrated its ability to detect unimolecular behaviour of neutrals in the gas phase. A number of methods have been devised and have been recently reviewed but three techniques in particular will be discussed here.[60]

1. *Neutralisation Collisional Activation Reionisation*

Pioneered by McLafferty and co-workers, this technique is similar to traditional NRMS except that it requires an instrument with three differentially pumped collision cells.[64] An incident ion is (i) neutralised in the first collision cell, (ii) the neutral formed is then passed to a second collision cell where it is collisionally activated and finally (iii) reionisation occurs in the final cell (Figure 1.5). The name neutralisation collisional activation reionisation (NCR) is derived from this sequence.
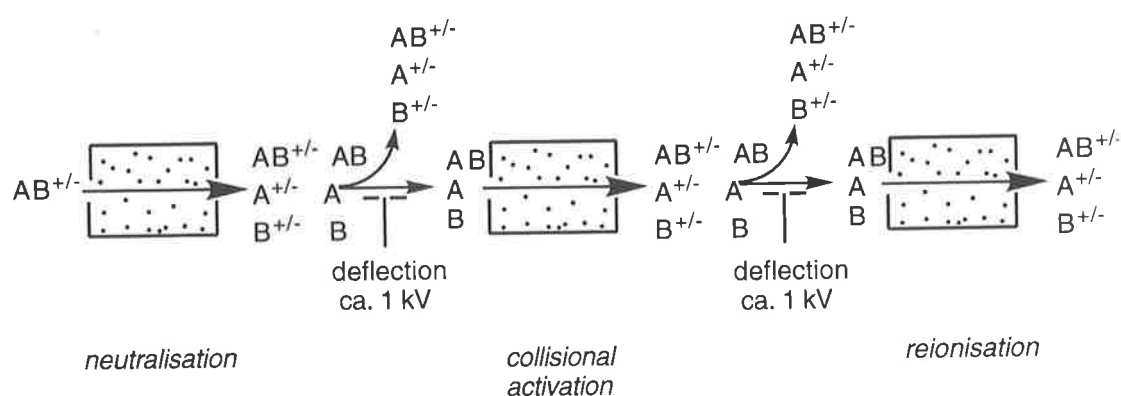
Figure 1.5 *The experimental arrangement for an NCR experiment.*

The NCR technique has been used to demonstrate the stability of transient neutrals generated by NRMS, and conversely, some studies show rearrangement of the activated neutral. An example of the latter is the CH_2OCH_2 diradical which has been shown to be a stable intermediate on the NRMS timescale but activation of this neutral in a NCR experiment shows isomerisation, predominantly to oxirane.[61]

2. *Variable lifetime NRMS*

Variable lifetime NRMS experiments can be carried out using an instrument with NCR capabilities. This technique is useful when rearrangement or decomposition of a transient neutral occurs on the approximate timescale of the NR experiment (ca. 10^{-6} s). In such an instance, comparing the NR spectra achieved with the neutral traversing first, a 'short distance' (SD-NR), and second a 'long distance' (LD-NR) may show some variations in peak abundance corresponding to the greater reaction time allowed in the latter experiment.[60] However, care must be taken to ensure that the collision conditions are as similar as possible for the two experiments, because the variation between spectra is usually subtle.[65]

3. *Neutral Ion Decomposition Difference*

Neutral ion decomposition difference (NIDD) spectrometry is the newest and perhaps the simplest way of investigating the unimolecular behaviour of neutrals formed by NRMS.[66] The advantage of this approach is that unlike the other methods discussed it requires no more specialist equipment than is necessary to run conventional NR spectra.

Consider the differences between the single step charge inversion, $^-CR^+$ and the stepwise charge inversion, $^-NR^+$ for a given anion. Peaks appearing in the $^-CR^+$ spectrum ideally correspond to cationic fragmentations whilst peaks appearing in the $^-NR^+$ spectrum form a superposition of cationic and neutral processes. Normalisation of the spectra to the sum of the intensities of all fragment ions (I), followed by subtraction of the normalised CR peaks from the NR, results in the NIDD spectrum (Equation 1.6). This spectrum elucidates the processes of the neutral shown on the positive scale with ionic contributions observed on the negative axis.

Equation 1.6

$$I_i(NIDD) = [I_i(NR)/\Sigma_i I_i(NR)] - [I_i(CR)/\Sigma_i I_i(CR)]$$

Scheme 1.14

$$HCO_2^- \xrightarrow{\text{NR (-e}^-)} [HCO_2]^\ddagger \rightarrow H^\cdot + CO_2 \xrightarrow{\text{NR (-e}^-)} CO_2^+ \qquad (a)$$

$$HCO_2^- \xrightarrow{\text{CR (-2e}^-)} [HCO_2^+]^\ddagger \rightarrow HCO^+ + O \qquad (b)$$
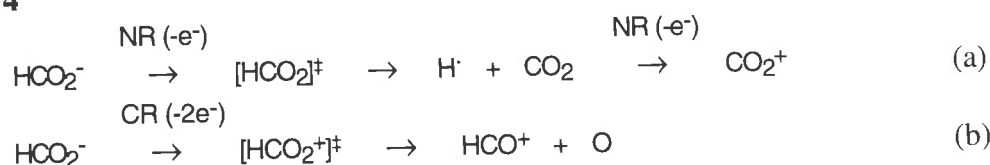
The technique is best illustrated by an example. The $^-NR^+$ and $^-CR^+$ spectra of the formate anion, HCO_2^-, are noticeably different from each other (Figure 1.6, a and b).[66] The former shows almost no recovery signal whereas the latter has an intense HCO_2^+ peak. In addition, the $^-CR^+$ spectrum shows an abundant HCO^+ signal which barely appears in the $^-NR^+$ spectrum. The $^-NIDD^+$ spectrum generated from $^-NR^+$ and $^-CR^+$ data is also shown in Figure 1.6. This representation clearly demonstrates the formation of CO_2, on the positive scale, as a neutral process, whereas the formation of HCO^+, seen on the negative scale, is predominantly formed from the cation. These observations are in line with theoretical predictions. Neutral HCO_2 is calculated to have only a small energy requirement to effect dissociation to form radical hydrogen and CO_2 (Scheme 1.14, a). Similarly, triplet HCO_2^+ requires little activation energy to cause dissociation to HCO^+ and triplet oxygen (Scheme 1.14, b).

Further examples of this technique include the investigation of unimolecular behaviour of the transient neutrals methyl hydroperoxide (CH_3OOH)[66] and the oxyallyl diradical $[CH_2C(O)CH_2]$.[25] A 1,5-hydrogen migration (as observed in solution by Barton and co-workers)[67] has also been identified occurring with long chain alkoxy radicals on the NRMS timescale.[68]

It is necessary to point out that for a meaningful comparison in a NIDD spectrum the component CR and NR spectra must be run under near identical conditions. This is generally achieved by utilising a typical NRMS configuration (i.e. collision gas in both cells) where the NR spectrum is recorded with the deflector electrode active and the CR with the deflector earthed.
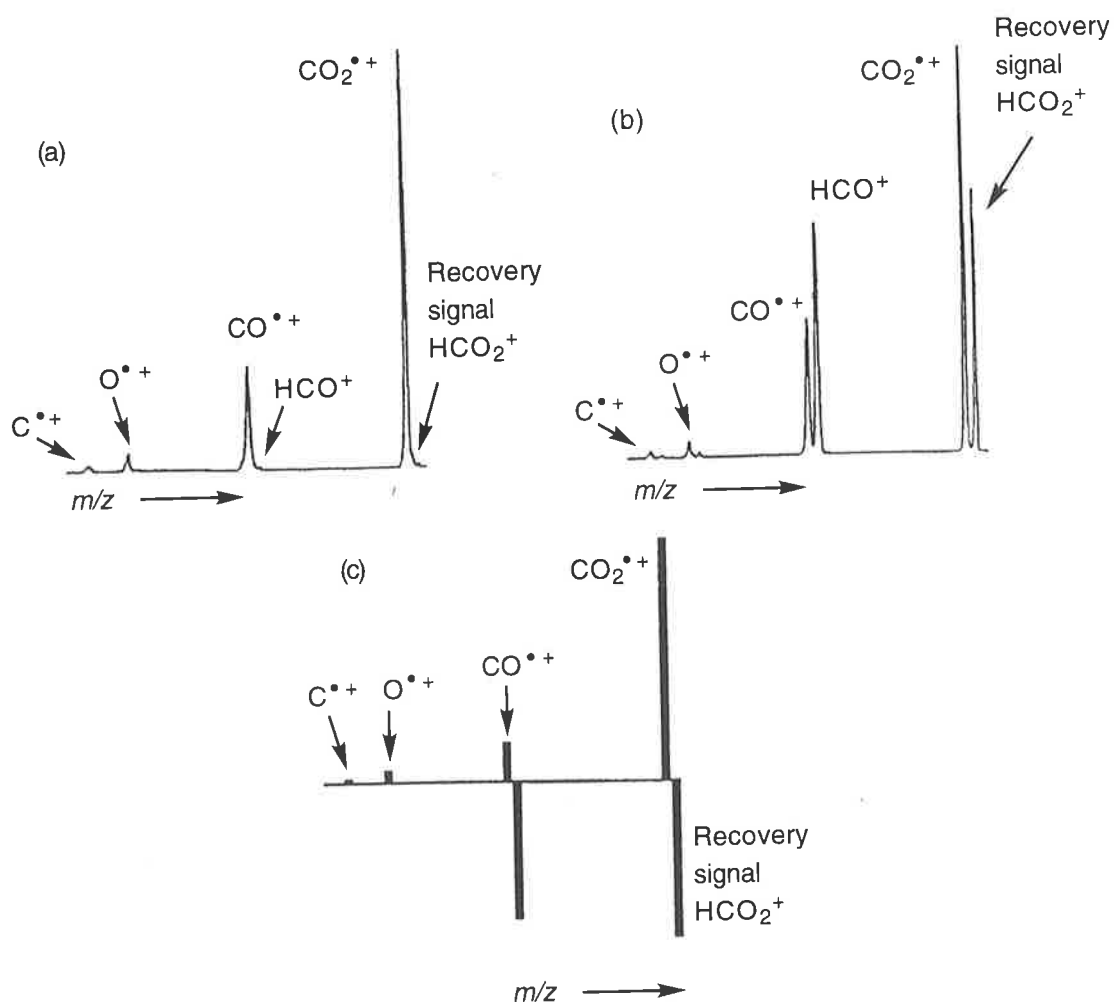
Figure 1.6 *(a)* $^-NR^+$, *(b)* $^-CR^+$ *and (c)* $^-NIDD^+$ *spectra for the formate anion* (HCO_2^-).[66]

(V) FRAGMENTATION BEHAVIOUR

The most useful probe of the structure of an ion is its fragmentation behaviour. Fragmentation may occur spontaneously if an ion is formed with sufficient internal energy, or alternatively it may be induced by collisional activation. Either way, the decomposition pathways of both positive and negative ions have been exhaustively investigated in order that mass spectrometry may be used as a tool for structural elucidation. Several general patterns have emerged from this work and are briefly outlined in this section.

A. Negative ions

The studies of even electron negative ion fragmentations allow a reasonable understanding and broad categorisation of their decomposition behaviour. Several comprehensive treatise are available.[14,15]

1. *Simple homolytic cleavages*

Most [M-H]$^-$ species lose a hydrogen radical to some extent. In systems where a stabilised radical anion is the product, this loss may be more pronounced. Such stability may also be the driving force for the loss of methyl, alkyl and sometimes more complex radicals from the parent anion (*cf.* Scheme 1.15, a and b).

Scheme 1.15

$$CH_3CO_2^- \rightarrow \ ^\cdot CH_2CO_2^- + H^\cdot \qquad \text{(a)}$$

$$[Et_2CCO_2CH_3]^- \rightarrow [Et_2CCO_2]^{\cdot -} + CH_3^\cdot \qquad \text{(b)}$$
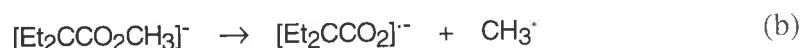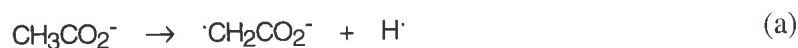
2. *Ion-neutral complex formation*

A decomposing [M-H]$^-$ ion may also undergo charge mediated heterolytic cleavage to form an ion and a neutral. These two entities may (i) separate (Scheme 1.16, a) or (ii) stay associated in a ion-neutral complex.[69] The complex is loosely bound by hydrogen bonds and ion-induced dipole interactions and can facilitate reaction of the anion on the neutral. This can take the form of deprotonation, S_N2 substitution or hydride donation (*cf.* Scheme 1.16).

Scheme 1.16

$$[Et_2CCO_2CH_3]^- \rightarrow [(Et_2C=C=O) \ ^-OCH_3] \rightarrow Et_2CCO + \ ^-OCH_3 \qquad \text{(a)}$$

$$\rightarrow [Et(CH_3CH)CCO]^- + HOCH_3 \qquad \text{(b)}$$

$$\rightarrow EtCCO^- + EtOCH_3 \qquad \text{(c)}$$

$$\rightarrow [Et_2CCHO]^- + OCH_2 \qquad \text{(d)}$$
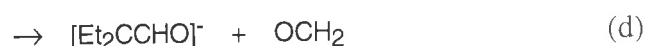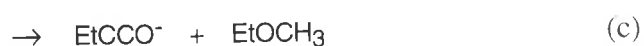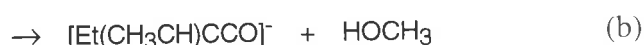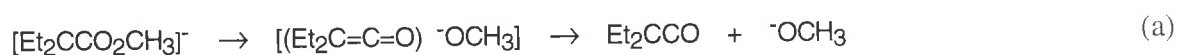
3. *Rearrangement preceding fragmentation*

In some instances it has been demonstrated that rearrangement of the initially formed anion precedes the observed fragmentation. This may take the form of simple proton transfer or a more complex skeletal rearrangement. These can be identified by the comparison of spectra of the rearranged species with those of the proposed rearrangement product synthesised by an independent means. Deprotonation of alkenyl alkyl ethers at the acidic allylic position generates an anion which undergoes proton transfer to form an unstable alkyl anion. The less stable species decomposes by loss of an alkene to generate the alkoxide anion (Scheme 1.17, a).[70] Deprotonated diallyl ethers however undergo skeletal rearrangement *via* sequential Wittig and Oxy Cope mechanisms to form the more stable enolate anion (Scheme 1.17, b).[71]

Scheme 1.17
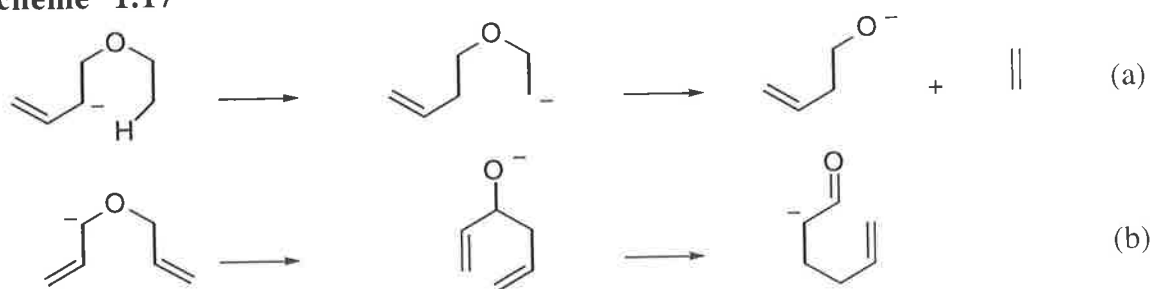
B. Charge inverted ions

1. *Fragmentation of positive ions*

The fragmentations of positive ions, in particular those of radical cations formed from EI ionisation have been thoroughly studied and exhaustively reviewed.[72-75] It is not our intention to attempt to condense this volume of work here. It is necessary however, to give some background to unimolecular decomposition by simple homolytic cleavage.

2. *Simple homolytic cleavage*

Radical cations formed by EI or similar ionisation techniques typically undergo facile homolytic cleavage of σ-bonds in order to form a stable cation and neutral radical (Scheme 1.18).

Scheme 1.18

$$ABC^{\cdot+} \rightarrow AB^+ + C^{\cdot}$$

In principle, mechanisms may be presented to show charge retention by either AB or C. In practice however, the relative stability of the two possible product cations determines the observed ratio of AB^+ and C^+. For example, in the case of ionised methyl benzoate [$PhCO_2Me^{\cdot+}$] homolysis of the ester C-OMe bond proceeds to form the phenyl acyl cation and the methoxide radical (Scheme 1.19).

Scheme 1.19

$$[PhC(O)\text{-}OCH_3]^{\cdot+} \rightarrow PhCO^+ + {\cdot}OCH_3$$
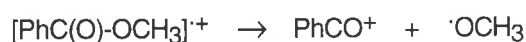
3. Charge inverted ions

From the earliest examples it is clear that the fragmentation of charge inverted ions (formed from either CR or NR processes) display a different fragmentation behaviour to the corresponding ions formed by direct ionisation. For example, Bowie and Blumenthal observed that the CR spectra achieved from the nitrobenzene anion is notably different to that of the nitrobenzene radical cation formed by EI.[39] This has been rationalised in terms of the differing internal energy of the ions formed in each processes. The corollary of this is that fragmentations appearing in CR and NR spectra may not adhere stringently to the types of behaviour outlined above. Even so, these types of spectra do provide a significant amount of structural information in their own right. Examples of the differentiation of isomeric ions by these methodologies have already been provided in the pertinent sections.

Chapter 2: Theoretical Methods for the Determination of Structure and Energetics

(I) ABSTRACT

The interplay between theory and experiment is now integral to modern chemistry. Advances in the application of quantum chemical theory make highly accurate prediction of chemical properties routinely available to the non-specialist. Quantum chemical calculations have proved particularly useful for investigating transient species such as the ions and neutrals which are commonly observed in the gas phase by mass spectrometry. Whereas in the early years molecular orbital theory was used to elucidate pre-existing problems, it is now common place for quantum chemical predictions to prompt an experimental investigation. The synergy between theory and experiment is apparent throughout this thesis. This Chapter provides a brief introduction to the different theoretical methods utilised in this study and the significance of the results obtained.

(II) MOLECULAR ORBITAL THEORY[76-78]

A. The Schrödinger Equation

The electronic structure of an atom or molecule may be described by the time-independent Schrödinger equation (Equation 2.1). Here, H is the Hamiltonian operator which can be applied to the mathematical function ψ, known as the wavefunction, and E is the electronic energy of the system.

Equation 2.1

$$H \, \psi(\mathbf{r}, \mathbf{R}) = E \, \psi(\mathbf{r}, \mathbf{R})$$

The wavefunction of the system, ψ, depends on (i) the coordinates of the electrons, comprising spatial and spin coordinates, represented by the vector $\mathbf{r}$ and (ii) the coordinates of the nuclei represented by the vector $\mathbf{R}$. The physical interpretation of ψ is that of a probability distribution, such that the probability of finding an electron at a given point in space is given by the scalar square of its wavefunction, $|\psi|^2$. Equation 2.1 can be expanded by considering the nuclei to be stationary with respect to the motion of the electrons in the molecule. This is known as the non-relativistic Born-Oppenheimer approximation[79] and leads to Equation 2.2.

Equation 2.2

$$H^{elec} \, \psi^{elec}(\mathbf{r}, \mathbf{R}) = [T^{elec}(\mathbf{r}) + V^{nuc\text{-}elec}(\mathbf{r},\mathbf{R}) + V^{elec\text{-}elec}(\mathbf{r})] \, \psi^{elec}(\mathbf{r}, \mathbf{R})$$

$$= E^{elec} \, \psi^{elec}(\mathbf{r}, \mathbf{R})$$

Here, the nuclear coordinates $\mathbf{R}$ are treated as fixed parameters determined by the given geometry of the molecular system under investigation. The Hamiltonian is reduced to the sum of electron kinetic energy (T^{elec}), nucleus-electron attraction energy ($V^{nuc\text{-}elec}$) and electron-electron repulsion energy ($V^{elec\text{-}elec}$) operators. Solving this equation for the electronic wavefunction (ψ^{elec}) produces the electronic energy (E^{elec}) of the molecular system. The total energy of the molecule however, depends also on the nucleus-nucleus

repulsive energy but this can be added in subsequent to the solution of the electronic energy. Once the energy of a given molecular geometry can be determined, the variation in energy with variation in geometry can be established and a potential surface can be calculated. Critical points on the potential energy surface such as local and global minima and first order saddle points (transition states) allow insight into the chemical behaviour of a molecular system (see further discussion pp 35). Furthermore, once the eigenfunctions of Equation 2.2 are calculated, all electronic and magnetic properties of a system become accessible by applying the corresponding operators to the electronic wavefunction. The power of the Schrödinger equation is apparent. However, for all but the most trivial of molecules an exact solution is not easily attained. This problem can be circumvented by applying a number of simplifying assumptions, which allow for an approximate solution to the Schrödinger equation for a broad range of systems.

B. Hartree-Fock Theory

The electronic wavefunction (ψ) can be approximated as the product of molecular orbitals (ϕ) which in turn can be estimated as a linear combination of one electron functions (χ) often called the basis functions (Equation 2.3). Basis functions are centred on nuclei and hence approximate atomic orbitals.

Equations 2.3

$$\phi_i = \Sigma\ c_{ik}\ \chi_k$$

The coefficients (c_{ik}) which determine the contribution of each basis function to the molecular orbital may be iteratively optimised with an approach known as the self-consistent field (SCF) procedure. This is done in order to minimise the electronic energy (E^{elec}) according to Equation 2.2, and is known as the Hartree-Fock (HF) method. The basis set is a well defined set of basis functions given to each type of atom: put simply the larger the basis set the greater the number of basis functions used to describe each molecular orbital. Expanding the basis to infinity however, does not lead to the true molecular wavefunction

but rather to the limit of the assumptions in the HF-SCF procedure. This is the so-called Hartree-Fock limit and produces an electronic energy higher than the real energy of the system. Inaccuracies arise for one, because the HF method treats electrons as independent particles and thus electron-electron interactions are treated as an averaged rather than as a many-body problem. Put simply, HF theory treats an electron's motion as if it moves in an averaged field of stationary electrons. In reality, electrons move in order to get out of each others' way. This is the so-called dynamic electron correlation effect. This problem must be addressed in order to accurately predict the energy of molecular systems.

C. Electron correlation

How significant is correlation energy? Correlation energy (E_{corr}) is the difference between the exact non-relativistic energy (E) of an atom or molecule and its HF energy (E_{HF}) and it is typically of the order of 0.5% to 1% of the energy of the system (Equation 2.4). This means, for example, that using HF theory the energy of a carbon atom is in error by approximately 5 eV. Therefore, in order to successfully calculate energies it is necessary to incorporate electron correlation energy.

Equation 2.4

$$E_{corr} = E - E_{HF}$$

One of the most common methods for the treatment of the electron correlation is the use of Møller-Plesset (MP) perturbation theory. Many body perturbation theory is used to describe systems of many interacting particles. It is therefore ideally suited to the problem of electron correlation where the interaction between electrons has to be addressed. In a general sense, it is based on dividing the Hamiltonian (H) into two parts: an exactly soluble H_0 and a correction or perturbation operator ($\lambda H'$) applied to it. It is assumed that the perturbation is small compared with H_0.

Equation 2.5

$$H = H_0 + \lambda H'$$

Møller-Plesset perturbation theory treats the contribution of electron correlation energy to the overall electronic energy as a series of perturbations to the (zeroth order) HF energy. The order that the perturbations are truncated at is defined in the name of the method. For example, MP2 includes a second order perturbation correction to the HF energy and is therefore the cheapest (computationally) of the MP methods. By extrapolation, the more accurate MP4 approach is more time consuming and thus expensive, because it produces fourth order perturbation. Qualitatively, MP perturbation theory adds higher electronic excitations to HF theory as a non-iterative correction.

A different approach to the treatment of electron correlation is the coupled-cluster (CC) method.[80] Here the HF-SCF wavefunction is augmented by the exponential operator e^T. according to Equation 2.6.

Equation 2.6

$$\psi_{CC} = e^T \psi_{SCF}$$

The effect of the e^T operator is to express the electronic wavefunction as a function of all possible excitations of electrons from occupied to vacant spin-orbitals. The mixing in of these excited states allows the electrons to keep away from each other and thereby provide for electron correlation. The cluster operator T is defined as the sum of one-electron (T_1), two-electron (T_2), three-electron (T_3) up to N-electron (T_N) excitation operators where N is the number of electrons in the system (Equation 2.7).

Equation 2.7

$$T = T_1 + T_2 + T_3 + \ldots\ldots + T_N$$

This summation must be truncated to make the calculation tractable. It is found that the T_2 operator is the most important and inclusion of this term only is known as the coupled cluster doubles (CCD) method. Further accuracy can be achieved by incorporating the T_1 and T_3 terms which give rise to, coupled cluster with singles and doubles (CCSD) and coupled cluster with singles doubles and triples (CCSDT), respectively.[81] The latter is computationally very expensive and hence a number of approximate forms have been developed, of which CCSD(T) is one.

D. Basis Sets

The role of basis functions in the calculation of the electron wavefunction has already been described (Equation 2.3). It is necessary however to give some insight into the nature of these sets of functions, or basis sets, and their importance for the accurate prediction of molecular energy.

Two types of mathematical functions have predominantly been used to generate basis functions. Slater-type Orbitals (STOs) were used early on but were found to generate mathematical difficulties and so for ease of calculation Gaussian-type Functions (GTFs) are most commonly adopted. Linear combinations of GTFs can be used to describe atomic orbitals (χ) which in turn are combined, linearly, to give molecular orbitals (ϕ) as outlined in Equation 2.3. It follows that the greater the number of functions used to describe an orbital, the greater the flexibility and hence, the greater the accuracy of the molecular orbital description. It is also important, particularly for valence-orbitals, to include more than one size of function. Such an approach is known as a split valence orbital. An example of this is the 6-31G basis set: here a linear combination of 6 primitive Gaussian functions are used to describe inner core orbitals (i.e., atomic $1s$ and $2s$ orbitals for atoms Li-Ne) , whereas the valence orbitals (i.e., atomic $2p$ orbitals for atoms Li-Ne) are split into 3 primitive Gaussians for the inner part of the orbital and 1 larger function for the outer. It is also possible to split the inner core orbitals in this way and such a basis is described as a double zeta (DZ) basis set.

While split valence and double zeta sets allow orbitals to change size they do not allow them to change shape. It is often the practice to add into the basis set orbitals with angular momentum higher than that required for the ground state description of the atom. For example, sometimes GTFs describing d -type atomic orbitals are added to second row atoms (Li-Ne) to form what are known as polarised basis sets. In a chemical sense, this allows the atomic d -orbitals to make a significant contribution to the bonding of second row atoms. Polarisation functions are designated with an asterisk or by the type of function added [eg. 6-31G* or 6-31G(d)]. In a similar way molecules with lone pairs of electrons, anions and systems which incorporate hydrogen bonding often have significant electron density far removed from the nuclei. This is best described by incorporating large versions of s and p -type functions into the basis set. These diffuse functions are designated with a "+" or sometimes with the prefix "aug" [eg. 6-31+G(d)].

Aside from electron correlation, the other major source of error in energy calculations of small molecular systems is the so-called basis set truncation error. If the basis set chosen for a particular calculation is too small then the energy of the system will be overestimated. So while a modest basis set may lead to an appropriate geometry in an optimisation calculation, accurate description of the energy of the system may require a larger basis set. A typical theoretical protocol is therefore likely to involve: (i) optimisation of the molecular structure at a level of theory which incorporates treatment of electron correlation and a modestly sized basis set, followed by (ii) accurate calculation of the energy for the optimised structure incorporating a more comprehensive treatment of electron correlation and a larger basis set including polarisation and diffuse functions. The nomenclature for such a protocol is a two part expression where the first part designates the level of theory and basis set of the final energy calculation and the second designates the level of theory and basis set used for the structural optimisation [eg. CCSD(T)/6-31+G(d)//MP2/6-31G(d)].

(III) DENSITY FUNCTIONAL THEORY[82]

A. Density Functional Theory

Density functional theory (DFT) is a completely different approach to the *ab initio* schemes previously discussed. Instead of attempting to generate the electron wavefunction, density functional theory targets its scalar square ($| \psi |^2$), which equates to the electron density (ρ), as the central quantity. The Hohenberg-Kohn theorem[83] proves that the ground-state molecular energy, wavefunction and all other molecular properties may in principle be described as functionals of the electron probability density ρ. Kohn-Sham orbitals[84] can be introduced to convert the many body problem to one-electron equations which may be solved in a self consistent manner, analogous to the HF-SCF approach.[#] The starting functional for most DFT methods is the local density approximation (LDA) which includes terms for kinetic energy, coulomb repulsion, exchange, and correlation as derived from the homogeneous electron gas. By itself, however, the LDA has problems in properly describing the properties of molecular systems. As such, gradient corrections to LDA have been introduced for exchange and correlation energy terms by Becke[85] and Perdew[86] to give the corrected LDA+BP functional. In fact, pure DFT methods are defined by pairing an exchange functional with a correlation functional in this way. Another common example is the pairing of Becke's gradient-corrected exchange functional with the gradient-corrected correlation functional of Lee, Yang and Parr[87] in the BLYP method. The major advantages of DFT methods are the inherent treatment of electron correlation and the inexpensive nature of the calculations.

B. Hybrid Methods

Electron exchange energy is treated exactly in HF theory. It is therefore possible to utilise a combination of DFT and HF terms to generate a so called hybrid functional. This idea was originally introduced by Becke[88] and has become increasingly popular because of its consistent generation of accurate results for a low computational cost. The most popular of the hybrid methods is the B3LYP approach which represents the exchange and correlation

---

[#] Kohn-Sham orbitals are mathematical auxiliary quanitities and are not directly related to molecular orbitals as is the case for the HF approach.

functional as a linear combination of the terms given by LDA, SCF, Becke and LYP functionals.[89] The coefficients for this combination have been determined in a semi-empirical fashion based on the computational reproduction of experimental heats of formation for various molecules. The B3LYP hybrid method generates an exchange and correlation functional (E_{xc}) as a linear combination of functionals given by LDA (E_x^{LDA}), SCF (E_x^{SCF}), Becke (E_x^B) and LYP (E_x^{LYP}) functionals. The coefficients for this expansion were determined semi-empirically with respect to computational reproduction of experimental heats of formation. The resultant combination is given in Equation 2.8.

Equation 2.8

$$E_{xc} (B3LYP) = 0.8\, E_x^{LDA} + 0.2\, E_x^{SCF} + 0.72\, E_x^B + 0.81\, E_x^{LYP}$$

The B3LYP method is the theory most used for the prediction of the molecular geometries appearing in this thesis.

(IV) CALCULATION OF MOLECULAR PROPERTIES

A. The Theoretical Protocols Adopted for This Study

This study is concerned with the prediction of structure and energy of cumulated carbon chains and their corresponding anions and cations. DFT and DFT/HF methods have proven themselves cost effective methods for the theoretical prediction of molecular geometries and their physical properties.[90] For example, used in conjunction with a moderately sized basis set such as 6-31G(d) the B3LYP method has been used to calculate vibrational frequencies for over 100 common organic and inorganic molecules with an average deviation from experimentally determined values of less than 50 cm^{-1}.[91] The structures presented in this thesis were therefore optimised using the B3LYP method with the 6-31G(d) or larger basis sets within the GAUSSIAN 94 suite of programs.[92]

Some concerns have been raised in the literature concerning the use of DFT and DFT/HF methods for accurate prediction of the energies of polycarbon systems. It is known, for

example, that at the B3LYP/6-31G(d) level, 1-propyne is determined to be almost 3 kcal mol^{-1} more positive in energy than allene. This is contrary to the experimentally known energetics which suggest the latter is less stable by 1.7 kcal mol^{-1}.[93] Further, many of the systems under investigation here involve anionic species and hence the incorporation of diffuse functions in the basis set is required for accurate prediction of energies. It is therefore pertinent to further probe the energetics of the predicted geometries at a higher level of theory. In this study, single point energy calculations for the B3LYP structures have been carried out using the coupled cluster approach, CCSD(T). These calculations have been carried out using the MOLPRO 97.4 program package.[94] It has been shown that accurate prediction of the energy of anions (and the cognate thermodynamic properties such as electron affinities) require extensive basis sets. Consequently, the correlation consistent basis sets of Dunning[95,96] have been employed in the energy calculations. In particular, the double zeta, aug-cc-pVDZ and triple zeta, aug-cc-pVTZ basis sets have been used. These basis sets include polarisation functions and large diffuse functions [such as $4s$, $3p$ and $2d$ orbitals on all second row atoms (Li-Ne)] in the calculation. The latter are particularly relevant to the determination of accurate energies for anionic species.[97]

The precise theoretical protocols are given in the relevant Chapters along with comparisons with other theoretical and experimental data where available.

(V) UNIMOLECULAR REACTIONS

The identification of critical points on the potential surface has already been mentioned. Once located these stationary points can be classified as either local minima (no imaginary frequencies) or transition states (one imaginary frequency) by calculation of the frequencies using analytical gradient procedures.[78] Chemically, it is important to ascertain which minima are connected by a given transition state. This can be determined by an intrinsic reaction coordinate (IRC) calculation which follows the reaction coordinate down-hill (in each direction) from the transition structure to the pertinent minimum.[98] The energy difference between a minimum and the transition state which connects it to a second

minimum represents the activation energy (E_a) required for the reaction. For example, the reaction coordinate diagram for the unimolecular rearrangement of ABC to ACB is shown in Figure 2.1. The two local minima are connected by the transition structure [ABC]‡ which is E_a kcal mol^{-1} more positive in energy than ABC and ACB.
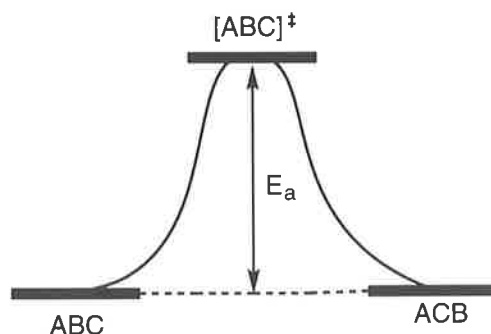
Figure 2.1 *The reaction coordinate diagram for the idealised unimolecular rearrangement of ABC to ACB*

It should be noted that the rate of this reaction depends on more than simply the activation energy (E_a). The empirical observation is that the rate of many chemical reactions (k) follows the Arrhenius equation (Equation 2.9).[99]

Equation 2.9

$$k = A \exp(-E_a / RT)$$

This relation demonstrates the dependence of rate on the activation energy (E_a), the gas constant (R), the temperature (T) and the pre-Arrhenius factor (A). The latter parameter is an experimentally determined value. Transition state theory provides one theoretical approach to allow estimation of the rate constant.[100] It gives the expression for unimolecular rate constant (k) shown in Equation 2.10 for a canonical ensemble of molecules at temperature, T.

Equation 2.10

$$k\,(T) = \frac{k_b T}{h} \frac{Q^{\ddagger}}{Q_R} \exp(-E_a / RT)$$

In this expression, k_b is Boltzman's constant, h is Planck's constant, E_a is the activation barrier at 0 K and $Q^{\ddagger}$ and Q_R are the molecular partition function densities of the transition state and reactants respectively. The equation can be considered in two parts, an exponential factor which is primarily dependent on the activation energy and a pre-exponential factor which effectively describes the entropy of the transition state. The rate of reaction is determined by both of these terms. While the activation energy may be calculated using the theoretical protocols discussed previously, estimation of the pre-exponential factor is more complex.

Chapter 3: Interstellar and Circumstellar Cumulenes. Mass Spectrometric and Related Studies

(I) ABSTRACT

The last few years have brought an increasing interest in the chemistry of the interstellar and circumstellar environs. Many of the molecular species discovered in remote galactic regions have been dubbed "non-terrestrial" because of their unique structures.[101] This has provided a challenge to chemists in many differing fields to attempt to generate these unusual species in the laboratory. Of particular interest have been the unsaturated hydrocarbon families C_nH and C_nH_2 which have been pursued by a number of diverse methodologies. Mass spectrometry has proved an invaluable tool in this quest, as it has the ability, in its many forms to (i), generate charged analogues of these species in the gas phase, (ii) probe their connectivity, ion chemistry and thermochemistry and (iii), in some cases elucidate the neutrals themselves. Here we will discuss the progress of these studies to this time in order to place in context the investigations described in this thesis.

(II) INTERSTELLAR CUMULENES

A. Detection of Molecules in Interstellar and Circumstellar Clouds

Advances in astrophysics over recent years have been responsible for both probing some of the furthest regions of the known universe and just as amazingly, uncovering its minutest secrets. More than 100 molecular species have now been positively identified across a range of disparate galactic media.[102] Molecules have been identified in diffuse interstellar clouds of low density (some 1-100 particles per cm^3), dark clouds (that are opaque to UV radiation), and circumstellar envelopes.[103] The latter category have proved to be some of the richest extraterrestrial molecular sources. The expanding envelopes of gas and dust surrounding carbon rich red giant stars contain a wide variety of carbon based molecules. Perhaps the best example of this is the carbon star IRC+10216, which is a source of more than 50 detected molecules and, in particular, a number of the more exotic cumulenes which will be discussed here.[104] The spatial distribution of the species HC_3N, HC_5N, C_4H and C_3N within the circumstellar envelope surrounding this star have been determined. In each case, a characteristic hollow shell has been observed indicating such species are more likely to have been synthesised in the outer regions of the envelope rather than in the dense regions close to the star (Figure 3.1).[105]
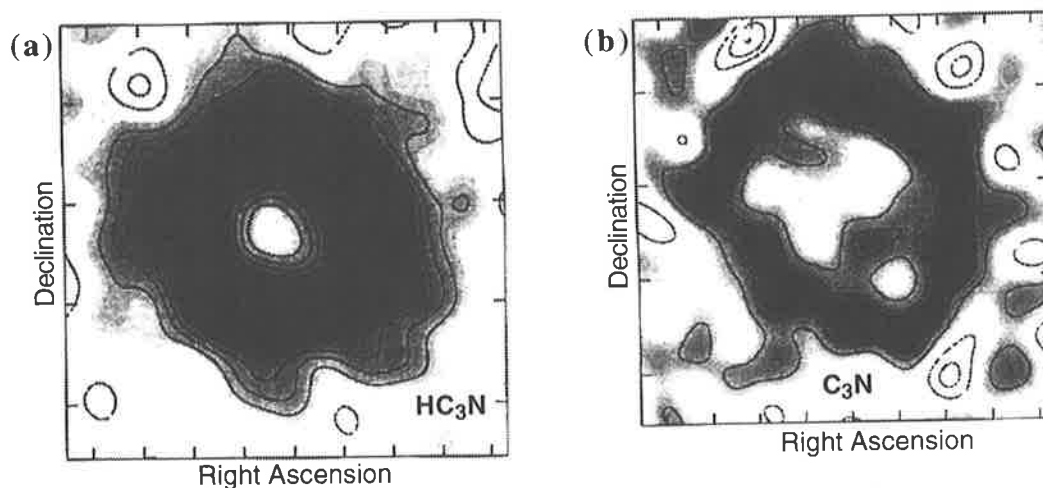
Figure 3.1 *Contour depiction of the annular distribution of (a) HC₃N and (b) C₃N in the circumstellar envelope surrounding the red giant star IRC+10216. The darker shading represents regions of higher molecular density.*[105]

Of the species detected in galactic sources, all but a handful have been initially detected by their rotational transitions which occur at radio/millimetre wavelengths. There are a number of reasons for this. Firstly, molecular sources such as those previously mentioned are typically low-temperature, low-density media, thus making vibrational and electronic transitions energetically improbable. Secondly, Earth based observation of astronomical lines is more strongly obscured at shorter wavelengths by interference from the terrestrial atmosphere. Finally, the nature of molecular clouds results in narrow line widths allowing for high resolution spectra (including fine and hyperfine structure) to be obtained. It is not our intention to discuss these detection methodologies which have been the subject of review.[106] However it is important to this discussion to consider what bias, if any, exists in these detection procedures in order to establish how representative the available data is, with reference to the chemistry of these environs. Consider the case of molecules which do not possess a permanent electric dipole moment and cannot, therefore, give rise to rotational transitions. Molecules of this type, inluding methane, oxygen and nitrogen cannot be detected by radioastronomy even though they are most probably ubiqitous in the galactic environment. Consider also the comparison between simple linear but highly polar molecules, which have only a few energetically separated rotational states giving rise to strong well defined emission spectra, and complicated asymmetric tops in which the population is spread over a number of closely spaced levels. This type of bias must be kept in mind when considering the molecular species so far identified in these galactic environs (Table 3.1). It is clear that these detection criteria strongly favour molecules such as the long chain cumulenic species targeted in this thesis. Most of these cumulenes have large dipole moments and relatively simple linear geometries giving rise to pronounced rotational transitions.

Table 3.1 Interstellar molecules detected so far.[102]

Number atoms	Molecular species
2-atomic	H_2, CH, OH, C_2, CN, CO, NO, HCl, CS, SiO, PN, PC, SN, SO, SiS, AlF, NaCl, AlCl, KCl.
3-atomic	H_2O, HCN, HNC, HCO, HNO, H_2S, OCS, SO_2, C_2Si, C_2H, C_2S, C_2O^*.
4-atomic	NH_3, H_2CO, C_2H_2, HNCO, H_2CS, HNCS, C_3N, C_3O, C_3S, l -C_3H, *cyc* -C_3H, HC_2N^*.
5-atomic	CH_2NH, CH_2CN, CH_2CO, NH_2CN, HCO_2H, C_4H, HC_3N, CH_4, SiH_4, *cyc* -C_3H_2, l -$C_3H_2^*$, C_4Si^*, C_5^*.
6-atomic	CH_3OH, CH_3CN, CH_3NC, NH_2CHO, CH_3SH, HC_2CHO, C_5H, C_2H_4, $C_4H_2^*$.
7-atomic	CH_3NH_2, CH_3C_2H, CH_3CHO, C_2H_3CN, C_6H, HC_5N.
8-atomic	CH_3C_3N, CH_3CO_2H, C_7H^*, $C_6H_2^*$.
9-atomic	C_2H_5OH, CH_3OCH_3, C_2H_5CN, CH_3C_4H, HC_7N, C_8H^*.
10-atomic	CH_3COCH_3, CH_3C_5N.
11-atomic	HC_9N.
13-atomic	$HC_{11}N$.
ions	CH^+, SO^+, HCO^+, HOC^+, HCS^+, N_2H^+, H_3O^+, HCO_2^+, H_2CN^+.

*These additional relevant species have been taken from NIST and NASA
  online databases.

Even a cursory inspection of the types of molecules detected, reveals many interesting and in some cases novel connectivities. Of particular note in the context of this thesis are the unsaturated hydrocarbons C_nH, starting with the trivial C_2H and progressing through to C_8H and C_nH_2, where n = 2, 3, 4 and 6. Higher analogues of both these families have been proposed as interstellar molecules and as good candidates for detection.[107,108] We have decided, for simplicity, to refer to species containing such unsaturated polycarbon chains as cumulenes, or heterocumulenes (where nitrogen, oxygen, sulphur, etc. are included in the chain), even though this may not be strictly correct in each case. It is significant to note that for some of these cumulenes there exist structural isomers as in the cases of C_3H and C_3H_2, where both linear and cyclic isomers have been detected. Along with the unsaturated hydrocarbons, many species which include heteroatoms in the carbon chain, such as C_nO, HC_nO, C_nN, HC_nN and C_nS have also been detected. In fact these molecules form some of

the largest (up to 13 atoms) thus far detected in interstellar and circumstellar clouds. It is worthwhile also to highlight the small number of charged species that have been detected (Table 3.1), lending support to models of ion-molecule chemistry in these environs as well as adding validity to investigations of charged analogues of the identified neutrals.

Despite the successes of radio-astronomy in detection of interstellar molecules, current limitations still encourage the pursuit of other methodologies. Of particular relevance to this discussion are ongoing investigations into spectroscopy in the IR, visible and UV regions. Many of the spectral features at these frequencies are as yet unassigned, for example the so called "UV hump" at 220 nm and the diffuse interstellar bands (DIBs) in the visible and near-IR regions. Interestingly, highly unsaturated hydrocarbons have been nominated as possible candidates to explain these spectroscopic characteristics. Linear carbon chains of the types C_n, C_nH, C_nH_2 and C_nH_4 (where n may be as high as 12), polycyclic aromatic hydrocarbons (PAHs) and even buckminster fullerenes have been investigated as possibilities.[109,110]

B. Molecule Formation in Galactic Gas Clouds.

With the increase in knowledge of the morphology of these molecular clouds, has come a growing interest in the types and rates of chemical reactions which evolve such a complex suite of species. A number of different models have been put forward to explain the astrophysical observations, as well as to make some further predictions about the types of molecules which may be present. Most models predict a chemistry dominated by positive ion-neutral and positive ion-electron type reactions (*cf.* Scheme 3.1) these have been thoroughly reviewed and can adequately account for the formation of long chain unsaturated hydrocarbons.[102] These reactions are favoured because they are not kinetically impaired by the low densities and temperatures which exist in these molecular clouds.

Scheme 3.1

Radiative association: $\qquad$ $C_3{}^{\cdot+}$ + C_2H_2 $\rightarrow$ $C_5H_2{}^{\cdot+}$ + $h\upsilon$

Dissociative recombination: $\qquad$ $C_5H_2{}^{\cdot+}$ + e^- $\rightarrow$ C_5H^- + $H^{\cdot}$

Although reactions between stable neutrals are likely to be slow at low temperatures, recent investigations have revealed that open shell neutrals may react rapidly with other uncharged species under these conditions. This has lead to the inclusion of this class of reaction into models of interstellar chemistry.[111,112] This has been supported by elegant laboratory investigations revealing possible new pathways to the synthesis of hydrocarbons in the interstellar environment (*cf.* Scheme 3.2).[113,114]

Scheme 3.2

Neutral-neutral reaction: $\qquad$ $^{\cdot}C$ + C_2H_2 $\rightarrow$ $^{\cdot}C_3H$ + $H^{\cdot}$

Despite the fact that no negative ions have been detected so far in any interstellar or circumstellar source, their contribution to the chemistry of these environments has been postulated. It was first thought that negative ion formation in interstellar clouds would be somewhat inefficient, particularly for small molecules with few vibrational and rotational modes through which to disperse excess energy acquired in a radiative attachment type process (Scheme 3.3).[115]

Scheme 3.3

Radiative attachment: $\qquad$ X + e^- $\leftrightarrow$ $[X^-]^{\ddagger}$ $\rightarrow$ X^- + $h\upsilon$

When X is a small molecule, electron attachment gives the energetically excited intermediate $[X^-]^{\ddagger}$, which has a very short lifetime against electron detachment (the reverse process). It has since been postulated however, that if larger species such as PAHs are present in interstellar clouds, then they may undergo more efficient radiative attachment to form large negative ions.[116,117] A number of larger linear cumulene anions of the forms C_nH^- and

$C_nH_2^{\cdot-}$ (where n = 10-23) appear in some models of the hydrocarbon chemistry of these environs.[118] The possibility of large negative charge carriers has led to the suggestion that charge transfer processes may take place involving relatively small neutrals with high electron affinities. A recent example of this is the cyanide anion. A detectable concentration of CN^- has been estimated for some interstellar gas clouds. This model predicts reasonably efficient formation of CN^- by charge transfer processes from large PAH anions [EA(CN) 3.82 ± 0.02 eV].[119] Similarly C_3N^- and C_3H^- have been proposed as possible small, detectable interstellar anions with a potential role in the chemistry of this environment.[120]

C. Laboratory Detection of Interstellar Cumulenes

The discovery of C_nH, C_nH_2 and other unusual molecular species in interstellar and circumstellar clouds has prompted a wealth of research into generating both these and their analogues in the laboratory. Most of these efforts have been focussed on utilising microwave (radio/millimetre) spectroscopy to probe electrical discharges in helium/acetylene or helium/diacetylene atmospheres. These investigations have lead to the detection and characterisation in the laboratory of a number of the C_nH and the C_nH_2 cumulenes.[101,121,122] In the last few years a technique employing a Fourier transform microwave spectrometer has been used to observe pulsed supersonic molecular beams.[108,123] These techniques have allowed for the characterisation of rotational lines for (i) C_nH, where n ≤ 14 and (ii) C_nH_2, where n ≤ 7, with a few exceptions. However, as may be expected from such techniques, a great many species are formed simultaneously, and a good deal of calculation and intuition is required to decipher the large range of signals generated. Despite these difficulties, the predictive advantages of this methodology are clear: a new species once characterised in the laboratory may be searched for directly amongst the unassigned astronomical radio/millimetre lines.

A different and perhaps a more structurally selective approach, is the use of low temperature matrix trapping techniques where UV photolysis or flash pyrolysis of suitable precursors is carried out and the products are trapped in a low temperature matrix. For example,

photolysis of diazopropyne in an argon matrix (12K) has generated propargylene (Scheme 3.4, **2**),[124] which was then characterised by infrared red (IR) spectroscopy. Similar trapping experiments have yielded cyclopropenylidene (Scheme 3.4, **1**)[125] and propadienylidene (Scheme 3.4, **3**),[126] stressing the structural selectivity of this approach.

Scheme 3.4
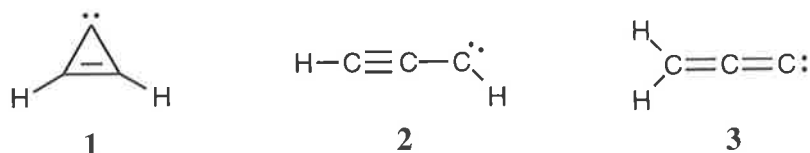
Generation and detection of unusual and transient ionic species has long been the domain of mass spectrometry and a number of advantages are evident when approaching the problem in this way. Firstly, the high dilution conditions used in mass spectrometry allow for the generation of unstable ionic species because of the low probabilities of destructive interactions with another reactive particle. These conditions are, in some ways, analogous to the diffuse atmosphere of galactic gas clouds. Secondly, tandem mass spectrometric techniques allow for the generation, detection and further investigation of the species of interest (a major advantage over the other techniques discussed). Thirdly, the application of many of the gas phase ionisation techniques outlined in Chapter 1 permits individual structural isomers to be generated. Mass spectrometry can also be used in conjunction with NRMS, photoelectron spectroscopy (PES), and related methods, to investigate transient neutrals. Finally, mass spectrometry allows for the study of reactions between cumulene ions and appropriate neutrals; this further elucidates reaction pathways operating in the interstellar medium. A surprisingly large volume of work exists in this area and forms an essential background to the investigations described in this thesis.

(III) GENERATION OF INTERSTELLAR CUMULENES BY MASS SPECTROMETRY

A. Isomers of C_3H_2

1. *Anionic approaches*

The most thoroughly investigated interstellar hydrocarbon species have been the isomers of C_3H_2. These have been studied by a range of mass spectrometric techniques. Some of the earliest work on this species was carried out as a part of broader investigations into the chemical ionisation behaviour of $O^{\cdot-}$.[20],# It was shown that reaction of methyl acetylene ($CH_3C\equiv CH$) and allene ($CH_2=C=CH_2$) with $O^{\cdot-}$ yielded some $C_3H_2^{\cdot-}$ species together with loss of water. A later study more fully investigated the mechanism of $H_2^{\cdot+}$ abstraction from methyl acetylene and showed that both 1,1- and 1,3-$H_2^{\cdot+}$ abstraction co-occurred, yielding $CH_2CC^{\cdot-}$ and $HCCCH^{\cdot-}$ isomers.[127] This was shown by deuterium labelling when d_3-methyl acetylene was allowed to react with $O^{\cdot-}$ in an ion-cyclotron resonance (ICR) mass spectrometer (Scheme 3.5).

Scheme 3.5

$$CD_3C\equiv CH \ + \ O^{\cdot-} \ \rightarrow \ CD_3C\equiv C^- \ + \ {}^{\cdot}OH \qquad (a)$$

$$\rightarrow \ [CD_2C\equiv CH]^- \ + \ {}^{\cdot}OD \qquad (b)$$

$$\rightarrow \ [CD_2C\equiv C]^{\cdot-} \ + \ HOD \qquad (c)$$

$$\rightarrow \ [CD=C=CH]^{\cdot-} \ + \ D_2O \qquad (d)$$
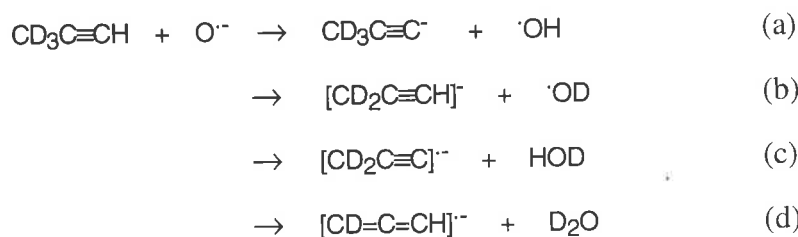
Further confirmation of these structural assignments was achieved by carrying out subsequent ion-molecule reactions. It was found that the mass selected ion $[CD_2C\equiv C]^{\cdot-}$ did not react with methyl formate while $[CD=C=CH]^{\cdot-}$ added to the ester and eliminated a methoxy radical to give a stabilised enolate (Scheme 3.6).

For a discussion on the chemical ionisation behaviour of $O^{\cdot-}$ see Chapter 1, pp 8.

Scheme 3.6

$$[CD_2C\equiv C]^{\cdot-} \quad + \quad HCO_2CH_3 \quad \rightarrow \quad \text{no reaction}$$

$$[DC=C=CH]^{\cdot-} \quad + \quad HCO_2CH_3 \quad \rightarrow \quad DC\equiv C\text{-}CH=CH\text{-}O^- \quad + \quad CH_3O^{\cdot}$$
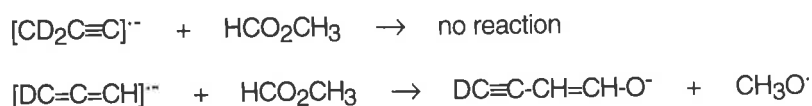
The structure of the $C_3H_2^{\cdot-}$ species formed from the analogous $O^{\cdot-}$ and allene reaction was probed by this chemistry. It was found here that only a "small fraction" of the $C_3H_2^{\cdot-}$ formed in this way reacted with methyl formate, thus suggesting very limited formation of HCCCH$^{\cdot-}$. This implied $1,1$-$H_2^{\cdot+}$ abstraction was the dominant process, leading to almost exclusive formation of $CH_2CC^{\cdot-}$ in this reaction. More recently, this ion chemistry has been used to generate precursors for both NRMS and PES experiments. These will be discussed later.

The species $C_3H_2^{\cdot-}$ has been the subject of a number of different spectroscopic investigations. In the earliest of these, the anion was generated along with C_3H^- and $C_3^{\cdot-}$ in a high pressure electrical discharge in a 4:1 propene and oxygen mixture.[128] The mass selected anions were then studied by photoelectron spectroscopy thus determining the electron affinity of C_3H_2 to be 1.794 ± 0.025 eV. The authors postulate that the photoelectron spectrum of $C_3H_2^{\cdot-}$ is not "highly structured", suggesting similarity between both anion and neutral geometries, favouring the CH_2CC over the HCCCH connectivity. Although early calculations predicted neutral HCCCH to be some 17 kcal mol^{-1} more stable than neutral CH_2CC.[129]

Subsequent *ab initio* studies have probed the structures of neutrals[130,131] and anions[132] at the much more comprehensive levels now available. In the case of the neutral isomers most theoretical studies maintain cyclic C_3H_2 as the global minimum, more stable than HCCCH which in turn is less energetic than CH_2CC. Significantly, theory shows the CH_2CC anion to be the global minimum at the CCSD(T)/aug-cc-pVTZ level of theory, some 13.5 kcal mol^{-1} more stable than the HCCCH anion and 40.3 kcal mol^{-1} more stable than electron attachment to the cyclic C_3H_2 isomer.[132] Calculation, at this level, of the electron affinity

(EA) of CH$_2$CC gives a value of 1.712 eV, in reasonable agreement with the photoelectron measurements mentioned, particularly when compared with the corresponding value of 1.10 eV, for HCCCH. This theoretical work is in agreement with the experimental structural assignment.

The EA of CH$_2$CC has been revisited by more recent photoelectron spectroscopic measurements: the ion was generated by the reaction of allene with O$^{\cdot -}$ as previously described.[133] Interestingly, this study also revealed a triplet excited state of the CH$_2$CC diradical, some 30 kcal mol^{-1} less stable than the ground state. This work included proton affinity bracketing experiments using flowing afterglow selected ion flow tube (FA-SIFT) methodologies to determine the gas phase acidity of the parent propargyl radical: ΔH_{acid}($^{\cdot}$CH$_2$CCH) = 372 ± 5 kcal mol^{-1}. When used in conjunction with the electron affinity data *via* a simple thermodynamic cycle, bond dissociation energies for the acetylenic hydrogen of the propargyl radical can be evaluated: BDE($^{\cdot}$CH$_2$CC-H) = 100 ± 5 kcal mol^{-1}. Significantly, by further manipulation of these data, the heat of formation of neutral propadienylidene, $\Delta H_{f,298}$(CH$_2$CC) = 129 ± 4 kcal mol^{-1}, was obtained from the simple relation given in Equation 3.1. The sensitivity of these techniques to probe both structure and thermochemistry of a neutral from its corresponding anion provides impetus for the development of gas phase anion syntheses, such as those described in Chapters 4-7.

Equation 3.1

$$\Delta H_{f,298}(CH_2CC) = BDE(^{\cdot}CH_2CC\text{-}H) + \Delta H_{f,298}(^{\cdot}CH_2CCH) - \Delta H_{f,298}(^{\cdot}H)$$

2. Cationic approaches

Despite a number of earlier studies on the empirical C$_3$H$_2$ radical cation, significant insight was not gained until structural investigations were performed with two C$_3$H$_2$$^{\cdot +}$ isomers found to be products of electron impact on methyl acetylene.[134] Reaction of C$_3$H$_2$$^{\cdot +}$ with CO and other neutral reagents in a selected ion flow tube (SIFT) apparatus yielded results inconsistent with a single reactant ion (Scheme 3.7). A rapid initial reaction quickly

terminated leaving the product formation dominated by a much slower process. This was rationalised in terms of an incident ion beam consisting of a reactive open chain $HCCCH^{\cdot+}$ isomer and a more stable, less reactive cyclic species, cyc -$C_3H_2^{\cdot+}$ (where the nomenclature cyc denotes a three membered ring system, *cf.* structure **1**, scheme 3.4).

Scheme 3.7

$$cyc\text{ -}C_3H_2^{\cdot+} \quad + \quad CO \quad \rightarrow \quad C_3H_2CO^{\cdot+} \qquad \text{(slow)}$$

$$HCCCH^{\cdot+} \quad + \quad CO \quad \rightarrow \quad C_3H_2CO^{\cdot+} \qquad \text{(fast)}$$
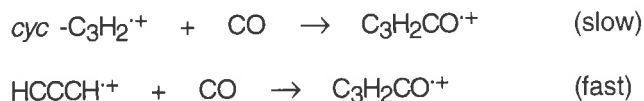
Structural assignments were confirmed from the reaction of C_3H^+ with D_2, in the SIFT, apparatus, where $C_3HD^{\cdot+}$ and $C_3D_2^{\cdot+}$ formed in the ratio of 2:1 (Scheme 3.8). It was proposed that this ratio was indicative of complete scrambling occurring through a symmetrical cyclic $C_3HD_2^{\cdot+}$ intermediate and hence forming the cyclic $C_3D_2(H)^{\cdot+}$ isomer exclusively. Furthermore, the $C_3D_2(H)^{\cdot+}$ reaction products reacted further with CO at rates consistent with the less reactive of the two species formed from methyl acetylene.

Scheme 3.8

$$C_3H^+ \quad + \quad D_2 \quad \rightarrow \quad cyc\text{ -}C_3HD_2^+$$

$$cyc\text{ -}C_3HD_2^+ \quad \rightarrow \quad cyc\text{ -}C_3D_2^{\cdot+} \quad + \quad H^{\cdot}$$

$$cyc\text{ -}C_3HD_2^+ \quad \rightarrow \quad cyc\text{ -}C_3HD^{\cdot+} \quad + \quad D^{\cdot}$$
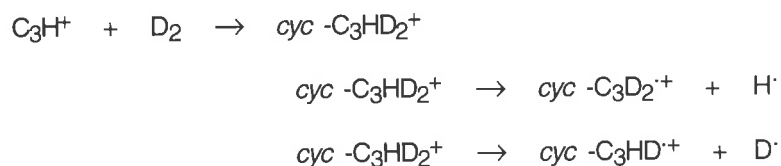
The overall reaction depicted in Scheme 3.8 was found to be endothermic by around 1 kcal mol^{-1}. The heat of formation of cyc -$C_3H_2^{\cdot+}$ is thus calculated as 329 ± 4 kcal mol^{-1}. The structural assignments have been further supported by subsequent *ab initio* studies which show cyc -$C_3H_2^{\cdot+}$ to be approximately 12.7 kcal mol^{-1} more stable than $HCCCH^{\cdot+}$ and 38.5 kcal mol^{-1} more stable than the $CH_2CC^{\cdot+}$ geometry at the CISD(Q)/6-311G** level of theory.[135] The differing reaction rates of these two isomeric C_3H_2 radical cations with CO and also N_2O allows quenching of the more reactive $HCCCH^{\cdot+}$ isomer. Subsequent

flowing afterglow (FA-SIFT) studies have utilised this technique to investigate *cyc* -$C_3H_2^{·+}$ in isolation and further probe the chemistry and thermochemistry of both isomers.[136-138]

Wong and Radom have critically evaluated the available thermochemical data: using G2 calculations, they propose the following heats of formation for the three stable isomeric cations, $\Delta H_{f,298}[cyc$ -$C_3H_2^{·+}] = 332$ kcal mol^{-1}, $\Delta H_{f,298}[HCCCH^{·+}] = 339$ kcal mol^{-1}, $\Delta H_{f,298}[CH_2CC^{·+}] = 379$ kcal mol^{-1}.[139] The stability of the 3-membered ring system relative to its open chain isomers is an interesting observation. It is presumably due to aromatic stabilisation energy in this cyclic 2π–electronic system. This is evident in consideration of the valence bond structure shown in Scheme 3.9 and is in contrast to the relative instability of the corresponding anion which does not adhere to Hückel's (4n + 2) π–electron rule. Aromatic stabilisation is also observed for the corresponding cyclic neutral, for which the thermochemistry has been reported. This data is reviewed in the following discussion.

Scheme 3.9
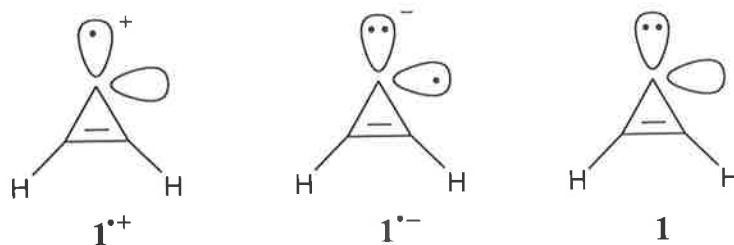
Another approach to the generation of $C_3H_2^{·+}$ isomers has been to use laser photoionisation time-of-flight (TOF) mass and photoelectron spectrometers to analyse supersonic expansions of the corresponding neutral carbenes.[140] In this study three isomeric carbenes were produced by supersonic jet flash pyrolysis of appropriate precursors (Scheme 3.10). The pyrolytes so produced were then expanded into a vacuum chamber and ionised with a 10.49 eV laser. Subsequent detection of ions and electrons was effected using TOF spectrometers.

Scheme 3.10
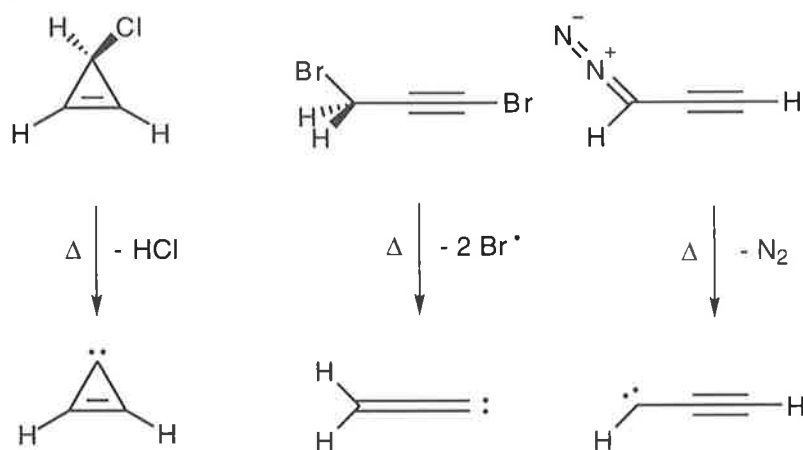
The three radical cations *cyc* -C_3H_2, CH_2CC and HCCCH, were detected, with ionisation potentials determined for all but the last isomer (ionisation potentials measured to be 9.15 ± 0.03 eV and 10.43 ± 0.02 eV respectively). These data are particularly useful in the case of the *cyc* -C_3H_2 radical cation since this represents the global minimum on the potential surface, and can thus be used in conjunction with other available data to calculate the heat of formation of neutral *cyc* -C_3H_2. The sum of the measured ionisation potential, IP[*cyc* -C_3H_2] = 9.15 ± 0.03 eV and the heat of formation of the product cation, $\Delta H_{f,298}[c\text{-}C_3H_2^{\cdot+}]$ = 322 ± 4 kcal mol^{-1} (use of this value has been questioned and will be further discussed) gave a heat of formation, $\Delta H_{f,298}[cyc$ -$C_3H_2]$ = 114 ± 4 kcal mol^{-1} for the neutral species.

The thermochemistry of *cyc* -C_3H_2 has also been addressed by a novel flowing afterglow-triple quadrupole study.[141] Here, the proton affinity of *cyc* -C_3H_2 was determined from the measured activation energy of the proton transfer from *cyc* -$C_3H_3^+$ to ammonia. Combined with the known heats of formation of *cyc* -$C_3H_3^+$ and H^+ (by the relation given in Equation 3.2), a heat of formation for *cyc* -C_3H_2 of 119.5 ± 2.2 kcal mol^{-1} was obtained. Although seemingly in conflict with the earlier result, it is interesting to note that if the IP from the former experiment is combined with the theoretically derived value[135] of $\Delta H_{f,298}[cyc$ -$C_3H_2^{\cdot+}]$ = 332 kcal mol^{-1} the resulting heat of formation $\Delta H_{f,298}[cyc$ -$C_3H_2]$ = 121 kcal mol^{-1} is in good agreement with the latter experiment.

Equation 3.2

$$\Delta H_{f,298}[cyc\text{ -}C_3H_2] = \Delta H_{f,298}[cyc\text{ -}C_3H_3^+] - \Delta H_{f,298}[H^+] - PA[cyc\text{ -}C_3H_2]$$

Worthwhile comparisons can be made between the heats of formation of *cyc* -C_3H_2 and the linear CH_2CC species previously discussed, remembering that the value $\Delta H_{f,298}[CH_2CC] = 129 \pm 4$ kcal mol^{-1}, was derived from experiments utilising the corresponding anion. Despite the large errors stated, these values seem at least in reasonable agreement with theoretical data referred to earlier which suggest that CH_2CC is less stable than *cyc* -C_3H_2 by anywhere from 8-14 kcal mol^{-1}.[130-132] The surprising stability of this highly strained cyclopropene structure compared with the open chain isomers is due to its aromatic character (see the valence bond structure depicted in Scheme 3.9).[142] It is significant to note how investigation of charged C_3H_2 anaolgues has produced useful thermochemical insight into the corresponding neutral isomers.

B. Isomers of C₃H

1. *Anionic approaches*

An investigation into possible candidates for remote reactions of energetic anions led to the serendipitous discovery of the novel gas phase ion chemistry of propargyl-oxy systems. This has provided a means for structurally specific syntheses of a number of negative ion analogues of interstellar hydrocarbons. The collisional activation mass analysed ion kinetic energy (CA-MIKE) spectrum of terminally deprotonated methylprop-2-ynyl ether ($^-C\equiv CCH_2OCH_3$) shows losses of formaldehyde, methoxide radical and methanol, yielding the product ions, $C_3H_3^-$, $C_3H_2^{-\cdot}$ and C_3H^- respectively (Figure 3.2).[143] This was rationalised in terms of decomposition of the parent ion *via* an ion-neutral complex, unambigously giving the connectivities shown in Scheme 3.11. In the case of formaldehyde loss, the possibility of hydride donation to the opposite terminus of the carbon chain was considered (Scheme 3.11, a) but was discounted by independent synthesis of the two possible $C_3H_3^-$ isomers.[143]

Scheme 3.11

$$^-C{\equiv}CCH_2OCH_3 \quad \rightarrow \quad [(CCCH_2)^-OCH_3] \quad \rightarrow \quad ^-CCCH_3 \ + \ OCH_2 \qquad \text{(a)}$$

$$\rightarrow \quad ^{--}CCCH_2 \ + \ ^-OCH_3 \qquad \text{(b)}$$

$$\rightarrow \quad ^-CCCH \ + \ HOCH_3 \qquad \text{(c)}$$
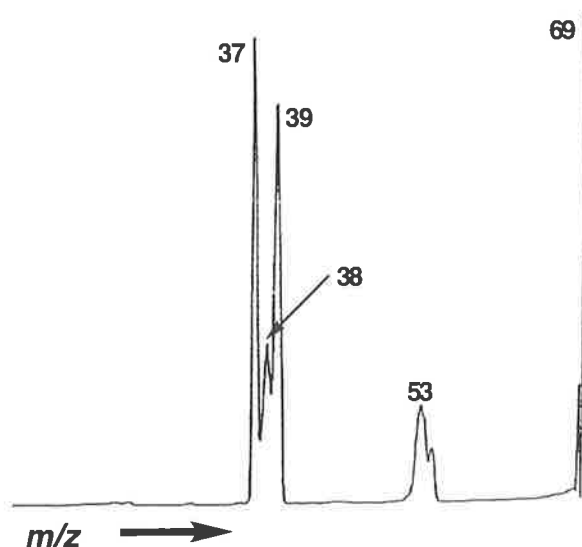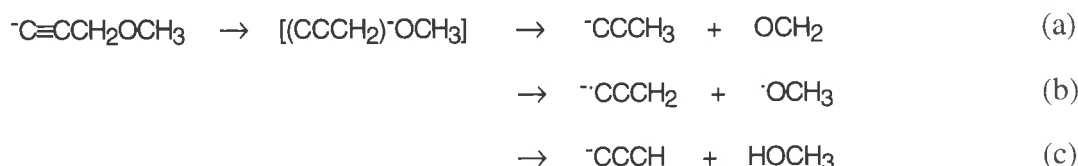
Figure 3.2 *The collisional activation MIKE spectrum of* $^-C{\equiv}CCH_2OCH_3$.[143] *Peaks at m/z 37, 38 and 39 correspond to the anionic species,* C_2CH^- $C_2CH_2^{-\cdot}$ *and* $C_2CH_3^-$ *respectively.*

This is only the second reported observation of the C_3H^- anion and the first whereby the structure could be unequivocally assigned to linear C_2CH^-. The first was the photoelectron spectroscopic study of Oakes and Ellison,[128] where the adiabatic electron affinity of some C_3H species was determined to be 1.858 ± 0.023 eV. The structure of this anion was unconfirmed until a recent high level *ab initio* study calculated the EA of the linear C_2CH to be 1.825 eV, corresponding well with the experimental value.[144] This may at first appear trivial for such a simple anionic system but as with the corresponding neutrals, the possibility of structural isomers must be considered. This is illustrated in another theoretical study.[145] The global minimum on the C_3H^- potential surface is in fact the cyclic singlet state, *cyc* $-C_3H^-$, stabilised by the aromatic character of the C_3-ring and > 5.0 kcal mol^{-1} more stable than both singlet and triplet electronic states of the experimentally observed C_2CH^- connectivity (*cf.* Scheme 3.12).

Scheme 3.12
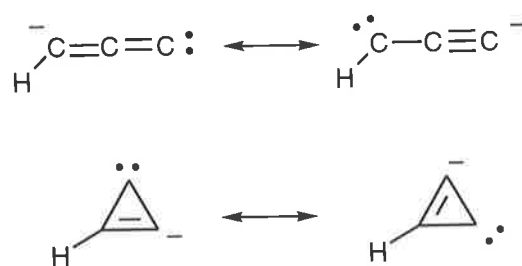
This further exemplifies the need for structurally specific synthesis in the gas phase, since *cyc* -C_3H^- is yet to be unequivocally generated. Interestingly, Ikuta has predicted neutral *cyc* -C_3H to be more stable than the linear structure by 1 kcal mol^{-1}, whereas in contrast the corresponding cyclic cation is less stable than its linear counterpart by some 17 kcal mol^{-1}.[146] All three charge states of the cyclic C_3H structure may be qualitatively considered as aromatic, with valence structures depicting 2π-electrons in each case (Scheme 3.13). The calculated π-electron population has been shown to decrease from the integer value of two in the order *cyc* -C_3H^-, *cyc* -C_3H, *cyc* -C_3H^+. This suggests decreasing aromatic character and may hence account for the decreasing stability of these species relative to their corresponding open chain isomers.[146]

Scheme 3.13
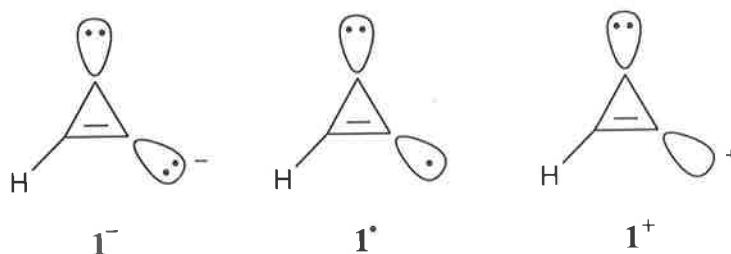
2. *Cationic approaches*

Experimentally, the C_3H cation is also known. It has been produced by electron impact ionisation on propylene ($CH_3CH=CH_2$), and the structure is presumed to be linear, in line with theoretical predictions. Flowing afterglow methodologies have probed a range of reactions of this cation.[147,148] Significantly, it has been shown that C_3H^+ proton transfers to methanol but not to acetonitrile, thus bracketing the proton affinity of C_3 as 184 ± 4 kcal

mol^{-1}. These data can then be combined with the known heats of formation of H$^+$ and C$_3$ by the thermochemical expression given in Equation 3.3 to yield the heat of formation, $\Delta H_{f,298}[C_3H^+] = 383 \pm 8$ kcal mol^{-1}.[149] This value was subsequently supported by Wong and Radom who calculated it to be 383 kcal mol^{-1} using G2 theory.[139] As yet there have been no reports of the generation or characterisation of any isomeric C$_3$H$^+$ species.

Equation 3.3

$$\Delta H_{f,298}[C_3H^+] = \Delta H_{f,298}[C_3] + \Delta H_{f,298}[H^+] + PA[C_3]$$

C. Longer chains, C$_n$H and C$_n$H$_2$

1. *C$_5$H*

The C$_4$H and C$_5$H cations have been generated by electron impact ionisation of diacetylene (HC≡CC≡CH) and 1,4-pentadiyne (HC≡CCH$_2$C≡CH) respectively. The connectivities have been presumed to be C$_3$CH and C$_4$CH. Reactions of these and similar ions with carbon monoxide have been investigated in a flowing afterglow study.[150] Interestingly, it has been found that ions of the form C$_n$H$^+$ undergo rapid reactions with carbon monoxide to generate HC$_{n+1}$O$^+$ (Scheme 3.14, a). It has been suggested that by either charge transfer or proton transfer to another molecule (X) such an ion may form neutral interstellar polycarbon monoxides of the types HC$_n$O and C$_n$O (Scheme 3.14, b and c).[151] Perhaps such reactions may be responsible for the galactic observation of these heterocumulenes (*cf.* Table 3.1).

Scheme 3.14

$$C_nH^+ \ + \ CO \ \rightarrow \ HC_{n+1}O^+ \qquad \qquad (a)$$

$$HC_{n+1}O^+ \ + \ X \ \rightarrow \ HC_{n+1}O \ + \ X^+ \qquad (b)$$

$$HC_{n+1}O^+ \ + \ X \ \rightarrow \ C_{n+1}O \ + \ HX^+ \qquad (c)$$

The C$_5$H anion has also been synthesised in the gas phase. The ionisation methodology utilised in this study allows unequivocal assignment of the ion structure. Chemistry directly analogous to that of the methylprop-2-ynyl ether system ($^-$C≡CCH$_2$OCH$_3$) was observed for

deprotonated methylpenta-2,4-dienyl ether ($^-$C≡CC≡CCH$_2$OCH$_3$) yielding linear, $^-$C$_4$CH by loss of methanol (Scheme 3.15).[152] Low level *ab initio* calculations performed in this study predict a bent triplet ground state for C$_4$CH$^-$ which is separated by only 12.7 kcal mol^{-1} from a singlet excited state. The geometries of these ions and a number of other stable C$_5$H$^-$ isomers are investigated by theory and experiment in Chapter 4.

Scheme 3.15

$^-$C≡CC≡CCH$_2$OCH$_3$ → [(CCCCCH$_2$)$^-$OCH$_3$] → $^-$CCCCCH + HOCH$_3$
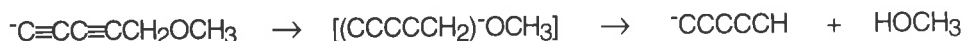
2. C$_2$H$_2$ and C$_4$H$_2$ isomers

We have shown how isomeric C$_3$H$_2$ cations and anions may be distinguished on the basis of differing rates of ion-molecule reactions in the gas phase (Schemes 3.6 and 3.7). Isomers have also been identified based on spectroscopic assignments (Scheme 3.10). It is however also possible to differentiate some isomeric cumulenes on the basis of their fragmentations in collision experiments. Two good examples of the structural sensitivity of this approach have been reported for C$_2$H$_2$ and C$_4$H$_2$ isomers. By analogy to the reaction of ethene with O$^{\cdot-}$ in the gas phase (Scheme 1.8, pp 8)[22] it was found that reaction of this reagent with butatriene (H$_2$C=C=C=CH$_2$) produced an abundance of the C$_3$CH$_2$ radical anion.[153] This ion was examined by neutralisation reionisation mass spectrometry, in this case designated $^-$NR$^+$. This spectrum was directly compared with the $^+$NR$^+$ spectrum of HC$_4$H$^{\cdot+}$, produced by electron impact ionisation of diacetylene (Figure 3.3). This comparison shows that only the C$_3$CH$_2$ structure gives peaks corresponding to C$_n$H$_2$$^{\cdot+}$ fragments. This is logical, as losses of carbon from a cation of HC$_4$H connectivity must include a concomitant loss of hydrogen, unless some rearrangement processes are occurring. This comparison serves to illustrate not only the structural differences between the incident ions but also, by extrapolation, the uniqueness of the neutrals. This is significant, as it suggests that the previously uncharacterised carbene C$_3$CH$_2$ is a stable species with a lifetime in the order of microseconds. Similar results were obtained for the neutral CCH$_2$ carbene when compared with acetylene.[154]
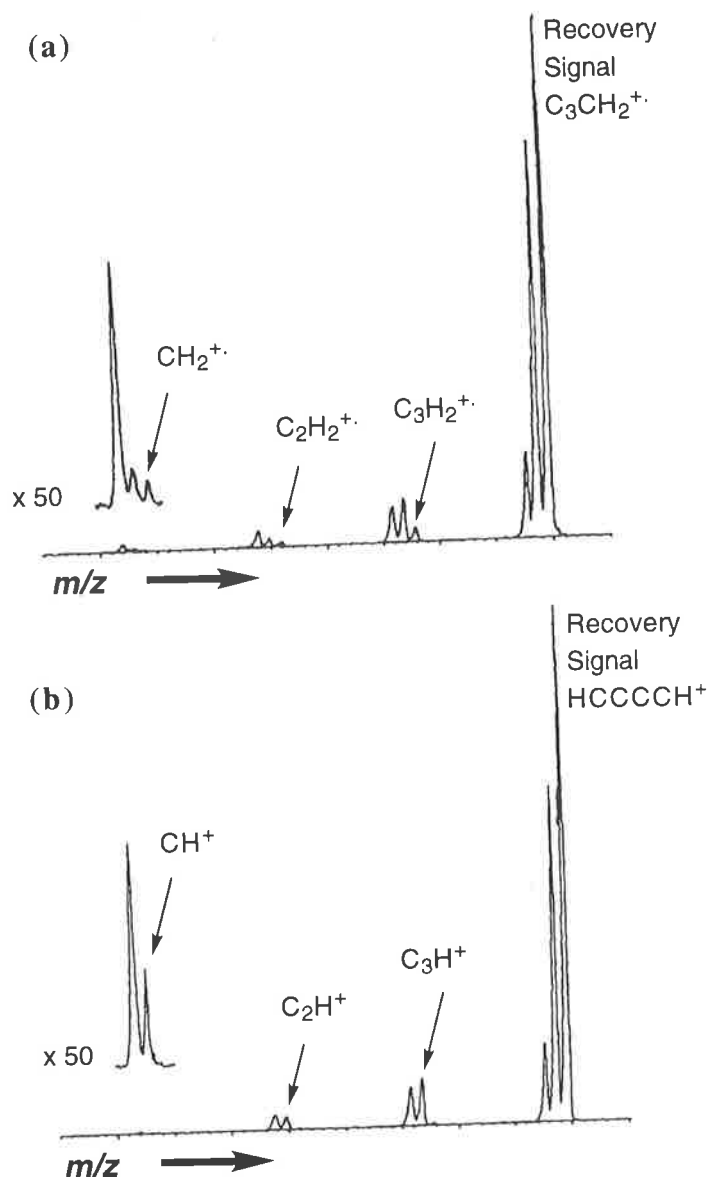
Figure 3.3 *Comparison of the NR spectra of (a) $C_3CH_2^{\cdot -}$ ($^-NR^+$) and (b) $HC_4H^{\cdot +}$ ($^+NR^+$). It is significant to note the low abundance of peaks corresponding to fragments of the type $C_nH_2^{\cdot +}$ in spectrum (a) compared to spectrum (b).*[153]

3. C_6H and higher homologues

An interesting study combined mass spectrometric and *ab initio* calculations to characterise triacetylene, C_6H_2, and the C_6H radical.[155] It was found that C_6H^- could be successfully generated under negative ion chemical ionisation conditions from both acetylene and fluorobenzene. Neither ionisation process can be readily rationalised but both produce the the same C_6H^- isomer which appears consistent with the C_5CH^- structure. This methodology allowed successful bracketing of the gas phase acidity of C_6H_2 in a FT-ICR instrument to $\Delta G_{acid} = 347 \pm 3$ kcal mol^{-1}, since proton transfer to C_6H^- was observed from

4-methylpyrazole but not N,N-hexamethyldisilazane. This determination was then used as the bench-mark from which to calculate (i) the C-H bond dissociation energy of C_6H_2 (126.8 $\pm$ 1.6 kcal mol^{-1}) and (ii) electron affinity of the C_6H radical (3.69 $\pm$ 0.05 eV). These results have been supported by subsequent spectroscopic investigation.[156]

A comprehensive survey of the even carbon, $C_{2n}H$, homologous series has recently been carried out.[156] Neumark and co-workers were able to generate $C_{2n}H$ anions, (n = 1-4) from a pulsed discharge in a molecular beam of acetylene and carbon dioxide. Once formed, the anions were mass selected, using a time-of-flight (TOF) mass spectrometer, photodetached and their photoelectron spectra collected. These spectra allowed determination of (i) electron affinities and (ii), some of the vibrational modes of the $C_{2n}H$ neutrals. The ground electronic states for each of the neutral homologues were also determined and are shown together with electron affinities in Table 3.2. The spectroscopic determination of the electron affinity of the C_6H radical is in reasonable agreement with the theoretical work previously described. A salient feature of these data is the very high electron affinities of all these polyacetylides. This seems significant in terms of the introductory discussion regarding the possible existence of interstellar anions. Each of these neutral species has been detected in interstellar and circumstellar environs and with such large electron binding energies it seems only reasonable to presume that the corresponding anions may be present also. This type of study is an example of the electronic and structural insight that can be gained for transient neutral species from spectroscopic interrogation of the corresponding negative ions. It stresses the importance of investigations into methodologies for generating structurally specific anions in the gas phase.

Table 3.2 Electron affinities of $C_{2n}H$ homologues for n = 1-4.[156]

Molecule	Ground electronic state	Electron Affinity (eV)
C_2H	$^2\Sigma^+$	2.956 $\pm$ 0.006
C_4H	$^2\Sigma^+$	3.558 $\pm$ 0.020
C_6H	$^2\Pi$	3.809 $\pm$ 0.015
C_8H	$^2\Pi$	3.966 $\pm$ 0.010

(IV) SUMMARY

Astrophysical studies have detected a number of cumulenic species of the forms C_nH and C_nH_2 in interstellar and circumstellar gas clouds. The expanding number of detected molecules reveals cumulenes of increasing carbon-chain length and also increasing complexity, with several examples of structural isomerism identified. These fascinating compounds have prompted extensive laboratory studies.

Previous mass spectrometric investigations have demonstrated the ability to generate charged analogues of the cumulenes C_nH and C_nH_2. Methods have been devised which produce reasonably long carbon chains as well as some structural isomers as positive and negatively charged ions. Examples have been provided, where the elucidation of the structure and energetics of neutral cumulenes has been achieved by investigation of the corresponding charged species. These include spectroscopic and ion-molecule reaction studies. Some neutral cumulene structures (for example, C_3CH_2) have been produced from their charged analogues by NRMS, where no other technique has demonstrated suitable structural selectivity. These studies highlight the need for further development of protocols for the gas phase preparation of charged analogues of cumulenes.

Previous mass spectral investigations combined with theoretical data have revealed something of the thermochemistry and relative energies of cumulenic anions, cations and neutrals. Some interesting trends have emerged from these data. For example, the surprising thermochemical stability of some cumulenic isomers which contain the highly strained, unsaturated C_3-ring system.

In this thesis methodologies for the generation and characterisation of a number of interstellar type cumulenes are described. Several isomeric C_5H, C_5H_2 and C_7H_2 anions have been produced and their structures identified by high energy collision experiments (Chapters 4, 5 and 6 respectively). NRMS has been employed to generate the corresponding neutral cumulenes all of which are found to be stable and most of which have not previously been

identified. The heterocumulene C_3N_2 has also been investigated by NRMS of its charged analogues. This neutral species provides an example of a system where unimolecular reactivity is observed on the mass spectrometric timescale.

Theoretical calculations are discussed which further elucidate the structure and energetics of these unusual species. Some surprising stability trends are observed for the cumulene families including indications of aromaticity in some cyclic structures. For some of these systems theoretical predictions of stability have prompted the experimental pursuit of a particular cumulene structure which may not have otherwise been considered. This synergy between experiment and theory is well illustrated by the results presented here.

Chapter 4: Generation of Two Isomers of C₅H From the Corresponding Anions.
A Theoretically Motivated Mass Spectrometric Study.

(I) ABSTRACT

Molecular orbital calculations have predicted the stability of a range of connectivities for the radical C_5H potential surface. The most energetically favourable of these include the linear C_4CH geometry and two ring-chain structures, HC_2C_3 and C_2C_3H. The corresponding anions are also shown to be theoretically stable and furthermore a fourth isomer, C_2CHC_2 is predicted to be the most stable anion connectivity. These results have motivated experimental efforts. Methodologies for the generation of the non-ring containing isomeric anions C_4CH and C_2CHC_2 have been developed utilising negative ion mass spectrometry. The absolute connectivities of the anions has been established using deuterium labelling and the collision based, charge reversal and neutralisation reionisation techniques. The success of the latter experiment confirms theoretical predictions of stability of the corresponding neutral species. This is the first reported observation of the neutral C_2CHC_2 species which calculations predict to be substantially less stable than the C_4CH connectivity but still bound relative to isomerisation processes.

(II) INTRODUCTION

The history of the homologous hydrocarbon series C_nH is an interesting one. The discovery of these species in interstellar and circumstellar clouds in many cases predates their characterisation in the laboratory. This has lead to them being broadly categorised, along with a number of other species, as "non-terrestrial" molecules.[101] The homologues with an even number of carbons, C_2H and C_4H were the first to be detected in both galactic features as well as in the laboratory.[157-160] It was later discovered that the odd carbon species, C_3H and C_5H were also present in circumstellar envelopes, detected virtually simultaneously in both astrophysical and terrestrial experiments.[161-164] It has been shown that C_nH species of odd n, are generally less abundant in the galactic environment, sometimes by an order of magnitude or more than their even n homologues.[104] It has been suggested that the even members of the series are relatively stable, formed from removal of a single hydrogen atom from an acetylenic chain. In contrast the odd members are likely to be much more reactive with up to three incomplete valencies.[163]

A range of theoretical and experimental studies has attempted to characterise and structurally elucidate this fascinating group of molecules. Microwave spectroscopy, Fourier transform microwave spectroscopy and photoelectron spectroscopy have so far been the most successful experimental techniques with linear chains as large as $C_{14}H$ now characterised.[123,128,156,#] Theoretical interest in C_nH radicals has also been high: a number of studies have been concerned with the structures and electronic natures of the linear $C_{n-1}CH$ connectivities.[107,144,165,166]

A   B
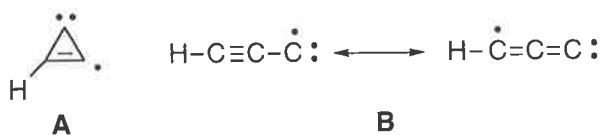
For a more comprehensive discussion of these techniques and the C_nH species which have been characterised thus far see Chapter 3.

Astrophysical detection of the cyclic C_3H structural isomer (**A**) has also been reported,[167] with the ratio of cyclic (**A**) to linear (**B**) varying from unity in some cold molecular clouds, to around 0.2 in circumstellar envelopes.[168] Theoretical studies have attempted to predict the structures and relative energies of the linear[144,165,166] and cyclic[167,169,170] isomers. Further, the anion[143-145] and cation[165,171] structures have also been investigated theoretically. Ikuta has established a stability trend across all three surfaces.[146] His studies using the CCSD(T) and multireference CI approaches have suggested that neutral cyclic C_3H (now denoted *cyc* -C_3H) is more stable than linear C_3H (now denoted *l* -C_3H) by only 1 kcal mol^{-1}. For the anion surface, *cyc* -C_3H is less energetic by 7 kcal mol^{-1} whilst for the corresponding cations, *l* -C_3H is lower in energy by some 17 kcal mol^{-1}. It should be noted that all three *cyc* -C_3H charge states can be described as aromatic, adhering to Hückel's ($4n$ + 2) π rule ($n = 0$). Calculations indicate that the π-electron populations on the C_3 ring decrease from the integer value of 2, in the order *cyc* -C_3H^-, *cyc* -C_3H and *cyc* -C_3H^+. This observation suggests a decrease in aromatic stabilisation and has been used to account for the relative energies of cyclic to linear structures across the three potential surfaces.

The neutrals C_3H and C_3H_2 are the only interstellar hydrocarbon species thus far to be detected with more than one structural connectivity. This is largely because of the strong astrophysical bias towards detection of linear species with large dipole moments.[*] The interplay between isomers in these environments is not yet fully resolved, however it has been demonstrated that both isomers may be formed in the binary collision between triplet carbon and acetylene.[168,172] Further, *ab initio* studies point to the possibility of isomerisation of the linear to the cyclic structure *via* electron attachment. Electron capture by linear C_3H should result in sufficient energy gain to overcome the isomerisation barrier on the anion surface: subsequent ejection of an electron gives neutral *cyc* -C_3H.[120]

By comparison with C_3H, isomeric studies of the higher C_nH homologues are relatively few. At this stage no experimental studies have shown the existence of a C_nH radical ($n > 3$)

---

[*] Detection bias in radioastronomy has been outlined in Chapter 1, pp 40.

which is not the linear connectivity. Previous theoretical studies have addressed the linear C_4CH neutral structure, but only recently have predictions emerged suggesting potentially stable non-linear geometries. The isomers, **1-7** have all been shown to be stable on the neutral potential surface.[173] The ring-chain species, HC_2C_3 (**2**) and C_2C_3H (**3**) are of particular significance since they are extensions of the *cyc* -C_3H geometry. By analogy with the *cyc* -C_3H radical, these species are surprisingly stable with respect to linear C_4CH (**1**): **2** and **3** are predicted to be less stable than **1** by only 4.9 and 22.0 kcal mol^{-1} respectively. A number of other intriguing geometries have been proposed as minima on this surface including the comparatively unstable C_2CHC_2 (**4**) geometry, predicted to be around 45 kcal mol^{-1} above C_4CH.
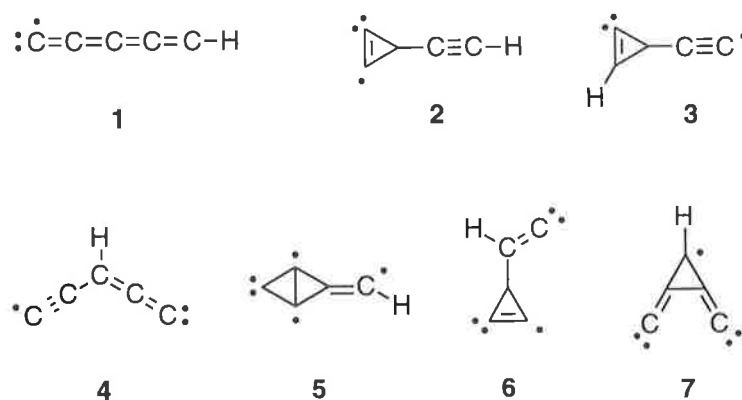
Charged analogues of C_5H have also received comparatively little attention. Bohme and co-workers have reported a number of ion-molecule reactions of the C_5H cation.[174] Formed from electron impact ionisation of 1,4-pentadiyne by a mechanism which is not clear, the C_5H^+ ion observed is assumed to adopt a linear structure (since low level calculations have suggested this cation to be stable with a linear geometry).[165] Of more interest however, is related work by the same group which shows that reaction between cationic carbon and neutral diacetylene leads to rapid formation of C_5H^+.[151] This is proposed as a possible synthon for both neutral C_5H and C_5 in the interstellar environment (Scheme 4.1).

Scheme 4.1

Experimental	$^+\!C$ + $HC{\equiv}C\text{-}C{\equiv}CH$ $\rightarrow$ $^+\!C{=}C{=}C{=}C{=}CH$ + H·
Proposed	$^+\!C{=}C{=}C{=}C{=}CH$ + X $\rightarrow$ ·$C{=}C{=}C{=}C{=}CH$ + X$^{+\cdot}$
Proposed	$^+\!C{=}C{=}C{=}C{=}CH$ + X $\rightarrow$ ·$C{=}C{=}C{=}C{=}C:$ + XH$^+$
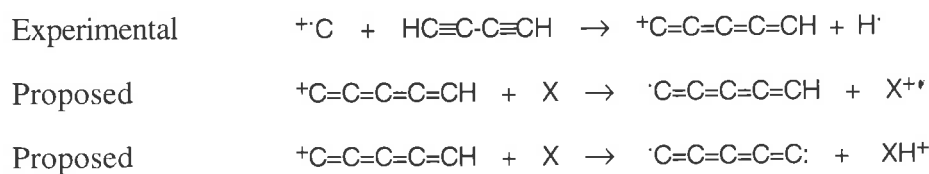
Theoretical calculations presented here suggest the stability of the anions C_4CH^-, $C_2CHC_2^-$, $HC_2C_3^-$ and $C_2C_3H^-$. A number of thermodynamically less favourable, yet still stable connectivities are also discussed. The energetics of the relevant neutral species are also outlined, with particular reference to the possibility of isomerisation. Methodology for the generation of C_4CH^- from a suitable precursor in the ion source of a mass spectrometer has been reported .[152],# In this Chapter we present the gas phase synthesis of $C_2CHC_2^-$ but suitable precursors for the remaining two stable anion minima could not be prepared.[175]

CR and NR mass spectrometry have been shown to be good methods for distinguishing isomeric ions (for example, isomers of C_2H_2 and C_4H_2).[153,154],* Further, NR experiments have shown the gas phase stability of the corresponding neutral species on the microsecond timescale. The results of NR experiments involving the C_4CH and C_2CHC_2 anions will be discussed here together with the experimental evidence that these provide for the stability of the corresponding neutrals.

This methodology is described in Chapter 3, pp 57.
* Differentiation of structural isomers by NR is well illustrated by the C_4H_2 example, see Figure 3.3 pp 40.

(III) RESULTS AND DISCUSSION

A. Theoretical Studies

1. *C₄CH*

Of the seven stable C_5H neutral geometries predicted by Crawford *et al.*, [173] the most stable anions are formed by electron attachment to structures **1-4**. The relative energies of the stable anionic species are given in Table 4.1 and their structures are depicted in Figures 4.1 and 4.3-4.5.

Table 4.1 Energies of various C_5H isomers on the anion potential surface. Calculated at the RCCSD(T)/aug-cc-pVDZ//B3LYP/aug-cc-pVDZ level of theory. ZPE uncorrected.

Isomer	Electronic State (point group)	Electronic Energy (Hartrees)	Zero-point Energy (Hartrees)	Relative Energy (kcal mol⁻¹)†
(**1⁻**) C_4CH^-	$^1A'$ (C$_S$)	-190.40983	0.02702	6.6
	triplet (C$_1$)	-190.41392	0.02612	3.5
(**2⁻**) $HC_2C_3^-$	$^1A_1$ (C$_{2v}$)	-190.41072	0.02779	6.5
	triplet	unstable‡		
(**3⁻**) $C_2C_3H^-$	$^1A'$ (C$_S$)	-190.42151	0.02950	0.8
	triplet (C$_1$)	-190.34509	0.02678	47.1
(**4⁻**) $C_2CHC_2^-$	$^1A_1$ (C$_{2v}$)	-190.42272	0.02940	0.0
	$^3B_1$ (C$_{2v}$)	-190.34205	0.02633	48.7
(**5⁻**) HCC_4^-	singlet	unstable		
	triplet	unstable		
(**6⁻**)*cyc* -C_3CHC^-	singlet	unstable		
	$^3A'$ (C$_S$)	-190.32661	0.02710	58.9
(**7⁻**) CC_3HC^-	singlet	unstable		
	triplet	unstable		
(**8⁻**) $C_2CC_2H^-$	$^1A'$ (C$_S$)	-190.36594	0.02723	34.3
	triplet	unstable		
(**9⁻**) *l* -C_3CHC^-	singlet	unstable		
	$^3A''$ (C$_S$)	-190.3394357	0.026059	50.2

† Relative energy given including ZPE, corrected by 0.9804.[91]
‡ These anions are unstable with respect to isomerisation processes.

Figure 4.1 *Optimised geometries for (a) triplet and (b) singlet electronic states of C_4CH^- (1⁻). These geometries were calculated at the B3LYP/aug-cc-pVDZ level of theory. All bond lengths are given in angstroms and all angles in degrees.*

66

The C_4CH anion shows two closely spaced electronic states: a singlet $^1A'$ state and a non-planar triplet state which is the more stable by 3.1 kcal mol^{-1}. The structure of the singlet state anion (Figure 4.1) is consistent with the valence bond picture of a cumulenic carbenoid, with a formal negative charge on the hydrogen bearing terminal carbon. For example, the C_3-C_4 and C_4-C_5 bond lengths are 1.28 Å and 1.32 Å respectively. The carbon-hydrogen bond length of 1.11 Å and bond angle of 115° are similar to those of a terminal sp^2 system. The slightly bent carbon chain (C_2-C_3-C_4 = 173° and C_3-C_4-C_5 = 170°) is in keeping with theoretical predictions made for the C_3H anion which suggest C-C-C bond angles of around 175°.[144,145] In contrast to the structure of the anion, the neutral ground state has the strictly linear structure of a polyacetylide: with alternating carbon-carbon bond lengths (C_3-C_4 = 1.33 Å and C_4-C_5 = 1.23 Å) and a contracted sp-like carbon hydrogen bond length of 1.07 Å.* The geometry of the stable triplet anion (Figure 4.1) falls somewhere between that of the singlet anion (carbenoid cumulene) and the neutral (polyacetylide) and can be represented, in valence bond terms, as a resonance hybrid of the two.
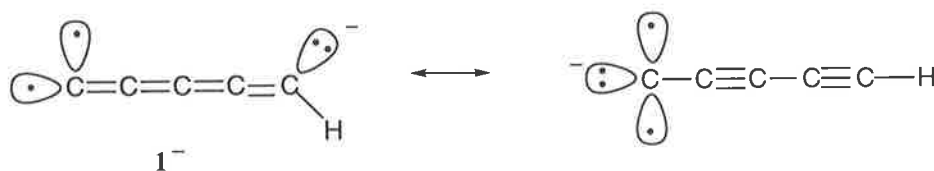
The geometric differences between both singlet and triplet anions and the radical neutral have significance for the neutralisation reionisation experiments carried out. The electronic transitions in such an experiment are considered as vertical[58,59] and in the case of C_4CH, Franck-Condon factors will lead to a vibrationally hot neutral being formed. However neutral C_4CH lies in a deep potential well on the radical C_5H surface (see Figure 4.2) and is thus unlikely to rearrange even when the small amount of surplus energy arising from the neutralisation process is considered. Rearrangement of C_4CH by cyclisation to either HC_2C_3 (**2**) or C_2C_3H (**3**), are high energy processes requiring some 29 and 50 kcal mol^{-1}

---

* The geometries of all neutrals calculated at the B3LYP/aug-cc-pVDZ level of theory are very similar to those reported by Crawford *et al.*[173] The structures calculated at this level appear as appendices to this Chapter (Table 4.6).

respectively (Figure 4.2).# These values were calculated at the B3LYP/aug-cc-pVDZ//B3LYP/6-31G level of theory and compare favourably with those obtained at higher level by Crawford *et al.*[173] Rearrangement by hydrogen transfer is also energetically demanding. Formation of C_2CHC_2 (**4**) from C_4CH (**1**) is endothermic by some 48 kcal mol^{-1} and requires a further 22 kcal mol^{-1} to overcome the barrier to this process. Calculations also predict C_4CH cations to be stable (Table 4.2). The theoretical results suggest that a $^-NR^+$ experiment should lead to successful gas phase generation of the C_4CH radical, which should not isomerise and should be observable by the detection of the analogous cation.
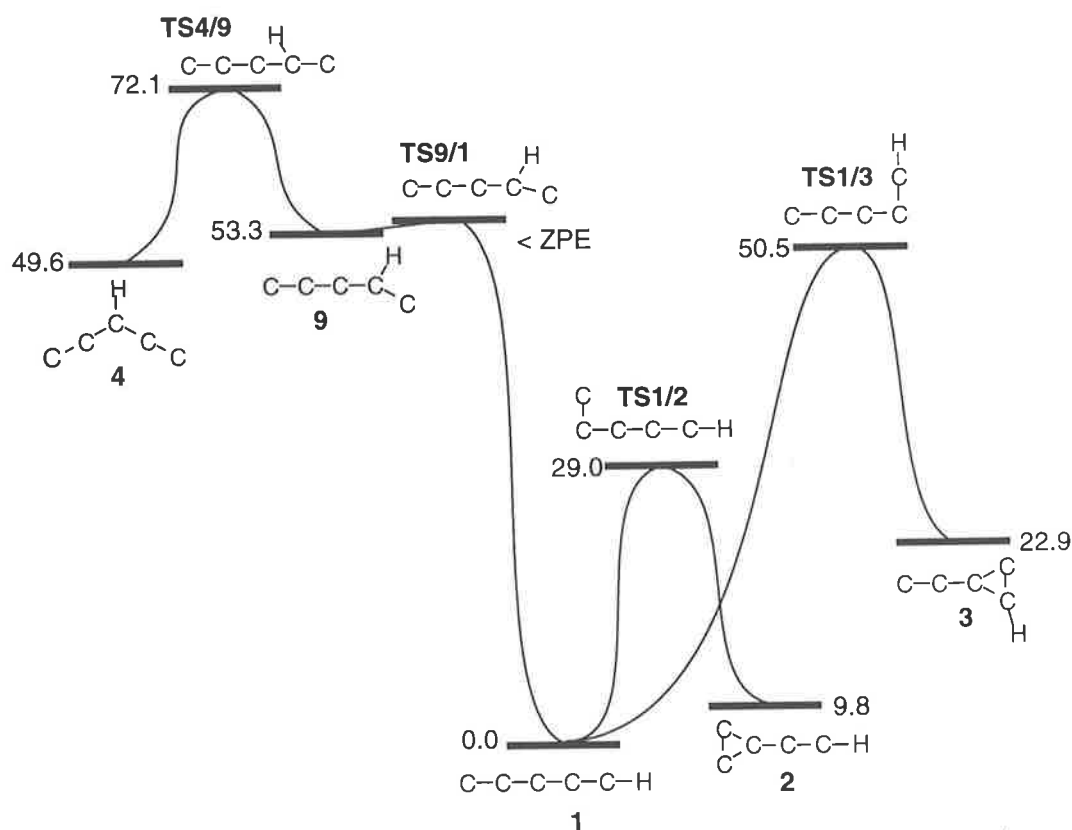
Figure 4.2 *The reaction coordinate diagram for rearrangement processes occurring on the neutral radical C_5H potential surface. The geometries of all stationary points were calculated at the B3LYP/6-31G level of theory: structures of the transition states and reactive intermediates appear as appendices to this Chapter (Table 4.7). The relative energies were calculated using the same theory with the larger, aug-cc-pVDZ basis set and are given in kcal mol^{-1}, with zero-point energy contributions included.*

The structures of all transition states and reactive intermediates were calculated at the B3LYP/6-31G level of theory and appear as appendices to this Chapter (Table 4.7). The activation barriers were calculated using the same level of theory with the larger aug-cc-pVDZ basis set.

Table 4.2 Relative energies of C_5H cations for which stable anions of the same connectivity have been calculated. Calculated at the RCCSD(T)/aug-cc-pVDZ//B3LYP/aug-cc-pVDZ[†] level of theory. ZPE uncorrected.

Isomer	Electronic State	Electronic Energy (Hartrees)	Zero-point Energy (Hartrees)	Relative Energy (kcal mol⁻¹)[‡]
(1⁺) C_4CH^+	$^1A'$	-190.02822	0.02907	0.0
(1⁺) C_4CH^+	$^3\Pi$	-189.96608	0.02691	37.6
(2⁺) $HC_2C_3^+$	singlet	unstable[¥]		
(2⁺) $HC_2C_3^+$	$^3B_2$	-189.97303	0.02947	34.8
(3⁺) $C_2C_3H^+$	singlet	unstable		
(3⁺) $C_2C_3H^+$	$^3A'$	-189.95031	0.03038	49.7
(4⁺) $C_2CHC_2^+$	$^1A_1$	-189.89883	0.02741	80.1
(4⁺) $C_2CHC_2^+$	$^3A'$	-189.88452	0.02536	87.8

[†] The geometries calculated at this level appear as appendices to this Chapter (Table 4.8).

[‡] Relative energy given including ZPE, corrected by 0.9804.[91]

[¥] These cations are unstable with respect to isomerisation processes.

2. HC_2C_3
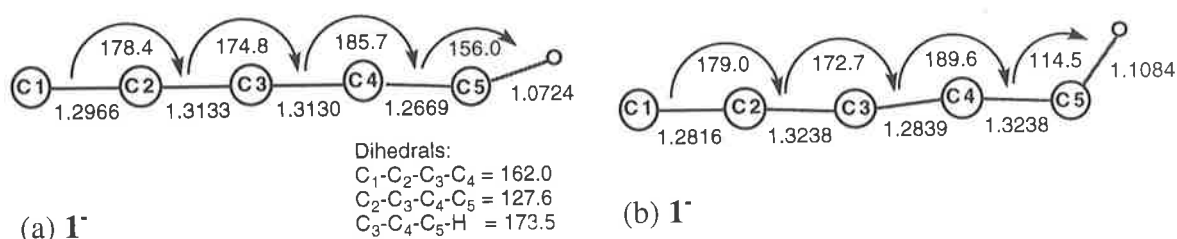

2⁻

Figure 4.3 *Optimised geometry for the $^1A_1$ ground state of $HC_2C_3^-$ (2⁻). The geometry was calculated at the B3LYP/aug-cc-pVDZ level of theory. All bond lengths are given in angstroms and all angles in degrees.*

The ground state HC_2C_3 anion was found to be a $^1A_1$ electronic state. No corresponding triplet structure could be found, with ring opening leading to formation of triplet C_4CH without barrier. The structure of the stable singlet state shown in Figure 4.3 is very similar to that of the corresponding neutral radical species.[*] It can be considered as a terminal alkyne bonded to one of the sp^2 carbons of cyclopropene, with the other ring carbons bearing a carbene and the negative charge.

---

[*] The geometries of all neutrals calculated at the B3LYP/aug-cc-pVDZ level of theory appear as appendices to this Chapter (Table 4.6).
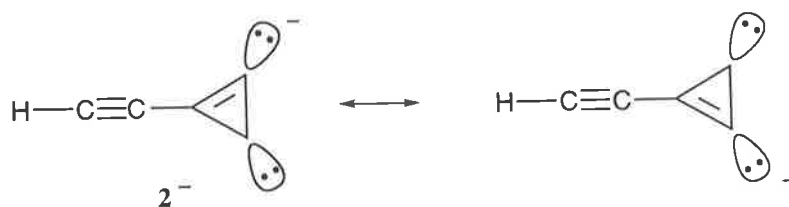
This structure is in keeping with the observed linearity of the H-C_1-C_2 moiety, and the contracted, acetylenic type, H-C_1 and C_1-C_2 bonds (1.07 Å and 1.23 Å respectively). Such a representation provides some insight into the stability of the anion (only some 3 kcal mol^{-1} above the triplet C_4CH ground state anion) as it possesses the $(4n + 2)$ π electrons $(n = 0)$ required for aromatic stabilisation. The same rationale has previously been applied to the *cyc* -C_3H anion.[145,146] In effect, $HC_2C_3^-$ may be considered as *cyc* -C_3H^- with the ring hydrogen replaced by an alkyne moiety. The stability of this anion suggests that it is a good candidate for formation in the gas phase if a suitable precursor can be found. The structural similarity between anion and neutral points to favourable overlap of the potential surfaces and hence a good probability of forming the neutral radical from the anion in either a collision based or spectroscopic neutralisation event.

Table 4.3 Energies of various C_5H isomers on the neutral potential surface. Calculated at the RCCSD(T)/aug-cc-pVDZ//B3LYP/aug-cc-pVDZ level of theory. The geometries are given as appendices to this Chapter (Table 4.6). ZPE uncorrected. Electron affinity estimated from indicated neutral and the corresponding ground state anion (Table 4.1).

Isomer	State	Electronic Energy (Hartrees)	Zero-point Energy (Hartrees)	Relative Energy‡ (kcalmol^{-1})	Previous Study† (kcalmol^{-1})	Electron Affinity (eV)
(1) C_4CH	$^2\Pi$	-190.32871	0.02622	0.0	0.0	2.44
(2) HC_2C_3	$^2B_2$	-190.32331	0.02814	4.6	4.9	2.39
(3) C_2C_3H	$^2A'$	-190.29798	0.02885	20.9	22.0	3.34
(4) C_2CHC_2	$^2B_2$	-190.25427	0.02773	47.6	49.7∂	4.54
(5) HCC_4	$^2A'$	-190.27670	0.02781	33.6	32.5	N/A§
(6)*cyc* -C_3CHC	$^2A'$	-190.25050	0.02693	49.5	49.1	N/A
(7) CC_3HC	N/A¥				67.0	

† CCSD(T)/DZP//CCSD(T)/DZP level of theory.[173]
‡ Relative energy given including ZPE, corrected by 0.9804.[91]
∂ Estimated from EOMIP-CCSD*/DZP//EOMIP-CCSD/DZP calculations.[173]
§ Electron affinities are not available at this level of theory because the corresponding minima on the anion surface are not stable for these geometries.
¥ A minimum corresponding to geometry **7** could not be located at this level of theory.
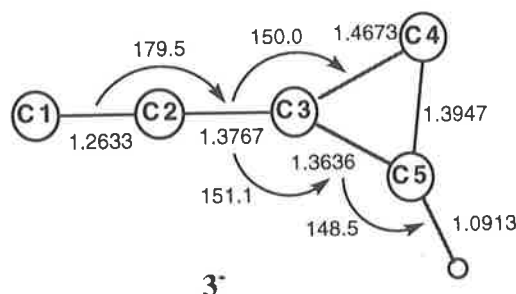
Figure 4.4 *Optimised geometry for the $^1A'$ ground state of $C_2C_3H^-$ (3⁻). The geometry was calculated at the B3LYP/aug-cc-pVDZ level of theory. All bond lengths are given in angstroms and all angles in degrees.*

3. C_2C_3H

The C_4CH structure is not the most stable arrangement on the anion potential surface. Whilst the C_4CH neutral radical is 21 kcal mol⁻¹ more stable than C_2C_3H, the trend is reversed for the anions (Tables 4.1 and 4.3). The ground state of $C_2C_3H^-$ is more stable than the triplet C_4CH anion by approximately 2 kcal mol⁻¹. The ground state C_2C_3H anion (Figure 4.4 and Table 4.1) is a singlet $^1A'$, with an excited non-planar triplet state calculated to be 46 kcal mol⁻¹ less stable (Tables 4.1). Once again it is reasonable to consider the structure of the C_2C_3H ground state anion based on the valence picture of the *cyc* -C_3H anion. If, in this instance, the negative charge of *cyc* -C_3H^- is replaced with an acetylide moiety, the resulting structure agrees with calculated parameters. These structural characteristics are best highlighted by the shortened acetylenic C_1-C_2 bond length (1.26 Å) and the two long sides (C_3-C_4 = 1.47 Å and C_4-C_5 = 1.39 Å) and the one short side (C_3-C_5 = 1.36 Å) of the 3-membered carbon ring.
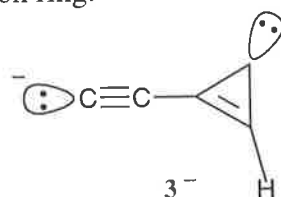
The ground state C_2C_3H anion may be thought of as possessing a carbon-carbon double bond bonded directly to the acetylide anion. This represents a contrast to the situation for the neutral. The neutral radical has less alternation in the bond lengths C_1-C_2 and C_2-C_3 (1.29

71

Å and 1.33 Å respectively).* The alkene like bond C_4-C_5 in the 3-membered ring is 1.35 Å, compared with C_3-C_4 and C_3-C_5 (1.46 Å and 1.42 Å respectively). This structure is more in keeping with an allenic carbene fused to a dehydro-cyclopropene.

3
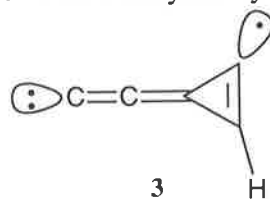
Some insight can be gained as to the relative stability of the anionic and radical species on their respective surfaces by contrasting these two valence structures. Whilst the anion may be considered aromatic with 2π electrons, the corresponding neutral has less aromatic stabilisation with a π-electron population of > 2, because of the greater π-overlap of carbons C_1, C_2 and C_3.
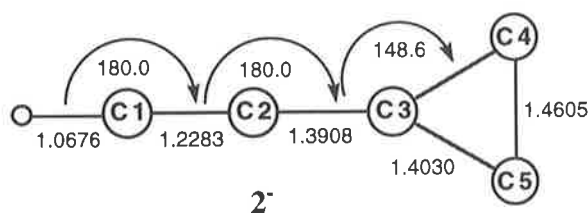
4. C_2CHC_2
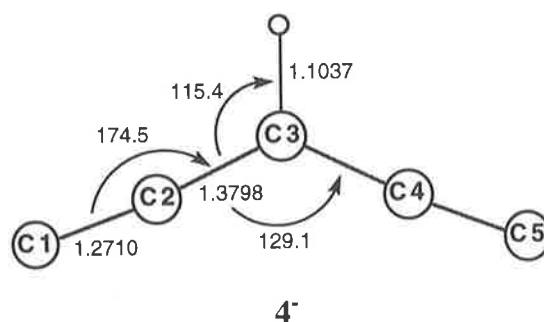
4⁻

Figure 4.5 *Optimised geometry for the $^1A_1$ ground state of $C_2CHC_2^-$ (4⁻). The geometry was calculated at the B3LYP/aug-cc-pVDZ level of theory. All bond lengths are given in angstroms and all angles in degrees.*

At the level of theory used in this investigation, C_2CHC_2 (**4**) proves to be the most stable anion (Table 4.1). However the ground state anions derived from **1-4** have energies within a 10 kcal mol⁻¹ range. The stability of $C_2CHC_2^-$ is surprising, since the corresponding neutral radical is almost 50 kcal mol⁻¹ less stable than C_4CH, the global minimum on the neutral surface (Table 4.3). Both singlet and triplet states have been calculated for $C_2CHC_2^-$

---

* The geometries of all neutrals calculated at the B3LYP/aug-cc-pVDZ level of theory appear as appendices to this Chapter (Table 4.6).

with the $^1A_1$ ground state being some 49 kcal mol^{-1} more stable that the $^3B_1$ state. The structures of these anions are given in Figure 4.5 and Table 4.4 (pp 75) respectively.

The ground state anion structure is best represented as an allene carbenoid substituted with hydrogen and an acetylide ion.
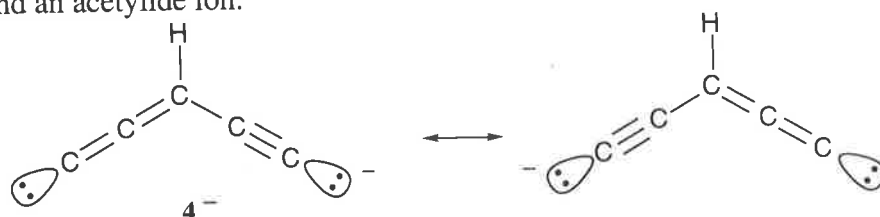
This structure is consistent with (i) the contracted C_1-C_2 and C_4-C_5 bond lengths of 1.27 Å, (ii) the C_2-C_3 and C_3-C_4 bond lengths of 1.38 Å (representative of carbon-carbon bonds between single and double bond character) and (iii) the C_2-C_3-H bond angle of 115° (close to the 120° expected for an sp^2 hybridised carbon). This anion structure differs somewhat from that calculated for the corresponding neutral. While the relative bond lengths remain almost the same, the C_2-C_3-C_4 bond angle is reduced from 129.1° in the anion to 112° in the neutral.# As with C$_4$CH, this geometric difference between the minimum energy geometries on the anion and neutral surfaces becomes significant when discussing neutralisation reionisation experiments. In this case a vertical neutralisation process will yield a vibrationally hot C$_2$CHC$_2$, particularly with respect to the C_2-C_3-C_4 bending mode. Calculation of the energy of the anion geometry on the neutral surface gives an indication of the excess energy which may be attained. At the B3LYP/aug-cc-pVDZ//B3LYP/6-31G level of theory the anion geometry on the neutral surface was found to be 4.5 kcal mol^{-1} above the radical minimum.* Transition state calculations for the neutral surface suggest that C$_2$CHC$_2$ is stable with respect to isomerisation processes even when generated with 4.5 kcal mol^{-1} of excess internal energy. Only one isomerisation pathway has been found leading from the C$_2$CHC$_2$ minimum (Figure 4.2, pp 68). This involves a 1,2-hydrogen shift *via* **TS4/9** which produces non-cyclic *l* -C$_3$CHC (**9**). Structure **9** is essentially unstable, with the

---

Crawford *et al.* obtained a geometry for neutral C$_2$CHC$_2$ with significant out of plane distortion. However these authors predict in plane twisting to be a very low energy process (< 0.1 kcal mol^{-1}) and hence the real equilibrium geometry may in fact be symmetrical.[173]
* This value does not include zero-point energy contributions.

barrier to a further 1,2-hydrogen shift below the zero-point energy of the minimum. Thus further rearrangement *via* **TS9/1** yields C_4CH. **TS4/9** lies some 22 kcal mol^{-1} above C_2CHC_2: this is therefore the barrier for isomerisation through to C_4CH. Isomerisation pathways leading from **4**, *via* cyclisation processes were not found. The energies of cationic C_2CHC_2 species have also been calculated (see Table 4.2, pp 69). Stable singlet and triplet electronic states were calculated and it is therefore expected that these cations would be observed in vertical electron transfers from either anion or neutral charged states. We conclude from these data that (i) $C_2CHC_2^-$ is stable and a good candidate for synthesis in the gas phase and (ii) we would predict this anion should be a suitable precursor for laboratory generation of the C_2CHC_2 radical by vertical neutralisation.

5. Other stable C$_5$H anions

Several other stable anion connectivities have been established by this computational approach. These species are dramatically less stable than the ground state anions discussed so far (for energies and structures see Table 4.1, pp 66 and Table 4.4, pp 75 respectively). The neutral *cyc* -C_3CHC is stable, although nearly 50 kcal mol^{-1} more energetic than C_4CH. Electron attachment to this radical produces a $^3A'$ species almost 60 kcal mol^{-1} above the anionic global minimum: the corresponding singlet is unstable and rearranges by ring closure to form a 3,3-bicyclic species which is referred to here as $C_2CC_2H^-$ (**8**). $C_2CC_2H^-$ is only 34 kcal mol^{-1} above $C_2CHC_2^-$. The remaining stable anion connectivity is *l* -C_3CHC (**9**). This has a $^3A''$ ground state and is 50 kcal mol^{-1} above the global minima. This structure is essentially a ring opened form of *cyc* -C_3CHC and is only stable on the anion surface. The corresponding neutral undergoes a barrierless 1,2-hydrogen transfer to give C_4CH in the manner previously discussed (Figure 4.2, pp 69).

Table 4.4 Geometries of excited electronic states and less stable C_5H anion minima (ground states for **1-4** are given in Figures 4.1 and 4.3-4.5). Calculated at the B3LYP/aug-cc-pVDZ level of theory. All bond lengths are given in angstroms and all angles in degrees.

3⁻ (C₁) triplet

|		
bond length	C_1-C_2	1.2760
	C_2-C_3	1.3488
	C_3-C_4	1.3554
	C_3-C_5	1.6260
	C_4-C_5	1.4025
	C_5-H	1.1019
angle	C_1-C_2-C_3	177.5
	C_2-C_3-C_4	166.7
	C_3-C_4-C_5	138.0
	C_3-C_5-H	122.8
dihedral angle	C_1-C_2-C_3-C_4	147.3
	C_2-C_3-C_4-C_5	-26.7
	C_3-C_4-C_5-H	57.2

6⁻ (C_S) ³A'

bond length	C_1-C_2	1.3751
	C_2-H	1.1109
	C_2-C_3	1.4146
	C_3-C_4	1.3927
	C_3-C_5	1.4579
	C_4-C_5	1.3576
angle	C_1-C_2-C_3	125.5
	H-C_2-C_3	113.5
	C_2-C_3-C_4	156.5
	C_2-C_3-C_5	146.7

9⁻ (C_S) ³A''

bond length	C_1-C_2	1.3047
	C_2-C_3	1.3003
	C_3-C_4	1.3886
	C_4-C_5	1.3599
	H-C_4	1.1030
angle	C_1-C_2-C_3	174.6
	C_2-C_3-C_4	171.4
	C_3-C_4-C_5	106.9
	H-C_4-C_3	124.7
dihedral angle	C_1-C_2-C_3-C_4	180.0
	C_2-C_3-C_4-C_5	0.0
	H-C_4-C_3-C_2	180.0

4⁻ (C₂ᵥ) ³B₁

bond length	C_1-C_2	1.2855
	C_2-C_3	1.3809
	C_3-C_4	1.3809
	C_4-C_5	1.2855
	C_5-H	1.1121
angle	C_1-C_2-C_3	180.1
	C_2-C_3-C_4	140.4
	C_3-C_4-C_5	180.1
	H-C_3-C_2	109.8

8⁻ (C_S) ¹A'

bond length	C_1-C_2	1.3234
	C_1-C_3	1.5193
	C_2-C_3	1.5952
	C_3-C_4	1.5437
	C_3-C_5	1.3948
	C_4-C_5	1.3543
	C_5-H	1.0909
angle	C_1-C_2-C_3	61.9
	C_2-C_3-C_4	178.6
	C_3-C_4-C_5	57.1
	H-C_5-C_4	151.3
dihedral angle	C_1-C_2-C_3-C_4	180.0
	C_2-C_3-C_4-C_5	0.0
	H-C_5-C_4-C_3	180.0

6. *Summary of theoretical results*

To summarise the theoretical results: (i) the radicals C_4CH (**1**), HC_2C_3 (**2**), C_2C_3H (**3**) are the most stable of the neutral C_5H isomers. Electron attachment to each of these species is a highly exothermic process with electron affinities estimated at 2.44, 2.39 and 3.34 eV respectively. Consequently, the corresponding anions would seem logical precursors for the neutral radicals in the gas phase, *via* an electron detachment process. (ii) The most stable C_5H anion structure is found to be C_2CHC_2 which represents the global minimum on the anion potential surface. The C_2CHC_2 anion would therefore be a logical starting point in attempts to generate the neutral C_2CHC_2 radical (and hence the first non-linear C_5H species) in the laboratory.

B. Syntheses of Two Isomeric C_5H Anions and their Neutrals. Experimental Confirmation of Structure.

1. *Gas phase syntheses of two isomeric C_5H anions*

Previous studies have established the negative ion decomposition behaviour of $^-C{\equiv}CCH_2\text{-}OCH_3$.[143] Collisional activation of this ion induced loss of methanol, forming l-C_3H^- as one of the major product ions. This process is rationalised as shown in Scheme 4.2.

Scheme 4.2

$$^-C{\equiv}CCH_2\text{-}OCH_3 \;\rightarrow\; [(:C{=}C{=}CH_2)\,^-OCH_3] \;\rightarrow\; :C{=}C{=}CH^- \;+\; HOCH_3$$
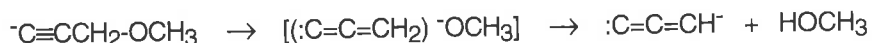
Simple extension of this procedure to the corresponding diacetylide precursor resulted in the formation of C_4CH^-.[152] The precursor ion $^-C{\equiv}CC{\equiv}CCH_2\text{-}OCH_3$ can be formed by deuterium abstraction from $DC{\equiv}CC{\equiv}CCH_2\text{-}OCH_3$ or by desilylation of $TMSC{\equiv}CC{\equiv}CCH_2\text{-}OCH_3$ by hydroxide ions under the same chemical ionisation conditions. The latter method is analogous to the general method originally developed by DePuy and coworkers.[10,#] Collisional activation of $^-C{\equiv}CC{\equiv}CCH_2OCH_3$ leads to losses of methanol, the methoxide radical and formaldehyde producing the anions of C_5H, C_5H_2 and C_5H_3 respectively (Table

---

See also Chapter 1, pp 6.

4.5). The $C_5H_3^-$ species should have the structure $C_4CH_3^-$ given that hydride donation from the methoxide ion occurs at the same terminus from which it was eliminated.[143] The ion C_5H_2 has been shown by deuterium labelling to be C_4CH_2,[*] whilst the loss of methanol from $^-C\equiv CC\equiv CCH_2$-OCH_3 can only generate the C_4CH anion. These processes can also occur in the ion source of the mass spectrometer. The C_4CH anion can therefore be mass selected and subjected to $^-CR^+$ and $^-NR^+$ experiments.

Table 4.5 The CA-MIKE spectra for C_4CH and C_2CHC_2 anion precursors.

Precursor ion (*m/z*)	Product ions [*m/z* (loss or formation) relative abundance[†]]
[TMSC≡CC≡CCH₂OCH₃ -TMS⁺]⁻ (*m/z* 93)	78 (CH₃˙) 43, 77 (CH₄) 54, 63 (CH₂O) 47, 62 (CH₃O˙) 42, 61 (CH₃OH) 100.
[HC≡CCH(OCOCH₃)C≡CH - H⁺]⁻ (*m/z* 121)	120 (H˙) 46, 95 (C₂H₂) 100, 93 (CO) 45, 79 (H₂C₂O) 44, 77 (CO₂) 39, 61 (C₅H⁻) 43, 59 (CH₃CO₂⁻) 37.
[HC≡CCD(OCOCH₃)C≡CH - H⁺]⁻ (*m/z* 122)	121 (H˙) 66, 96 (C₂H₂) 95, 95 (C₂HD) 100, 80 (H₂C₂O) 49, 78 (CO₂) 36, 62 (C₅D⁻) 29, 59 (CH₃CO₂⁻) 14.
[DC≡CCH(OCOCH₃)C≡CD - D⁺]⁻ (*m/z* 122)	121 (H˙) 66, 95 (C₂HD) 100, 80 (H₂C₂O) 41, 78 (CO₂) 24, 61 (C₅H⁻) 41, 59 (CH₃CO₂⁻) 30.
[HC≡CCH(OCOH)C≡CH - H⁺]⁻ (*m/z* 107)	106 (H˙) 53, 81 (C₂H₂) 16, 79 (CO) 40, 77 (H₂CO) 5, 63 (C₅H₃⁻) 100, 61 (C₅H⁻) 16, 51 (C₄H₃⁻) 5, 49 (C₄H⁻) 5, 45 (HCO₂⁻) 9.
[HC≡CCH(OCOCH₂CH₃)C≡CH - H⁺]⁻ (*m/z* 135)	134 (H˙) 60, 120 (CH₃˙) 21, 109 (C₂H₂) 100, 107 (CO) 67, 91 (CO₂) 26, 73 (CH₃CH₂CO₂⁻) 27, 61 (C₅H⁻) 11.

† The abundances presented here are relative to the base peak of the CA-MIKE spectrum.

Theoretical predictions of the stability of the symmetrical C_2CHC_2 anion led us to investigate ways to generate this ion in the gas phase. Initially it was proposed that an analogous chemistry could be used for this system as for C_4CH described, that is, loss of methanol from a 3-substituted pentadiyne precursor. Methanol is lost from the precursor ion

---

* This experiment is presented and discussed in Chapter 5.

$^-C\equiv CCH(OCH_3)C\equiv CD$ under collisional activation however deuterium labelling at the acetylenic positions shows exclusive loss of CH_3OH to form C_4CD^- (Scheme 4.3).

Scheme 4.3

$$^-C\equiv CCH(OCH_3)C\equiv CD \rightarrow [(:C=C=CHC\equiv CD)^- OCH_3] \rightarrow C_4CD^- + HOCH_3$$
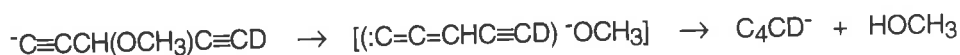
The methoxide ion shows preference for removing the proton from the 3-position, rather than migration of CH_3O^- to the end of the carbon chain and removal of the more acidic acetylenic deuterium. A new approach was therefore required in order to synthesise $C_2CHC_2^-$ in the gas phase. The acetylide anion, $^-C\equiv CCH(OCOCH_3)C\equiv CH$ was formed by deprotonation of 3-penta-1,4-diynyl acetate under typical negative ion chemical ionisation conditions. The collisional activation spectrum of this ion showed formation of "C_5H^-" at m/z 61 (Table 4.5). Deuterium labelling assisted with structure determination of the product ion. The precursor ion $[HC\equiv CCD(OCOCH_3)C\equiv CH - H^+]^-$, yields only m/z 62 whilst $[DC\equiv CCH(OCOCH_3)C\equiv CD - D^+]^-$ gives exclusively m/z 61 (Table 4.5). The products of these two reactions are thus $C_2CDC_2^-$ and $C_2CHC_2^-$ respectively. The mechanism of this reaction has been probed by examination of the labelling data and by investigation of the behaviour of some related esters. The CA-MIKE spectrum of $[DC\equiv CCH(OCOCH_3)C\equiv CD - D^+]^-$ shows formation of $C_2CHC_2^-$, suggesting that the precursor ion is an acetylide rather than an enolate anion. This points to either elimination of acetic acid or loss of carbon dioxide and methane as two possible reaction pathways (Scheme 4.4).

Scheme 4.4

$$^-C\equiv CCH(OCOCH_3)C\equiv CH \rightarrow C_2CHC_2^- + CH_3CO_2H$$

$$^-C\equiv CCH(OCOCH_3)C\equiv CH \rightarrow C_2CHC_2^- + CO_2 + CH_4$$
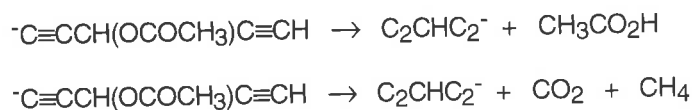
The corresponding formate and propionate esters have also been synthesised. The $[M-H]^-$ ions of both of these precursors show m/z 61 in their respective CA mass spectra.# Source

---

The propionate ester is used as the C_2CHC_2 anion precursor for the CR and NR spectra shown here as it gives a particularly intense source signal.

formed C_5H anions from all these ester precursors gave identical $^-CR^+$ spectra confirming the proposal of the same atom connectivity in each case.

2. *Characterisation of isomeric C_5H anions by charge reversal*

Further support for the structures of the two C_5H anions can be gained by examining their spectra. The conventional CA mass spectra of the respective ions yield virtually no structural information since both species show only loss of a hydrogen radical with formation of $C_5^{\cdot-}$. In comparison, the $^-CR^+$ spectra show extensive fragmentation, with the decomposition of the carbon chain giving fragments C_nH^+ and $C_n^{\cdot+}$ (n = 2-5). The charge reversal spectra of both isomers show the formation of common fragments but the abundances of some peaks are dramatically different (Figure 4.6, pp 80).

Consideration of the charge reversed parent ion C_5H^+ in each spectrum serves to illustrate the difference between the species. The ion corresponding to C_4CH^+ is the base peak in the $^-CR^+$ spectrum of C_4CH^- suggesting this cation is a very stable species with respect to decomposition processes. The major fragmentation observed is loss of a hydrogen radical (79% of the base peak) while further decompositions are minor processes with the largest of these being the formation of $C_4^{\cdot+}$ at *m/z* 48 (9%). This is in contrast to the situation for the isomeric C_2CHC_2 anion. The $^-CR^+$ spectrum of this species shows not the charge reversed parent ion but a fragment ion, namely $C_5^{\cdot+}$, as the base peak of the spectrum. Further fragmentations to lower mass product ions are also much more pronounced, with $C_4^{\cdot+}$ (37%) of comparable intensity with the parent cation (49%). This result suggests a much lower stability of the cation produced in the latter charge reversal experiment over that generated in the former. This is in line with the trend predicted for connectivities C_4CH and C_2CHC_2 by the molecular orbital calculations previously described. That is, while the anions of these geometries are of comparable energy their corresponding cations (formed here by vertical two electron transfer in the charge reversal process)[41,44] differ significantly in stability. Ground state C_4CH^+ is some 80 kcal mol^{-1} lower in energy than singlet $C_2CHC_2^+$ (Table 4.2, pp 69) and as such is significantly more stable with respect to

decomposition processes. These charge reversal spectra clearly distinguish the structures of the two C_5H^- anions by the differing abundances of each fragmentation from their corresponding cations. This established, it would seem that these anions are suitable precursors for the formation of the corresponding neutrals by neutralisation reionisation mass spectrometry.
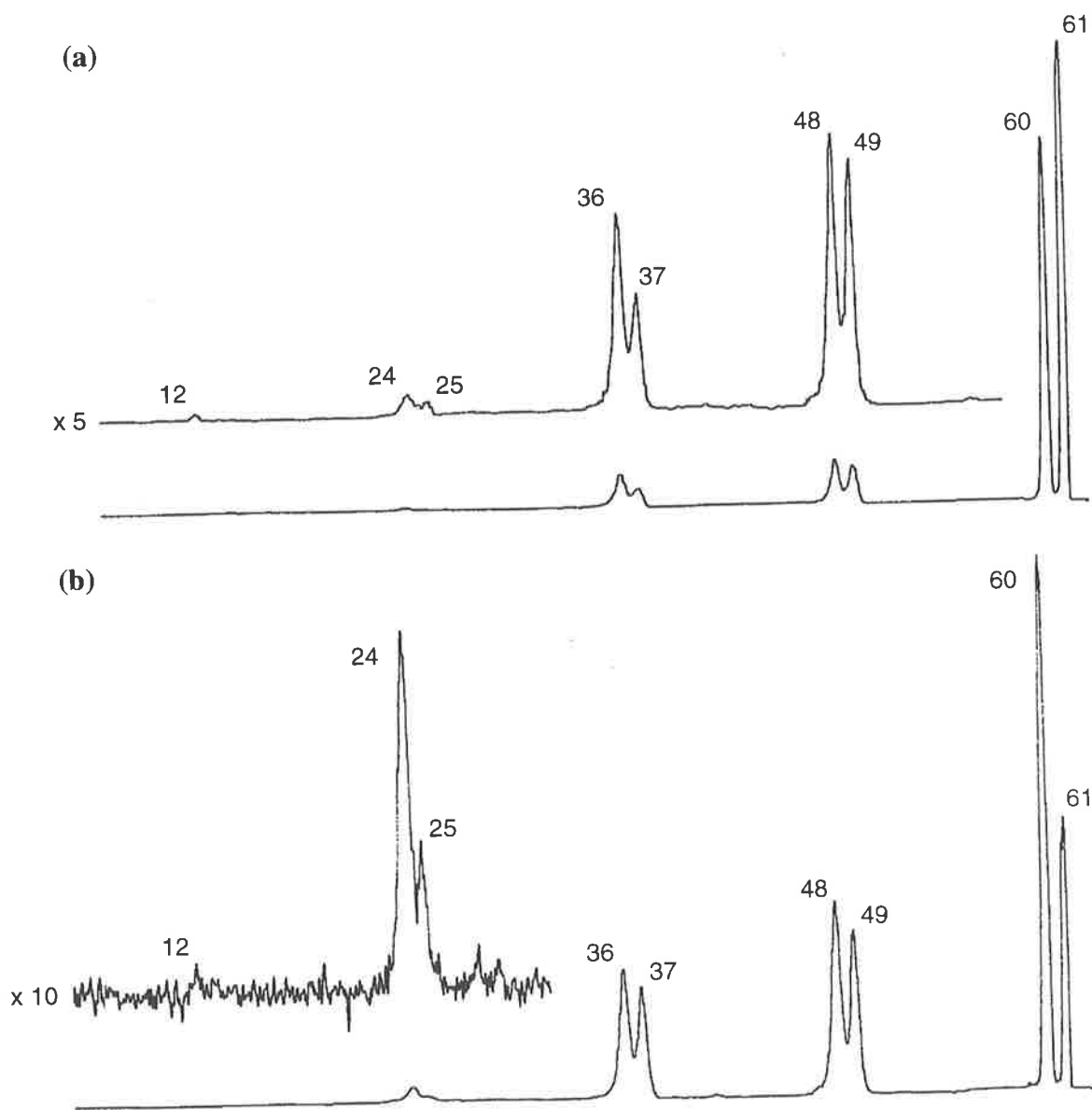
Figure 4.6 $^-CR^+$ *(O_2, 80% T; O_2, 80% T) spectra of m/z 61 from (a) TMSC$\equiv$CC$\equiv$CCH$_2$OCH$_3$, giving C$_4$CH$^-$ and (b) HC$\equiv$CCH(OCOCH$_2$CH$_3$)C$\equiv$CH giving C$_2$CHC$_2^-$. These spectra both show fragments of the forms C_nH^+ and $C_n^{\cdot+}$.*

3. *Gas phase syntheses of neutral C₄CH and C₂CHC₂*

3. *Gas phase syntheses of neutral C_4CH and C_2CHC_2*

The $^-NR^+$ spectra of both C_4CH^- and $C_2CHC_2^-$ are shown in Figure 4.7. As with the charge reversal spectra, the peaks observed in these spectra are of masses corresponding to the ions C_nH^+ and $C_n^{\cdot+}$ (n = 2-5). Significantly, survivor ions (ions of *m/z* 61, corresponding to C_5H^+ species) are detected in the $^-NR^+$ spectra of C_4CH^- and $C_2CHC_2^-$. This can only occur if some stable neutral "C_5H" is accessed in the neutralisation reionisation process. From the molecular orbital calculations previously outlined it has been shown that both C_4CH and C_2CHC_2 have stable anions, neutrals and cations and as such it is expected that the neutral produced in each NR experiment is of the same connectivity as the incident anion. Experimentally, should isomerisation of the neutral occur it would be expected that there should be major discrepancies between the corresponding $^-CR^+$ and $^-NR^+$ spectra. The cations resulting from both processes should have different geometries and energies and should display different fragmentations, *cf.* [25,66,68]. Comparison of the charge reversal and neutralisation reionisation spectra of C_2CHC_2 [Figures 4.6(b) and 4.7(b)] reveal a consistency between the fragmentations observed. Most noticeably, the parent cation (*m/z* 61) remains at about the same intensity with respect to the C_5^+ fragment (56%). The similarities between these spectra point to (i) structural continuity between the incident C_2CHC_2 anion and the neutral and cation formed in this experiment and (ii) favourable Franck-Condon overlap of the three surfaces.[58] It can be concluded that the neutral C_2CHC_2 radical has been generated in this experiment.

A similar inspection of the C_4CH^- spectra [Figures 4.6(a) and 4.7(a)] reveals some subtle variation, most notably in the region of the parent cation. Whilst *m/z* 61 is the base peak in the $^-CR^+$ spectrum it is slightly less intense than the C_5^+ signal (92%) in the $^-NR^+$ spectrum. This is most likely due to some fragmentation of the neutral. In their theoretical work, Crawford *et al.* discovered that along with the stable $^2\Pi$ ground state of neutral C_4CH there exists a dissociative $^2\Sigma^+$ surface which leads to production of C_2H and C_3.[173] This surface could be accessible by vertical excitation of the C_4CH anion by collision, producing neutral fragments concomitant with the generation of the stable C_4CH neutral $^2\Pi$ state. This

rationale is proposed to account for the different abundances of *m/z* 61 in CR and NR experiments. Such a process is more probable than isomerisation of neutral C_4CH (Figure 4.2.2). The recovery signal observed in the $^-NR^+$ spectrum of C_4CH^- is thus attributed to the neutral $^2\Pi$ C_4CH species.
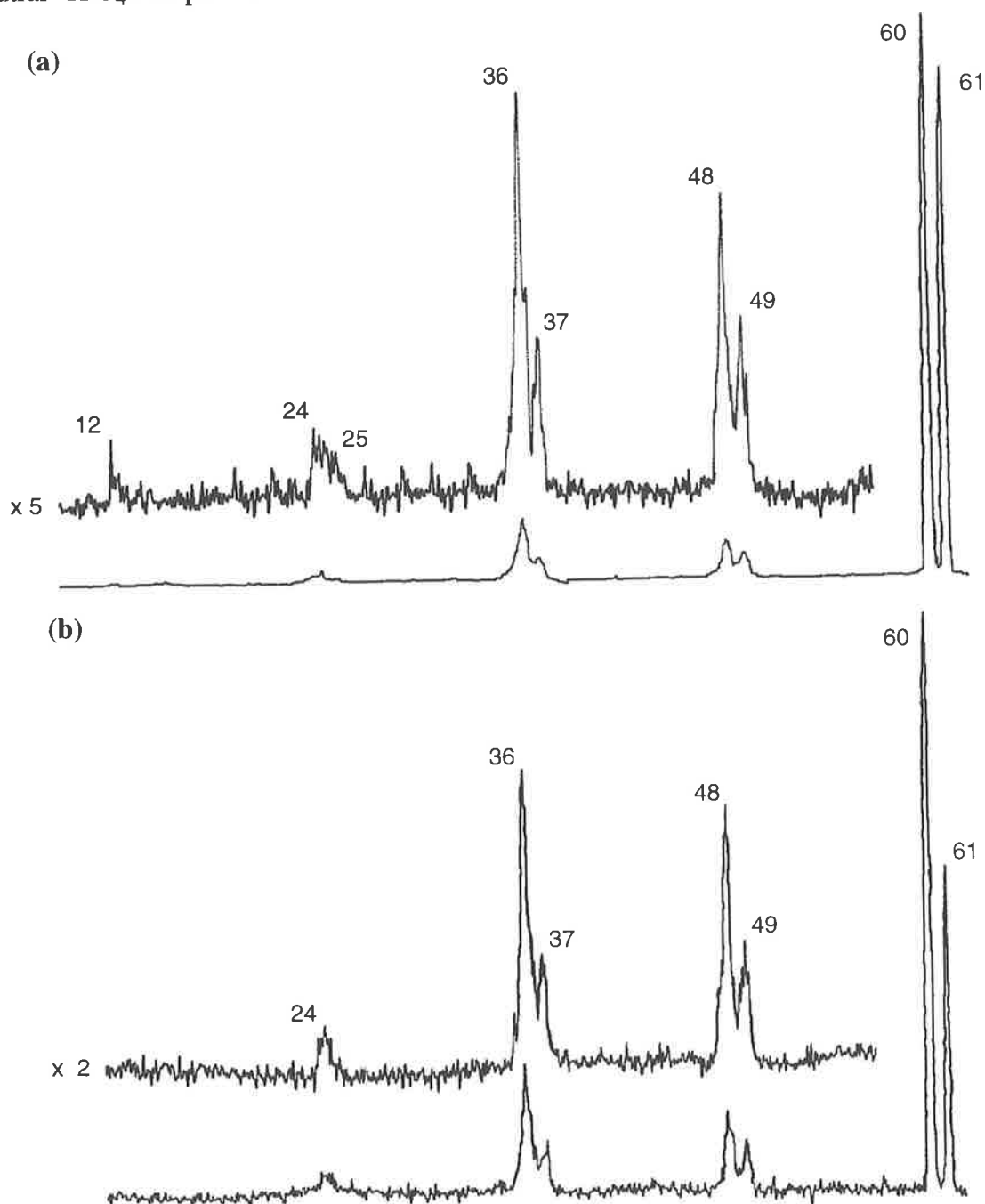
Figure 4.7 $^-NR^+$ *(O_2, 80% T; O_2, 80% T) spectra of m/z 61 from (a)* $TMSC{\equiv}CC{\equiv}CCH_2OCH_3$, *giving* C_4CH^- *and (b)* $HC{\equiv}CCH(OCOCH_2CH_3)C{\equiv}CH$ *giving* $C_2CHC_2^-$. *These spectra both show fragments of the forms* C_nH^+ *and* $C_n^{\cdot+}$.

(IV) CONCLUSIONS

Theoretical studies have shown the stability of a range of anions of the form C_5H. This has prompted attempts to use these charged species as gas phase precursors of the corresponding neutrals by neutralisation reionisation mass spectrometry. Anions and neutrals with the connectivities C_4CH and C_2CHC_2 have been synthesised in the gas phase with the neutrals shown to be stable on the time scale of the NR experiment (ca. 10^{-6} s). This is the first report of the observation of a non-linear C_nH isomer (where $n > 3$). The stability of this molecule in the laboratory lends support to its candidacy as a possible interstellar species. Further, the large electron affinities of the radicals C_4CH and C_2CHC_2 (2.44 and 4.54 eV) suggest the anions too may be present in these galactic environments.

(V) EXPERIMENTAL SECTION

A. Computational Methods

Geometry optimisations were carried out with the Becke 3LYP method[88,89] initially using the 6-31G basis within the GAUSSIAN 94[92] suite of programs. The larger Dunning aug-cc-pVDZ[95,96] basis was used to further optimise minima on the anion, neutral and cation surfaces. Stationary points were characterised as either minima (no imaginary frequencies) or transition states (one imaginary frequency) by calculation of the frequencies using analytical gradient procedures. The minima connected by a given transition structure were confirmed by intrinsic reaction coordinate (IRC) calculations. The calculated frequencies were also used to determine the zero-point vibrational energies which were then scaled by 0.9804[91] and used as a zero-point energy correction for the electronic energies calculated at this and higher levels of theory. Some problems with the linear C_4CH radical structure arose using these methods. The B3LYP methods predicted a very slightly bent geometry (deviating by less than a degree). With $C_{\infty v}$ symmetry imposed, the resulting stationary point was almost identical in geometry and energy to that of lower symmetry, but a number of imaginary frequencies were observed. In this case the linear geometry is reported, in agreement with higher level optimisations.[144,173] More accurate energies for the B3LYP geometries were determined with the RCCSD(T)[176-181] method, using the Dunning aug-cc-pVDZ basis set, within the MOLPRO package.[94] The described computational method was tested using l-C_3H (**B**) giving a computed electron affinity of 1.79 eV compared with the experimentally determined 1.858 ± 0.023 eV.[128] Calculations involving GAUSSIAN 94 geometry optimisation were carried out using the Power Challenge Super Computer at the South Australian Super Computing Centre (Adelaide). MOLPRO single point energy calculations were carried out with the Power Challenge Super Computer at the Australian National University Super Computing Facility (Canberra).

B. Mass Spectrometric Methods

CA, CR and NR spectra were measured using a two-sector reversed geometry VG ZAB 2HF spectrometer. This instrument and the typical experimental conditions for NICI, CA, CR and NR experiments have been described in Chapter 1. Specifically however, spectra were generated in the following manner. Samples were introduced into the source *via* a heated septum inlet, producing a measured pressure of 5 x 10^{-6} Torr inside the source housing. Typical ionisation conditions were: source temperature, 200°C; ionising energy, 70eV (tungsten filament); accelerating voltage, -7kV. All slits were fully open in order to minimise mass discrimination effects due to energy resolution.[46,182] The reagent ions HO⁻ and CH_3O^- were generated respectively from substrates H_2O and CH_3OH (introduced through the heated septum inlet) to give an operating pressure inside the source housing of ca. 5 x 10^{-5} Torr, and thus an estimated pressure inside the ion source of close to 0.1 Torr. Negative ion chemical ionisation of the sample either effected (i) deprotonation or dedeuteration as appropriate, or (ii) desilylation of a neutral trimethylsilylated substrate, by analogy to the method originally developed by DePuy and coworkers.[10] Collisional activation (CA) spectra were obtained by collision of the incident anions with argon in the first of two collision cells at a pressure typically around 10^{-7} Torr. Neutralisation of the anion beam in the first collision cell was achieved by collision with oxygen gas at a typical pressure of 5x10^{-6} Torr: this reduces the main beam to 80% of its initial value, producing essentially single collision conditions in the collision cell.[183] Residual ions were removed using the deflector electrode, with neutrals passing into the second cell where they were reionised to the corresponding cation under identical conditions to those used in the first cell. The spectra were collected by reversing the polarity of the electric sector voltage and scanning the sector voltage. CR spectra were measured under the same conditions as those used for NR spectra, except that the deflector electrode is grounded. Although this CR method does increase the likelihood of double collisions, it allows direct comparison between NR and CR spectra.[25,60,66,68,#] All spectra were repeated a minimum of three times in order to establish their reproducibility.

Comparison of the NR and CR spectra collected in this way equates to a qualitative NIDD treatment (see Chapter 1, pp 20).

C. Synthesis of Precursor Molecules

Many of the precursor compounds necessary for this study had not previously been reported. The synthetic procedures employed to prepare them are given in this section.

1. *Methyl (5-trimethylsilyl)penta-2,4-diynyl ether* [TMSC≡CC≡CCH$_2$OCH$_3$].

A solution of trimethylsilylbutadiyne lithiate was prepared by dropwise addition of methyl lithium-lithium bromide complex (1.7 cm^3, 1.5 M solution in ether) to a stirred solution of (bistrimethylsilyl)butadiyne (0.5 g) in anhydrous tetrahydrofuran (20 cm^3), at 0°C, under a nitrogen atmosphere.[184] The resultant mixture was stirred at 0°C for 15 min, warmed to 20°C and stirred for 2 hr, cooled to 0°C and freshly distilled chloromethyl methyl ether (0.23 cm^3) was added dropwise, the mixture stirred at 20°C for 12 hr. The reaction mixture was cooled to 0°C, quenched with aqueous ammonium chloride (saturated, 10 cm^3), extracted with diethyl ether (3 x 20 cm^3), the ethereal extract separated, washed with water (20 cm^3) and sodium chloride (saturated, 10 cm^3) and dried (MgSO$_4$). The solvent was then removed *in vacuo* to yield methyl (5-trimethylsilyl)penta-2,4-diynyl ether (0.36 g, 87%), [M-H]$^-$ = 165.0725 C$_9$H$_{14}$OSi requires 165.0736. ^{1}H NMR (200MHz, CDCl$_3$) δ 0.16 (s, 9H), 3.36 (s, 3H), 4.13 (s, 2H).*

2. *3-Penta-1,4-diynyl acetate* [HC≡CCH(OCOCH$_3$)C≡CH].

1,4-Pentadiyn-3-ol[186,187] (0.5 g) was heated at 120°C in acetic anhydride (3 cm^3) for 1 hr, with vigorous stirring. The resultant mixture was quenched with ice (10 g), neutralised with aqueous sodium hydrogen carbonate (saturated, ca. 10 cm^3), extracted with diethyl ether (3 x 20 cm^3), the ethereal extract separated, washed with water (20 cm^3) and aqueous sodium chloride (saturated, 10 cm^3) and dried (MgSO$_4$). The solvent was removed *in vacuo* to yield 3-penta-1,4-diynyl acetate (0.76 g, 90%). ^{1}H NMR (200 MHz, CDCl$_3$) δ 2.09 (s, 3H), 2.54 (d, 2H), 5.98 (t, 1H).#

---

* Polyacetylenes are known to be unstable and potentially explosive hence further purification of these compounds was not attempted unless absolutely necessary.[185]
# Accurate mass data is presented for the D$_2$-labelled species pp 87.

3. *[3-D_1]-Penta-1,4-diyn-3-ol* [HC≡CCD(OH)C≡CH].

[3-D_1]-Penta-1,4-diyn-3-ol was prepared by a standard procedure[186,187] except that methyl-[D_1]-formate was used in place of ethyl formate. Yield = 73%. D_1 = 98%.

4. *3-[D_1]-3-Penta-1,4-diynyl acetate* [HC≡CCD(OCOCH$_3$)C≡CH]

3-[D_1]-3-Penta-1,4-diynyl acetate was prepared as for the unlabelled species excepting [3-D_1]-penta-1,4-diyn-3-ol was used as the starting material. Yield = 88%. D_1 = 98%.

5. *1,5-Bis(trimethylsilyl)-3-penta-1,4-diynyl acetate* [TMSC≡CCH(OCOCH$_3$)C≡CTMS].

1,5-Bis(trimethylsilyl)penta-1,4-diyn-3-ol[188] (0.5 g) was heated at 120°C in acetic anhydride (3 cm^3) for 1 hr, with vigorous stirring. The resultant mixture was quenched with ice (10 g), neutralised with aqueous sodium hydrogen carbonate (saturated, ca. 10 cm^3), extracted with diethyl ether (3 x 20 cm^3), the ethereal extract separated, washed with water (20 cm^3) and aqueous sodium chloride (saturated, 10 cm^3) and dried (MgSO$_4$). The solvent was removed *in vacuo* to yield 1,5-bis(trimethylsilyl)-3-penta-1,4-diynyl acetate (0.55 g, 88%). ^{1}H NMR (200 MHz, CDCl$_3$) δ 0.16 (s, 18H), 2.10 (s, 3H), 6.02 (s, 1H).

6. *[1,5-D_2]-3-Penta-1,4-diynyl acetate* [DC≡CCH(OCOCH$_3$)C≡CD].

A solution containing 1,5-bis(trimethylsilyl)-3-penta-1,4-diynyl acetate (0.55 g) and 18-crown-6 (0.005 g) in anhydrous tetrahydrofuran (10 cm^3) was added dropwise over 0.5 hr to a stirred solution of dry potassium fluoride (1.0 g) in deuterium oxide (1 cm^3), at 0°C, under a nitrogen atmosphere. The solution was then stirred at 25°C for 12 hr, dried (MgSO$_4$), followed by removal of the solvent *in vacuo* to give [1,5-D_2]-3-penta-1,4-diynyl acetate (0.22 g, 95%, D_2 > 97%). [M-H]$^-$ = 123.0423 C$_7$H$_3$D$_2$O requires 123.0415.

7. *3-Penta-1,4-diynyl propionate* [HC≡CCH(OCOCH₂CH₃)C≡CH]

Procedure adapted from that of Vogel.[189] 1,4-Pentadiyn-3-ol (0.6 g) in anhydrous dichloromethane (20 cm^3) was cooled to 0°C, and a mixture of propionyl chloride (3.89 cm^3) in anhydrous dichloromethane (30 cm^3) was added dropwise at 0°C under a nitrogen atmosphere. The mixture was then heated under reflux for 2 hr, cooled to 20°C, ice (10 g) was added and the mixture was extracted with dichloromethane (3 x 20 cm^3). The combined organic extract was washed with aqueous sodium hydrogen carbonate (saturated, 3 x 20 cm^3), dried (MgSO₄), the solvent was removed *in vacuo* and the product purified on a short silica column (eluted with ethyl acetate:hexane, 30:70) to give 3-penta-1,4-diynyl propionate (0.83 g, 81%). [M-H]⁻ = 135.0447 C₈H₇O₂ requires 135.0446. ^{1}H NMR (200 MHz, CDCl₃) δ 1.15 (t, 3H), 2.34 (q, 2H), 2.55 (d, 2H), 6.03 (t, 1H).

8. *3-Penta-1,4-diynyl formate* [HC≡CCH(OCOH)C≡CH]

Procedure adapted from that of Carlson *et al.* [190] 3-Penta-1,4-diynol (0.5 g) was added to a mixture of boron oxide (0.12 g), *para*-toluenesulfonic acid (0.12 g), formic acid (0.33 g) and anhydrous dichloromethane (20 cm^3) at 20°C under an atmosphere of nitrogen. The mixture was heated under reflux for 1 hr, cooled to 0°C, filtered, and the filtrate stirred with potassium carbonate (0.5 g) for 0.25 hr, refiltered and the solvent removed *in vacuo*. The residue was purified on a short silica column (eluting with dichloromethane) to give 3-penta-1,4-diynyl formate (0.07 g, 14%). [M-H]⁻ = 107.0127 C₆H₃O₂ requires 107.0133. ^{1}H NMR (200 MHz, CDCl₃) δ 2.60 (d, 2H), 6.10 (t, 1H), 8.04 (s, 1H).

(VI) APPENDICES

Table 4.6 Geometries of minima on the C_5H neutral radical potential surface. Calculated at the B3LYP/aug-cc-pVDZ level of theory. All bond lengths are given in angstroms and all angles in degrees.

$C_1—C_2—C_3—C_4—C_5—H$

1 $(C_{\infty v})$ $^2\Pi$

bond length		
	C_1-C_2	1.3177
	C_2-C_3	1.2757
	C_3-C_4	1.3301
	C_4-C_5	1.2335
	C_5-H	1.0709
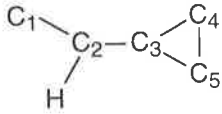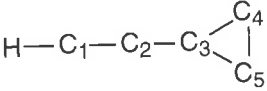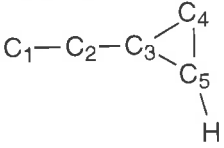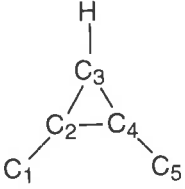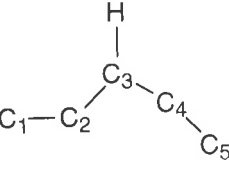
2 (C_{2v}) $^2B_2$

bond length		
	C_1-H	1.0713
	C_1-C_2	1.2183
	C_2-C_3	1.3832
	C_3-C_4	1.4011
	C_3-C_5	1.4011
angle	C_2-C_1-H	180.0
	C_1-C_2-C_3	180.0
	C_2-C_3-C_4	150.8
	C_2-C_3-C_5	150.8

3 (C_S) $^2A'$

bond length		
	C_1-C_2	1.2897
	C_2-C_3	1.3285
	C_3-C_4	1.4575
	C_3-C_5	1.4160
	C_4-C_5	1.3478
	C_5-H	1.0860
angle	C_1-C_2-C_3	181.1
	C_2-C_3-C_4	156.4
	C_2-C_3-C_5	147.7
	C_3-C_5-H	140.8

4 (C_{2v}) $^2B_2$

bond length		
	C_1-C_2	1.2930
	C_2-C_3	1.3707
	C_3-C_4	1.3707
	C_4-C_5	1.2930
	C_3-H	1.0950
angle	C_1-C_2-C_3	184.6
	C_2-C_3-C_4	112.0
	C_3-C_4-C_5	184.6
	H-C_3-C_2	124.0

5 (C_S) $^2A'$

bond length		
	C_1-H	1.0805
	C_1-C_2	1.2973
	C_2-C_3	1.4448
	C_2-C_4	1.4715
	C_3-C_5	1.4255
angle	H-C_1-C_2	144.6
	C_1-C_2-C_3	148.3
	C_1-C_2-C_4	148.6
	C_2-C_3-C_5	117.2

6 (C_S) $^2A'$

bond length		
	C_1-C_2	1.3179
	C_2-H	1.1037
	C_2-C_3	1.4391
	C_3-C_4	1.3754
	C_3-C_5	1.4056
angle	C_1-C_2-C_3	126.4
	H-C_2-C_3	120.1
	C_2-C_3-C_4	153.0
	C_2-C_3-C_5	147.8

Table 4.7 Geometries of transition states and unstable intermediates on the C_5H neutral radical potential surface. Calculated at the B3LYP/6-31G level of theory. All bond lengths are given in angstroms and all angles in degrees.

$$H$$
$$\diagdown$$
$$C_1-C_2-C_3-C_4-C_5$$

TS4/9

bond length	C_1-C_2	1.3005
	C_2-C_3	1.2983
	C_3-C_4	1.3259
	C_4-C_5	1.3359
	H-C_4	1.3222
angle	C_1-C_2-C_3	179.1
	C_2-C_3-C_4	175.1
	C_3-C_4-C_5	173.5
	H-C_4-C_3	62.5
dihedral angle	C_1-C_2-C_3-C_4	180.0
	C_2-C_3-C_4-C_5	0.0
	H-C_4-C_3-C_2	180.0

$$H$$
$$\diagup$$
$$C_1-C_2-C_3-C_4$$
$$\diagdown C_5$$

9

bond length	C_1-C_2	1.3305
	C_2-C_3	1.2674
	C_3-C_4	1.3721
	C_4-C_5	1.3577
	H-C_4	1.1039
angle	C_1-C_2-C_3	179.6
	C_2-C_3-C_4	179.5
	C_3-C_4-C_5	134.7
	H-C_4-C_3	118.2
dihedral angle	C_1-C_2-C_3-C_4	0.0
	C_2-C_3-C_4-C_5	0.0
	H-C_4-C_3-C_2	180.0

$$H$$
$$\diagup$$
$$C_1-C_2-C_3-C_4$$
$$\diagdown C_5$$

TS9/1

bond length	C_1-C_2	1.3308
	C_2-C_3	1.2692
	C_3-C_4	1.3524
	C_4-C_5	1.3146
	H-C_4	1.2017
angle	C_1-C_2-C_3	178.9
	C_2-C_3-C_4	174.9
	C_3-C_4-C_5	160.5
	H-C_4-C_3	125.6
dihedral angle	C_1-C_2-C_3-C_4	180.0
	C_2-C_3-C_4-C_5	180.0
	H-C_4-C_3-C_2	0.0

$$C_5$$
$$|$$
$$H-C_1-C_2-C_3-C_4$$

TS1/2

bond length	C_1-C_2	1.2436
	C_2-C_3	1.3177
	C_3-C_4	1.3548
	C_4-C_5	1.3393
	H-C_1	1.0660
angle	C_1-C_2-C_3	176.7
	C_2-C_3-C_4	174.8
	C_3-C_4-C_5	95.8
	H-C_1-C_2	171.0
dihedral angle	C_1-C_2-C_3-C_4	180.0
	C_2-C_3-C_4-C_5	0.0
	H-C_1-C_2-C_3	180.0

$$H$$
$$|$$
$$C_5$$
$$|$$
$$C_1-C_2-C_3-C_4$$

TS1/3

bond length	C_1-C_2	1.3209
	C_2-C_3	1.2776
	C_3-C_4	1.4379
	C_4-C_5	1.2797
	H-C_5	1.0714
angle	C_1-C_2-C_3	174.8
	C_2-C_3-C_4	170.5
	C_3-C_4-C_5	96.4
	H-C_5-C_4	174.7
dihedral angle	C_1-C_2-C_3-C_4	180.0
	C_2-C_3-C_4-C_5	0.0
	H-C_5-C_4-C_3	180.0

Table 4.8 Geometries of minima on the C_5H cation potential surface. Calculated at the B3LYP/aug-cc-pVDZ level of theory. All bond lengths are given in angstroms and all angles in degrees.
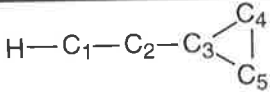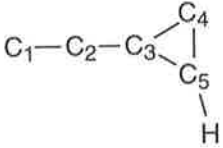
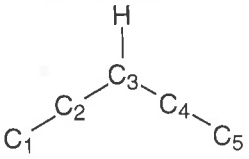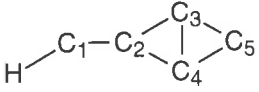C_1—C_2—C_3—C_4—C_5—H C_1—C_2—C_3—C_4—C_5—H

1+ (C$_S$) ^{1}A'   **1+** (C$_{\infty v}$) $^3\Pi$

bond length	C_1-C_2	1.3311
	C_2-C_3	1.2599
	C_3-C_4	1.3271
	C_4-C_5	1.2294
	C_5-H	1.0815
angle	C_1-C_2-C_3	176.3
	C_2-C_3-C_4	178.1
	C_3-C_4-C_5	177.5
	C_4-C_5-H	179.2

bond length	C_1-C_2	1.2566
	C_2-C_3	1.2975
	C_3-C_4	1.3067
	C_4-C_5	1.2433
	C_5-H	1.0802
angle	C_1-C_2-C_3	180.0
	C_2-C_3-C_4	180.0
	C_3-C_4-C_5	180.0
	C_4-C_5-H	180.0

H—C_1—C_2—$C_3$$\diagdown$$^{C_4}_{C_5}$ C_1—C_2—$C_3$$\diagdown$$^{C_4}_{C_5}$—H

2+ (C$_{2v}$) ^{3}B$_2$ **3+** (C$_S$) ^{1}A'

bond length	C_1-H	1.0792
	C_1-C_2	1.2231
	C_2-C_3	1.3581
	C_3-C_4	1.4236
	C_3-C_5	1.4236
	C_4-C_5	1.3657
angle	C_2-C_1-H	180.0
	C_1-C_2-C_3	180.0
	C_2-C_3-C_4	151.3
	C_2-C_3-C_5	151.3

bond length	C_1-C_2	1.2272
	C_2-C_3	1.3648
	C_3-C_4	1.3929
	C_3-C_5	1.4233
	C_4-C_5	1.3494
	C_5-H	1.0907
angle	C_1-C_2-C_3	183.8
	C_2-C_3-C_4	155.9
	C_2-C_3-C_5	146.9
	C_3-C_5-H	143.5

4+ (C$_{2v}$) ^{1}A$_1$

bond length	C_1-C_2	1.3503
	C_2-C_3	1.3744
	C_3-C_4	1.3744
	C_4-C_5	1.3503
	C_2-C_4	1.5353
	C_5-H	1.0935
angle	C_1-C_2-C_3	152.7
	C_2-C_3-C_4	67.9
	C_3-C_4-C_5	152.7
	H-C_3-C_2	146.0

4+ (C$_S$) ^{3}A'

bond length	C_1-C_2	1.2701
	C_2-C_3	1.3786
	C_3-C_4	1.3731
	C_4-C_5	1.2879
	C_5-H	1.1043
angle	C_1-C_2-C_3	199.1
	C_2-C_3-C_4	124.3
	C_3-C_4-C_5	155.7
	H-C_3-C_2	117.7

Chapter 5: Gas Phase Syntheses of Three Isomeric C_5H_2 Radical Anions and Their Elusive Neutrals. A Joint Experimental and Theoretical Study.

(I) ABSTRACT

Three different radical anions of the empirical formula C_5H_2 have been generated by negative ion chemical ionisation mass spectrometry in the gas phase. The isomers $C_4CH_2^{\cdot-}$, $C_2CHC_2H^{\cdot-}$ and $HC_5H^{\cdot-}$ have been synthesised by unequivocal routes and their structures confirmed by deuterium labelling and the collision based, charge reversal and neutralisation reionisation experiments. The results also provide evidence for the existence of neutrals C_4CH_2, C_2CHC_2H and HC_5H as stable species: this is the first reported observation of C_2CHC_2H. Theoretical calculations confirm these structures to be minima on the anion and neutral potential energy surfaces. Electron attachment to two stable cyclic C_5H_2 neutrals has also been investigated theoretically to probe the possibility of using anion precursors to generate these neutrals in the gas phase.

(II) INTRODUCTION

Since the discovery of the cyclic carbene C_3H_2 (**1**) in interstellar and circumstellar environments, interest in the generation and characterisation of carbenes of the form C_nH_2 has increased.[101,191] Cyclic C_3H_2, together with its isomers and charged analogues, has been the subject of intensive investigation in recent years. Matrix trapping experiments have characterised the neutrals cyclopropenylidene (**1**), propargylene (**2**) and propadienylidene (**3**),[124-126,130,192] while mass spectrometry has probed the molecular cations of **1** - **3**[134,136,137,140,141] and the molecular anions of **2** and **3**.[20,127,133] A number of theoretical studies have also been reported pertaining to these elusive systems.[132,193] These studies have all been outlined in some detail in Chapter 3.
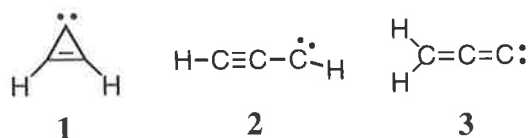
Some isomers of neutral C_5H_2 have also been described. Pentadiynylidene (**4**), has been trapped in a neon matrix and characterised by its electronic spectrum,[194] while pentatetraenylidene (**5**) and ethynylcyclopropenylidene (**6**) have been identified in a molecular beam using Fourier transform microwave spectroscopy.[108]
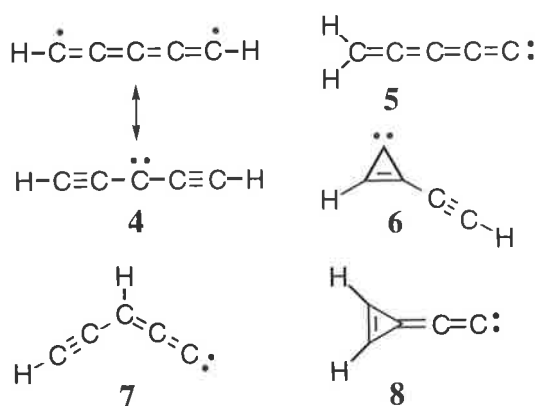
The related even numbered cumulenes C_nH_2 (n = 2, 4) have been studied by mass spectrometric techniques.[153,154] In these cases, radical anions of the type C_nCH_2 (n = 1, 3) were formed in the gas phase by negative ion chemical ionisation of appropriate precursors.

Comparison of the $^-NR^+$ spectra of these radical anions with the $^+NR^+$ spectra of acetylene ($HC_2H^{\cdot+}$) and diacetylene ($HC_4H^{\cdot+}$) radical cations proves to be surprisingly diagnostic of structure.[153,154] The spectrum of $C_3CH_2^{\cdot-}$ shows fragments $C_mCH_2^{\cdot+}$ (where m = 1 and 2), whilst these fragmentations are minimal for the $HC_4H^{\cdot+}$ isomer (Chapter 3, Figure 3.3, pp 57). The C_2H_2 system also shows this trend.[154] Similarly, we have demonstrated in Chapter 4 that the CR and NR spectra of C_5H^- and $C_2CHC_2^-$ are diagnostic of structural connectivity. Following from this work, three isomeric C_5H_2 radical anions have been generated by procedures outlined in this Chapter. CR and NR techniques have been employed to establish the uniqueness of the structures in each case, with the latter experiment providing an indication of the stability of the corresponding neutrals.

The stabilities of **4, 5** and **6** have been studied using various *ab initio* methods,[165,195,196] and a thorough investigation of the C_5H_2 potential surface at high level has revealed two further stable isomers of neutral C_5H_2, namely ethynylpropadienylidene (**7**) and 3-(dihydrovinylidene)cyclopropene (**8**).[193] In this Chapter theoretical calculations are presented which investigate the effect of electron attachment to these stable C_5H_2 neutral isomers. The structures and relative energies of these anions are discussed.

(III) RESULTS AND DISCUSSION

A. Synthesis of Isomeric C_5H_2 Radical Anions and their Neutrals. Experimental Confirmation of Structure.

1. *Gas phase syntheses of three isomeric C_5H_2 anions*

Our initial approach to this problem followed earlier work on the collision induced dissociation (CID) behaviour of $^-C{\equiv}CCH_2OCH_3$ (Chapter 3, Figure 3.2, pp 53).[143] This anion decomposes in a number of ways including loss of $CH_3O^{\cdot}$ to yield $C_2CH_2^{\cdot-}$ (Scheme 5.1, a). The analogous process from $^-C{\equiv}CC{\equiv}CCH_2OCH_3$ should give $C_4CH_2^{\cdot-}$ (the radical anion of **5**). The precursor anion is formed by the reaction between methyl (5-trimethylsilyl)penta-2,4-diynyl ether and HO^- in the ion source of the mass spectrometer. This ion-molecule reaction is analogous to the method developed by DePuy *et al.* where the fluoride ion is used as the reagent species.[10] However this reaction has also been shown to be effective with the use of hydroxide as the nucleophile.[11] Once formed the $^-C{\equiv}CC{\equiv}CCH_2OCH_3$ ion then undergoes facile metastable decomposition to yield a pronounced peak (*m/z* 62) corresponding to an ion of formula $C_5H_2^{\cdot-}$ (Scheme 5.1, b). This anion must be $C_4CH_2^{\cdot-}$ unless either hydrogen or carbon rearrangement accompanies or precedes the formation of the ion. To support this assignment the corresponding deuterium analogue $C_4CD_2^{\cdot-}$ has also been synthesised: in this case from precursor anion $^-C{\equiv}CC{\equiv}CCD_2OH$ (Scheme 5.1, c) formed by the reaction between $TMSC{\equiv}CC{\equiv}CCD_2OH$ and HO^-, followed by loss of hydroxide radical.

Scheme 5.1

$$^-C{\equiv}CCH_2OCH_3 \;\rightarrow\; [C{=}C{=}CH_2]^{\cdot-} \;+\; {}^{\cdot}OCH_3 \qquad\qquad (a)$$

$$TMSC{\equiv}CC{\equiv}CCH_2OCH_3 \;+\; {}^-OH \;\rightarrow\; {}^-C{\equiv}CC{\equiv}CCH_2OCH_3 \;+\; TMSOH$$

$$^-C{\equiv}CC{\equiv}CCH_2OCH_3 \;\rightarrow\; [C{=}C{=}C{=}C{=}CH_2]^{\cdot-} \;+\; {}^{\cdot}OCH_3 \qquad (b)$$

$$TMSC{\equiv}CC{\equiv}CCD_2OH \;+\; {}^-OH \;\rightarrow\; {}^-C{\equiv}CC{\equiv}CCD_2OH \;+\; TMSOH$$

$$^-C{\equiv}CC{\equiv}CCD_2OH \;\rightarrow\; [C{=}C{=}C{=}C{=}CD_2]^{\cdot-} \;+\; {}^{\cdot}OH \qquad\qquad (c)$$
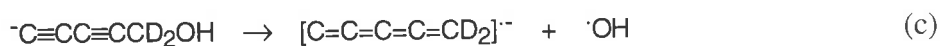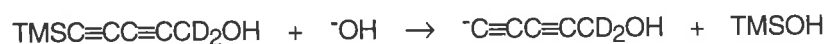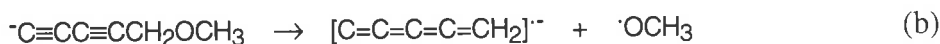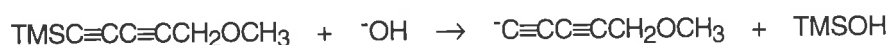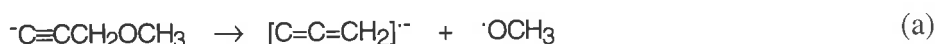
We next effected the synthesis of HC$_5$H$^{\cdot-}$ (the radical anion of neutral **4**). In principle, HC$_5$H$^{\cdot-}$ can be formed from anion [HC≡C-C(OH)C≡CH]$^-$ following loss of HO$^\cdot$ and indeed reaction of HC≡CCD(OH)C≡CH and DC≡CCH(OH)C≡CD with HO$^-$ in the ion source yielded C$_5$H$_2^{\cdot-}$ (*m/z* 62, Scheme 5.2)$^{\#}$ and C$_5$D$_2^{\cdot-}$ (*m/z* 64) respectively. These isotopomers should have the desired HC$_5$H (also DC$_5$D) connectivity provided that no hydrogen (or deuterium) or carbon rearrangement precedes or accompanies formation of the anion. Coincident to the synthesis of the desired species, C$_5$HD (*m/z* 63) radical anions were observed as products, in the source reactions of both labelled precursors.* This could occur *via* loss of HO$^\cdot$ from the ions [C≡C-CD(OH)C≡CH]$^-$ and [C≡C-CH(OH)C≡CD]$^-$ thus suggesting C$_2$CDC$_2$H$^{\cdot-}$ (*m/z* 63, Scheme 5.2) and C$_2$CHC$_2$D$^{\cdot-}$, respectively, to be the structures of the observed ions. To further investigate this novel connectivity, the precursor TMSC≡CCH(OH)C≡CH was ionised under the same conditions and in a process analogous to Scheme 5.1(b), yielded a peak of *m/z* 62, corresponding to C$_2$CHC$_2$H$^{\cdot-}$, the radical anion of **7**.

Scheme 5.2

HC≡CCD(OH)C≡CH + $^-$OH → HC≡CCD(OH)C≡C$^-$ + H$_2$O

HC≡CCD(OH)C≡C$^-$ → [HC≡CCDC≡C]$^{\cdot-}$ + $^\cdot$OH
m/z 63

HC≡CCD(OH)C≡CH + $^-$OH → [HC≡CC(OH)C≡CH]$^-$ + HOD

[HC≡CC(OH)C≡CH]$^-$ → [HC≡CCC≡CH]$^{\cdot-}$ + $^\cdot$OH
m/z 62
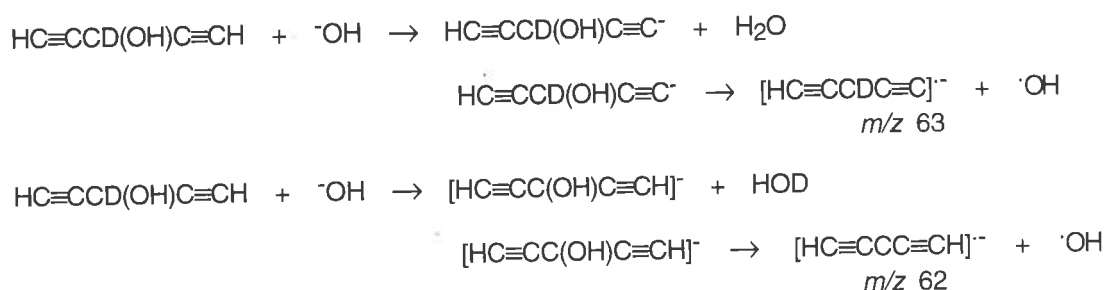
We have used the HO substituent instead of CH$_3$O, because the latter, although forming C$_5$H$_2^{\cdot-}$ also undergoes some hydride transfer to form C$_5$H$_3^-$ (*m/z* 63) and CH$_2$O. Use of a hydroxide substituent does open reaction channels through deprotonation at the HO moiety, however the resulting alkoxide ion cannot fragment to give C$_5$H$_2^{\cdot-}$.

* The CH$_3$O substituted precursor also gave C$_2$CHC$_2$D$^{\cdot-}$ (*m/z* 63) and is the precursor of choice here because its higher isotopic purity precludes a contribution from HC$_5$D$^{\cdot-}$ in the spectrum.

2. *Characterisation of isomeric C_5H_2 anions by CR and NR*

Despite the simple logic of the formation of these isomeric radical anions, further evidence is needed to confirm their connectivities. The conventional negative ion CA spectra of these isomers show only losses of H· and H_2, and thus do not differentiate the isomers. In contrast, the $^-CR^+$ and $^-NR^+$ spectra may be used as probes of structure as was demonstrated in Chapter 4. Consider first, the deuterated isomers $DC_5D^{·-}$ and $C_4CD_2^{·-}$ (the radical anions of deuterated **4** and **5** respectively). Their $^-CR^+$ spectra are listed in Table 5.1, while the $^-NR^+$ spectra are illustrated, for comparative purposes, in Figure 5.1.

Both sets of spectra show peaks corresponding to $C_nD_2^{·+}$, C_nD^+ and $C_n^{·+}$ (n = 1-5) confirming the empirical assignments made for the parent anions. Closer inspection of the spectra of the isomer $DC_5D^{·-}$ reveals a low abundance of peaks corresponding to fragments $C_mD_2^{·+}$ (m = 2-4).# This seems intuitive for the anticipated DC_5D structure given that formation of these ions must occur through loss of carbon with deuterium migration: that is, loss of carbon with concomitant loss of deuterium (C_mD) is much more probable than pure carbon losses (C_m). Such fragmentation behaviour is directly analogous to the decomposition observed in the $^+NR^+$ spectrum of $HC_4H^{·+}$ reported by Goldberg *et al.* (Chapter 3, Figure 3.3, pp 57).[153] The $^-NR^+$ spectrum of $C_4CD_2^{·-}$ contrasts markedly to that of $DC_5D^{·-}$, with the former showing $C_mD_2^{·+}$ (m = 2-4) fragment peaks with a relative abundance more than twice that observed for $DC_5D^{·-}$ (Figure 5.1). Identical trends are observed for the respective $^-CR^+$ spectra (Table 5.1) The significant differences between these two isomeric species in their $^-NR^+$ and $^-CR^+$ spectra appear logical and support the assignment of distinct structures to these ions.

It should be noted that the spectrum of $DC_5D^{·-}$ also shows a number of very small peaks at *m/z* 63 and 61, it is suggested that these are fragmentations from the ^{13}C isotopomer of $C_2CDC_2H^{·-}$ which may make a small contribution to the *m/z* 64 parent ion.
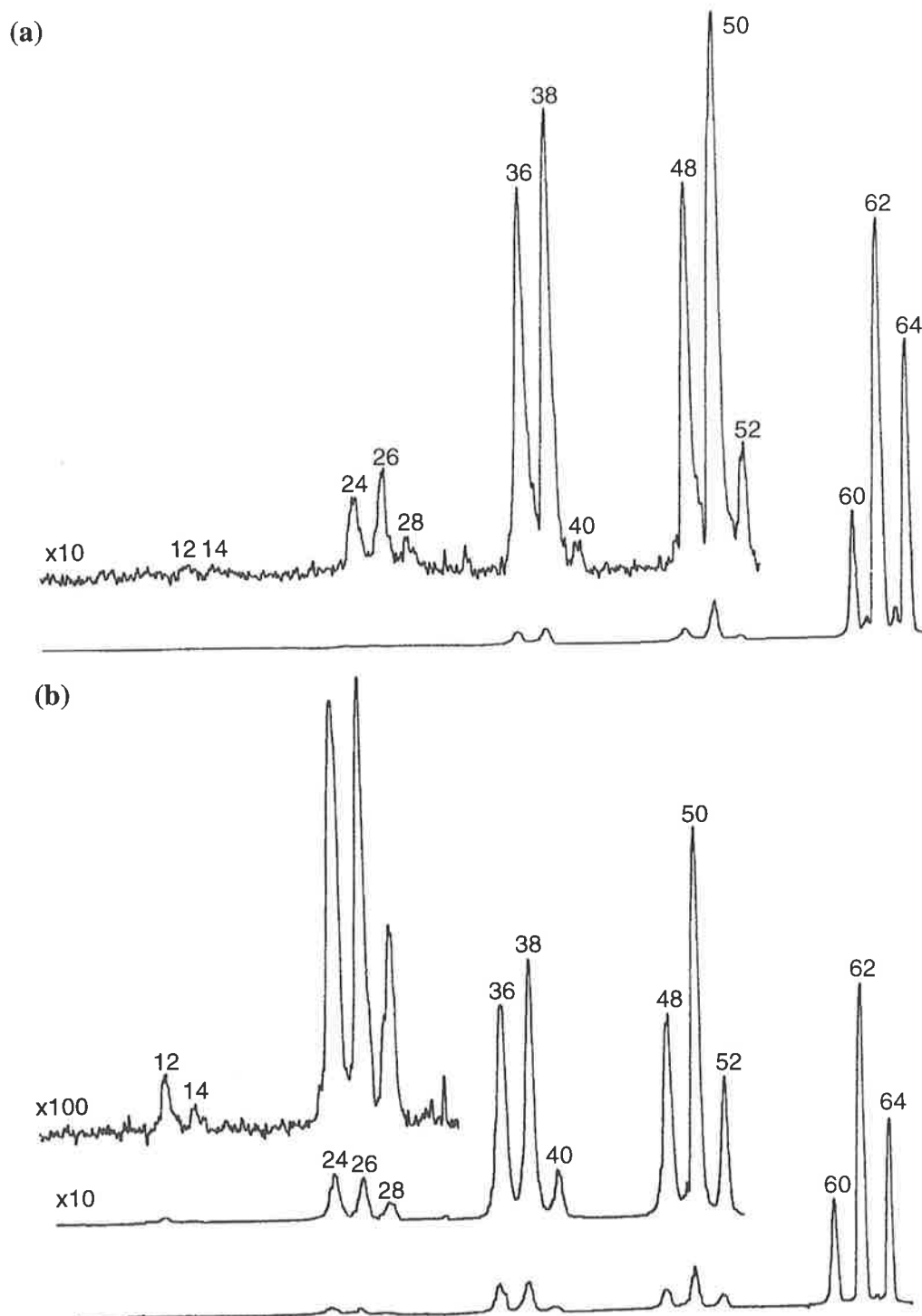
(a)

(b)

Figure 5.1 $^-NR^+$ *(O_2, 80% T; O_2, 80% T) spectra of m/z 64 from (a) DC≡CCH(OH)C≡CD, giving $DC_5D^{\cdot-}$ and (b) TMSC≡CC≡CCD$_2$OH, giving $C_4CD_2^{\cdot-}$. These spectra both show fragment ions of the forms, $C_nD_2^{\cdot+}$, $C_nD^{\cdot+}$ and $C_n^{\cdot+}$ (where n = 1-5).*

Table 5.1 Charge Reversal ($^-$CR$^+$) and Neutralisation Reionisation ($^-$NR$^+$) spectra for the [D$_1$] and [D$_2$] analogues of three C$_5$H$_2$$^{\cdot-}$ isomers.

Precursor	Fragmentations: *m/z* (intensity relative to base peak)
m/z 64 from DC≡CCH(OH)C≡CD **DC$_5$D$^{\cdot-}$**	**CR** 64(88), 62(100), 60(34), 52(2), 50(27), 48(6), 40(.3), 38(7.5), 36(3.5), 28(0.1), 26(1), 24(0.6), 16(<0.02), 14(<0.1), 12(<0.1). **NR** 64(70), 62(100), 60(31), 52(2), 50(14), 48(7), 40(0.5), 38(8), 36(7), 28(0.7), 26(2), 24(1.3), 16(<0.02), 14(0.2), 12(0.2).
m/z 64 from TMSC≡CC≡CCD$_2$OH **C$_4$CD$_2$$^{\cdot-}$**	**CR** 64(49), 62(100), 60(33), 52(14), 50(23), 48(11), 40(3), 38(8), 36(5), 28(.3), 26(.7), 24(.8), 16(<0.02), 14(<0.02), 12(.1). **NR** 64(58), 62(100), 60(33), 52(5), 50(14), 48(7), 40(2), 38(9), 36(8), 28(0.6), 26(1.5), 24(1.5), 16(<0.02), 14(0.1), 12(0.2).
m/z 63 from DC≡CCH(OCH$_3$)C≡CD **C$_2$CHC$_2$D$^{\cdot-}$**	**CR** 63(68), 62(100), 61(48), 60(27), 51(11), 50(7.5), 49(9), 48(7.5), 39(5.5), 38(5), 37(8), 36(6), 27(0.5), 26(1.4), 25(1), 24(1.4), 15(<0.02), 14(<0.1), 13(<0.02), 12(0.2). **NR** 63(97), 62(100), 61(69), 60(66), 51(8), 50(9), 49(11), 48(15), 39(4), 38(13), 37(15), 36(23), 27(<0.02), 26(3), 25(<0.02), 24(6), 15(<0.02), 14(<0.02), 13(<0.02), 12(<0.02).
m/z 63 from HC≡CCD(OH)C≡CH **C$_2$CDC$_2$H$^{\cdot-}$**	**CR** 63(71), 62(100), 61(35), 60(7), 51(3), 50(11), 49(8), 48(2.5), 39(1.5), 38(7), 37(7), 36(4.5), 27(0.2), 26(0.9), 25(1.5), 24(1), 15(<0.02), 14(<0.02), 13(<0.1), 12(<0.1). **NR** 63(73), 62(100), 61(47), 60(9), 51(3), 50(14), 49(10), 48(4), 39(4), 38(11), 37(16), 36(10), 27(1), 26(3), 25(4), 24(4), 15(<0.02), 14(<0.02), 13(<0.02), 12(<0.02).

While it is difficult to compare the spectra in Figure 5.1 directly with those of the third labelled isomer it is useful to compare the results from the two isotopomers $C_2CDC_2H^{\cdot-}$ and $C_2CHC_2D^{\cdot-}$ (Table 5.1). If we consider here the $^-CR^+$ spectra, both show the isotopically analogous fragment ions to those already discussed, namely, $C_nDH^{\cdot+}$, C_nD^+, C_nH^+ and $C_n^{\cdot+}$ (where n = 1-5). Significantly, however, in the spectrum of $C_2CHC_2D^{\cdot-}$ the losses of $CD^{\cdot}$ and $C_2D^{\cdot}$ predominate over losses of $CH^{\cdot}$ and $C_2H^{\cdot}$ while the opposite is observed for $C_2CDC_2H^{\cdot-}$. This would be in accord with the assigned connectivities, with the terminal CH/D unit lost preferentially to that at the central position, where some rearrangement or migration would be required. In particular, the comparison of the two different monolabelled $C_5HD^{\cdot-}$ ions unambiguously demonstrates that the radical anion formed has two non-equivalent hydrogen atoms, thus excluding structures, HC_5H and C_4CH_2.

The $^-CR^+$ spectra of the unlabelled analogues $HC_5H^{\cdot-}$, $C_4CH_2^{\cdot-}$ and $C_2CHC_2H^{\cdot-}$ are illustrated in Figure 5.2. These spectra show the same trends as do those of their labelled counterparts (*cf.* Table 5.1). The $^-CR^+$ spectrum of $HC_5H^{\cdot-}$ shows low abundance peaks from ions $C_mH_2^{\cdot+}$ (m = 2-4): in contrast, such peaks are more abundant in the CR spectrum of $C_4CH_2^{\cdot-}$. The $^-CR^+$ spectrum of the final isomer (Figure 5.2, c) is hardly characteristic, appearing quite similar to that of $C_4CH_2^{\cdot-}$. However the propensity for $CH^{\cdot}$ and $C_2H^{\cdot}$ loss from this structure, established previously from the labelled ions, is consistent with the major losses observed in this spectrum. The $^-NR^+$ spectra of all three isomers are given in Table 5.2 and are analogous to the $^-CR^+$ spectra discussed.
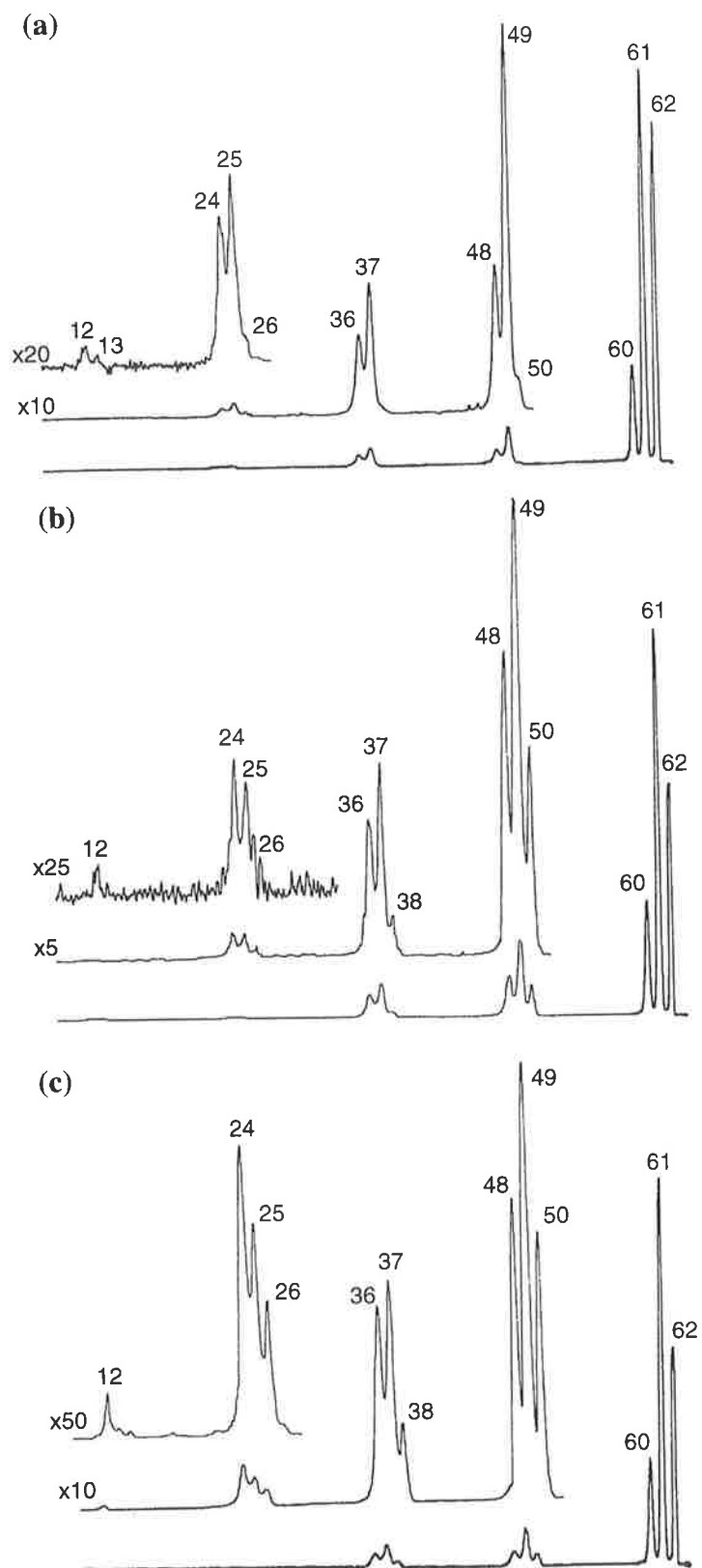
Figure 5.2 $^-CR^+$ $(O_2, 80\% \ T; \ O_2, 80\% \ T)$ spectra of m/z 62 from (a) $HC{\equiv}CCD(OH)C{\equiv}CH$, giving $HC_5H^{\cdot-}$ (b) $TMSC{\equiv}CC{\equiv}CCH_2OCH_3$, giving $C_4CH_2^{\cdot-}$ and (c) $TMSC{\equiv}CCH(OH)C{\equiv}CH$, giving $C_2CHC_2H^{\cdot-}$. These spectra each show fragment ions of the forms, $C_nH_2^{\cdot+}$, $C_nH^{\cdot+}$ and $C_n^{\cdot+}$ (where n = 1-5).

Table 5.2 Charge Reversal ($^-CR^+$) and Neutralisation Reionisation ($^-NR^+$) spectra for the three $C_5H_2^{\cdot-}$ isomers.

Precursor	Fragmentations: *m/z* (intensity relative to base peak)
m/z 62 from HC≡CCD(OH)C≡CH **HC$_5$H$^{\cdot-}$**	**CR** 62(87), 61(100), 60(25), 50(0.8), 49(9.5), 48(4), 38(0.2), 37(3), 36(2), 26(0.03), 25(0.25), 24(0.2), 14(<0.02), 13(<0.02), 12(<0.1). **NR** 62(76), 61(100), 60(44), 50(1), 49(6), 48(4), 38(0.5), 37(3.5), 36(4), 26(0.15), 25(0.6), 24(0.75), 14(<0.02), 13(<0.02), 12(<0.1).
m/z 62 from TMSC≡CC≡CCH$_2$OCH$_3$ **C$_4$CH$_2$$^{\cdot-}$**	**CR** 62(60), 61(100), 60(26), 50(10), 49(21), 48(14), 38(2), 37(9), 36(6), 26(0.4), 25(0.9), 24(1), 14(<0.02), 13(<0.02), 12(0.25). **NR** 62(62), 61(100), 60(36), 50(3), 49(11), 48(9), 38(1), 37(8), 36(8), 26(0.5), 25(1.5), 24(2), 14(<0.02), 13(<0.02), 12(<0.02).
m/z 62 from TMSC≡CCH(OH)C≡CH **C$_2$CHC$_2$H$^{\cdot-}$**	**CR** 62(56), 61(100), 60(27), 50(6), 49(10.5), 48(7), 38(2), 37(5), 36(5), 26(0.5), 25(0.8), 24(1), 14(<0.02), 13(<0.1), 12(0.15). **NR** 62(54), 61(100), 60(34), 50(3), 49(7), 48(6), 38(0.7), 37(3.5), 36(4.5), 26(0.3), 25(0.6), 24(1), 14(<0.02), 13(<0.02), 12(0.15).

3. *Possible pathways for anion rearrangement*

The charge reversal and neutralisation reionisation data (including labelling studies) presented thus far clearly demonstrate that the three isomeric C_5H_2 radical anions formed do not rearrange to a common species or a common mixture of species in the gas phase. These experimental results do not however exclude the possibility of some individual rearrangement processes occurring for one or more of the initially formed radical anions to give rearranged but still distinct ions. Mechanisms which might lead to isomerisation include: (i) intramolecular hydride transfer around the C_5-carbon skeleton (i.e. 1,2-H, 1,3-H and 1,5-H shifts); (ii) cyclisation followed by ring opening of the carbon skeleton; and (iii) intermolecular base catalysed proton transfer. The first two possibilities are energetically unfavourable. Given the high degree of unsaturation of the carbon chain, the barriers

involved in forming the strained intermediates and transition states will be considerable. Examples of such rearrangement processes have been investigated computationally and will be discussed in the theoretical section of this Chapter. The third possibility is summarised in Scheme 5.3. This has been discounted by labelling studies which show that isotopic abundances of the product radical anions do not change in the presence of deuterated CI reagent gases in the ion source of the mass spectrometer (i.e. precursors ionised in the presence of either D_2O or H_2O show the same isotopic ratios for each of the $C_5H_2^{\cdot-}$ isomers). Mechanisms for isomerisation are thus either energetically unfavourable or inconsistent with labelling data.* We conclude therefore that the data presented indicates that $HC_5H^{\cdot-}$, $C_4CH_2^{\cdot-}$ and $C_2CHC_2H^{\cdot-}$ are generated as discrete species, and that isomerisation of these species is unfavourable under the experimental conditions.

Scheme 5.3

$$^{-\cdot}C{=}C{=}C{=}C{=}CH_2 \;+\; H_2O \;\rightleftharpoons\; \left[\left(H\overset{\cdot}{C}{=}C{=}C{=}C{=}CH_2\right)^{-}OH\right]$$

$$\mathbf{5^{\cdot-}}$$

$$\rightleftharpoons\; H\overset{\cdot}{C}{=}C{=}C{=}C{=}CH^{-} \;+\; H_2O$$

$$\mathbf{4^{\cdot-}}$$
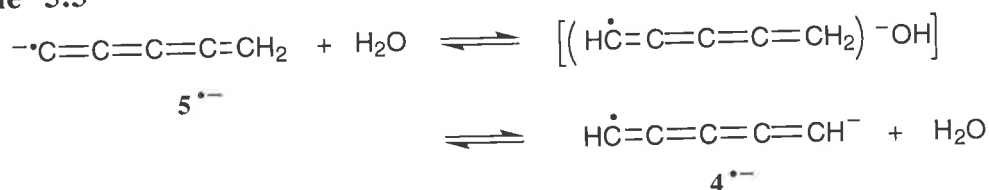
4. Generation of three isomeric C5H2 neutrals by NR

There are abundant peaks corresponding to parent cations (survivor ions) in all of the NR spectra. In addition, the NR and CR spectra of each C_5H_2 radical anion are very similar (Table 5.1 and 5.2). This suggests (i) a structural continuity between anion, neutral and cation, since rearrangement of the neutral during the NR experiment should yield a spectrum quite distinct from that obtained from the vertical CR transition,[25,60,66,68] and (ii) favourable Franck-Condon overlap linking the three surfaces.[58] Therefore as the three radical anions have been shown to be distinct, we propose that the three neutral species **4, 5** and **7** have been generated successfully and that they are stable species on the timescale of the neutralisation reionisation experiment (ca. 10^{-6} s). This is in line with existing theoretical

---

* It is also theoretically possible that isotopic scrambling could occur during the ionisation process itself. For example, the hydroxide or methoxide leaving group may act as a catalyst for proton transfer in an intramolecular process similar to Scheme 5.3. This possibility cannot be rigorously excluded however the spectral data presented indicates that if occurring at all this must be a minor process.

calculations which predict these species to be stable.[193] However it further seems likely that there should be reasonable structural similarity between anions and neutrals for each of these isomers. This hypothesis has been investigated by calculation and the results are discussed in the following section.

B. Theoretical Studies

Energy minima corresponding to $HC_5H^{\bullet-}$, $C_4CH_2^{\bullet-}$ and $C_2CHC_2H^{\bullet-}$ on the radical anion surface are shown in Figures 5.3-5.5 whilst their relative energies, along with those of the corresponding neutrals and cations are summarised in Table 5.3. Consideration of these structures in traditional valence bond terms is by no means trivial as can be seen from the geometries given. Resonance hybrid contributors can be written which give a classic organic chemistry perspective of these species.

Table 5.3 Energies of anions, neutrals and cations of connectivities **4** (HC_5H), **5** (C_4CH_2), **6** (*cyc* -HC_3C_2H), **7** (C_2CHC_2H) and **8** (*cyc* -$H_2C_3C_2$). The energies of **TS5**$^{\bullet-}$/**7**$^{\bullet-}$ and **TS4**$^{\bullet-}$/**6**$^{\bullet-}$ from the radical anion surface are also included.

		Electronic Energy (Hartrees) CCSD(T)/aug-cc-pVDZ//B3LYP/6-31G		Zero-Point Energy† (Hartrees) B3LYP/6-31G	Relative Energies‡ (kcal mol⁻¹)
4$^{\bullet-}$	$^2B_1$	-191.03443		0.03671	12.9
4	$^3\Sigma_g$	-190.98130		0.03928	47.8
4	$^1A_1$	-190.95806		0.03849	61.9
4$^{\bullet+}$	$^2\Pi_g$	-190.68274		0.04161	236.6
5$^{\bullet-}$	$^2B_1$	-191.05879		0.04063	0.00
5	$^1A_1$	-190.97271		0.04187	54.8
5	$^3A''$	-190.93165		0.03948	79.1
5$^{\bullet+}$	$^2A'$	-190.63081		0.04042	268.4
6$^{\bullet-}$		-191.00526		0.04042	32.6
6	$^1A'$	-190.99143		0.04246	43.4
7$^{\bullet-}$	$^2A''$	-191.04789		0.03964	6.2
7	$^1A'$	-190.97136		0.04206	55.8
7	$^3A''$	-190.90262		0.04126	98.4
7$^{\bullet+}$	$^2A'$	-190.58837		0.04273	296.5
8$^{\bullet-}$		-191.00003		0.04012	36.5
8	$^1A_1$	-190.96341		0.04254	61.0
TS5$^{\bullet-}$/**7**$^{\bullet-}$		-190.91523		0.03358	85.8
TS4$^{\bullet-}$/**6**$^{\bullet-}$		-190.94083		0.03320	69.5

† Zero-point energy scaled by 0.9804.[91]
‡ Includes zero-point energy correction.

1. HC_5H

Figure 5.3 *Optimised geometry for the C_5H_2 radical anion isomer* **4**$^{\cdot-}$ *(C_{2v}). Optimisation was carried out at the B3LYP/6-31G level of theory, with bond lengths given in angstroms and angles in degrees.*

The optimised geometry of $HC_5H^{\cdot-}$ is illustrated in Figure 5.3. The C_{2v} structure can be rationalised in terms of the cumulenic valence representation, $[HC=C=C=C=CH]^{\cdot-}$. This is best illustrated by the similarities between adjacent bond lengths, for example the bonds C_1-C_2 and C_2-C_3 are 1.28 Å and 1.31 Å respectively, and also the sp^2 nature of the terminal C_5-H bond lengths (1.08 Å). The slight bending of the carbon chain and the C-C-H bond angle of 138º which is between that expected for sp^2 and sp hybridised carbons, suggests resonance contributions from acetylide species.[*]
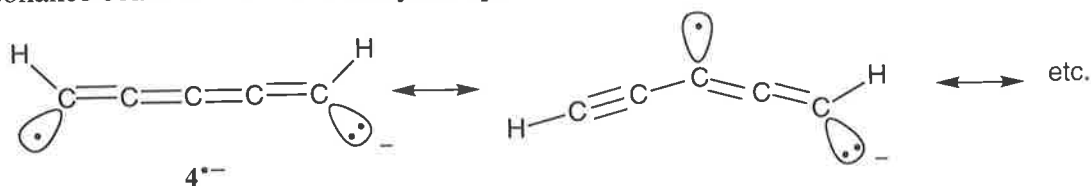
The bent configuration of $HC_5H^{\cdot-}$ contrasts markedly with the linear diyne type structure of the triplet ground state neutral ($^3\Sigma_g$, **4**), where the bonds C_1-C_2 and H-C_1 are 1.25 Å and 1.06 Å, characteristic of sp hybridised carbons. Interestingly, the geometry of the singlet excited state ($^1A'$, **4**) contains both cumulenic and acetylenic functionality. Hence, the geometry of the singlet more closely approximates that of the anion. Due to the fact that, electron transfers in CR and NR experiments can be considered to occur as vertical processes, electron detachment is expected to yield predominantly the excited singlet state of the neutral species.[58] The geometries of all neutrals discussed here are given as appendices to this Chapter (Table 5.4). The B3LYP structures show excellent agreement with the recent work of Seburg and co-workers,[193] who optimised the ground state neutral geometries of

---

[*] It is worth mentioning that the connectivity $HC_5H^{\cdot-}$ lends itself to geometric isomerism, the second isomer is a *trans* -type arrangement with C_2 symmetry. This is also a stable minimum, only 0.33 kcal mol^{-1} less stable than the species shown.

C_5H_2 isomers **4-8** at the CCSD(T) level.* A stable HC_5H radical cation structure has also been identified (Table 5.4). These theoretical predictions are in agreement with the $^-NR^+$ experiments performed: with stepwise oxidation of the HC_5H radical anion producing the neutral and cationic HC_5H species.
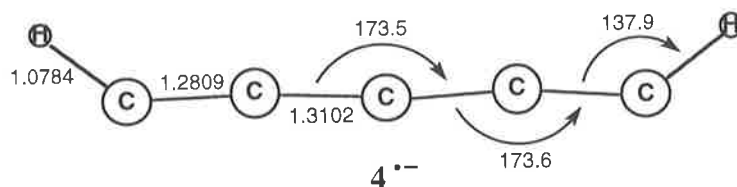
2. C_4CH_2
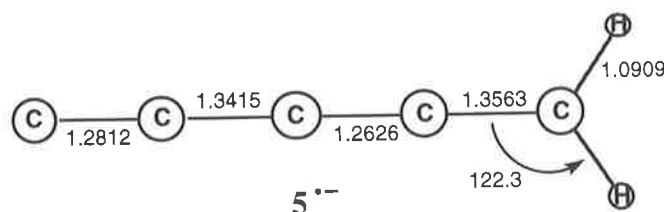
$5^{\cdot-}$

Figure 5.4 *Optimised geometry for the C_5H_2 radical anion isomer $5^{\cdot-}$ (C_{2v}). Optimisation was carried out at the B3LYP/6-31G level of theory, with bond lengths given in angstroms and angles in degrees.*

The optimised structure for $C_4CH_2^{\cdot-}$ is shown in Figure 5.4. The C_{2v} symmetric structure may be described in valence bond terms as a cumulene with the C-H bond lengths and angles, 1.09 Å and 122°, characteristically sp^2. There is an alternation of C-C bond lengths down the carbon chain however which suggests a resonance contribution from a localised acetylide anion hybrid. Both of these resonance contributors point to a HOMO anti-symmetric with respect to the C-C-H plane which is consistent with the predicted $^2B_1$ electronic term.

$5^{\cdot-}$
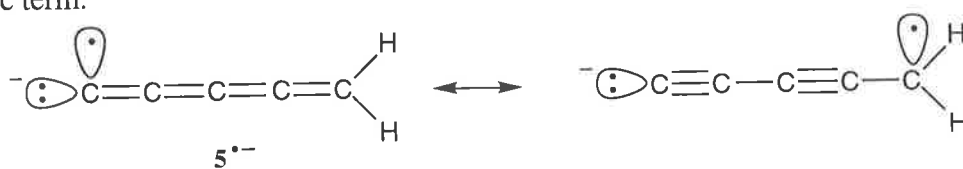
$C_4CH_2^{\cdot-}$ is structurally similar to the corresponding singlet ground state neutral (Table 5.4) indicating that this is highly likely to be accessed in the NR experiment. A C_4CH_2 radical cation structure has also been calculated and shown to be a stable species (Table 5.4). Formed by reionisation of neutral **5**, $C_4CH_2^{\cdot+}$ is the species ultimately detected in the $^-NR^+$

---

* There is a suggestion in the literature that the B3LYP method may not cope well with cumulene/polyacetylene systems such as C_5H_2.[93] We have therefore repeated the geometry optimisations of the three ground state neutrals **4**, **5** and **7** at the MP2/cc-pVDZ level. These data appear as appendices to this Chapter (Table 5.5). It is found however that the B3LYP treatment reported here gives much better agreement with the high level CCSD(T) structures of Seburg and co-workers.[193]

experiment. The relative energies of the anions (Table 5.2) show that $C_4CH_2^{\cdot-}$ is more stable than $HC_5H^{\cdot-}$ by 12.9 kcal mol^{-1} at the level of theory indicated. This is the reversal of the trend for the corresponding neutrals but is similar to that observed previously by Ikuta[132] for the analogous C_3H_2 radical anions, where $C_2CH_2^{\cdot-}$ was found to be more stable than $HC_3H^{\cdot-}$ by 15.8 kcal mol^{-1}.

3. C_2CHC_2H
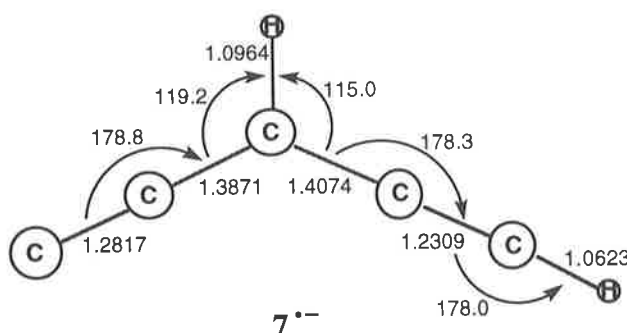
Figure 5.5 *Optimised geometry for the C_5H_2 radical anion isomer 7$^{\cdot-}$ (C_S). Optimisation was carried out at the B3LYP/6-31G level of theory, with bond lengths given in angstroms and angles in degrees.*

The optimised structure for $C_2CHC_2H^{\cdot-}$ is shown in Figure 5.5. This C_S symmetric structure is consistent with valence bond contributions from both localised acetylide as well as cumulenic representations. It is best thought of as an extension of the C_2CH_2 radical anion (3$^{\cdot-}$) where one of the hydrogens is replaced with an acetylide function. These hybrids suggest a HOMO for this ion anti-symmetric with respect to the C_S plane which is consistent with the calculated $^2A''$ electronic term.
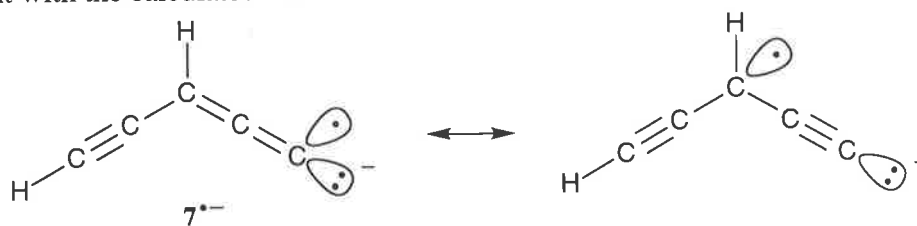
$C_2CHC_2H^{\cdot-}$ is structurally similar to the corresponding singlet ground state neutral (7) and radical cation (7$^{\cdot+}$) indicating favourable overlap between the three potential surfaces. This provides some insight into the successful NR experiments previously described, supporting the proposed gas phase generation of neutral C_2CHC_2H. The geometric data for the ground

state neutral, triplet excited state and radical cation are listed in Table 5.4. The isomer $C_2CHC_2H^{\cdot-}$ is 6.2 kcal mol^{-1} less stable than $C_4CH_2^{\cdot-}$ which makes it a more stable configuration than $HC_5H^{\cdot-}$. This is in contrast to the situation for the corresponding ground state neutrals where the order of stability is $HC_5H > C_4CH_2 \approx C_2CHC_2H$ (Table 5.3). The computational results discussed up to this point allow estimation of the adiabatic electron affinities (EA) of the three neutrals HC_5H, C_4CH_2 and C_2CHC_2H: these are 1.51, 2.38 and 2.15 eV respectively.

4. *cyc-HC₃C₂H and cyc-H₂C₃C₂*

Calculations concerning the C_5H_2 isomers **4**, **5** and **7** demonstrate that all three species have stable anion and neutral structures with similar geometries across both potential surfaces. These theoretical predictions would suggest that all three are ideal targets for a $^-NR^+$ study which is consistent with the experimental data presented. Analogous calculations for the two remaining connectivities, **6** and **8** (see pp 93), which were proposed in the study of Seburg and co-workers, have been performed to ascertain whether these would be suitable candidates for a similar synthetic strategy.[193]
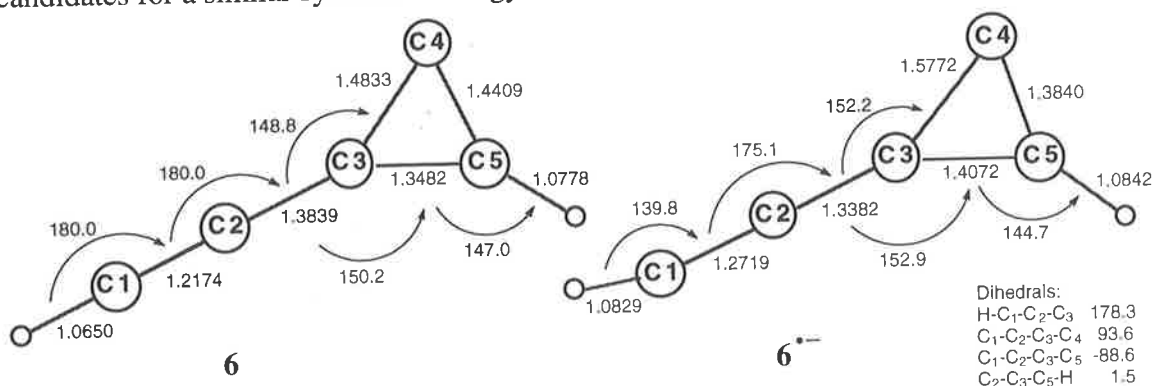
Figure 5.6 *Optimised geometries for the cyclic C_5H_2 isomer **6** (C_S) and the corresponding radical anion isomer **6·⁻** (C_1). Optimisation was carried out at the B3LYP/6-31G level of theory, with bond lengths given in angstroms and angles in degrees.*

In their theoretical study of neutral C_5H_2 isomers Seburg and co-workers demonstrated the surprising stability of the cyclic HC_3C_2H (**6**) structure.[193] Calculated using the RCCSD(T)/aug-cc-pVDZ//B3LYP/6-31G protocol this $^1A'$ species is found to be slightly more stable than ground state HC_5H (**4**, Table 5.3). The predicted structure is given in

Figure 5.6 and may be considered in valence bond terms as an extension of the aromatic *cyc-*

C_3H_2 species (**1**) where one of the hydrogens is substituted for an acetylene moiety.

6
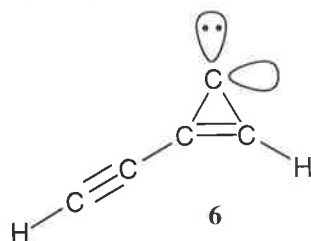
This assignment is borne out by the contracted $H\text{-}C_1$ and $C_1\text{-}C_2$ bond lengths (1.07 and 1.22

Å respectively) which are characteristic of acetylenic functionality and the $C_3\text{-}C_5$ bond length

(1.35 Å) which has double bond character. Such a structure maintains a 2π-electron

population on the C_3-ring which, along with the C_S molecular symmetry, fulfils the

requirements for aromaticity and may hence account for the stability of this isomer. Electron

attachment to this neutral carbene generates a relatively unstable radical anion of C_1

symmetry (Figure 5.6). The bonding environment surrounding C_1 in this structure can be

considered as between sp and sp^2 in nature, given the $H\text{-}C_1\text{-}C_2$ bond angle of 140° and the

lengthened $C_1\text{-}C_2$ bond (1.27 Å). This is best described by the valence contributors shown

below.

6·−
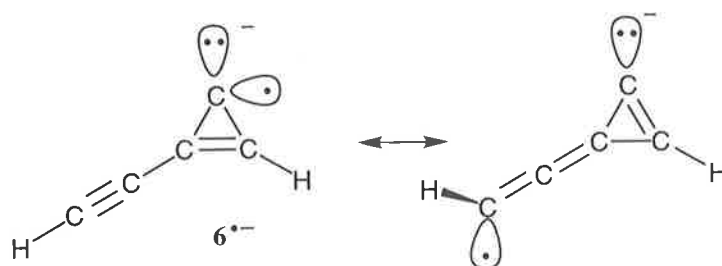
In both cases the π-electron population on the C_3-ring is greater than two and such bonding

representations also rationalise the deviation of this ion from planarity. Thus no aromatic

stabilisation is expected for **6·−**. Energy calculations support this suggestion with *cyc*

$-HC_3C_2H^{·-}$ nearly 33 kcal mol^{-1} less stable than the global minimum $C_4CH_2^{·-}$ and with

electron attachment exothermic by only 0.47 eV.
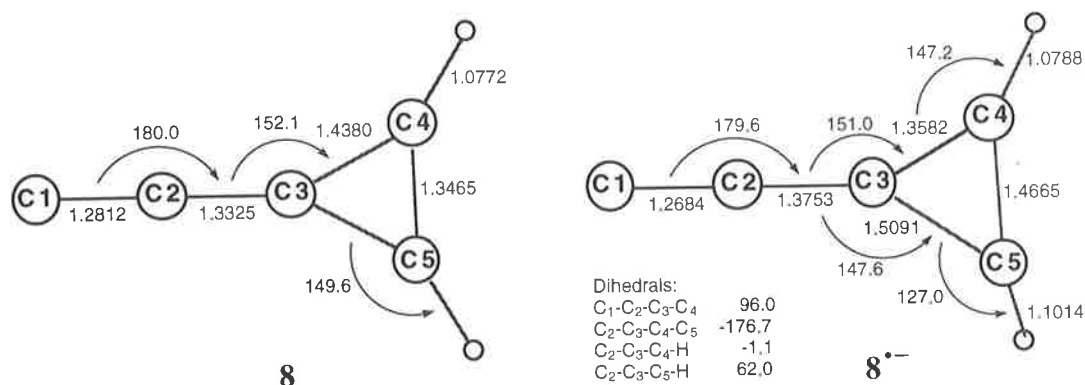
Figure 5.7 *Optimised geometries for the cyclic C_5H_2 isomer 8 (C_{2v}) and the corresponding radical anion isomer 8·⁻ (C_1). Optimisation was carried out at the B3LYP/6-31G level of theory, with bond lengths given in angstroms and angles in degrees.*

The structure of neutral isomer **8** is given in Figure 5.7. This C_{2v} symmetric species has a ground $^1A_1$ electronic state and is calculated to be 13 kcal mol⁻¹ less stable than **4**, making it the least thermochemically stable C_5H_2 neutral carbene discussed thus far (Table 5.3). This instability is due to the ring strain energy of the cyclopropene ring which is not, in this case, offset by significant aromatic stabilisation. The bond lengths C_1-C_2 and C_2-C_3 (1.28 and 1.33 Å respectively) demonstrate little alternation, suggesting allenic carbene character for the carbon chain. This points to extended π-overlap over carbons C_1-C_2-C_3 and hence a π-electron population of > 2 for the C_3-ring.
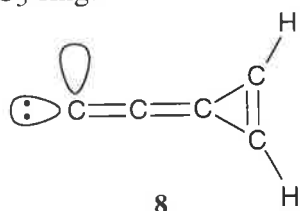
Electron attachment to **8** is exothermic by only 1.06 eV and produces an anion 37 kcal mol⁻¹ less stable than the global minimum on the radical anion potential surface (Table 5.3). The structure of this species is given in Figure 5.7 and a deviation from the planar structure of the neutral is observed. In valence bond terms this can be considered as a resonance hybrid of the following structures.
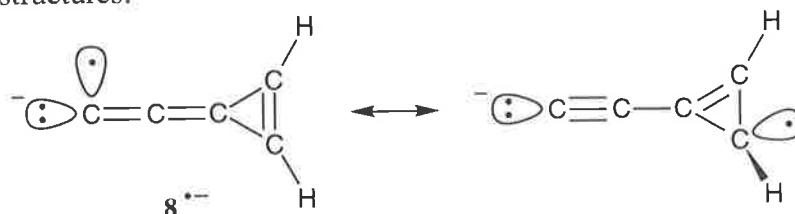
These resonance contributors provide some rationale for the contraction of the C_3-C_4 bond length from single bond character in the neutral carbene (1.44 Å), to double bond character in the radical anion (1.36 Å).

These calculations suggest that the cyclic C_5H_2 isomeric anions $6^{\cdot-}$ and $8^{\cdot-}$ present difficult targets for synthesis in the gas phase, at least by the negative ion methodologies used in this study. For example, extrapolation of the anion syntheses presented for isomers $4^{\cdot-}$, $5^{\cdot-}$ and $7^{\cdot-}$ would suggest a hydroxy-substituted cyclopropene as a suitable precursor for anions $6^{\cdot-}$ and $8^{\cdot-}$ (Scheme 5.4). Assuming similar chemistry, namely carbon-oxygen bond homolysis, facile electron transfer to the nascent OH radical (Scheme 5.4, b) seems the more probable outcome given the low electron affinities of both cyclic C_5H_2 species. Thus a unimolecular reaction such as outlined in Scheme 5.4 is likely to give a greater abundance of hydroxide ions than of the desired radical anion due to the discrepancy in electron affinities (1.36 eV in the case of **6**).[#] On the basis of the theoretical data it appears that the radical anions $6^{\cdot-}$ and $8^{\cdot-}$ would present difficult targets for generation in the gas phase.

Scheme 5.4
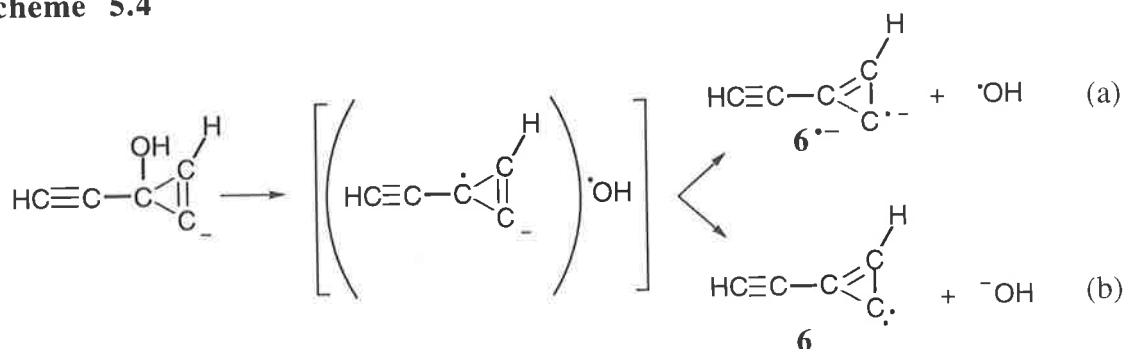
5. *Unimolecular isomerisation pathways*

The possibility of isomerisation of these radical anions has also been investigated computationally. Two typical examples are shown in Scheme 5.5 which represent the two types of processes previously discussed, namely a 1,3-hydride shift (**TS5$^{\cdot-}$/7$^{\cdot-}$**) and a 3-membered ring formation (**TS4$^{\cdot-}$/6$^{\cdot-}$**). The geometries of these transition states appear as

[#] The electron affintiy of the hydroxide ion is reported as 1.827 67 ± 0.000 021 eV.[197]

appendices to this Chapter (Table 5.6). These rearrangements have activation barriers of 85.8 and 56.5 kcal mol^{-1} respectively (Table 5.3), suggesting that these processes are much more energy demanding than electron loss and as such are unlikely to be observed under the experimental conditions.

Scheme 5.5
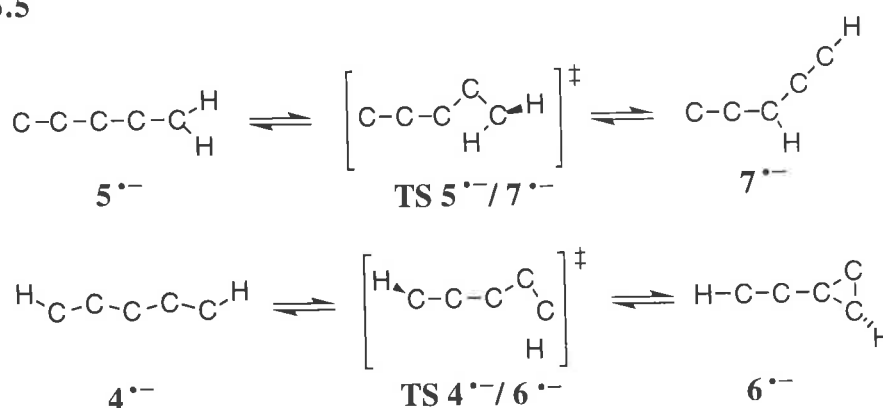
(IV) CONCLUSIONS

Gas phase negative ion chemistry has been shown to be an efficient and structurally sensitive method of generating isomers of C_5H_2 radical anions. The technique of neutralisation reionisation mass spectrometry allows the formation of their neutral counterparts. The radical anions **4$^{•-}$**, **5$^{•-}$** and **7$^{•-}$** have been synthesised in the gas phase and have been shown to have discrete structures. The corresponding neutrals have been generated in NR experiments, with this forming the first reported observation of C_2CHC_2H. The stability of the radical anions **4$^{•-}$**, **5$^{•-}$** and **7$^{•-}$** and the corresponding neutrals has been supported by theoretical calculations indicating these connectivities to be bound on both surfaces. Two further anions **6$^{•-}$** and **8$^{•-}$** have also been investigated theoretically and prove to be much less stable than their open chain counter-parts. These calculations suggest that gas phase synthesis of **6$^{•-}$** and **8$^{•-}$** by the type of methodologies employed in this study would be inefficient. The experimental and theoretical evidence demonstrating the stability of C_5H_2 transient neutrals lends support to their candidacy as possible interstellar species. Further, the large electron affinities of the open chain species **4, 5** and **7** suggests that the corresponding anions may also play a role in the chemistry of these galactic environs.

(V) EXPERIMENTAL SECTION

A. Mass spectrometric methods

CR and NR spectra were measured using a two-sector reversed geometry VG ZAB 2HF spectrometer. This instrument and the typical experimental conditions for NICI, CR and NR experiments have been described in Chapter 1. Specifically however, spectra were generated in the following manner. Samples were placed in glass capillaries which were drawn to a fine point and inserted into the chemical ionisation source *via* the solid inlet probe, in order to produce a measured pressure of 5×10^{-6} Torr, inside the source housing. Typical ionisation conditions were; source temperature, 200°C; ionising energy, 70 eV (tungsten filament); accelerating voltage, -7 kV. All slits were fully open in order to minimise mass discrimination effects due to energy resolution.[46,182] The reagent ions HO⁻, DO⁻ and CH_3O^- were generated respectively from substrates H_2O, D_2O and CH_3OH (introduced through the heated septum inlet) to give an operating pressure inside the source housing of ca. 5×10^{-5} Torr, and thus an estimated pressure inside the ion source of close to 0.1 Torr. Negative ion chemical ionisation of the sample either effected (i) deprotonation or dedeuteration as appropriate, or (ii) desilylation of a neutral trimethylsilated substrate by the method developed by DePuy and coworkers.[10] Neutralisation of the anion beam in the first collision cell was achieved by collision with oxygen gas at a typical pressure of 5×10^{-6} Torr: this reduces the main beam to 80% of its initial value, producing essentially single collision conditions in the collision cell.[183] Residual ions were removed using the deflector electrode, with neutrals passing into the second cell where they were reionised to the corresponding cation under identical conditions to those used in the first cell. The spectra were collected by reversing the polarity of the electric sector voltage and scanning the sector voltage. CR spectra were measured under the same conditions as those used for NR spectra, except that the deflector electrode is grounded. Although this CR method does increase the likelihood of double collisions, it allows direct comparison between NR and CR spectra.[25,60,66,68,#] All spectra were repeated a minimum of three times in order to establish their reproducibility.

Comparison of the NR and CR spectra collected in this way equates to a qualitative NIDD treatment (*cf.* Chapter 1, pp 20).

B. Syntheses of Precursor Molecules

Many of the precursor compounds necessary for this study had not previously been reported. The synthetic procedures employed to prepare them are given in this section.

1. *Methyl (5-trimethylsilyl)penta-2,4-diynyl ether* [$TMSC\equiv CC\equiv CCH_2OCH_3$].

This preparation is described in Chapter 4, pp 86.

2. *[1,1-D$_2$]-5-Trimethylsilylpenta-2,4-diyn-1-ol* [$TMSC\equiv CC\equiv CCD_2OH$][198,199]

[1,1-D$_2$]-5-Trimethylsilylpenta-2,4-diyn-1-ol was prepared by a standard procedure[200] except that [D$_2$]-paraformaldehyde was used in place of the unlabelled reagent. Yield = 83%. D$_2$ > 99%.*

3. *[3-D$_1$]-Penta-1,4-diyn-3-ol* [$HC\equiv CCD(OH)C\equiv CH$].

[3-D$_1$]-Penta-1,4-diyn-3-ol was prepared by a standard procedure[186,187] except that methyl-[D$_1$]-formate was used in place of ethyl formate. Yield = 73%. D$_1$ = 98%.

4. *[1,5-D$_2$]-Penta-1,4-diyn-3-ol* [$DC\equiv CCH(OH)C\equiv CD$].

A solution containing 1,5-bis(trimethylsilyl)penta-1,4-diyn-3-ol[188] (1.5 g) and 18-crown-6 (0.005 g) in anhydrous tetrahydrofuran (20 cm^3) was added dropwise over 0.5 hr to a stirred solution of potassium fluoride (1.0 g) in deuterium oxide (1 cm^3), at 0°C, under a nitrogen atmosphere. The solution was then stirred at 25°C for 12 hr, before being dried (MgSO$_4$). Removal of the solvent *in vacuo* gave [1,5-D$_2$]-penta-1,4-diyn-3-ol (0.31 g, 76% , D$_2$ = 85%).

---

* Polyacetylenes are known to be unstable and potentially explosive hence further purification of these compounds was not attempted unless absolutely necessary.[185]

5. *(1-Trimethylsilyl)penta-1,4-diyn-3-ol* [TMSC≡CCH(OH)C≡CH].

Ethynyl magnesium bromide (0.74 cm^3, 0.5 M in anhydrous tetrahydrofuran), was added dropwise under nitrogen to a stirred solution of (3-trimethylsilyl)propynal[201,202] (0.03 g), in anhydrous tetrahydrofuran (10 cm^3), at 0°C, the mixture stirred for 12 hr at 25°C, cooled to 0°C, quenched with aqueous ammonium chloride (saturated, 10 cm^3) at 0°C, and extracted with diethyl ether (3 x 20 cm^3). The organic extract was washed with water (20 cm^3), sodium chloride (saturated 10 cm^3), dried (MgSO$_4$) and the solvent removed *in vacuo* to yield (1-trimethylsilyl)penta-1,4-diyn-3-ol, (0.03 g, 80%). [M-H$^+$]$^-$ = 151.0565. C$_8$H$_{10}$OSi requires 151.0579. ^{1}H NMR (200 MHz, CDCl$_3$) δ 0.17 (s, 9H), 2.52 (d,1H), 2.90 (br, 1H), 5.10 (d,1H).

6. *Methyl-3-[1,5-bis(trimethylsilyl)]penta-1,4-diynyl ether*

[TMSC≡CCH(OCH$_3$)C≡CTMS].

Freshly distilled dichloromethyl methyl ether (1.61 cm^3) in anhydrous tetrahydrofuran (20 cm^3) was added dropwise to a stirred solution of trimethylsilylethynyl magnesium bromide[188] (7.83 g) in tetrahydrofuran (100 cm^3) over 0.5 hr, at 0°C, under a nitrogen atmosphere and the reaction mixture stirred at 25°C for 12 hr. The reaction was quenched with aqueous ammonium chloride (saturated, 50 cm^3), extracted with diethyl ether (3 x 50 cm^3), the ethereal extract separated, washed with water (20 cm^3), aqueous sodium chloride (saturated, 20 cm^3) and dried (MgSO$_4$). The solvent was removed *in vacuo* and the crude product purified by distillation at reduced pressure (b.p. 76-80°C @ 0.07 Torr) to yield methyl-3-[1,5-bis(trimethylsilyl)]penta-1,4-diynyl ether (1.74 g, 24%). [M$^{·+}$] = 238.1192. C$_{12}$H$_{22}$OSi$_2$ requires 238.1209. ^{1}H NMR (200 MHz, CDCl$_3$) δ 0.19 (s, 18 H), 3.40 (s, 3H), 4.89 (s, 1H).

7. *Methyl-3-[1,5-D$_2$]-penta-1,4-diynyl ether* [DC≡CCH(OCH$_3$)C≡CD].

This preparation was carried out by the same procedure outlined for the corresponding alcohol; using methyl-3-[1,5-bis(trimethylsilyl)]penta-1,4-diynyl ether (0.75 g) gave methyl-3-[1,5-D$_2$]-penta-1,4-diynyl ether (0.17 g, 59% , D$_2$ > 97%).

C. Computational Methods

Geometry optimisations were carried out with the Becke 3LYP method[88,89] using the 6-31G basis within the GAUSSIAN 94 suite of programs.[92] Stationary points were characterised as either minima (no imaginary frequencies) or transition states (one imaginary frequency) by calculation of the frequencies using analytical gradient procedures. The minima connected by a given transition structure were confirmed by intrinsic reaction coordinate (IRC) calculations. The calculated frequencies were also used to determine the zero-point vibrational energies which were then scaled[91] by 0.9804 and used as a zero-point energy correction for the electronic energies calculated at this and higher levels of theory. More accurate energies for the B3LYP/6-31G geometries were determined with the RCCSD(T) method[176-181], using the Dunning aug-cc-pVDZ basis set,[95,96,203] within the MOLPRO package.[94] The described computational method was tested using C_2CH_2 (**3**) giving a computed electron affinity of 1.67eV compared with the experimentally determined 1.794 ± 0.025eV.[128] Calculations involving GAUSSIAN 94 geometry optimisation were carried out using both PC and Unix machines. MOLPRO single point energy calculations were carried out with both the Cray J 932 computer at the Konrad-Zuse-Zentrum (Berlin), and the Power Challenge Super Computer at the Australian National University Super Computing Centre (Canberra).

(VI) APPENDICES

Table 5.4 Optimised geometries for C_5H_2 neutral and radical cation isomers corresponding to the anions of interest. Optimisations performed using the B3LYP/6-31G level of theory. All bond lengths are in angstroms and all angles in degrees.

4 $(D_{\infty h})$ $^3\Sigma_g$

$H-C_1-C_2 \cdot C_3-C_4-C_5-H$

bond length H-C_1 1.0648
C_1-C_2 1.2497
C_2-C_3 1.3111

4 (C_S) $^1A'$

$H_7 \cdot C_1-C_2 \cdot C_3-C_4-C_5 \cdot H_6$

bond length H_7-C_1 1.0808
C_1-C_2 1.2850
C_2-C_3 1.2901
C_2-C_3 1.3251
C_2-C_3 1.2389
H_6-C_5 1.0648

angle H_7-C_1-C_2 135.0
C_1-C_2-C_3 169.4
C_2-C_3-C_4 164.2
C_3-C_4-C_5 177.5
C_4-C_5-H_6 172.8

4 $^{\cdot+}$ $(D_{\infty h})$ $^2\Pi_g$

$H-C_1-C_2 \cdot C_3-C_4-C_5-H$

bond length H-C_1 1.0741
C_1-C_2 1.2466
C_2-C_3 1.3028

5 (C_{2v}) $^1A_1$

$C_1-C_2 \cdot C_3-C_4-C_5 \overset{H}{\underset{H}{\diagup}}$

bond length C_1-C_2 1.2981
C_2-C_3 1.3037
C_3-C_4 1.2726
C_4-C_5 1.3242
C_5-H 1.0891

angle C_1-C_2-C_3 180.0
C_2-C_3-C_4 180.0
C_3-C_4-C_5 180.0
H-C_5-C_4 122.0

5 (C_S) $^3A''$

$C_1-C_2 \cdot C_3-C_4-C_5 \overset{H_6}{\underset{H_7}{\diagup}}$

bond length C_1-C_2 1.3156
C_2-C_3 1.3075
C_3-C_4 1.2764
C_4-C_5 1.3372
C_5-H_6 1.0862
C_5-H_7 1.0862

angle C_1-C_2-C_3 169.4
C_2-C_3-C_4 180.0
C_3-C_4-C_5 180.0
H_6-C_5-C_4 121.4
H_7-C_5-C_4 121.4

5 $^{\cdot+}$ (C_S) $^2A'$

$C_1-C_2 \cdot C_3-C_4-C_5 \overset{H_6}{\underset{H_7}{\diagup}}$

bond length C_1-C_2 1.3401
C_2-C_3 1.2821
C_3-C_4 1.2895
C_4-C_5 1.3178
C_5-H_6 1.0928
C_5-H_7 1.0928

angle C_1-C_2-C_3 170.4
C_2-C_3-C_4 180.0
C_3-C_4-C_5 180.0
H_6-C_5-C_4 121.6
H_7-C_5-C_4 121.6

7 (C_S) $^1A'$

bond length C_1-C_2 1.2955
C_2-C_3 1.3449
C_3-C_4 1.4119
C_4-C_5 1.2181
C_5-H_6 1.0656
C_3-H_7 1.0941

angle C_1-C_2-C_3 179.5
C_2-C_3-C_4 125.0
C_3-C_4-C_5 179.8
H_6-C_5-C_4 179.1
H_7-C_3-C_2 119.3

7 (C_S) $^3A''$

bond length C_1-C_2 1.2367
C_2-C_3 1.3869
C_3-C_4 1.3964
C_4-C_5 1.2244
C_5-H_6 1.0645
C_3-H_7 1.0887

angle C_1-C_2-C_3 179.2
C_2-C_3-C_4 124.0
C_3-C_4-C_5 179.0
H_6-C_5-C_4 179.7
H_7-C_3-C_2 117.8

7 $^{\cdot+}$ (C_S) $^2A'$

bond length C_1-C_2 1.2323
C_2-C_3 1.3817
C_3-C_4 1.3757
C_4-C_5 1.2287
C_5-H_6 1.0733
C_3-H_7 1.0944

angle C_1-C_2-C_3 178.6
C_2-C_3-C_4 124.3
C_3-C_4-C_5 178.2
H_6-C_5-C_4 179.8
H_7-C_3-C_2 118.1

Table 5.5 The optimised geometries of the three ground state neutral C_5H_2 isomers **4**, **5** and **7**. A comparison between the B3LYP/6-31G results discussed in this Chapter, MP2/cc-pVDZ and the CCSD(T)/cc-pVTZ data of Seburg and co-workers.[193]

B3LYP/6-31G	MP2/cc-pVDZ[†]	CCSD(T)/cc-pVTZ
4 $D_{\infty h}$ (triplet ground state) $H-C_1-C_2\cdot C_3-C_4\cdot C_5-H$ bond length $H-C_1$ 1.0648 $\quad C_1-C_2$ 1.2497 $\quad C_2-C_3$ 1.3111	**4** C_{2v} $H-C_1-C_2\cdot C_3-C_4-C_5-H$ bond length H_7-C_1 1.0744 $\quad C_1-C_2$ 1.2304 $\quad C_2-C_3$ 1.3258 angle $H-C_1-C_2$ 179.8 $\quad C_1-C_2-C_3$ 179.8 $\quad C_2-C_3-C_4$ 178.9	**4** $D_{\infty h}$ $H-C_1-C_2\cdot C_3-C_4-C_5-H$ bond length $H-C_1$ 1.0594 $\quad C_1-C_2$ 1.2365 $\quad C_2-C_3$ 1.3079
5 C_{2v} (singlet ground state) $C_1-C_2\cdot C_3-C_4-C_5$ (H, H) bond length C_1-C_2 1.2981 $\quad C_2-C_3$ 1.3037 $\quad C_3-C_4$ 1.2726 $\quad C_4-C_5$ 1.3242 $\quad C_5-H$ 1.0891 angle $C_1-C_2-C_3$ 180.0 $\quad C_2-C_3-C_4$ 180.0 $\quad C_3-C_4-C_5$ 180.0 $\quad H-C_5-C_4$ 122.0	**5** C_S $C_1-C_2\cdot C_3-C_4-C_5$ (H, H) bond length C_1-C_2 1.3027 $\quad C_2-C_3$ 1.3227 $\quad C_3-C_4$ 1.2822 $\quad C_4-C_5$ 1.3406 $\quad C_5-H_6$ 1.0981 $\quad C_5-H_7$ 1.0980 angle $C_1-C_2-C_3$ 179.8 $\quad C_2-C_3-C_4$ 179.9 $\quad C_3-C_4-C_5$ 179.9 $\quad H_6-C_5-C_4$ 121.1 $\quad H_7-C_5-C_4$ 121.2	**5** C_{2v} $C_1-C_2\cdot C_3-C_4-C_5$ (H, H) bond length C_1-C_2 1.2879 $\quad C_2-C_3$ 1.2988 $\quad C_3-C_4$ 1.2655 $\quad C_4-C_5$ 1.3219 $\quad C_5-H$ 1.0803 angle $C_1-C_2-C_3$ 180.0 $\quad C_2-C_3-C_4$ 180.0 $\quad C_3-C_4-C_5$ 180.0 $\quad H-C_5-C_4$ 121.0
7 C_S (singlet ground state) $C_1-C_2-C_3(H_7)-C_4\cdot C_5-H_6$ bond length C_1-C_2 1.2955 $\quad C_2-C_3$ 1.3449 $\quad C_3-C_4$ 1.4119 $\quad C_4-C_5$ 1.2181 $\quad C_5-H_6$ 1.0656 $\quad C_3-H_7$ 1.0941 angle $C_1-C_2-C_3$ 179.5 $\quad C_2-C_3-C_4$ 125.0 $\quad C_3-C_4-C_5$ 179.8 $\quad H_6-C_5-C_4$ 179.1 $\quad H_7-C_3-C_2$ 119.3	**7** C_S $C_1-C_2-C_3(H_7)-C_4\cdot C_5-H_6$ bond length C_1-C_2 1.3019 $\quad C_2-C_3$ 1.3598 $\quad C_3-C_4$ 1.4236 $\quad C_4-C_5$ 1.2368 $\quad C_5-H_6$ 1.0774 $\quad C_3-H_7$ 1.0102 angle $C_1-C_2-C_3$ 178.2 $\quad C_2-C_3-C_4$ 123.4 $\quad C_3-C_4-C_5$ 178.5 $\quad H_6-C_5-C_4$ 178.3 $\quad H_7-C_3-C_2$ 119.9	**7** C_S $C_1-C_2-C_3(H_7)-C_4\cdot C_5-H_6$ bond length C_1-C_2 1.2858 $\quad C_2-C_3$ 1.3372 $\quad C_3-C_4$ 1.4128 $\quad C_4-C_5$ 1.2105 $\quad C_5-H_6$ 1.0595 $\quad C_3-H_7$ 1.0836 angle $C_1-C_2-C_3$ 177.5 $\quad C_2-C_3-C_4$ 124.3 $\quad C_3-C_4-C_5$ 177.9 $\quad H_6-C_5-C_4$ 178.5 $\quad H_7-C_3-C_2$ 119.3

[†] MP2/cc-pVDZ calculations were performed using the GAUSSIAN 94 suite of programs, following the same protocols outlined in the text for the other methods.

Table 5.6 The geometries of the two transition states calculated at the B3LYP/6-31G level of theory. All bond lengths are in angstroms and all angles in degrees.

	TS 5·⁻/7·⁻			TS 4·⁻/6·⁻	

		TS5·⁻/7·⁻			TS4·⁻/6·⁻	
bond length	C_1-C_2	1.3860	bond length	C_1-C_2	1.2552
	C_2-C_3	1.4708		C_2-C_3	1.3487
	C_3-C_4	1.3572		C_3-C_4	1.4299
	C_4-C_5	1.2763		C_4-C_5	1.4212
	C_3-H_6	1.3503		C_5-H_6	1.3077
	C_3-H_7	1.0936		C_3-H_7	1.0712
angle	C_1-C_2-C_3	81.4	angle	C_1-C_2-C_3	175.4
	C_2-C_3-C_4	137.2		C_2-C_3-C_4	149.5
	C_3-C_4-C_5	174.6		C_3-C_4-C_5	75.9
	H_6-C_3-C_2	98.3		H_6-C_5-C_3	52.5
	H_7-C_1-C_2	131.5		H_7-C_1-C_2	150.1
dihedral angle	C_1-C_2-C_3-C_4	132.5	dihedral angle	C_1-C_2-C_3-C_4	-107.1
	C_2-C_3-C_4-C_5	152.8		C_2-C_3-C_4-C_5	-175.6
	H_6-C_3-C_2-C_1	-9.7		H_6-C_5-C_3-C_2	-6.5
	H_7-C_1-C_2-C_3	-124.2		H_7-C_1-C_2-C_3	-169.4

Chapter 6: Gas Phase Syntheses of Three Isomeric C_7H_2 Radical Anions and Their Elusive Neutrals. A Joint Experimental and Theoretical Study.

(I) ABSTRACT

Theoretical calculations predict a number of stable structures for neutral C_7H_2 with some of the more stable geometries possessing the aromatic C_3-ring moiety. Electron attachment to all neutral C_7H_2 isomers produces bound isomeric radical anions. The most stable anion isomers are found to be linear structures which may prove good candidates for formation in the gas phase. Three radical anions, C_6CH_2, $HC_2C(C_2)C_2H$ and $C_2CH_2C_4$, have been synthesised in the gas phase, utilising a range of precursors and NICI techniques. The structures of these ions have been probed by collisional activation and charge reversal mass spectrometric techniques. Neutralisation reionisation experiments confirm the theoretically predicted stability of the corresponding neutrals: this constitutes the first reported observation of these species.

(II) INTRODUCTION

The astrophysical and terrestrial interest in the unsaturated carbenes C_nH_2 (where, $n \leq 7$) has been well documented in this thesis.[#] Both theoretical and experimental studies concerning the odd homologues C_3H_2 and, increasingly, C_5H_2 are prevalent in the literature. By comparison little is known about the C_7H_2 carbenes. C_7H_2 isomers have yet to be detected in interstellar or circumstellar gas clouds[204,205] however models for the chemistry of these regions predict such species to be present in detectable concentrations (although no particular isomer is specified).[206] Further, the C_6CH_2 (**6**) isomer has been proposed as a prime candidate for astrophysical detection due to its predicted dipole moment of more than seven Debye.[108,207]

Scheme 6.1
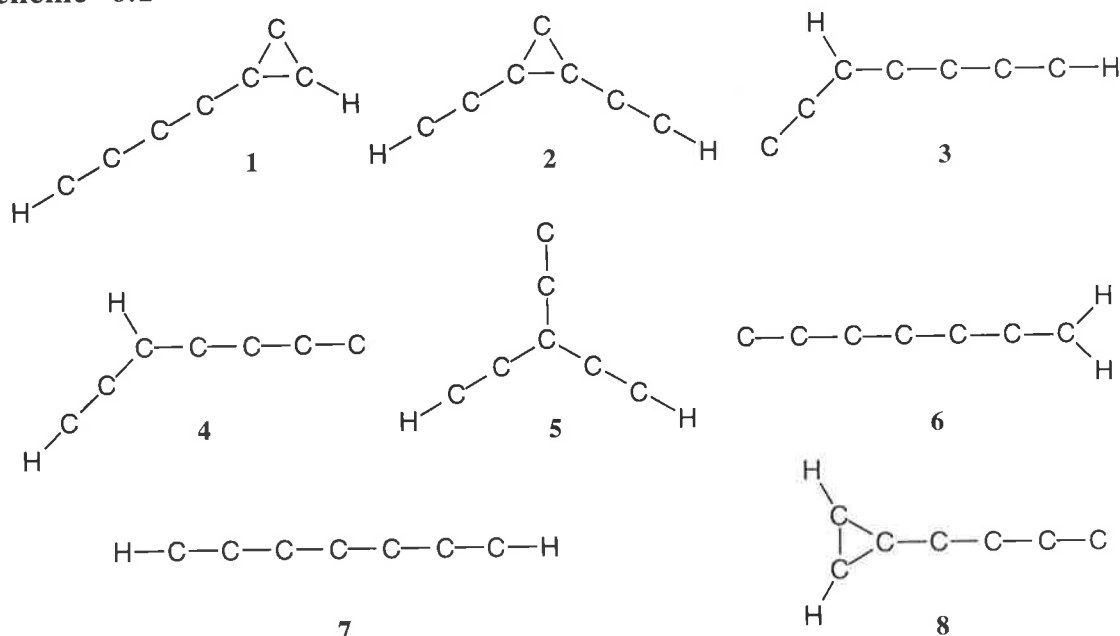
Aoki and Ikuta have calculated the mimum energy structures for a number of the most stable neutral C_7H_2 isomers at the MP2/D95** level of theory.[208] For the connectivities **1-7** (Scheme 6.1) all were found to have singlet ground states with the exception of **7**, the HC$_7$H isomer, which is a linear triplet species. All the ground states were determined to fall within an energy range of less than 22 kcal mol^{-1} (determined by single point energy calculations utilising the ACPF/ANO//MP2/D95** level of theory). The two most stable species were determined to be the C_3-ring chain carbenes **1** and **2**. Both of these have $(4n + 2)$ π-electron

---

[#] See Chapters 3 and 5.

occupation (where n = 0) of the ring, thus aromaticity may account for the stability of these systems. This is perhaps most obvious by consideration of possible valence bond structures of the singlet carbenes **1** and **2**.
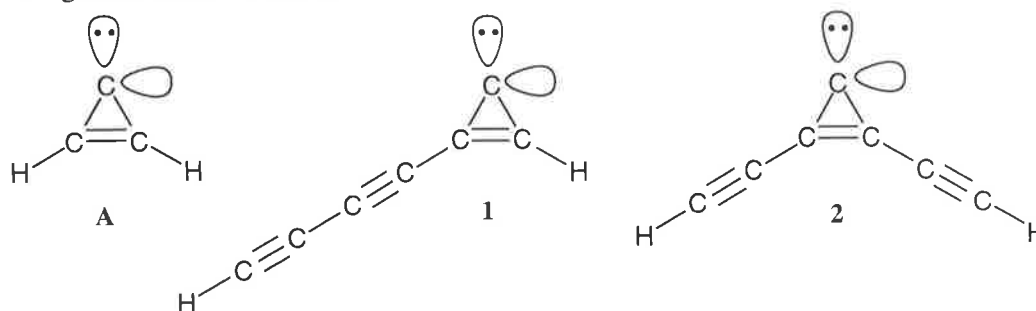
The structures of **1** and **2** may in fact be considered as extensions of aromatic cyclopropenylidene **(A)**[142] with the hydrogens substituted with diacetylene and acetylene respectively. A third C_3-ring chain structure **8** (Scheme 6.1) has also been proposed by some authors, however the relative stability of this species has not been theoretically determined.[209] The energetics of electron attachment and its effect on structure for the species **1-8** has been investigated theoretically and the results are described here. The stability and suitability of these anions as potential precursors to the corresponding neutral carbenes *via* NRMS techniques will be discussed.

Previously, only two C_7H_2 isomers have been detected in the laboratory. (i) Rotational transitions corresponding to the cyclic carbene **1** have been detected in a DC electrical discharge in a neon-diacetylene environment.[209] It is found to be 15 times less abundant than C_5H_2 isomers generated in the same experiment. (ii) The electronic spectrum of HC_7H, **7**, trapped in a low temperature matrix has been recorded and provides evidence for a linear triplet ground state as predicted by theory.[194] The capacity of neutralisation reionisation to generate transient neutral species and in particular unsaturated carbenes in the gas phase has been amply illustrated in this thesis* and by other authors.[153,154] The generation and characterisation of three isomeric C_7H_2 radical anions will be described. NRMS experiments conducted on these provide evidence for the stability of the corresponding neutrals in the gas phase.

---

* See Chapters 4 and 5.

(III) RESULTS AND DISCUSSION

A. Theoretical predictions for C_7H_2 isomers

1. Relative stability of isomeric C_7H_2 neutrals and anions

The neutral C_7H_2 isomers **1-7** were optimised at the economical B3LYP level of theory, with the modest 6-31G(d) basis set. The structures predicted in this way are in excellent agreement with those calculated by Aoki and Ikuta and are given as appendices to this Chapter (Table 6.5).[208] The relative energies of these isomers have been determined using the larger Dunning, aug-cc-pVDZ basis set and are given in Table 6.1. Although the energy trend differs slightly from that previously reported,[208] the isomers **1-6** all fall within 1 eV of each other as demonstrated by these authors. The exception is the linear HC_7H (**7**) isomer which our calculations place some 14 kcal mol^{-1} lower in energy than **1**. Estimation of the electron affinity of HC_7H at this level gives 1.86 eV which is in reasonable accord with the value obtained using a coupled-cluster approach (EA = 1.72 eV, see appendices to this Chapter, Table 6.4). Therefore despite some energy discrepancies between this and previously reported data, the economical B3LYP computational regime seems in accord with high level treatments and is thus sufficient for comparison of C_7H_2 isomers.

Table 6.1 The relative energies of the ground state C_7H_2 neutrals of isomers **1-9** are given here, along with the symmetry and electronic term. With the exception of **7** which is a triplet, all isomers were found to have a singlet ground electronic state. The geometries were optimised at the B3LYP/6-31G(d) level and are given as appendices to this Chapter (Table 6.5). The energies of these species were then recalculated at the same level with the larger aug-cc-pVDZ basis set.

C_7H_2 Isomers	Electronic State (Point Group)	Electronic Energy (Hartrees)	Zero-point Energy (Hartrees)[†]	Relative Energy (kcal mol^{-1})[‡]
1 *cyc* -HC_4C_3H	$^1A'$ (C_S)	-267.69151	0.05261	13.65
2 *cyc* -$HC_2C_3C_2H$	$^1A_1$ (C_{2v})	-267.68456	0.05178	17.51
3 C_2CHC_4H	$^1A'$ (C_S)	-267.67072	0.05252	26.65
4 HC_2CHC_4	$^1A'$ (C_S)	-267.67097	0.05230	26.36
5 $HC_2C(C_2)C_2H$	$^1A_1$ (C_{2v})	-267.65590	0.05115	35.11
6 C_6CH_2	$^1A_1$ (C_{2v})	-267.67825	0.05293	22.17
7 HC_7H	$^3\Sigma_g$ ($D_{\infty h}$)	-267.71051	0.04979	0.00
8 *cyc* -$H_2C_3C_4$	$^1A_1$ (C_{2v})	-267.65971	0.05322	33.99
9 $C_2CH_2C_4$	$^1A'$ (C_S)	-267.57510	0.05128	85.89

[†] ZPE uncorrected

[‡] Relative energy includes ZPE corrected by 0.9804.[91]

2. *cyc-H₂C₃C₄*
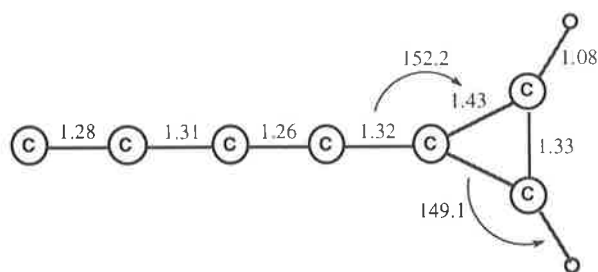
Figure 6.1 *Optimised geometry of neutral C_7H_2 isomer 8 (all bond lengths are given in angstroms and all angles in degrees). The C_{2v} structure is the singlet $^1A_1$ ground state calculated at the B3LYP/6-31G(d) level of theory. The results of energy calculations on this species can be found in Table 6.1.*

The structure of the cyclic C_7H_2 isomer **8** was calculated at the B3LYP/6-31G(d) level. This structure was initially proposed by McCarthy and co-workers[209] who extrapolated from the C_5H_2 calculations of Seburg *et al.* (see in particular structure **8**, Chapter 5, pp 93).[193] The optimised structure of **8** is shown in Figure 6.1 and is found to be more than 15 kcal mol⁻¹ less stable than the other cyclic C_7H_2 isomers, namely **1** and **2** (Table 6.1). Why should **8** be less stable than the other two C_3-carbon ring systems? Some insight can be gained by inspection of the predicted geometry and electronic state of the former species. The linear C_5-carbon chain in this molecule shows little alternation in C-C bond lengths, with all four bonds falling between 1.26 and 1.32 Å. This is characteristic of a cumulenic carbene system with the lone pair of electrons residing on the terminal carbon. Such a valence structure also accounts for the $^1A_1$ electronic term: suggesting a HOMO orbital symmetric to the C-C-H plane of the molecule and symmetrical with respect to the C_2-axis of rotation.
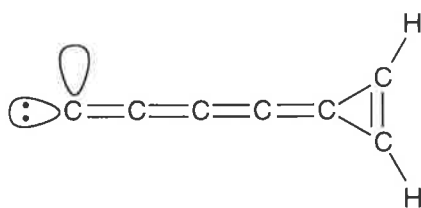
This valence picture points to a π-electron contribution of greater than two on the C_3-ring and consequently no aromatic stabilisation is expected.

3. *cyc-HC₄C₃H and cyc-HC₂C₃C₂H*
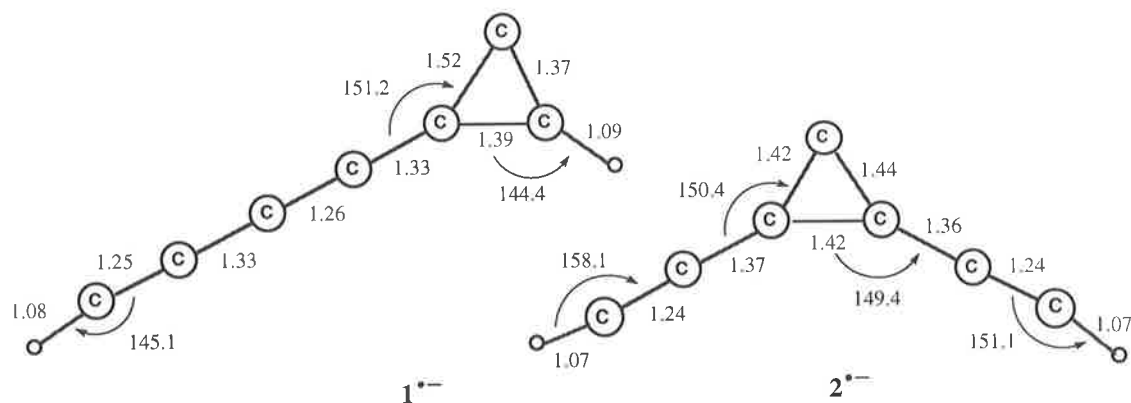
Figure 6.2 *Optimised geomteries of the C₇H₂ radical anion isomers 1·⁻ and 2·⁻ (all bond lengths are given in angstroms and all angles in degrees). The structures are both C₁ and full geometric details including dihedral angles are given as appendices to this chapter (see Table 6.5). Both structures are calculated at the B3LYP/6-31G(d) level of theory. The relative energies for these anions are given in Table 6.2.*

The relative energies of the neutral C_3-ring systems **1**, **2** and **8** illustrate the importance of aromatic stabilisation to these types of molecules. Similar considerations provide a rationale for the relative instability of the anionic species **1·⁻** and **2·⁻** compared with open chain isomers (Table 6.2). Addition of a further electron to the valence structures of singlet neutrals **1** and **2** (illustrated previously) suggests three π-electrons populating the C_3-ring. The calculated geometries of **1** and **2** are shown in Figure 6.2 and demonstrate a marked deviation from planarity which can be depicted in valence bond terms as a series of resonance hybrids.

$2^{\bullet-}$
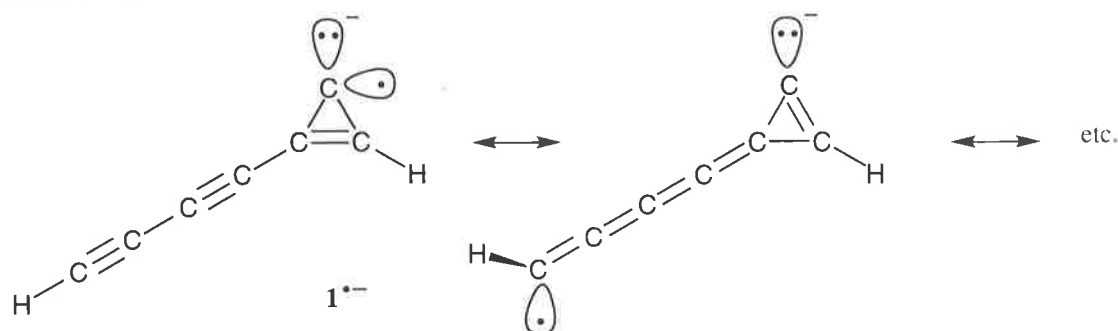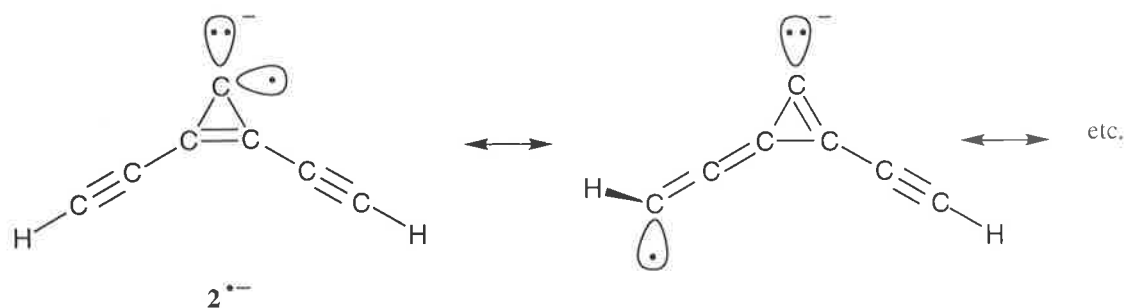
All of these contributing structures have either three or four π-electrons on the C_3-ring. Further, the predicted geometries show the C_3-rings to be non-planar. Consequently these cyclopropenyl systems with (i) more than 2π-electrons and (ii) lack of planarity, possess no aromatic stabilisation to compensate for the large ring strain energy. As a result the ring containing anions $1^{\bullet-}$, $2^{\bullet-}$ and also $8^{\bullet-}$ are at least 30 kcal mol^{-1} more positive in energy than the open chain global minimum on the C_7H_2 radical anion potential surface (Table 6.2). Therefore despite the stability of the neutral cyclic C_7H_2 isomers their relatively low propensity for electron attachment suggests that the anions may be difficult to form in the gas phase.

Table 6.2 The relative energies of the ground state C_7H_2 radical anions of isomers **1-9** are given here, along with the symmetry and electronic term. The geometries were optimised at the B3LYP/6-31G(d) level and are given as appendicies to this Chapter (Table 6.5). The energies of these species were then recalculated at the same level with the larger aug-cc-pVDZ basis set.

C_7H_2 Isomers	Electronic State (Point Group)	Electronic Energy (Hartrees)	Zero-point Energy (Hartrees)[†]	Relative Energy (kcal mol^{-1})[‡]
$1^{\bullet-}$ cyc -HC_4C_3H	(C_1)	-267.74078	0.04934	29.87
$2^{\bullet-}$ cyc -$HC_2C_3C_2H$	(C_1)	-267.72606	0.04730	37.85
$3^{\bullet-}$ C_2CHC_4H	(C_1)	-267.76903	0.05045	12.82
$4^{\bullet-}$ HC_2CHC_4	$^2A''$ (C_s)	-267.77685	0.05025	7.79
$5^{\bullet-}$ $HC_2C(C_2)C_2H$	$^2B_1$ (C_{2v})	-267.75364	0.04827	21.14
$6^{\bullet-}$ C_6CH_2	$^2B_1$ (C_{2v})	-267.79110	0.05211	0.00
$7^{\bullet-}$ HC_7H	$^2B_1$ (C_{2v})	-267.77781	0.04886	6.34
$8^{\bullet-}$ cyc -$H_2C_3C_4$	(C_1)	-267.72191	0.05103	42.75
$9^{\bullet-}$ $C_2CH_2C_4$	$^2A'$ (C_s)	-267.69990	0.05202	57.17
TS4/9$^{\bullet-}$	(C_1)	-267.630596	0.04624	97.10

[†] ZPE uncorrected

[‡] Relative energy includes ZPE corrected by 0.9804.[91]

4. C_6CH_2 and HC_7H

By comparison with the ring containing structures the linear C_6CH_2 (**6**) and HC_7H (**7**) species form relatively stable anions (Table 6.2). In fact the former represents the global minimum on the C_7H_2 radical anion potential surface whilst the latter is less than 7 kcal mol^{-1} higher in energy. This energy trend is analogous to that observed in theoretical studies of isomeric C_3H_2 and C_5H_2 radical anions. $C_2CH_2{}^{\cdot-}$ is calculated to be 15.8 kcal mol^{-1} more stable than $HC_3H^{\cdot-}$ whilst $C_4CH_2{}^{\cdot-}$ is predicted to be 12.9 kcal mol^{-1} more stable than $HC_5H^{\cdot-}$.[146,210,#] The predicted structures of the radical anions **6** and **7** are shown in Figure 6.3 and may be considered as simple extensions of the corresponding $C_5H_2{}^{\cdot-}$ isomers discussed in Chapter 5.
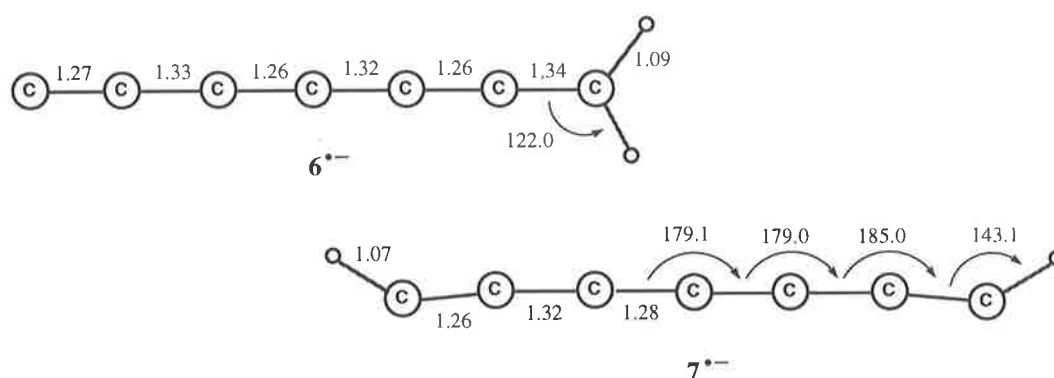
Figure 6.3 *Optimised geometries of the C_7H_2 radical anion isomers **6**$^{\cdot-}$ and **7**$^{\cdot-}$ (all bond lengths are given in angstroms and all angles in degrees). The structures both possess C_{2v} symmetry and full geometric details are given as appendices to this Chapter (see Table 6.5). Both structures are calculated at the B3LYP/6-31G(d) level of theory. The relative energies for these anions are given in Table 6.2.*

The ion $C_6CH_2{}^{\cdot-}$ (**6**) has a strictly linear carbon chain with only minor alternation between C-C bond lengths (between 1.26 and 1.34 Å) and a C-C-H bond angle of 122° characteristic of an sp^2 hybridised carbon. This suggests a cumulenic structure in valence bond terms with some resonance contribution from a polyacetylenic species. Both contributors point to a HOMO anti-symmetric to the C-C-H plane which is consistent with the predicted $^2B_1$ state.
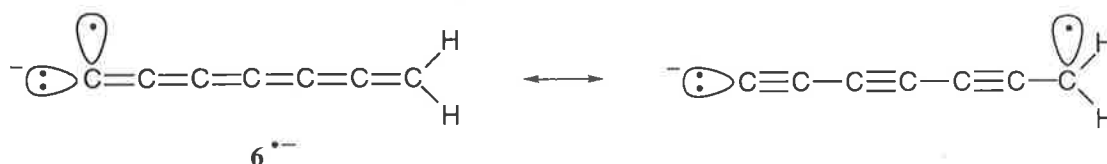
See also Table 5.3, pp 104.

The predicted structure of $HC_7H^{\cdot-}$ (**7**) initially seems unusual, however it is very similar to the corresponding HC_5H structure. In particular, the C-C-H bond angle of approximately 140° is common to both calculated $HC_7H^{\cdot-}$ and $HC_5H^{\cdot-}$ geometries. This angle falls between that anticipated for typical sp^2 (ca. 120°) and sp (ca. 180°) hybrised carbons. Therefore in valence bond terms, $HC_7H^{\cdot-}$ can be viewed as a resonance hybrid incorporating both acetylenic and allenic functionality.
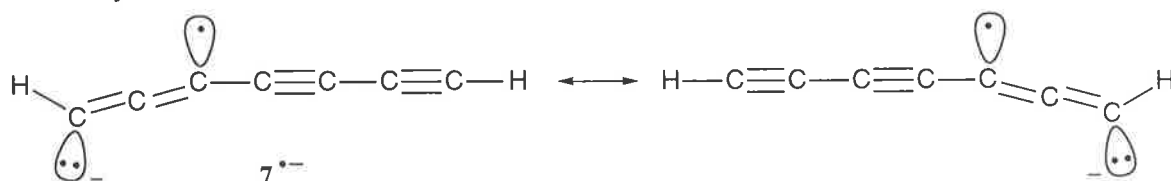
The structural isomers **6** and **7** are predicted to be stable as anions and neutrals and consequently both present good targets for generation in the mass spectrometer. There is also favourable Franck-Condon overlap between the anion, neutral and cation potential surfaces of both these connectivities. The predicted structures for C_6CH_2 (i) radical anion, (ii) singlet and triplet neutral# and (iii) radical cation# are strikingly similar. It is therefore anticipated that neutralisation of $C_6CH_2^{\cdot-}$ should efficiently generate neutral C_6CH_2 in both spin states# and subsequent reionisation should yield the corresponding cation. The ground state HC_7H neutral is calculated to be a linear triplet species with this geometry in contrast to the bent C_{2v} structure of the radical anion already discussed. HC_7H also possess a singlet neutral electronic state# of higher energy than the triplet and with an equilibrium geometry closer to the bent C_{2v} structure of the anion. In a $^-NR^+$ experiment the singlet neutral would be preferentially formed due to Franck-Condon factors, however the internal energy of the incident anion makes the production of the triplet also plausible. Interestingly, of the two neutral spin states the triplet should be more efficiently reionised to the cation as this species also possess a linear $D_{\infty h}$ geometry (see appendices to this Chapter, Table 6.6).

5. C_2CHC_4H, HC_2CHC_4 and $C_2CH_2C_4$

The radical anions of structures C_2CHC_4H (**3**) and HC_2CHC_4 (**4**) are calculated to be stable, only 12.8 and 7.8 kcal mol^{-1} respectively above the global minimum (structures and

---

Calculated structures for excited state neutrals and ground state cations are given as appendices to this Chapter (Table 6.6).

relative energies of these species are given in Tables 6.2 and 6.5). Conceptually these species are simply chain extensions of the C_2CHC_2H radical anion discussed in Chapter 5. By contrast, placing both hydrogens onto the C_3-position generates the rather unstable $C_2CH_2C_4$ (**9**) radical anion which is nearly 60 kcal mol^{-1} more energetic than C_6CH_2·¯ (structure and relative energy of this species are given in Tables 6.2 and 6.5). The instability in this structure arises.from the disruption of the π-overlap caused by an sp^3 carbon at the C_3-position. This is best illustrated by the valence bond structure which necessarily possess an unstable radical acetylide moiety.
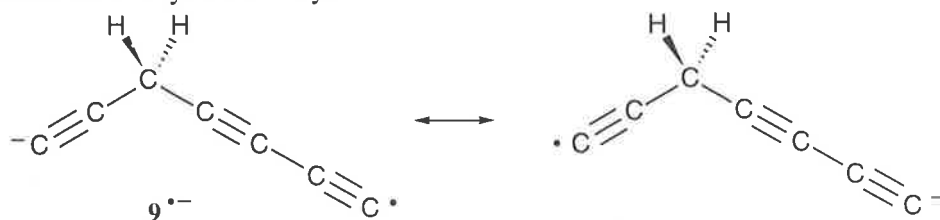
This species provides an interesting target for experimental studies. It poses a number of questions: (i) is it possible to generate such an anion in the mass spectrometer? (ii) Will such an unstable anion maintain its structure or rearrange to a more energetically favourable connectivity? (iii) Can the very unstable neutral **9** be formed from this anion (see Table 6.1)? If this anion can be generated experimentally and is shown to maintain its structure this suggests that other, perhaps more significant, species may be pursued from their negative ions. For example the cyclic geometries **1**·¯, **2**·¯ and **8**·¯ already discussed are all calculated to be more stable than **9**·¯. The ground state neutral **9** is also rather unstable with a calculated energy some 70 kcal mol^{-1} above the cyclic aromatic neutral **1** (Table 6.1). Interestingly this species is found to adopt a C_3-ring structure upon optimisation, producing quite a different geometry to that of the corresponding radical anion (for structural details see appendicies to this Chapter, Table 6.5). It seems therefore that vertical oxidation of the anion, as would be achieved in a ¯NR$^+$ experiment, would most likely produce the triplet neutral species which shares its open-chain geometry and is only 5 kcal mol^{-1} above the singlet (Table 6.4).# The triplet neutral should be efficiently reionised to the corresponding cation# which has a very similar structure.

Calculated structures for excited state neutrals and ground state cations are given as appendices to this Chapter (Table 6.6).

6. $HC_2C(C_2)C_2H$
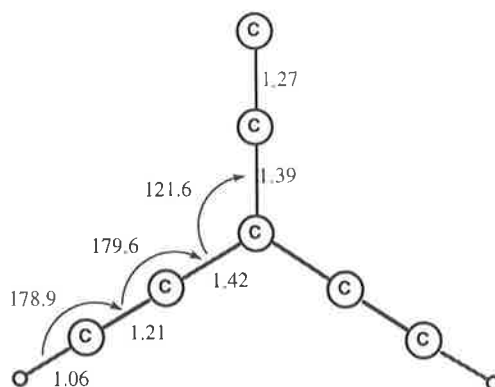
Figure 6.4 *Optimised geomtery of the $HC_2C(C_2)C_2H$ (5) radical anion (all bond lengths are given in angstroms and all angles in degrees). The structure is C_{2v} symmetric and full geometric details are given as appendices to this Chapter (Table 6.5). Calculated at the B3LYP/6-31G(d) level of theory. The relative energy for this anion compared with other C_7H_2·⁻ species is given in Table 6.2.*

The possibility of branched structures such as $HC_2C(C_2)C_2H$ (**5**) arises with C_7H_2 isomers. The calculated structure of **5**·⁻ is given in Figure 6.4 and shows C_{2v} symmetry. The C-C-H bond angles are nearly 180° and the corresponding bond lengths, r(C-C) = 1.22 Å and r(C-H) = 1.06 Å. These data are consistent with pure acetylenic functionality, whilst the remaining C-C bond lengths of 1.39 Å and 1.27 Å suggest a resonance hybrid of allenic and propynyl radical anions.
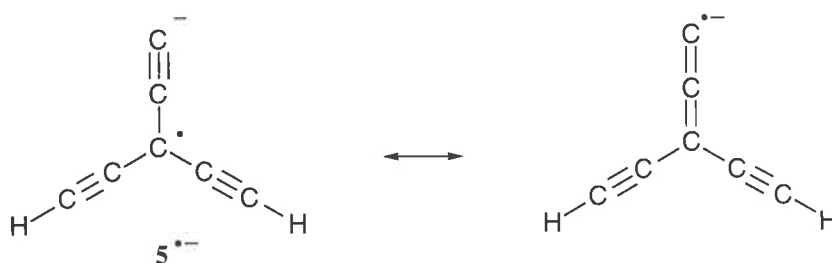
The ion **5**·⁻ is calculated to be some 21 kcal mol⁻¹ less stable than the global minimum on the radical anion potential surface, with the singlet ground state neutral also 21 kcal mol⁻¹ more energetic than the cyclic aromatic neutral **1** (Tables 6.1 and 6.2). Consequently, $HC_2C(C_2)C_2H$ (**5**) would seem a realistic target for synthesis in the gas phase *via* a negative ion pathway. Further, the predicted structures for $HC_2C(C_2)C_2H$ (i) radical anion, (ii) singlet and triplet neutral# and (iii) radical cation# are strikingly similar. It is therefore

---

Calculated structures for excited state neutrals and ground state cations are given as appendices to this Chapter (Table 6.6).

anticipated that neutralisation of $HC_2C(C_2)C_2H^{\cdot-}$ should efficiently generate neutral $HC_2C(C_2)C_2H$ in both spin states and subsequent reionisation should yield the corresponding cation.

B. Syntheses of C_7H_2 isomers

1. *Gas phase syntheses of isomeric C_7H_2 radical anions*

It has been previously demonstrated that the acetylide anions $^-C\equiv CCH_2OCH_3$ and $^-C\equiv CC\equiv CCH_2OCH_3$ decompose by loss of the methoxide radical in the source of the mass spectrometer, to generate the radical anions $C_2CH_2^{\cdot-}$ and $C_4CH_2^{\cdot-}$ respectively.[143,152] It seems reasonable to anticipate therefore that the triyne anion $^-C\equiv CC\equiv CC\equiv CCH_2OCH_3$ should behave in a similar manner. This ion was formed by (i) desilylation of the trimethylsilylated heptatriyne, $TMSC\equiv CC\equiv CC\equiv CCH_2OCH_3$ and (ii) dedeuteration of the labelled precursor $DC\equiv CC\equiv CC\equiv CCH_2OCH_3$. In both cases an abundant peak corresponding to the anion *m/z* 86 was detected in the source of the mass spectrometer which must correspond to the C_6CH_2 radical anion (**6**$^{\cdot-}$). The mechanism for this formation is likely the homolytic cleavage of the carbon oxygen bond (Scheme 6.2)

Scheme 6.2

$$TMSC\equiv CC\equiv CC\equiv CCH_2OCH_3 \; + \; ^-OH \; \rightarrow \; ^-C\equiv CC\equiv CC\equiv CCH_2OCH_3 \; + \; TMSOH$$

$$DC\equiv CC\equiv CC\equiv CCH_2OCH_3 \; + \; ^-OH \; \rightarrow \; ^-C\equiv CC\equiv CC\equiv CCH_2OCH_3 \; + \; DOH$$

$$^-C\equiv CC\equiv CC\equiv CCH_2OCH_3 \; \rightarrow \; ^-C\equiv CC\equiv CC\equiv CCH_2^{\cdot} \; + \; CH_3O^{\cdot}$$
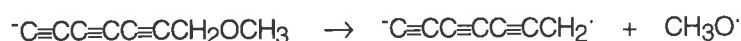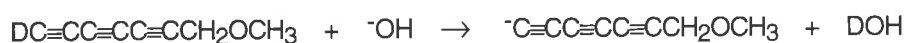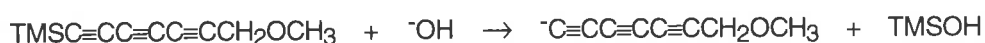
Attempts were made to prepare the HC_7H radical anion (**7**$^{\cdot-}$) in the gas phase by the analogous pathway to that used for the corresponding, $HC_5H^{\cdot-}$ isomer.* That is, dedeuteration of the labelled heptatriyne precursor, $HC\equiv CCD(OH)C\equiv CC\equiv CH$ followed by homolytic cleavage of the carbon oxygen bond as shown in Scheme 6.3. Unfortunately this precursor proved to be unstable and could not be synthesised.

---

* See Chapter 5, pp 96.

Scheme 6.3

$$HC{\equiv}CCD(OH)C{\equiv}CC{\equiv}CH \; + \; {}^-OH \; \rightarrow \; [HC{\equiv}CC(OH)C{\equiv}CC{\equiv}CH]^- \; + \; DOH$$

$$[HC{\equiv}CC(OH)C{\equiv}CC{\equiv}CH]^- \; \rightarrow \; [HC{\equiv}CCC{\equiv}CC{\equiv}CH]^{\cdot-} \; + \; HO^\cdot$$
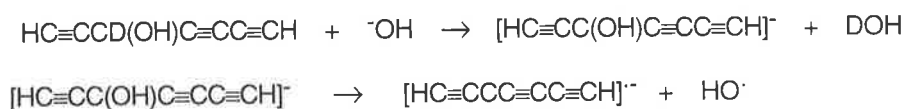
The branched $HC_2C(C_2)C_2H$ radical anion (**5**$^{\cdot-}$) is formed by a very similar methodology to that described above. The precursor for this anion is 3-ethynyl penta-1,4-diyn-3-ol or more commonly triethynyl methanol. Deprotonation of this species at one of the terminal positions, under NICI conditions, yields an acetylide ion which readily loses the hydroxide moiety as a radical in the source of the mass spectrometer to form the $HC_2C(C_2)C_2H$ radical anion (Scheme 6.4).

Scheme 6.4

$$(HC{\equiv}C)_3COH \; + \; {}^-OH \; \rightarrow \; (HC{\equiv}C)_2C(OH)C{\equiv}C^- \; + \; HOH$$

$$(HC{\equiv}C)_2C(OH)C{\equiv}C^- \; \rightarrow \; [(HC{\equiv}C)_2CC{\equiv}C]^{\cdot-} \; + \; HO^\cdot$$
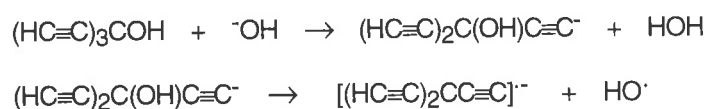
The least stable of these C_7H_2 radical anion isomers, namely $C_2CH_2C_4$ (**9**$^{\cdot-}$) was formed using the so-called "double-desilylation" method devised by Squires and co-workers.[26,27] The bistrimethylsilyl heptatriyne precusor, $TMSC{\equiv}CCH_2C{\equiv}CC{\equiv}CTMS$, was prepared and reacted in the gas phase with the sulphur hexafluoride radical anion which acts as the NICI reagent. The mechanism for this process is not fully established but it seems likely to proceed by the stepwise process outlined in Scheme 6.5. A large source formed peak at *m/z* 86 is observed under these conditions and may be assigned as the radical anion of isomer **9** provided that no rearrangement process accompanies or follows the formation of this ion.

Scheme 6.5

$$TMSC{\equiv}CCH_2C{\equiv}CC{\equiv}CTMS \; + \; SF_6{}^{\cdot-} \; \rightarrow \; [TMSC{\equiv}CCH_2C{\equiv}CC{\equiv}C^- \, (SF_5{}^\cdot)] \; + \; TMSF$$

$$[TMSC{\equiv}CCH_2C{\equiv}CC{\equiv}C^- \, (SF_5{}^\cdot)] \; \rightarrow \; [(TMSC{\equiv}CCH_2C{\equiv}CC{\equiv}C^\cdot)SF_5{}^-]$$

$$[(TMSC{\equiv}CCH_2C{\equiv}CC{\equiv}C^\cdot)SF_5{}^-] \; \rightarrow \; {}^-C{\equiv}CCH_2C{\equiv}CC{\equiv}C^\cdot \; + \; SF_4 \; + \; TMSF$$
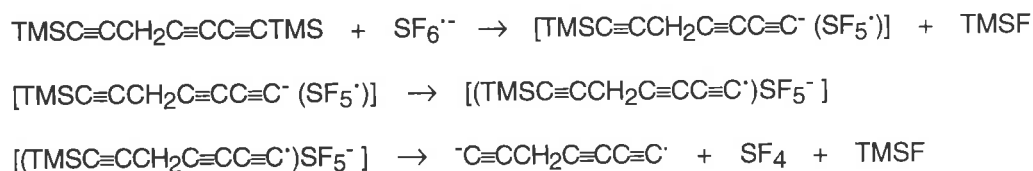
2. Characterisation of isomeric C_7H_2 radical anions by charge reversal

With the exception of the double desilylation approach these methods of forming radical anions have been thoroughly investigated for the C_5H_2 system (*cf.* Chapter 5). Some confidence can therefore be placed in the structural assignments of the C_7H_2 isomers **5**$^{\bullet-}$ and **6**$^{\bullet-}$. Similarly, the gas phase synthesis of **9**$^{\bullet-}$ is also straight forward. Comparison of the charge reversal (CR) spectra of the *m/z* 86 ions from the various precursors may however reveal more information regarding the connectivity of the anions. These spectra are shown in Figure 6.5 and are at first inspection notably different from each other. This points to the fact that at the very least these ions are structurally distinct species. A more thorough analysis reveals that the observed fragmentations can be attributed to the structure of the ions.

Consider first the branched $HC_2C(C_2)C_2H$ (**5**$^{\bullet-}$) radical ion (Figure 6.5, a). Aside from the ubiquitous loss of H$^{\bullet}$ the major fragment ion in the charge reversal spectrum corresponds to loss of C_2H (*m/z* 61). This seems consistent with the assigned structure: cleavage of the C-C single bond connecting one of the acetylide moieties to the central carbon should require less energy compared with disruption of the multiple bonding in this system. Further, the linear C_5H^+ ion (*m/z* 61) which is the product of this decompostion is known to be stable from previous work discussed in this thesis (*cf.* Chapter 4).

By comparison, the CR spectrum of the C_6CH_2 (**6**$^{\bullet-}$) radical anion shows a more sequential decrease in the abundance of peaks corresponding to fragment ions. That is, the C_6H^+ (*m/z* 73) fragment ion is more intense than the C_5H^+ ion (*m/z* 61) which is in turn more intense than C_4H^+ (*m/z* 49). This trend would be consistent with a linear structure with reasonably homogenous C-C bonding throughout, as is the case for the assigned C_6CH_2 geometry of this ion. Interestingly, this spectrum shows very weak signals corresponding to $C_nH_2^{\bullet+}$ ions (where n = 3-6) which proved characteristic of the corresponding C_4CH_2 radical anion (*cf.* Figure 5.2, pp 101). The CR spectrum of C_6CH_2 shows more pronounced losses of H$^{\bullet}$ and 2H$^{\bullet}$ from the parent species than those observed for C_4CH_2. Hence a greater
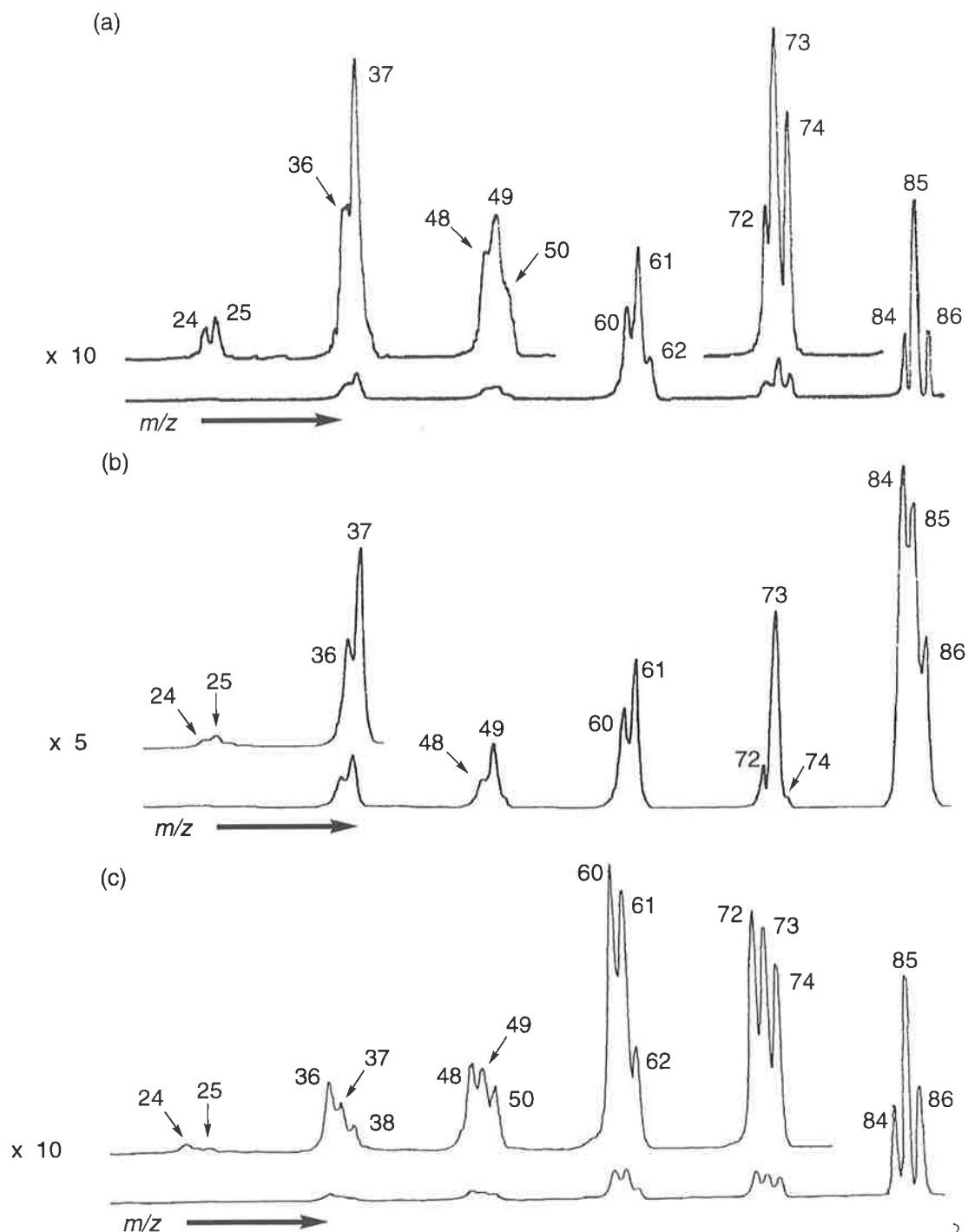
Figure 6.5 $^-CR^+$ *(O_2, 80% T; O_2 80% T) spectra of m/z 86 from (a) $(HC\equiv C)_3^? COH$, giving $HC_2C(C_2)C_2H^{\cdot-}$ (**5$^{\cdot-}$**), (b) $DC\equiv CC\equiv CC\equiv CCH_2OCH_3$, giving $C_6CH_2^{\cdot-}$ (**6$^{\cdot-}$**) and (c) $TMSC\equiv CCH_2C\equiv CC\equiv CTMS$, giving $C_2CH_2C_4^{\cdot-}$ (**9$^{\cdot-}$**).*

proportion of secondary fragmentation arising from decomposition of $C_7^{\cdot+}$ and C_7H^+ cations may contribute to the spectrum of the former. This would result in an increase in the intensity of signals due to C_nH^+ and C_n^+ (where n= 3-6) fragment ions and thus some

rationale for the lack of uniformity between C_6CH_2 and C_4CH_2 spectra. It appears therefore that there are some differences in the unimolecular behaviour of the homologues C_6CH_2 and C_4CH_2. Further evidence of this is the observation of fragment ions in the negative ion CA spectrum of C_6CH_2 whereas no such fragments are observed for the C_4CH_2 system (Table 6.3). These spectra will be discussed in the subsequent section.

The assignment of the $C_2CH_2C_4$ (**9**$^{•-}$) structure to the C_7H_2 radical anion which results from the reaction of (1,7-bistrimethylsilyl)hepta-1,4,6-triyne and $SF_6^{•-}$ is perhaps the most difficult to confirm given the predicted instability of this anion. The charge reversal spectrum of this ion does however tend to support the ion-chemistry assignment (Figure 6.5, c). The spectrum, in the first instance, is notably different from those of the other two C_7H_2 isomers which suggests that if the unstable ion has rearranged, it has not undergone major rearrangement to either of the more stable configurations which have been independently synthesised. The second significant feature of this spectrum is the relatively high abundance of peaks corresponding to $C_nH_2^{•+}$ and $C_n^{•+}$ (where n = 3-6) fragment ions. This trend is unique to this spectrum and whilst it is not easy to attribute it directly to the $C_2CH_2C_4$ structure the following observations can be made: (i) a predominance of $C_nH_2^{•+}$ fragments has been shown, at least in C_5H_2 systems, to indicate the presence of the CH_2 methylene moiety and (ii) large peaks corresponding to $C_n^{•+}$ fragments (compared with $C_nH_2^{•+}$ and C_nH^+ ions) are unusual in both C_7H_2 and C_5H_2 systems. Such pronounced fragments point to an instability in the parent species as multiple fragmentations are generally required to yield naked carbon chains. Both these observations are consistent with the assigned $C_2CH_2C_4$ (**9**$^{•-}$) structure, however it must be stressed that such CR fragmentation behaviour may not be unique to $C_2CH_2C_4$. Even so, further evidence in the form of collisional activation and theoretical results are presented in the two subsequent sections which are also consistent with the $C_2CH_2C_4$ assignment of structure.

Table 6.3 Collisional activation (CA), charge reversal (CR) and neutralisation reionisation (NR) spectra for the $C_7H_2^{\cdot-}$ isomers.

Precursor and C_7H_2 isomer	Fragmentations: *m/z* (intensity relative to base peak)[†]
m/z 86 from $(HC\equiv C)_3COH$ **5**$^{\cdot-}$, $HC_2C(C_2)C_2H^{\cdot-}$	**CA** 86, 85(100), 84(56), 73(63), 72(67), 61(48), 60(44), 49(28). **CR** 86(44), 85(100), 84(84), 74(13), 73(22), 72(9), 62(22), 61(78), 60(47), 50(4), 49(9), 48(7), 37(13), 36(9), 25(2), 24(1.5). **NR**[‡] 86(56), 85(90), 84(100), 74(23), 73(37), 61(77), 60(76), 50(21), 49(43), 48(32), 37(22), 36(21).
m/z 86 from $DC\equiv CC\equiv CC\equiv CCH_2OCH_3$ **6**$^{\cdot-}$, $C_6CH_2^{\cdot-}$	**CA** 86, 85(100), 84(37), 73(85), 72(55), 61(71), 60(27), 49(21). **CR** 86(49), 85(88), 84(100), 74(4), 73(57), 72(13), 61(43), 60(29), 50(3), 49(19), 48(9), 37(15), 36(9), 25(1), 24(0.5). **NR** 86(67), 85(93), 84(100), 74(8), 73(58), 72(22), 61(44), 60(45), 50(10), 49(21), 48(15), 37(15), 36(15), 25(2), 24(2).
m/z 86 from $TMSC\equiv CCH_2C\equiv CC\equiv CTMS$ **9**$^{\cdot-}$, $C_2CH_2C_4^{\cdot-}$	**CA** 86, 85(100), 84(39), 74(11), 73(25), 72(19), 62(8), 60(47), 38(16), 36(5). **CR** 86(47), 85(100), 84(40), 74(9), 73(10), 72(11), 62(5), 61(14), 60(13), 50(3), 49(4), 48(5), 38(1), 37(2), 36(4), 26(0.3), 25(0.3), 24(0.6). **NR** 86(63), 85(100), 84(54), 74(3), 73(6), 72(9), 62(4), 61(13), 60(4), 50(5), 49(8), 48(8), 37(5), 36(8), 26(1), 25(1), 24(2).

† For CA spectra the parent signal is excluded and the most abundant fragment peak is used to calculate relative intensity.

‡ This spectrum is quite weak with a low signal to noise ratio. Differences between this spectrum and the corresponding CR spectrum are not thought to be significant.

3. *Characterisation of isomeric C_7H_2 radical anions by collisional activation*

For the C_7H_2 radical anion isomers studied here the unique situation arises where fragmentation of the carbon chain in the negative ion CA spectra is observed. This has not been previously noted for any of the cumulenic anions studied. The negative ion CA spectra

for radical anions **5**, **6** and **9** are given in Table 6.3. The nature of the observed fragmentation is more surprising because it involves losses of rather unstable atomic and diatomic neutrals and does not seem to fall under the auspices of the predictable negative ion decomposition which are commonly reported.[14,15] For example, the decomposition of the branched $HC_2C(C_2)C_2H$ (**5**$^{•-}$) radical anion shows formation of fragments corresponding to the ions $C_n^{•-}$ and C_nH^- (where n = 5 and 6). It is not clear how these ions can be formed simply. Only stepwise atomic losses of hydrogen and carbon can account for the observation of the ions $C_6^{•-}$ and C_6H^- assuming no structural rearrangement occurs. Formation of $C_5^{•-}$ seems the only decomposition for which it is possible to write a conventional negative ion mechanism (Scheme 6.6).

Scheme 6.6
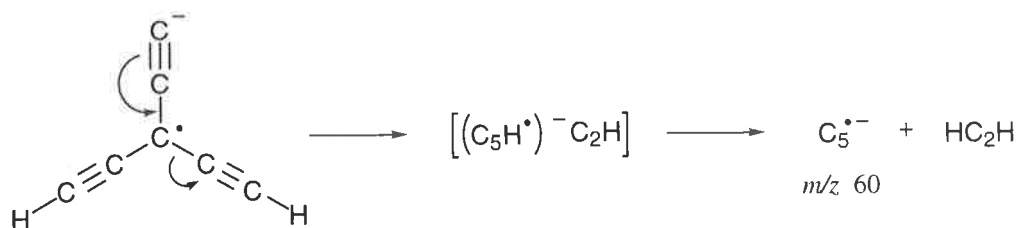
Although not readily explained in terms of unimolecular negative ion chemistry, the CA fragmentations of these ions provide a further means of comparison of the C_7H_2 structural isomers examined so far. The linear isomer, C_6CH_2 (**6**$^{•-}$) shows formation of the same fragment ions as **5**$^{•-}$ in its negative ion CA spectrum. However the relative abundances of the peaks corresponding to $C_6^{•-}$ and $C_5^{•-}$ (*m/z* 72 and 60) compared with the C_6H^- and C_5H^- fragments (*m/z* 73 and 61) are substantially lower than those in the spectrum of the branched species. Whilst these differences cannot be easily attributed to the respective anion geometries, the different abundances of the fragment ions clearly demonstrate that two distinct anionic structures have been generated.

The least stable of the C_7H_2 radical anions generated, namely $C_2CH_2C_4$ (**9**$^{•-}$), shows a unique fragmentation behaviour in its CA spectrum. Aside from the ubiquitous losses of H$^•$ and 2H$^•$ the largest peak in the spectrum corresponds to the C_5 radical anion (*m/z* 60).

Although speculative, a mechanistic scheme can be written for a unimolecular reaction of $C_2CH_2C_4{}^{\cdot-}$ resulting in formation of the C_5 radical anion (Scheme 6.7). It seems probable that upon activation, the $C_2CH_2C_4$ radical anion would decompose to form the ion-neutral complex, $[(C_5H_2)^{\cdot-}C_2]$. The C_2 radical anion may then abstract a hydrogen radical and a proton (perhaps in a stepwise process analogous to that of the oxygen radical anion)[21] resulting in loss of neutral acetlyene and formation of $C_5{}^{\cdot-}$. Other fragments in the spectrum also point to the assigned $C_2CH_2C_4$ connectivity. The appearance of the C_3H_2 radical anion is the most noticable: this is consistent with loss of the C_4 chain as a neutral from $C_2CH_2C_4{}^{\cdot-}$. As with the charge reversal data, the CA spectrum is by no means conclusive of structure. However the observed fragmentations (i) can at least be accounted for qualitatively in terms of the assigned structure and (ii) the CA spectrum is unique to this ion, showing quite a different CA behaviour to the other species analysed.

Scheme 6.7

$$\left[\left(C_4CH_2\right)C_2^{\cdot-}\right] \longrightarrow C_5^{\cdot-} + HC_2H$$
$$m/z\ 60$$
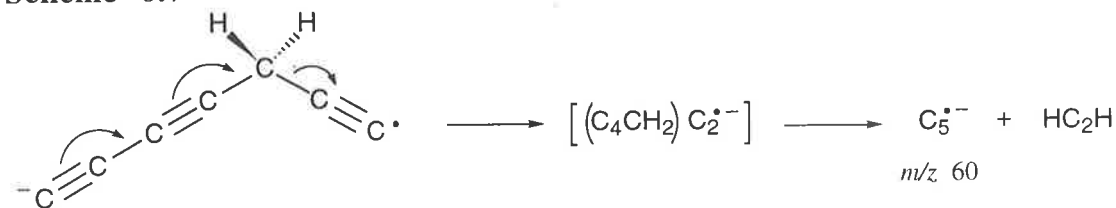
Generally, the CA spectra demonstrate unusual fragmentations which are not always easy to rationalise. However it is significant that distinct spectra are obtained for all isomers. This not only points to three structurally distinct anions but to three distinct anions that do not rearrange to a common stable connectivity even upon activation.

4. Possibilities for rearrangement of isomeric C_7H_2 radical anions

The CR and negative ion CA data presented thus far demonstrate that the three C_7H_2 radical anion species generated have different structures. If rearrangement processes are occurring either during or after the formation of these anions, such processes certainly do not result in a single stable structure or indeed a common mixture of stable structures. Both of these scenarios would lead to common fragmentation in the spectra described. Having said this

however, some degree of isomerisation cannot be excluded and the possible pathways are as follows: (i) intramolecular hydride transfer around the C_7-carbon skeleton, (ii) cyclisation followed by ring opening of the carbon-skeleton and (iii) intermolecular base catalysed proton transfer.

The first two possibilities seem rather unlikely. Given the high degree of unsaturation of these C_7H_2 systems, the intermediates and transitions states required to achieve rearrangement must be exceedingly strained and consequently rather energetic. For the C_5H_2 system a few possible pathways were investigated theoretically and it was found that a typical 1,3-hydrogen shift involved an activation barrier of 85.8 kcal mol^{-1} while formation of a three membered ring required 56.5 kcal mol^{-1}.* It is expected that for C_7H_2 radical anions hydride transfers and skeletal rearrangements are also likely to be energetically unattainable. The $C_2CH_2C_4$ (**9**) radical anion is a possible exception to this, as its inherent instability (nearly 60 kcal mol^{-1} less stable than **6·⁻**) suggests that little activation may be required to undergo hyride transfer or cyclisation. With such an excess of energy it might be expected that **9·⁻** could rearrange to one of the more stable anions, such as **6·⁻**. This possibility at least can be excluded based on comparison of CA and CR spectra, but it is possible that nascent **9·⁻** rearranges to some other stable C_7H_2·⁻ configuration (*cf.* Scheme 6.8). A transition state for this 1,3-hydrogen shift has been identified by calculation and is found to be nearly 40 kcal mol^{-1} above **9·⁻** (Table 6.2). This presents a substantial barrier to isomerisation and it would be expected that other rearrangement pathways would require similar activation energies. Thus it seems unlikely that once formed, **9·⁻** should undergo extensive unimolecular rearrangement.

Scheme 6.8

---
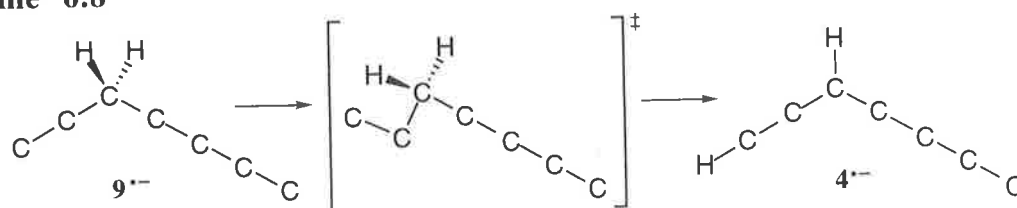
* These calculations are discussed in Chapter 5, pp 112.

Intermolecular base catalysed proton transfer must also be considered as a possible pathway to isomerisation. The formation of $HC_2C(C_2)C_2H$ (**5**$^{•-}$) and C_6CH_2 (**6**$^{•-}$) radical anions involve the loss of an oxy-radical, either hydroxide or methoxide, from a parent anion and follow closely procedures established for $C_5H_2^{•-}$ species. As an example, a possible intermolecular base catalysed proton transfer for **6**$^{•-}$ is outlined in Scheme 6.9.

Scheme 6.9

$$^{-•}C{=}C{=}C{=}C{=}C{=}C{=}CH_2 \; + \; H_2O \; \rightleftharpoons \; \left[\left(H\overset{\bullet}{C}{=}C{=}C{=}C{=}C{=}C{=}CH_2\right)^- OH\right]$$

$$\mathbf{6}^{\,\bullet-}$$

$$\rightleftharpoons \quad H\overset{\bullet}{C}{=}C{=}C{=}C{=}C{=}C{=}CH^- \; + \; H_2O$$

$$\mathbf{7}^{\,\bullet-}$$
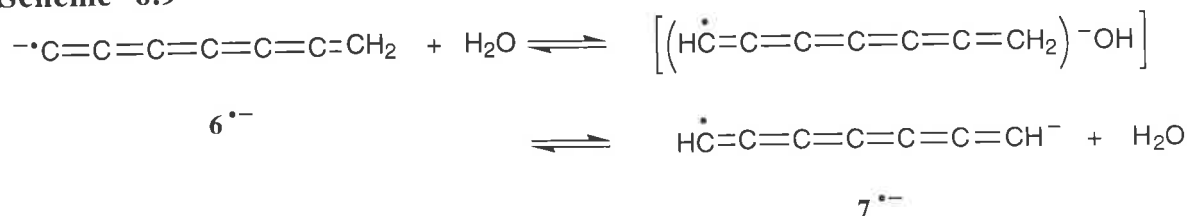
The possibility of the NICI reagent gas acting as the catalyst base for this process can be excluded given that the use of labelled NICI reagents does not lead to the incorporation of deuterium labels. However the analogous intramolecular process where the hydroxide or methoxide leaving group acts as the catalyst cannot be rigorously excluded. This possibility does not need to be considered for the $C_2CH_2C_4$ (**9**) radical anion as the double-desilylation method employed for its formation does not involve a potential base catalyst.

To summarise, there do exist a few possibilities for isomerisation of the C_7H_2 radical anions generated in this study: (i) for isomers **5**$^{•-}$ and **6**$^{•-}$ rearrangement accompanying formation, where the leaving group acts a base catalyst for proton transfer, cannot be excluded. (ii) Unimolecular isomerisation of the radical anions subsequent to formation *via* hydride transfer or skeletal rearrangement, cannot be entirely ruled out. It must be stressed that the latter possibility appears extremely unlikely on the basis of theoretically predicted energy requirements for such isomerisation processes. Having conceded these possibilities, no evidence exists suggesting the operation of any such processes. The weight of evidence, including theoretical data and CA and CR spectra, suggests that all three of these anions exist as discrete species.

2. Gas phase synthesis of isomeric C_7H_2 neutrals

Given that three isomeric C_7H_2 radical anions have been generated in this study it now remains to examine the stability or otherwise of the corresponding neutrals. The neutralisation reionisation spectra of each of the isomers are reported in Table 6.3. The NR spectra of all three isomers show a strong recovery signal at *m/z* 86 indicative of some surviving "C_7H_2" neutral.

The theoretical results previously discussed suggest that the neutrals **5**, **6** and **9** exist as discrete species on the C_7H_2 potential surface. These are, therefore, the most probable products of the step-wise oxidation of the corresponding radical anions in the NR experiment. In addition, the structural similarity between the anions **5·⁻** and **6·⁻** and their ground state neutrals suggests favourable Franck-Condon overlap between these potential surfaces (Table 6.5).[58] Similarly, the radical anion **9·⁻** shares a geometry analogous to that of the low lying triplet neutral (Table 6.5 and 6.6). Consequently, little excess internal energy would be deposited in the neutrals by the anion-neutral electronic transition. Experience has shown that structural rearrangement of these unsaturated cumulene species (anions or neutrals) are high energy processes requiring activation energy upwards of 20 kcal mol⁻¹ (*cf.* Chapters 4, 5 or 6). Hence rearrangement on the neutral surface is unlikely in these NR experiments. The theoretical evidence suggests therefore that the C_7H_2 cation signals detected in the NR spectra of all three isomers correspond to the reionised neutrals **5**, **6** and **9**.

This conclusion is evidenced experimentally by the similarity between ⁻NR⁺ and ⁻CR⁺ spectra of each isomer (Table 6.3). For each of the three anion isomers **5·⁻**, **6·⁻** and **9·⁻** the fragments and fragment peak abundances show little variation between ⁻NR⁺ and ⁻CR⁺ spectra. Major rearrangement of the neutral species during the ⁻NR⁺ experiment should result in the formation of a different cation to that resulting from the ⁻CR⁺ procedure. Consequently, different fragmentation would be observed in the two spectra.[25,60,66,68] It

appears therefore that the neutral C_7H_2 isomers **5**, **6** and **9** are stable species on the mass spectrometry timescale (ca. 10^{-6} s).

(IV) CONCLUSIONS

Theoretical calculations, both ours and those of other researchers, have predicted the structures and relative energies of nine isomeric C_7H_2 neutrals. It has been calculated that electron attachment to these species will generate stable radical anions which may provide suitable targets for synthesis in the gas phase. The relative order of stability of the isomers has been shown to alter between neutral and anionic potential surfaces, with the aromaticity of neutral C_3-ring structures **1**, **2** and **8** disrupted by the attachment of an electron. Three of these C_7H_2 radical anions have been generated in the mass spectrometer by different NICI techniques. Two theoretically stable anions (**5**$^{•-}$and **6**$^{•-}$) and one substantially less stable C_7H_2 isomer (**9**$^{•-}$) have been synthesised in the gas phase. Spectral data collected from these ions has been shown to be unique for each isomer and at least qualitatively consistent with the assigned structures. The corresponding neutrals have also been generated using neutralisation reionisation mass spectrometry. This is the first experimental report of the neutrals $HC_2C(C_2)C_2H$ (**5**), C_6CH_2 (**6**) and $C_2CH_2C_4$ (**9**).

It is significant that this synthetic protocol has allowed the generation of **9**$^{•-}$ and **9**. Both anion and neutral are predicted by theoretical calculations to be rather unstable on their respective potential surfaces. That NICI should yield such an anion and NR such a neutral is testament to the sensitivity of these techniques. In principle, it suggests that other unstable anions such as the ring chain isomers **1**$^{•-}$, **2**$^{•-}$ and **8**$^{•-}$ may be pursued (providing that suitable precursor compounds can be identified) as potential precursors for these corresponding neutrals in the gas phase.

The neutrals $HC_2C(C_2)C_2H$ (**5**), C_6CH_2 (**6**) and $C_2CH_2C_4$ (**9**) are all potential interstellar molecules and with their high calculated electron affinities: 2.47, 2.82 and 3.37 eV

respectively (Table 6.4), the possibility exists that the corresponding anions may also be present in galactic environments.

(V) EXPERIMENTAL SECTION

A. Mass Spectrometric Methods

CA, CR and NR spectra were measured using a two-sector reversed geometry VG ZAB 2HF spectrometer. This instrument is described in detail in Chapter 1. The typical experimental conditions and procedures are similar to those discussed in previous chapters.[#] Those routines unique to this study are outlined below.

Samples were introduced into the source *via* a heated septum inlet, with solid samples dissolved in a small amount of methanol or tetrahydrofuran. This was done to produce a measured pressure of 5×10^{-6} Torr inside the source housing. $[M-H]^-$ ions were obtained using H_2O or CH_3OH as NICI reagents at an operating pressure inside the source housing of ca. 5×10^{-5} Torr, and thus an estimated pressure inside the ion source of close to 0.1 Torr. $[M-TMS]^-$ ions were generated by desilylation of the precursor using the method developed by DePuy and co-workers[10] except that hydroxide ions were used as the gas phase nucleophile. This has also been demonstrated to be an effective methodology for formation of anions in the gas phase.[11] $[M-2TMS]$ radical anions were generated from bistrimethylsilylated precursors utilising SF_6 as the NICI reagent by the method of Squires and co-workers.[*][26] CA spectra were measured using argon as the collision gas at a typical pressure of 5×10^{-7} Torr, giving predominantly single collision conditions.[183] $^-NR^+$ and $^-CR^+$ spectra of the anions were measured under typical O_2/O_2 conditions.[#] All spectra were repeated a minimum of three times in order to establish their reproducibility.

[#] See Chapter 4, pp 85 for a discussion of typical experimental conditions.
[*] See Chapter 1, pp 6 and Chapter 1, pp 9 respectively for detailed discussion of $[M-TMS]^-$ and $[M-2TMS]^-$ ionisation techniques.

B. Syntheses of Precursor Molecules

The precursor molecules used in this study were prepared by Dr Suresh Dua. The synthetic schemes utilised and references to preparative procedures are given below.

1. *Methyl (7-trimethylsilyl)hepta-2,4,6-triynyl ether* [TMSC≡CC≡CC≡CCH$_2$OCH$_3$][211]

$$TMSC≡CC≡CCu \quad + \quad BrC≡CCH_2OCH_3 \quad \xrightarrow[-CuBr]{} \quad TMSC≡CC≡CC≡CCH_2OCH_3$$
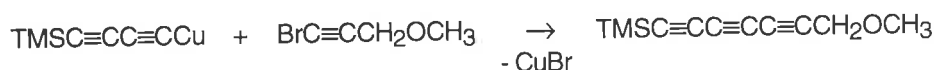
2. *Methyl [D₁]-hepta-2,4,6-triynyl ether* [DC≡CC≡CC≡CCH$_2$OCH$_3$][211]
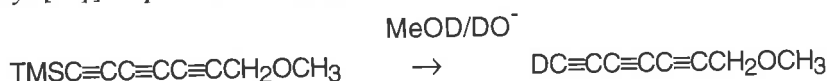
$$TMSC≡CC≡CC≡CCH_2OCH_3 \quad \xrightarrow{MeOD/DO^-} \quad DC≡CC≡CC≡CCH_2OCH_3$$

3. *3-Ethynyl penta-1,4-diyn-3-ol* [(HC≡C)$_3$COH][212,213]

$$TMSC≡CCH(OH)C≡CTMS \quad \xrightarrow{CrO_3/H^+} \quad TMSC≡CCOC≡CTMS \qquad (a)$$

$$TMSC≡CCOC≡CTMS \quad + \quad TMSC≡CLi \quad \rightarrow \quad (TMSC≡C)_3COH \qquad (b)$$

$$(TMSC≡C)_3COH \quad \xrightarrow{KF} \quad (HC≡C)_3COH \qquad (c)$$

4. *1,7-Bis(trimethylsilyl)hepta-1,4,6-triyne* [TMSC≡CCH$_2$C≡CC≡CTMS]
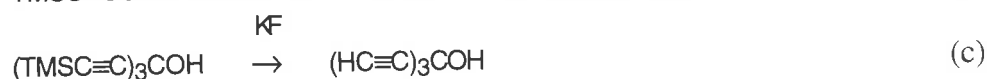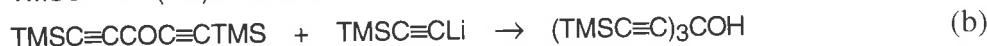
$$TMSC≡CCH_2Br \quad + \quad TMSC≡CC≡CCu \quad \xrightarrow[-CuBr]{} \quad TMSC≡CCH_2C≡CC≡CTMS$$

C. Computational Methods

Theoretical protocols utilised in this study are very similar to those outlined in preceding chapters. Briefly however, geometry optimisations were carried out with the Becke 3LYP method[88,89] using the 6-31G(d) basis within the GAUSSIAN 94 suite of programs.[92] Stationary points were characterised as either minima (no imaginary frequencies) or transition states (one imaginary frequency) by calculation of the frequencies using analytical gradient procedures. The minima connected by a given transition state were confirmed by intrinsic reaction coordinate (IRC) calculations. The calculated frequencies were also used to determine the zero-point vibrational energies which were then scaled[91] by 0.9804 and used as a zero-point energy correction for the electronic energies calculated at this and higher levels of theory. More accurate energies for the B3LYP/6-31G(d) geometries were determined using the larger Dunning aug-cc-pVDZ basis set.[95,96] Where possible the RCCSD(T) method,[176-181] using the Dunning aug-cc-pVDZ basis set, within the MOLPRO

97.4 package[94] was used for calculation of thermochemical properties such as electron affinity. Calculations involving GAUSSIAN 94 geometry optimisation were carried out using the Power Challenge Super Computer at the South Australian Super Computing Centre (Adelaide). MOLPRO 97.4 single point energy calculations were carried out with the Power Challenge Super Computer at the Australian National University Super Computing Facility (Canberra).

(VI) APPENDICES

Table 6.4 The relative energies of the C_7H_2 (i) radical anions and (ii) singlet and triplet neutrals are given here, along with the symmetry and electronic terms. The geometries were optimised at the B3LYP/6-31G(d) level and are given as appendicies to this Chapter (Tables 6.5 and 6.6). The energies of these species were then recalculated at the RCCSD(T) level with the larger aug-cc-pVDZ basis set.
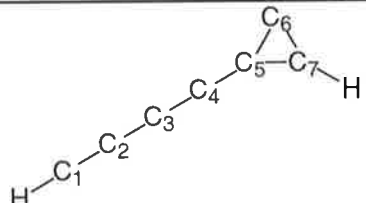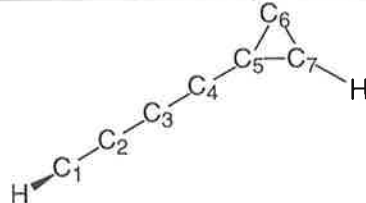
C_7H_2 Isomers (anions and neutrals)	Electronic State (Point Group)	Electronic Energy (Hartrees)[a]	Relative Energy (eV)[b]
5·⁻ $HC_2C(C_2)C_2H$	$^2B_1$ (C_{2v})	-267.00154	0.00
5 $HC_2C(C_2)C_2H$	$^1A_1$ (C_{2v})	-266.91350	2.47[c]
5 $HC_2C(C_2)C_2H$	$^3B_1$ (C_{2v})	-266.86944	3.63
6·⁻ C_6CH_2	$^2B_1$ (C_{2v})	-267.02102	0.00
6 C_6CH_2	$^1A_1$ (C_{2v})	-266.91808	2.82[c]
6 C_6CH_2	$^3A_2$ (C_{2v})	-266.88310	3.71
7·⁻ HC_7H	$^1A_2$ (C_{2v})	-267.00196	0.00
7 HC_7H	$^1A_1$ (C_{2v})	-266.91157	2.47
7 HC_7H	$^3\Sigma_g$ ($D_{\infty h}$)	-266.93956	1.72[c]
9·⁻ $C_2CH_2C_4$[c]	$^2A'$ (C_S)	-267.69990	0.00
9 $C_2CH_2C_4$	$^1A'$ (C_S)	-267.57510	3.37[c]
9 $C_2CH_2C_4$	$^3A''$ (C_S)	-267.51057	3.60

[a] Energies calculated at the RCCSD(T)/aug-cc-pVDZ//B3LYP/6-31G(d) level of theory except isomer **9** and do not include ZPE contributions. For isomer **9** the lack of high order symmetry renders the single point energy calculation at RCCSD(T) level intractable and so these results were calculated at the lesser B3LYP/aug-cc-pVDZ//B3LYP/6-31G(d) level.

[b] Relative energies are calculated including corrected ZPE contributions.

[c] Corresponds to an estimate of adiabatic electron affinity.

Table 6.5 Geometries of C_7H_2 isomers on the neutral and radical anion potential surfaces. The geometries of the electronic ground states are given only. For the neutrals that is the singlet electronic state for all but isomer HC_7H (**7**), which has a linear triplet ground state and for the anions the ground state is a doublet in all cases. Calculated at the B3LYP/6-31G(d). All bond lengths given in angstroms and all angles in degrees.

1 (C_S) $^1A'$

bond length		
H-C_1	1.0668
C_1-C_2	1.2147
C_2-C_3	1.3591
C_3-C_4	1.2238
C_4-C_5	1.3782
C_5-C_6	1.4582
C_5-C_7	1.3419
C_6-C_7	1.4079
C_7-H	1.0833

angle		
H-C_1-C_2	179.6
C_1-C_2-C_3	179.9
C_2-C_3-C_4	179.6
C_3-C_4-C_5	179.9
C_4-C_5-C_6	149.0
C_4-C_5-C_7	150.8
C_5-C_6-C_7	55.8
C_5-C_7-H	146.5

1·⁻ (C_1) Doublet

bond length		
H-C_1	1.0753
C_1-C_2	1.2535
C_2-C_3	1.3308
C_3-C_4	1.2632
C_4-C_5	1.3320
C_5-C_6	1.5241
C_5-C_7	1.3890
C_6-C_7	1.3660
C_7-H	1.0873

angle		
H-C_1-C_2	145.1
C_1-C_2-C_3	175.1
C_2-C_3-C_4	180.0
C_3-C_4-C_5	179.3
C_4-C_5-C_6	151.2
C_4-C_5-C_7	153.1
C_5-C_6-C_7	57.1
C_5-C_7-H	144.4

dihedral angle		
H-C_1-C_2-C_3	-177.9
C_1-C_2-C_3-C_4	151.8
C_2-C_3-C_4-C_5	-25.1
C_3-C_4-C_5-C_6	140.3
C_3-C_4-C_5-C_7	-40.3
C_4-C_5-C_6-H	0.3
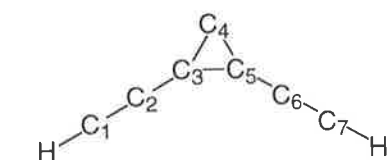
2 (C$_{2v}$) ^{1}A$_1$

bond	H-C$_1$	1.0671
length	C$_1$-C$_2$	1.2116
	C$_2$-C$_3$	1.3908
	C$_3$-C$_4$	1.4341
	C$_3$-C$_5$	1.3500
angle	H-C$_1$-C$_2$	179.5
	C$_1$-C$_2$-C$_3$	179.8
	C$_2$-C$_3$-C$_4$	149.6
	C$_2$-C$_3$-C$_5$	148.5
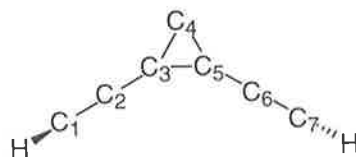
2$^{\cdot-}$ (C$_1$) Doublet

bond	H-C$_1$	1.0682
length	C$_1$-C$_2$	1.2353
	C$_2$-C$_3$	1.3697
	C$_3$-C$_4$	1.4231
	C$_4$-C$_5$	1.4350
	C$_3$-C$_5$	1.4203
	C$_5$-C$_6$	1.3631
	C$_6$-C$_7$	1.2424
	C$_7$-H	1.0721
angle	H-C$_1$-C$_2$	158.1
	C$_1$-C$_2$-C$_3$	175.9
	C$_2$-C$_3$-C$_4$	150.4
	C$_2$-C$_3$-C$_5$	149.0
	C$_3$-C$_4$-C$_5$	59.6
	C$_3$-C$_5$-C$_6$	149.4
	C$_5$-C$_6$-C$_7$	175.0
	C$_6$-C$_7$-H	151.1
dihedral	H-C$_1$-C$_2$-C$_3$	170.4
angle	C$_1$-C$_2$-C$_3$-C$_4$	101.7
	C$_2$-C$_3$-C$_4$-C$_5$	178.2
	C$_2$-C$_3$-C$_5$-C$_6$	3.7
	C$_3$-C$_5$-C$_6$-C$_7$	-85.1
	C$_5$-C$_6$-C$_7$-H	174.0
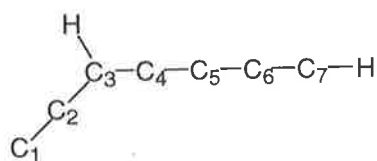
3 (C$_S$) ^{1}A'

bond	C$_1$-C$_2$	1.2854
length	C$_2$-C$_3$	1.3463
	C$_3$-H	1.0951
	C$_3$-C$_4$	1.4015
	C$_4$-C$_5$	1.2239
	C$_5$-C$_6$	1.3580
	C$_6$-C$_7$	1.2147
	C$_7$-H	1.0673
angle	C$_1$-C$_2$-C$_3$	179.5
	C$_2$-C$_3$-C$_4$	124.3
	C$_2$-C$_3$-H	119.7
	C$_3$-C$_4$-C$_5$	178.7
	C$_4$-C$_5$-C$_6$	179.6
	C$_5$-C$_6$-C$_7$	180.0
	C$_6$-C$_7$-H	179.9
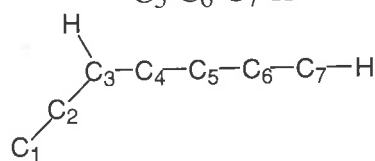
3$^{\cdot-}$ (C$_1$) Doublet

bond	C$_1$-C$_2$	1.2715
length	C$_2$-C$_3$	1.3848
	C$_3$-H	1.0972
	C$_3$-C$_4$	1.3864
	C$_4$-C$_5$	1.2393
	C$_5$-C$_6$	1.3533
	C$_6$-C$_7$	1.2255
	C$_7$-H	1.0642
angle	C$_1$-C$_2$-C$_3$	178.4
	C$_2$-C$_3$-C$_4$	125.8
	C$_2$-C$_3$-H	119.1
	C$_3$-C$_4$-C$_5$	178.1
	C$_4$-C$_5$-C$_6$	179.8
	C$_5$-C$_6$-C$_7$	178.6
	C$_6$-C$_7$-H	171.6
dihedral	C$_1$-C$_2$-C$_3$-C$_4$	179.0
angle	C$_1$-C$_2$-C$_3$-H	-1.1
	C$_2$-C$_3$-C$_4$-C$_5$	-176.5
	C$_3$-C$_4$-C$_5$-C$_6$	47.1
	C$_4$-C$_5$-C$_6$-C$_7$	-131.3
	C$_5$-C$_6$-C$_7$-H	172.8

148
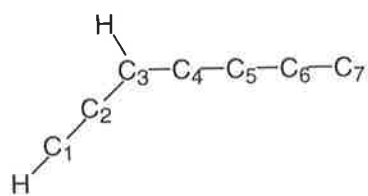
4 (C_S) $^1A'$

bond	H-C_1	1.0675
length	C_1-C_2	1.2129
	C_2-C_3	1.4109
	C_3-C_4	1.3378
	C_3-H	1.0935
	C_4-C_5	1.2626
	C_5-C_6	1.3061
	C_6-C_7	1.2872
angle	H-C_1-C_2	179.0
	C_1-C_2-C_3	178.5
	C_2-C_3-C_4	124.1
	C_2-C_3-H	116.5
	C_3-C_4-C_5	179.3
	C_4-C_5-C_6	180.0
	C_5-C_6-C_7	179.9
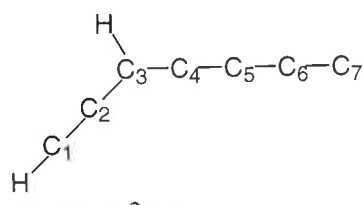
4·‾ (C_S) $^2A''$

bond	H-C_1	1.0642
length	C_1-C_2	1.2211
	C_2-C_3	1.4082
	C_3-C_4	1.3690
	C_3-H	1.0941
	C_4-C_5	1.2513
	C_5-C_6	1.3395
	C_6-C_7	1.2715
angle	H-C_1-C_2	177.8
	C_1-C_2-C_3	178.0
	C_2-C_3-C_4	124.8
	C_2-C_3-H	116.0
	C_3-C_4-C_5	178.4
	C_4-C_5-C_6	179.7
	C_5-C_6-C_7	179.8
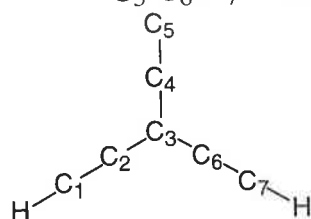
5 (C_{2v}) $^1A_1$

bond	H-C_1	1.0676
length	C_1-C_2	1.2110
	C_2-C_3	1.4240
	C_3-C_4	1.3554
	C_4-C_5	1.2832
angle	H-C_1-C_2	179.1
	C_1-C_2-C_3	179.5
	C_2-C_3-C_4	121.4
	C_2-C_3-C_6	117.1
	C_3-C_4-C_5	180.0
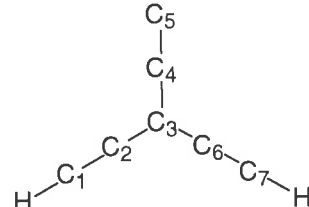
5·‾ (C_{2v}) $^2B_1$

bond	H-C_1	1.0642
length	C_1-C_2	1.2188
	C_2-C_3	1.4231
	C_3-C_4	1.3939
	C_4-C_5	1.2705
angle	H-C_1-C_2	178.9
	C_1-C_2-C_3	179.6
	C_2-C_3-C_4	121.6
	C_2-C_3-C_6	116.8
	C_3-C_4-C_5	180.0
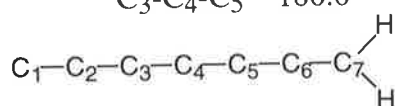
6 (C_{2v}) $^1A_1$

bond	C_1-C_2	1.2886
length	C_2-C_3	1.3011
	C_3-C_4	1.2701
	C_4-C_5	1.2930
	C_5-C_6	1.2710
	C_6-C_7	1.3204
	C_7-H	1.0896
angle	C_1-C_2-C_3	180.0
	C_2-C_3-C_4	180.0
	C_3-C_4-C_5	180.0
	C_4-C_5-C_6	180.0
	C_5-C_6-C_7	180.0
	C_6-C_7-H	121.6
	H-C_7-H	116.8
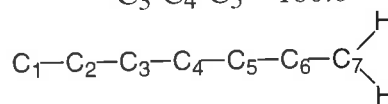
6·‾ (C_{2v}) $^2B_1$

bond	C_1-C_2	1.2721
length	C_2-C_3	1.3339
	C_3-C_4	1.2563
	C_4-C_5	1.3233
	C_5-C_6	1.2612
	C_6-C_7	1.3449
	C_7-H	1.0903
angle	C_1-C_2-C_3	180.0
	C_2-C_3-C_4	180.0
	C_3-C_4-C_5	180.0
	C_4-C_5-C_6	180.0
	C_5-C_6-C_7	180.0
	C_6-C_7-H	122.0
	H-C_7-H	116.0

H—C₁—C₂—C₃—C₄—C₅—C₆—C₇—H

$$H-C_1-C_2-C_3-C_4-C_5-C_6-C_7-H$$
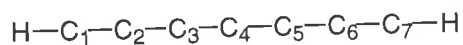
7 ($D_{\infty h}$) $^3\Sigma_g$

bond length	H-C$_1$	1.0663
	C$_1$-C$_2$	1.2330
	C$_2$-C$_3$	1.3257
	C$_3$-C$_4$	1.2770

$$H-C_1-C_2-C_3-C_4-C_5-C_6-C_7-H$$

7·⁻ (C_{2v}) $^2A_2$

bond length	H-C$_1$	1.0740
	C$_1$-C$_2$	1.2582
	C$_2$-C$_3$	1.3202
	C$_3$-C$_4$	1.2833
angle	H-C$_1$-C$_2$	143.1
	C$_1$-C$_2$-C$_3$	175.0
	C$_2$-C$_3$-C$_4$	179.0
	C$_3$-C$_4$-C$_5$	179.1

C₁—C₂—C₃—C₄—C₅ (triangle: C₆ with H, C₇ with H)
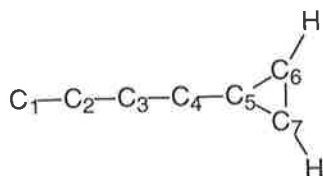
8 (C_{2v}) $^1A_1$

bond length	C$_1$-C$_2$	1.2789
	C$_2$-C$_3$	1.3117
	C$_3$-C$_4$	1.2576
	C$_4$-C$_5$	1.3248
	C$_5$-C$_6$	1.4271
	C$_6$-C$_7$	1.3306
	C$_6$-H	1.0820
angle	C$_1$-C$_2$-C$_3$	180.0
	C$_2$-C$_3$-C$_4$	180.0
	C$_3$-C$_4$-C$_5$	180.0
	C$_4$-C$_5$-C$_6$	152.2
	C$_5$-C$_6$-C$_7$	62.2
	C$_5$-C$_6$-H	149.1

C₁—C₂—C₃—C₄—C₅ (triangle: C₆ with H, C₇ with H)
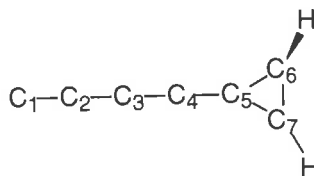
8·⁻ (C_1) Doublet

bond length	C$_1$-C$_2$	1.2647
	C$_2$-C$_3$	1.3448
	C$_3$-C$_4$	1.2424
	C$_4$-C$_5$	1.3662
	C$_5$-C$_6$	1.5394
	C$_5$-C$_7$	1.3445
	C$_6$-C$_7$	1.4380
	C$_6$-H	1.1021
	C$_7$-H	1.0831
angle	C$_1$-C$_2$-C$_3$	179.8
	C$_2$-C$_3$-C$_4$	179.5
	C$_3$-C$_4$-C$_5$	178.5
	C$_4$-C$_5$-C$_6$	150.9
	C$_4$-C$_5$-C$_7$	151.4
	C$_5$-C$_6$-C$_7$	54.6
	C$_5$-C$_6$-H	126.7
	C$_5$-C$_7$-H	146.3
dihedral angle	C$_1$-C$_2$-C$_3$-C$_4$	5.0
	C$_2$-C$_3$-C$_4$-C$_5$	-153.1
	C$_3$-C$_4$-C$_5$-C$_6$	-148.2
	C$_3$-C$_4$-C$_5$-C$_7$	166.3
	C$_4$-C$_5$-C$_6$-H	63.4
	C$_4$-C$_5$-C$_7$-H	-5.7
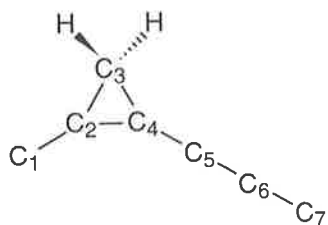
9 (C_s) ^{1}A'

bond	C_1-C_2	1.2994
length	C_2-C_3	1.5409
	C_2-C_4	1.4295
	C_3-C_4	1.4740
	C_4-C_5	1.2974
	C_5-C_6	1.2900
	C_6-C_7	1.2931
	C_3-H	1.0892
	C_3-H	1.0892

angle	C_1-C_2-C_3	137.0
	C_1-C_2-C_4	163.6
	C_2-C_3-C_4	56.6
	C_2-C_4-C_5	146.2
	C_4-C_5-C_6	179.4
	C_5-C_6-C_7	179.7
	C_2-C_3-H	116.5
	C_2-C_3-H	116.5

dihedral	C_1-C_2-C_3-C_4	180.0
angle	C_2-C_3-C_4-C_5	180.0
	C_2-C_4-C_5-C_6	180.0
	C_4-C_5-C_6-C_7	0.0
	C_1-C_2-C_3-H	71.8
	C_1-C_2-C_3-H	-71.8

9$^{\cdot-}$ (C_s) ^{2}A'
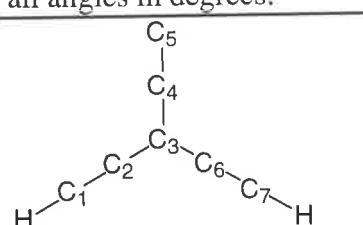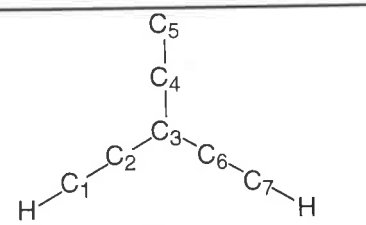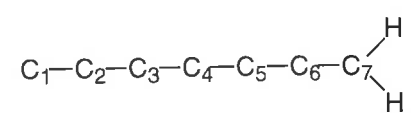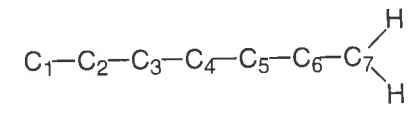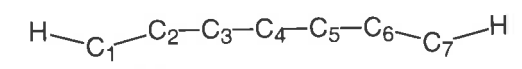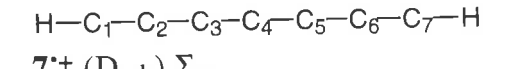
bond	C_1-C_2	1.2629
length	C_2-C_3	1.4715
	C_3-C_4	1.4603
	C_4-C_5	1.2366
	C_5-C_6	1.3432
	C_6-C_7	1.2718
	C_3-H	1.1029
	C_3-H	1.1029

angle	C_1-C_2-C_3	176.3
	C_2-C_3-C_4	102.6
	C_3-C_4-C_5	176.3
	C_4-C_5-C_6	177.5
	C_5-C_6-C_7	178.9
	C_2-C_3-H	112.5
	C_2-C_3-H	112.5

dihedral	C_1-C_2-C_3-C_4	180.0
angle	C_2-C_3-C_4-C_5	0.0
	C_3-C_4-C_5-C_6	180.0
	C_4-C_5-C_6-C_7	0.0
	C_1-C_2-C_3-H	60.2
	C_1-C_2-C_3-H	-60.2

151
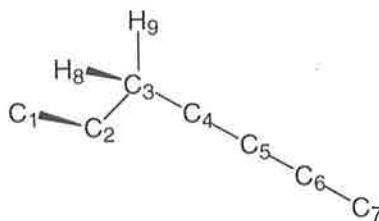
TS9/4·⁻ (C$_1$) Doublet

bond	C$_1$-C$_2$	1.2981	
length	C$_2$-C$_3$	1.5595	
	C$_3$-C$_4$	1.4091	
	C$_4$-C$_5$	1.2416	
	C$_5$-C$_6$	1.3394	
	C$_6$-C$_7$	1.2731	
	C$_3$-H$_8$	1.2552	
	C$_3$-H$_9$	1.0962	
angle	C$_1$-C$_2$-C$_3$	83.5	
	C$_2$-C$_3$-C$_4$	123.0	
	C$_3$-C$_4$-C$_5$	177.2	
	C$_4$-C$_5$-C$_6$	179.3	
	C$_5$-C$_6$-C$_7$	179.4	
	C$_2$-C$_3$-H$_8$	92.5	
	C$_2$-C$_3$-H$_9$	113.7	
dihedral	C$_1$-C$_2$-C$_3$-C$_4$	109.7	
angle	C$_2$-C$_3$-C$_4$-C$_5$	-154.8	
	C$_3$-C$_4$-C$_5$-C$_6$	-66.3	
	C$_4$-C$_5$-C$_6$-C$_7$	16.8	
	C$_1$-C$_2$-C$_3$-H$_8$	1.0	
	C$_1$-C$_2$-C$_3$-H$_9$	-105.0	

Table 6.6 Excited state neutral and ground state cation geometries of the C_7H_2 isomers **5**, **6**, **7** and **9**. Calculated at the B3LYP/6-31G(d). All bond lengths given in angstroms and all angles in degrees.

5 (C_{2v}) $^3B_1$

bond length	H-C_1	1.0665
	C_1-C_2	1.2153
	C_2-C_3	1.4099
	C_3-C_4	1.4047
	C_4-C_5	1.2246
angle	H-C_1-C_2	179.8
	C_1-C_2-C_3	179.7
	C_2-C_3-C_4	119.9
	C_2-C_3-C_6	120.3
	C_3-C_4-C_5	180.0

5·+ (C_{2v}) $^2A_1$

bond length	H-C_1	1.0735
	C_1-C_2	1.2176
	C_2-C_3	1.3956
	C_3-C_4	1.4028
	C_4-C_5	1.2208
angle	H-C_1-C_2	179.8
	C_1-C_2-C_3	179.9
	C_2-C_3-C_4	119.7
	C_2-C_3-C_6	120.6
	C_3-C_4-C_5	180.0

6 (C_{2v}) $^3A_2$

bond length	C_1-C_2	1.3009
	C_2-C_3	1.3012
	C_3-C_4	1.2736
	C_4-C_5	1.2969
	C_5-C_6	1.2719
	C_6-C_7	1.3291
	C_7-H	1.0873
angle	C_1-C_2-C_3	180.0
	C_2-C_3-C_4	180.0
	C_3-C_4-C_5	180.0
	C_4-C_5-C_6	180.0
	C_5-C_6-C_7	180.0
	C_6-C_7-H	121.2
	H-C_7-H	117.7

6·+ (C_{2v}) $^2B_2$

bond length	C_1-C_2	1.2272
	C_2-C_3	1.3354
	C_3-C_4	1.2442
	C_4-C_5	1.3139
	C_5-C_6	1.2570
	C_6-C_7	1.3295
	C_7-H	1.0906
angle	C_1-C_2-C_3	180.0
	C_2-C_3-C_4	180.0
	C_3-C_4-C_5	180.0
	C_4-C_5-C_6	180.0
	C_5-C_6-C_7	180.0
	C_6-C_7-H	121.1
	H-C_7-H	117.8

7 (C_{2v}) $^1A_1$

bond length	H-C_1	1.0687
	C_1-C_2	1.2385
	C_2-C_3	1.3202
	C_3-C_4	1.2753
angle	H-C_1-C_2	158.8
	C_1-C_2-C_3	176.5
	C_2-C_3-C_4	179.0
	C_3-C_4-C_5	179.7

7·+ ($D_{\infty h}$) Σ_g

bond length	H-C_1	1.0736
	C_1-C_2	1.2318
	C_2-C_3	1.3175
	C_3-C_4	1.2728
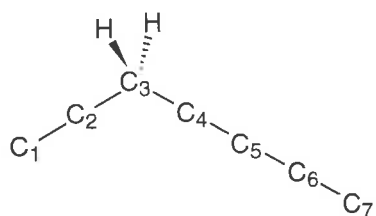
9 (C$_s$) ^{3}A''

bond length		
	C$_1$-C$_2$	1.2395
	C$_2$-C$_3$	1.4743
	C$_3$-C$_4$	1.4560
	C$_4$-C$_5$	1.2363
	C$_5$-C$_6$	1.3291
	C$_6$-C$_7$	1.2932
	C$_3$-H	1.1012
	C$_3$-H	1.1012

angle		
	C$_1$-C$_2$-C$_3$	164.0
	C$_2$-C$_3$-C$_4$	111.1
	C$_3$-C$_4$-C$_5$	177.7
	C$_4$-C$_5$-C$_6$	181.1
	C$_5$-C$_6$-C$_7$	180.1
	C$_2$-C$_3$-H	110.9
	C$_2$-C$_3$-H	110.9

dihedral angle		
	C$_1$-C$_2$-C$_3$-C$_4$	180.0
	C$_2$-C$_3$-C$_4$-C$_5$	0.0
	C$_3$-C$_4$-C$_5$-C$_6$	180.0
	C$_4$-C$_5$-C$_6$-C$_7$	0.0
	C$_1$-C$_2$-C$_3$-H	58.6
	C$_1$-C$_2$-C$_3$-H	-58.6
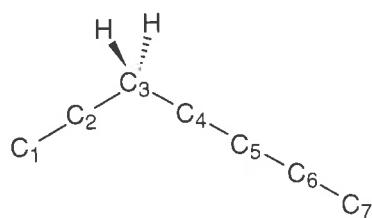
9$^{\cdot+}$ (C$_s$) ^{2}A'

bond length		
	C$_1$-C$_2$	1.2113
	C$_2$-C$_3$	1.4656
	C$_3$-C$_4$	1.4457
	C$_4$-C$_5$	1.2600
	C$_5$-C$_6$	1.2979
	C$_6$-C$_7$	1.3352
	C$_3$-H	1.1055
	C$_3$-H	1.1055

angle		
	C$_1$-C$_2$-C$_3$	181.5
	C$_2$-C$_3$-C$_4$	108.6
	C$_3$-C$_4$-C$_5$	183.2
	C$_4$-C$_5$-C$_6$	178.9
	C$_5$-C$_6$-C$_7$	184.6
	C$_2$-C$_3$-H	112.0
	C$_2$-C$_3$-H	112.0

dihedral angle		
	C$_1$-C$_2$-C$_3$-C$_4$	180.0
	C$_2$-C$_3$-C$_4$-C$_5$	0.0
	C$_3$-C$_4$-C$_5$-C$_6$	180.0
	C$_4$-C$_5$-C$_6$-C$_7$	0.0
	C$_1$-C$_2$-C$_3$-H	53.0
	C$_1$-C$_2$-C$_3$-H	-53.0

154

Chapter 7: The Gas Phase Synthesis and Unimolecular Behaviour of NCCCN

(I) ABSTRACT

The radical anion and cation of NCCCN have been generated in the gas phase by a number of methodologies. The neutral has been probed using neutralisation reionisation mass spectrometry. These experiments demonstrate NCCCN to have some unimolecular reactivity on the microsecond timescale . By contrast, the most simple homologue NCN appears stable. Molecular orbital calculations have been carried out for both species on anion, neutral and cation surfaces in order to elucidate the structure and behaviour of these intermediates.

(II) INTRODUCTION

Small, highly unsaturated molecules are of much interest to chemist and astrophysicist alike. Reactive organic species containing the C_3-cumulene unit have received considerable attention. The interstellar heterocumulenes C_3O, C_3S and C_3N have all been targets of intensive laboratory and theoretical effort.[214-217] Di-heterocumulenes of the form XC_3Y have also been the subject of laboratory study although as yet none has been detected in galactic gas clouds.[#] Carbon suboxide ($X = Y = O$) is a relatively stable organic reagent,[218] while NC_3O has been observed in NRMS experiments.[219] HNC_3Y where $Y = NH, O, S$ have been also been generated by this technique.[220-222] NC_3N is also a member of this family of compounds. Little is known about this transient species but it has for many years been implicated as a key intermediate in chemical reactions.

Throughout the late 1950's and the 1960's, NCCCN or dicyanocarbene was frequently invoked as a reactive intermediate in a number of addition reactions. It was postulated that dibromo malononitrile heated in the presence of copper gave tetracyanoethylene *via* the coupling of two dicyanocarbenes (Scheme 7.1, a).[223] Reaction of bromo malononitrile and triethylamine in the presence of an alkene gave a dicyano cyclopropane: the involvement of dicyanocarbene was again proposed by way of explanation (Scheme 7.1, b).[224]

Scheme 7.1

$$2\ NCCBr_2CN + 2\ Cu \xrightarrow[-2\ CuBr_2]{} 2\ NC\ddot{C}CN \longrightarrow \begin{array}{c} NC \\ NC \end{array}\!\!\!>\!\!=\!\!<\!\!\!\begin{array}{c} CN \\ CN \end{array} \tag{a}$$

$$NCCH(Br)CN + NEt_3 \xrightarrow[-Et_3NH^+Br^-]{} NC\ddot{C}CN \longrightarrow \tag{b}$$
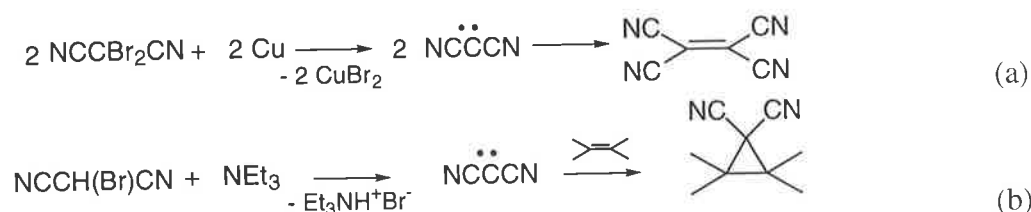
Subsequent studies have suggested that the intermediacy of dicyanocarbene is not necessary for either reaction.[225,226] However the interest generated by this work stimulated efforts to

---

[#] Linear, symmetrical XC_3X species do not possess permanent dipole moments. Radioastronomical detection is therefore not plausible. See Chapter 3 for a more detailed account of this type of detection bias. Infrared or other spectroscopic investigation however may yet establish the presence of these species in interstellar or circumstellar gas clouds.

form the carbene in a less ambiguous manner. Dicyanodiazomethane was found to be a suitable precursor for the generation of the carbene by either photolysis or pyrolysis.[227] Dicyanocarbene produced by either method was found to insert rapidly into aliphatic C-H bonds and to add across C-C double bonds (Scheme 7.2, a and b).[228]

Scheme 7.2
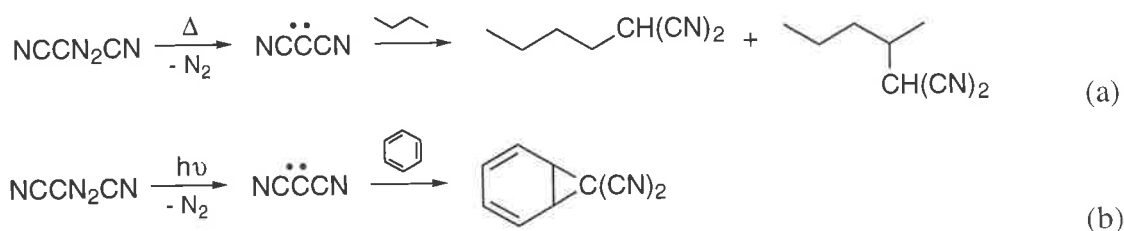
Thermolysis of dicyanodiazomethane in the presence of *cis* and *trans* 2-butene proved informative, with reactions carried out in the neat olefin proceeding with > 90% retention of stereochemistry.[228] However if this reaction is carried out with *cis* or *trans* olefin diluted in an unreactive solvent, the product ratio approaches 30 : 70 (*cis* : *trans*). That is, the thermodynamic *trans* product is the major product under dilute conditions, regardless of the original stereochemistry of the alkene. It was suggested that this is indicative of concerted addition of singlet dicyanocarbene formed originally from thermolysis of the diazo precursor, resulting in retention of stereochemistry. However, dilution of the olefin in this reaction allows collisional deactivation of the singlet dicyanocarbene to a triplet ground state prior to addition. The triplet then adds in a stepwise manner to give predominantly the thermodynamic *trans* product. The assignment of the triplet ground electronic state was confirmed by the electron spin resonance spectrum.[229] The carbene was generated by photolysis of dicyanodiazomethane and trapped in a low temperature matrix where its electron spin resonance spectrum was measured. These results further predict a linear structure for the triplet ground state of NCCCN.

The pyrolysis of dicyanodiazomethane in a stream of helium at 220 °C has also been carried out with products identified by mass spectrometry.[230] Dinitrogen and tetracyanoethylene

were detected as expected, surprisingly however, cyanogen and dicyanoacetylene were also found as major products. It was suggested that these are formed by subsequent decomposition of the tetracyanoethylene (Scheme 7.3). However pyrolysis of neat tertracyanoethylene at 700 °C is necessary before these products are observed. This problem was explained in terms of excess internal energy resulting from the coupling of the two dicyanocarbenes.

Scheme 7.3
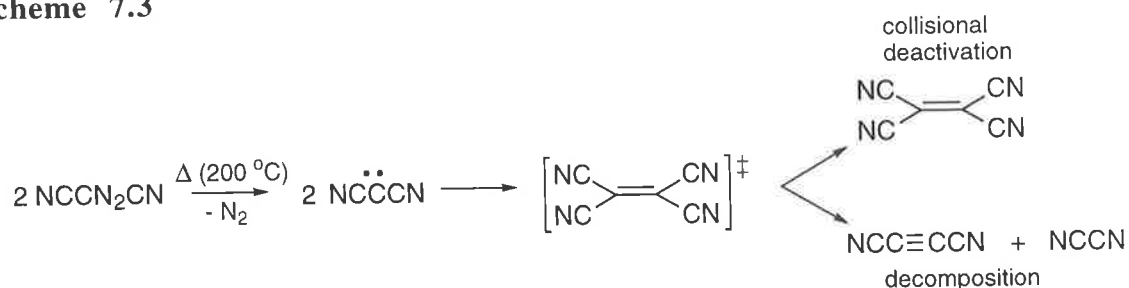
Similar experimental trends were observed for the NCN homologue. Produced either photolytically of pyrolytically from cyanogen azide (NCN_3), NCN inserts into C-H bonds, in a stereospecific manner when high concentrations of an aliphatic substrate are present.[231,232] This was rationalised in terms of singlet carbene as the reactive species. Dilution of the substrate with an unreactive solvent leads to the reaction proceeding in a stereo-random fashion. This was once again rationalised in terms of an initially formed singlet state undergoing collisional deactivation under dilute conditions to yield the triplet ground state. The triplet ground state then undergoes stepwise insertion.[226] Further support for this postulate was the detection of triplet NCN trapped in low temperature matrix, by electron spin resonance.[229]

More recent spectroscopic studies have been carried out on both NCCCN and NCN. Infrared absorptions of NCCCN trapped in low temperature matrix have been measured.[233,234] Electronic, laser induced fluorescence and infrared spectra have been reported for NCN.[235-237] Both NCN and NCCCN have also been the subject of theoretical investigations. A non-linear $^3B_1$ ground state NCCCN structure was calculated in early

studies and found to be some 17 kcal mol^{-1} more stable than the lowest energy singlet state.[238-240] Recent high level *ab initio* investigations[241] for NCN have found linear $^3\Sigma_g^-$ to be the ground state with a C-N bond length of 1.2334 Å in good agreement with the experimental determination of 1.2309 Å.[242,243]

Previous negative ion chemical ionisation studies have shown that the radical anions NCCCN$^{\cdot-}$ and NCN$^{\cdot-}$ can be formed by ion molecule reactions. Reaction of malononitrile with O$^{\cdot-}$ was found to give NCCCN$^{\cdot-}$ in the gas phase, whilst the same reagent reacted with cyanamide yields NCN$^{\cdot-}$ (Scheme 7.4, a and b).[244,245]

Scheme 7.4

$$(NC)_2CH_2 \;+\; O^{\cdot-} \;\rightarrow\; (NC)_2C^{\cdot-} \;+\; H_2O \qquad\qquad (a)$$

$$NCNH_2 \;+\; O^{\cdot-} \;\rightarrow\; NCN^{\cdot-} \;+\; H_2O \qquad\qquad (b)$$
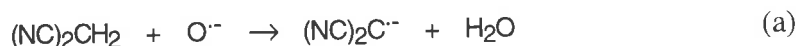
Whilst little work has been done on the NCCCN anion, NCN$^{\cdot-}$ has been probed in photoelectron spectroscopic experiments. The electron affinity of NCN has been determined to be 2.484 ± 0.006 eV and the ground electronic state has been confirmed to be the triplet.[246]

(III) RESULTS AND DISCUSSION

A. Synthesis of NCN

1. *Gas phase synthesis of neutral NCN*

The NCN radical anion was synthesised by reaction of cyanamide with $O^{\cdot-}$ in the source of the mass spectrometer (Scheme 7.4, b). This reaction gives a peak at *m/z* 40 of high abundance corresponding to a "$CN_2^{\cdot-}$" species. A previous investigation has shown that this reaction produces $NCN^{\cdot-}$ (**A**) exclusively: neither of the two other possible geometries (**B** and **C**) are formed.[245]

Scheme 7.5

$$^{-}N=C=N^{\cdot} \qquad ^{-\cdot}C=N=N \qquad$$

A   B   C
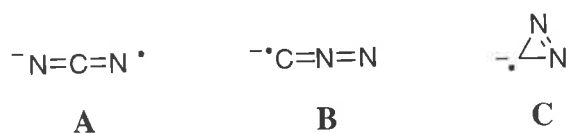
This structural assignment is further confirmed by the $^{-}CR^{+}$ spectrum which shows loss of atomic nitrogen and formation of the cyanide cation as the major fragmentation. Although a peak corresponding to $N_2^{\cdot+}$ does appear in the spectrum it is of substantially lower abundance than the CN^{+} signal (Figure 7.1, a). The opposite trend would be anticipated for structures **B** and **C** where fragmentation yielding the dinitrogen radical cation should dominate.

The $^{-}NR^{+}$ spectrum of $NCN^{\cdot-}$ shows a strong recovery signal (Figure 7.1, b) suggesting the stability of neutral NCN on the microsecond timescale. A qualitative comparison of the $^{-}CR^{+}$ and $^{-}NR^{+}$ spectra indicates a slight increase in fragmentation (relative to the recovery signal) in the latter. The spectra are however ostensibly the same and it can be concluded that (i) there is favourable Franck-Condon overlap between the anion, neutral and cation potential surfaces (a conclusion borne out by theoretical predictions of structure, see subsequent section) and (ii) there is no major unimolecular behaviour (either rearrangement or fragmentation) which can be attributed to the transient neutral.
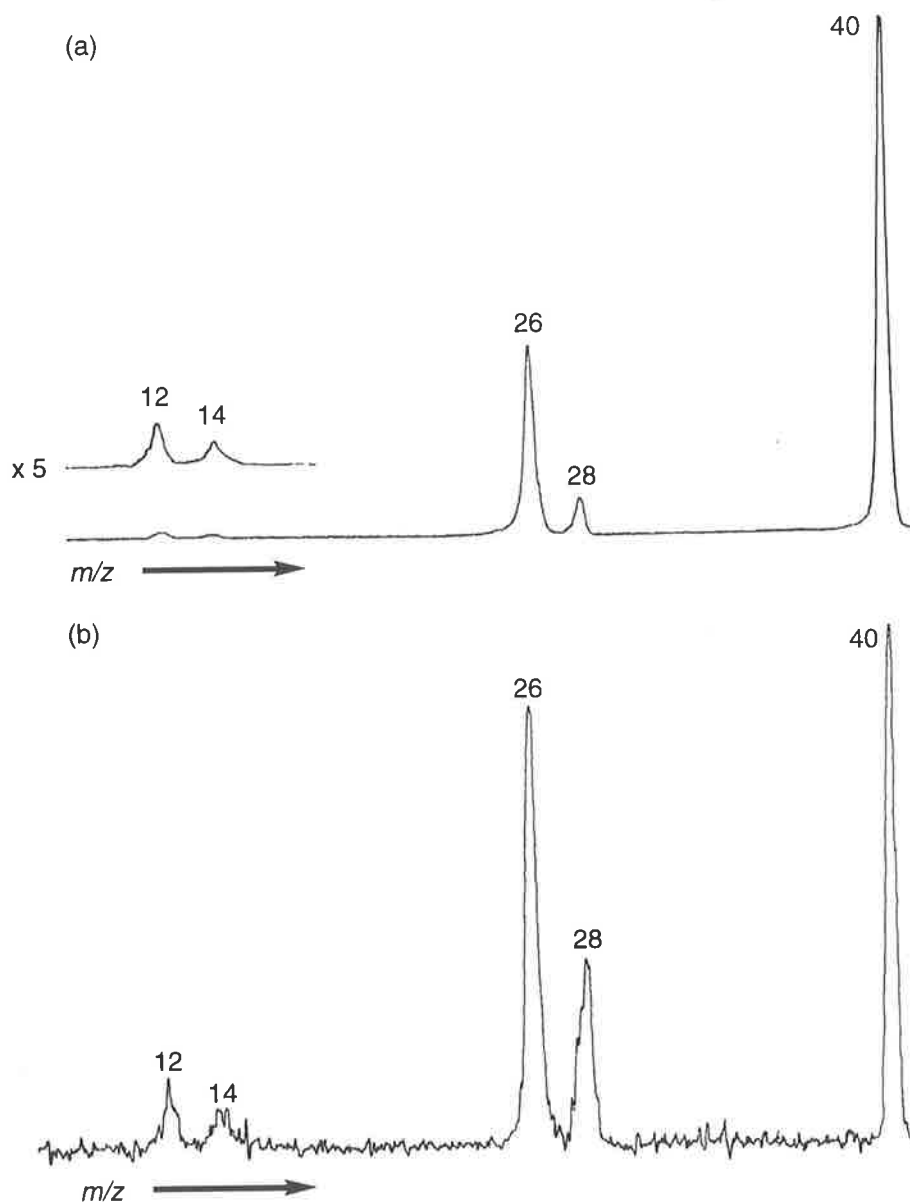
Figure 7.1 *(a) ⁻CR⁺ (O₂, 80% T; O₂, 80% T) and (b) ⁻NR⁺ (O₂, 80% T; O₂, 80% T) spectra of NCN⁻⁻.*

2. Theoretical predictions of NCN structure

The hybrid density functional Becke 3LYP method using the modest 6-31+G(d) basis predicts a ground state triplet ($^3\Sigma_g^-$) for NCN neutral with a C-N bond length of 1.2341 Å. This value is in good agreement with both the experimental [r(C-N) = 1.2309 Å][242,243] and high level theoretical data available [r(C-N) = 1.2334 Å].[241] An excited singlet $^1\Delta_g^-$ state is also predicted with r(C-N) = 1.2312 Å but almost 1.5 eV above the ground state (Table 7.1). This method predicts linear $D_{\infty h}$ geometries for both anionic and cationic charge states. The

$^2\Pi_g$ anion ground state is calculated to have r(C-N) = 1.2404 Å whilst for the $^2\Pi_g$ cation ground state r(C-N) = 1.2377 Å. These geometries were used to predict adiabatic electron affinities and ionisation potentials using coupled cluster theory. The results are given in Table 7.1 along with the experimentally determined electron affinity of NCN (electronic energies, zero-point energy corrections and relative energies are given in Table 7.2). It is apparent from these results that (i) the B3LYP method performs surprisingly well, providing a good estimate of electron affinity and (ii) for the RCCSD(T) method, the larger cc-pVTZ basis set out-performs the cc-pVDZ basis set for prediction of the EA. Photoelectron spectroscopy experiments carried out on NCN·⁻ were unable to detect excited singlet states for neutral NCN but a lower bound of 0.85 eV was established.[246] That is, the singlet electronic state must be at least 0.85 eV more energetic than the triplet ground state. This result is consistent with the singlet-triplet energy gap calculated by all three methods (Table 7.1).

Table 7.1 Thermochemical properties for NCN calculated at different levels of theory. The geometries and electronic energies from which these properties are derived are listed in Table 7.2, pp 164.

Level of theory or Experiment type	Electron affinity (eV)	Ionisation Potential (eV)	Singlet-Triplet splitting (eV)[b]
B3LYP/6-31+G(d)	2.50	15.31	1.46
RCCSD(T)/aug-cc-pVDZ// B3LYP/6-31+G(d)	2.23	14.60	1.35
RCCSD(T)/aug-cc-pVTZ// B3LYP/6-31+G(d)	2.42	14.94	1.25
CBS-QCI/APNO[a]	2.52	N/A	N/A
Photoelectron spectroscopy[a]	2.484 ± 0.006	N/A	> 0.85

[a] Taken from the work of Ellison and co-workers.[246]
[b] The energy separation between the triplet ground state and the excited singlet electronic state.

In valence bond terms the theoretical data suggests structures for ground state anion, neutral and cation as shown in Scheme 7.6. The linear geometry and contracted C-N bond lengths suggest a resonance hybrid of a cyano-nitrene and allenic type structures. For the triplet

ground state neutral two unpaired electrons in orthogonal Π orbitals gives rise to the $^3\Sigma_g^-$ term. The ground state anion and cation may be considered by simply adding or removing an electron from the HOMO orbital.

Scheme 7.6
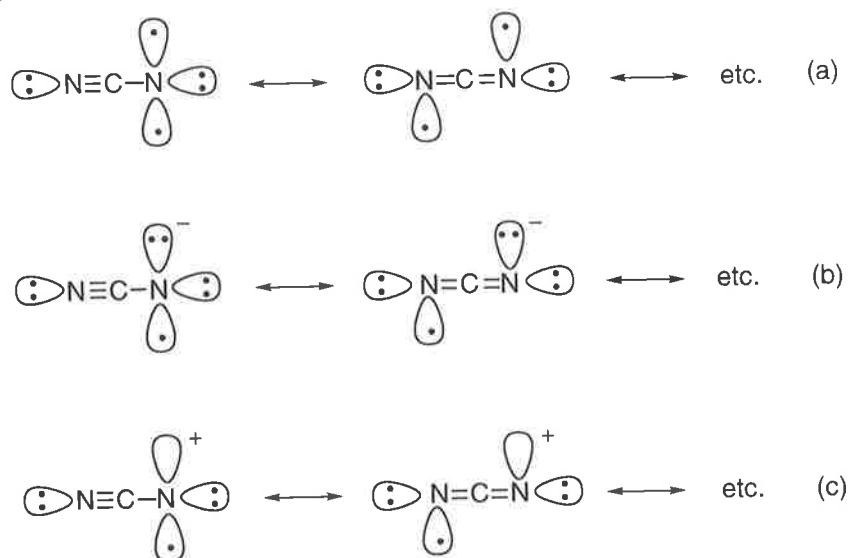
The geometric uniformity between the three charge states may give some insight into the observed NRMS behaviour of this species. With linear structures for the anion, neutral and cation the only geometric differences are the C-N bond lengths which differ by less than 0.01 Å. This suggests favourable Franck-Condon factors governing vertical electronic transitions between (i) anion and cation ($^-CR^+$), (ii) anion and neutral and (iii) neutral and cation ($^-NR^+$) surfaces. From the theoretical data it would be expected that neutral NCN would be formed in an NRMS experiment and observed as the NCN$^{\cdot+}$ signal in the spectrum. Due to the favourable Franck-Condon considerations for the anion and both triplet and singlet neutral potential surfaces it is probable that both spin states would be accessed during this experiment. The large recovery signal in the $^-NR^+$ spectrum of NCN$^{\cdot-}$ has already been discussed (Figure 7.1, b) and is consistent with these theoretical predictions.

Table 7.2 The results of theoretical calculations for anion, neutral and cation charge states of NCN. The geometries are calculated at the B3LYP/6-31+G(d) level of theory with high level single point energies calculated at the RCCSD(T)/aug-cc-pVDZ and RCCSD(T)/aug-cc-pVTZ levels.

NCN Species	Electronic State	r(C-N) angstroms	Electronic Energy (Hartrees)	Zero-point Energy (Hartrees)[†]	Relative Energy (kcal mol^{-1})[‡]
NCN$^{\cdot-}$	$^2\Pi_g$	1.2404[a]	-147.59103[a]	0.00922[a]	0.0
			-147.22972[b]		0.0
			-147.34793[c]		0.0
NCN	$^3\Sigma_g^-$	1.2341	-147.49851	0.00842	57.6
			-147.14696		51.4
			-147.25819		55.8
NCN	$^1\Delta_g^-$	1.2312	-147.44571	0.00915	91.2
			-147.09823		82.5
			-147.21279		84.8
NCN$^{\cdot+}$	$^2\Pi_g$	1.2377	-147.02683	0.00844	353.1
			-146.69248		336.6
			-146.79796		344.6

[a] Calculated using B3LYP/6-31+G(d)//B3LYP/6-31+G(d)
[b] Calculated using RCCSD(T)/aug-cc-pVDZ//B3LYP/6-31+G(d)
[c] Calculated using RCCSD(T)/aug-cc-pVTZ//B3LYP/6-31+G(d)
† ZPE uncorrected
‡ Relative energy includes ZPE corrected by 0.9804.[91]

B. Synthesis of NCCCN and its Unimolecular Behaviour

1. *Gas phase synthesis of NCCCN ions*

Two methods were found for generating the NCCCN radical anion in the mass spectrometer. The first, involves the reaction of malononitrile with $O^{\cdot-}$ as previously reported by Dawson and Nibbering (Scheme 7.4).[244] The resultant loss of H_2O, gives a peak corresponding to "$C_3N_2^{\cdot-}$" in good abundance. The structure of this ion was assumed in the literature to have NCCCN connectivity consistent with the structure of the malononitrile precursor. This is borne out by the $^-CR^+$ spectrum, which shows losses of N, NC and NCC as the major fragmentations consistent with C-N and C-C cleavages from an NCCCN backbone (Table 7.3, pp 167). Sequential fragmentation of activated cumulenic cations along the carbon backbone has been observed previously.* A comparable example involves the fragmentation of $H_2N=C=C=C=O^+$ under CA and $^+NR^+$ conditions.[221] Here, the fragmentations are dominated by losses of (i) O, CO, C_2O as well as (ii) NH_2, CNH_2, C_2NH_2 originating from simple cleavages along the carbon backbone. Notably, no loss of C or C_2 is observed which

---

* See also CR fragmentation of HC_5H, Chapter 5.

would require more complex decomposition pathways. Thus for a linear cumulenic cation species the sequence of fragment ions observed may be used for assignment of structure.

The second method for generation of $C_3N_2^{\cdot-}$ involves the fragmentation of the tetracyanoethylene oxide radical anion. Under NICI conditions, tetracyanoethylene oxide gives a source formed parent radical anion with concomitant production of a C_3N_2 radical anion (*m/z* 64).[247] The $^-CR^+$ spectrum of the latter ion confirms the empirical assignment and its connectivity, showing identical fragmentation to that observed in the spectrum obtained from malononitrile (Table 7.3, pp 167). The structure of this ion is therefore assigned as the radical anion NCCCN. The source formed NCCCN radical anion gives a more abundant peak from tetracyanoethylene oxide than from malononitrile and hence a more intense CR spectrum was obtained from the former. As a consequence, a few minor fragmentations not previously observed, such as the loss of carbon and formation of $C_3^{\cdot+}$, were noted. Formation of NCCCN$^{\cdot-}$ from tetracyanoethylene oxide could occur *via* a number of mechanisms but it is notable that the CA spectrum of the parent radical anion shows only limited formation of *m/z* 64.[247] It is therefore most probable that dissociative resonance capture competes with thermal electron capture under NICI conditions, forming internally excited ions along with the stable [M]$^{\cdot-}$ ions. The former may decompose rapidly to NCCCN$^{\cdot-}$ by a mechanism such as that described in Scheme 7.7.

Scheme 7.7
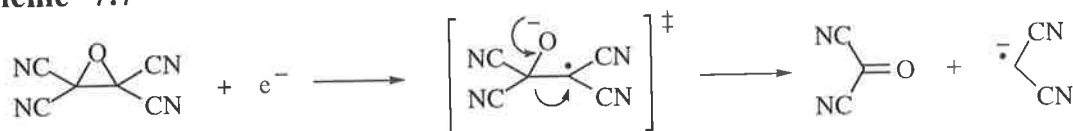
This type of decomposition of cyano substituted oxiranes has been induced photolytically in solution chemistry. 2-Cyanooxiranes undergo photolytic cleavage in a number of cases to give substituted cyanocarbenes which can be trapped by insertion or addition to the reaction solvent. For example, 2,3,3-triphenyl-2-cyanooxirane under prolonged photolysis gives

phenylcyanocarbene, which adds to the double bond in 2-methyl-2-butene, the reaction solvent (Scheme 7.8).[248]

Scheme 7.8

The analogous C_3N_2 radical cation is formed upon EI ionisation of tetracyanoethylene oxide. If this ion is formed by a dissociative ionisation pathway, as for the anion and neutral mechanisms discussed, NCCCN connectivity would be anticipated. Comparison of the CA spectrum of this positive ion with the $^-CR^+$ spectra of the anion can only be a qualitative guide to ion structure.# Having said this however, the fragment ions observed in the CA spectrum of the C_3N_2 radical cation are very similar to those observed in the CR spectrum of the radical anion. The former shows major losses of N, NC and NCC consistent with NCCCN connectivity (Table 7.3, pp 167).

Malononitrile also gives the C_3N_2 radical cation under EI conditions, presumably *via* step-wise loss of hydrogen radicals from the parent ion. Loss of two or more hydrogen radicals from a cumulenic backbone has previously been observed and utilised in the generation of unsaturated carbon cations in the gas phase.[148,150] The structure of the precursor molecule suggests the connectivity is NCCCN in this case unless some skeletal rearrangement is involved in the ionisation or fragmentation process. The geometry is confirmed by the CA spectrum, which is identical to that of the same ion obtained from tetracyanoethylene oxide (Table 7.3, pp 167).

The internal energies deposited in the ions in each of the two experiments are quite different and hence more often than not the abundances of the fragment ions appearing in each spectrum are not the same.[39] See Chapter 1, pp 25 for more discussion of this observation.

In summary, NCCCN radical anions and cations may be generated in the gas phase by ionisation (under varying conditions) of the neutral substrates malononitrile and tetracyanoethylene oxide.

Table 7.3 CR and CA spectra of NCCCN$^{\cdot-}$ and NCCCN$^{\cdot+}$ respectively.

Precursor Molecule	Ionisation method	Spectrum type	Fragmentations mass/charge ratio (relative intensity)[a]
malononitrile	NICI (N$_2$O)	$^-$CR$^+$	64(100), 52(0), 50(63), 38(88), 36(0), 26(9), 24(4), 12(0)
tetracyanoethylene oxide	NICI (N$_2$O)	$^-$CR$^+$	64(93), 52(5), 50(58), 38(100), 36(3), 26(13), 24(4), 12(1)
malononitrile	EI	CA (positive)	64, 52(4), 50(10), 38(100), 36(0.4), 26(1), 24 (0.4), 12(<0.2)
tetracyanoethylene oxide	EI	CA (positive)	64, 52(2), 50(7), 38(100), 36 (0.5), 26(2), 24 (1), 12(0.2)

[a] For convenience the relative abundance is given relative to that of the base peak (excluding the parent ion signal for positive ion CA spectra).

2. *Behaviour of neutral NCCCN*

With the connectivity of the radical anion and cation of NCCCN established, it remains to investigate the stability of the corresponding neutral on the mass spectrometric timescale. $^-$NR$^+$ and $^+$NR$^+$ spectra of the precursor ions show strong recovery signals consistent with the survival of a "C$_3$N$_2$" neutral species between neutralisation and reionisation collisions (ca. 10^{-6} s). It is of particular interest to note the abundance of peak *m/z* 52, corresponding to loss of carbon, in (i) the $^-$NR$^+$ compared with the $^-$CR$^+$ spectrum and (ii) the $^+$NR$^+$ compared with the positive ion CA (Figures 7.2 and 7.3 respectively).

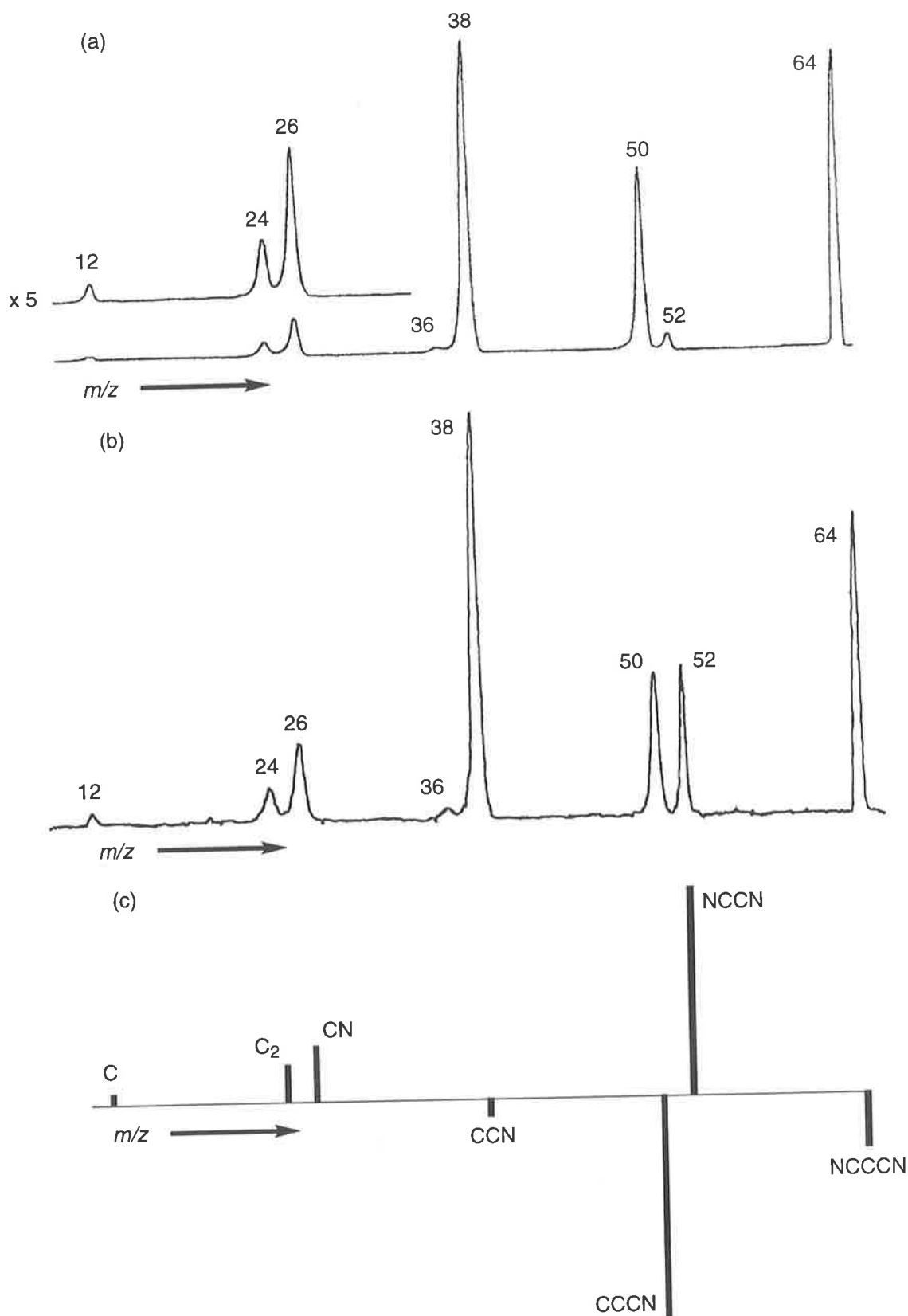**Figure 7.2** *(a)* $^-CR^+$ *(O_2, 80% T; O_2, 80% T) and (b)* $^-NR^+$ *(O_2, 80% T; O_2, 80% T) spectra of NCCCN^{--}. (c)* $^-NIDD^+$ *spectrum.*

Consider the case of the radical anion in the first instance. Vertical excitation of the anion to the cation surface in the $^-CR^+$ experiment generates the NCCCN radical cation as has been demonstrated by the fragmentation pattern (see preceding $^-CR^+$ discussion, pp 164). However the corresponding $^-NR^+$ spectrum shows a pronounced loss of carbon, not observed for the $^-CR^+$ spectrum, suggesting one of two possibilities, each involving a unimolecular reaction of the neutral NCCCN (Scheme 7.9).

Scheme 7.9

$$NCCCN^{\bullet-} \xrightarrow{NR\ (-e^-)} \left[NCCCN\right]^{\ddagger} \xrightarrow[\text{fragmentation}]{\text{neutral}} C_2N_2 + C \xrightarrow{NR\ (-e^-)} C_2N_2^{\bullet+} \quad (a)$$
$$\phantom{NCCCN^{\bullet-} \xrightarrow{NR\ (-e^-)} \left[NCCCN\right]^{\ddagger} \xrightarrow[\text{fragmentation}]{\text{neutral}} C_2N_2 + C \xrightarrow{NR\ (-e^-)}} m/z\ 52$$

$$NCCCN^{\bullet-} \xrightarrow{NR\ (-e^-)} \left[NCCCN\right]^{\ddagger} \xrightarrow[\text{rearrangement}]{\text{neutral}} NCCNC \xrightarrow{NR\ (-e^-)} \left[NCCNC^{\bullet+}\right]^{\ddagger}$$

$$\left[NCCNC^{\bullet+}\right]^{\ddagger} \xrightarrow[\text{fragmentation}]{\text{positive ion}} NCCN^{\bullet+} + C \quad (b)$$
$$\phantom{\left[NCCNC^{\bullet+}\right]^{\ddagger} \xrightarrow[\text{fragmentation}]{\text{positive ion}}} m/z\ 52$$

Direct loss of carbon from reionised $NCCCN^{\bullet+}$ can be ruled out as this fragmentation is only minor in the $^-CR^+$ spectrum. Therefore, the first possible rationale for the observed loss of atomic carbon is fragmentation of neutral NCCCN to form C and C_2N_2 (Scheme 7.9, a). The larger neutral fragment would then be efficiently reionised and the C_2N_2 cation observed in the $^-NR^+$ spectrum. It would be expected that the increased abundance of the C_2N_2 peak in the $^-NR^+$ spectrum should be accompanied by a concomitant reduction in the recovery signal. This should be most apparent in a comparison in peak abundances between $^-NR^+$ and $^-CR^+$ spectra. Such a comparison can be observed in the NIDD analysis, derived by subtraction of the normalised $^-CR^+$ from the normalised $^-NR^+$ spectrum (Figure 7.2, c).[#] The NIDD spectrum shows (i) a positive signal for loss of carbon, as expected for a species formed by fragmentation of the neutral and (ii) a negative intensity for the parent species, indicative of a reduction in the number of surviving neutrals. Whilst this seems in agreement with the proposed mechanism, the abundance of the two peaks in the NIDD spectrum are

---

[#] The method by which the NIDD spectrum was obtained is outlined in the Experimental section of this Chapter. A discussion of this method and its application appears in Chapter 1, pp 20.

quite different. The magnitude of the increase in carbon loss (*m/z* 52) in the ⁻NR⁺ compared with the ⁻CR⁺ spectrum far exceeds the magnitude of the reduction in the parent species (*m/z* 64).

By contrast, the NIDD spectrum shows that the loss of nitrogen to give *m/z* 50 is reduced in the ⁻NR⁺ compared with the ⁻CR⁺ spectrum by approximately the same magnitude as the increase in the loss of carbon which gives rise to *m/z* 52. This may point toward a second scenario for a neutral process giving rise to the loss of carbon in the ⁻NR⁺ spectrum (Scheme 7.9, b). Isomerisation of the neutral to form an isocyano species with the NCCNC connectivity, followed by reionisation would yield an activated NCCNC radical cation. In keeping with the previous discussion, such a cation would be expected to fragment by a series of sequential cleavages along the molecular backbone. Such fragmentation would result in the observation of comparable losses of carbon and nitrogen in the ⁻NR⁺ spectrum (see preceding ⁻CR⁺ discussion, pp 164). This is indeed the case, with the peaks corresponding to losses of carbon and nitrogen (*m/z* 52 and 50 respectively) of comparable abundance (Figure 7.3, b). The NIDD analysis also highlights this trend, with the loss of carbon as positive and the loss of nitrogen as negative and of almost equal intensity (Figure 7.2, c). This suggests that loss of carbon from the C_3N_2 cation formed in the stepwise oxidation (⁻NR⁺) comes at the expense of the nitrogen loss observed in the ⁻CR⁺ experiment. Such an observation is consistent with the proposal of complete or partial isomerisation from NCCCN to NCCNC at the neutral stage of the ⁻NR⁺ experiment.
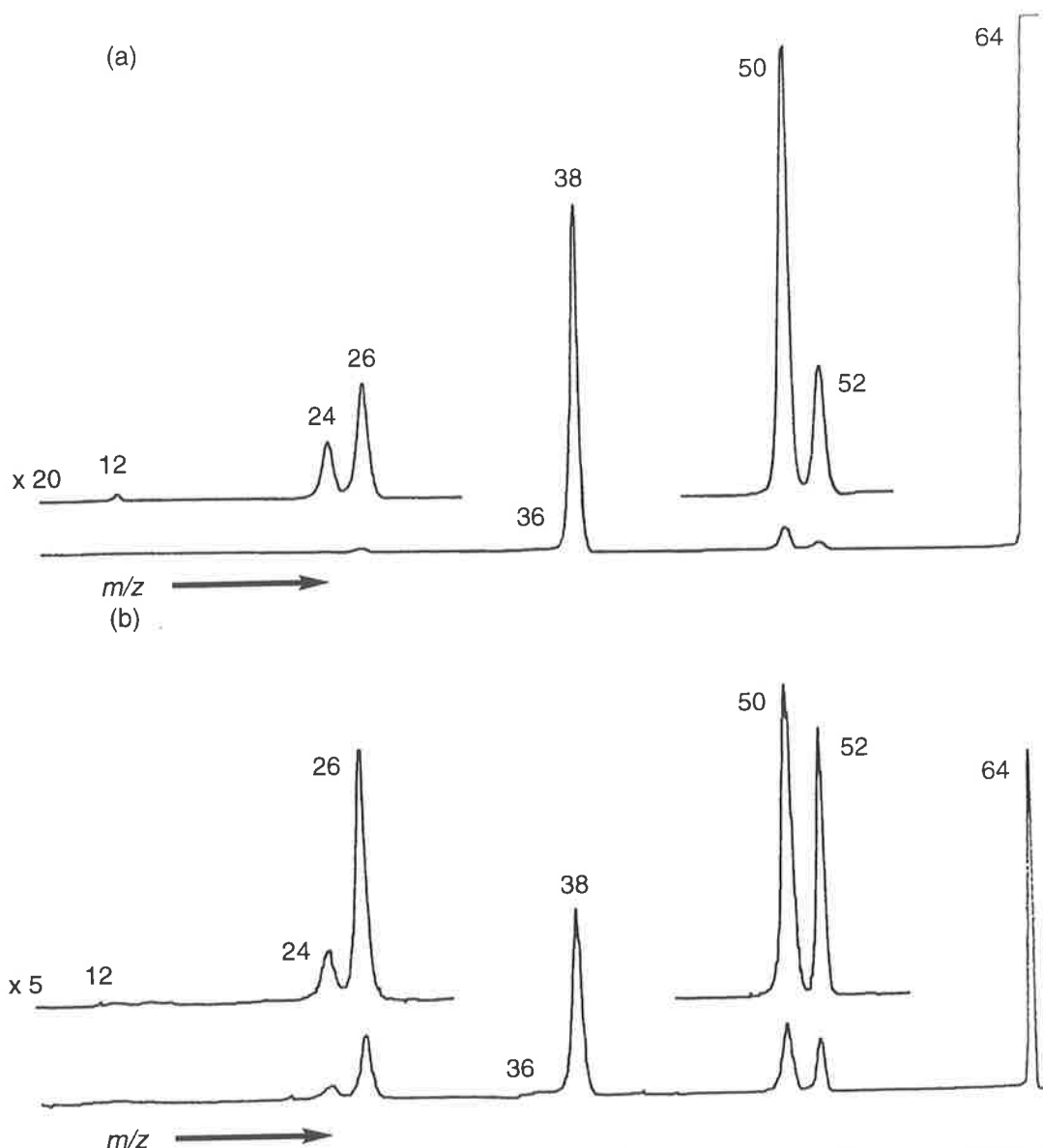
Figure 7.3 *(a) CA (benzene, 70% T; O₂, 80% T) and (b) ⁺NR⁺ (benzene, 70% T; O₂, 80% T) spectra of NCCCN⁺.*

Whilst it is not possible to quantitatively compare the positive ion CA and $^+NR^+$ spectra shown in Figure 7.3 it is informative to contrast them in a qualitative sense. The general trend is toward greater fragmentation in the $^+NR^+$ with respect to the parent ion signal, than that observed for the CA experiment. Amongst this however the most striking contrast remains the increase in abundance of the *m/z* 52 signal between the CA and $^+NR^+$ spectra. The same possibilities exist here as in the negative ion case. Namely, the increased loss of carbon in the $^+NR^+$ spectrum could be due to (i) loss of atomic carbon from neutral NCCCN and subsequent reionisation of the C_2N_2 fragment or (ii) skeletal rearrangement of the

NCCCN chain to an isocyanide species such as NCCNC and subsequent reionisation and fragmentation by loss of the terminal carbon (Scheme 7.9, a and b respectively). In the absence of any quantitative analysis (such as the NIDD comparison) it is difficult to favour one of these proposals over the other. In light of the $^-NR^+$ data it is tempting to favour the mechanism for neutral isomerisation (Scheme 7.9, b). However geometric differences between anion, neutral and cation (see subsequent theoretical discussion) may result in two different processes occurring in each of the NR charge permutations discussed. This is because the Franck-Condon factors are likely to be different for the anion-neutral and cation-neutral electronic transitions. The $^+NR^+$ data by itself does not give any further insight into the mechanism for carbon loss in the neutral spectra, except that it does suggest the process is independent of the charge state of the precursor ion.

If it could be established whether the carbon loss is from the central carbene position (NC<u>C</u>CN) or one of the nitrile moieties (N<u>C</u>CCN) this may further elucidate the mechanism of this process. As such, malononitriles labelled with carbon-13 at (i) the methylene position and (ii) one of the nitrile carbons were prepared. These precursors were reacted with the $O^{\cdot-}$ in the source of the mass spectrometer to generate gas phase NCCCN radical anions with labels incorporated as indicated in Scheme 7.10.

Scheme 7.10

$$NC\text{-}^{13}CH_2\text{-}CN \ + \ O^{\cdot-} \ \rightarrow \ NC\text{-}^{13}C\text{-}CN^{\cdot-} \ + \ H_2O \hspace{2cm} (a)$$

$$NC\text{-}CH_2\text{-}^{13}CN \ + \ O^{\cdot-} \ \rightarrow \ NC\text{-}C\text{-}^{13}CN^{\cdot-} \ + \ H_2O \hspace{2cm} (b)$$

The collisional activation, charge reversal and neutralisation reionisation data from these anions are listed in Table 7.4, pp 174. The most critical observation arising from the $^-NR^+$ spectra of the labelled precursor ions is that the loss of carbon-12 and carbon-13 occurs in an almost statistical manner from both configurations. That is, the peaks *m/z* 52 and 53 appear in a ratio of approximately 1 : 2. This suggests a scrambling of the label which may occur at either the anion, neutral or cation stage of the $^-NR^+$ experiment.

The negative ion CA spectra for both carbon-13 labelled species are given in Table 7.4, pp 174. The NC-^{13}C-CN radical anion is found to lose predominantly the unlabelled cyanide radical and form the unlabelled cyanide anion. A comparatively small fraction of ^{13}CN$^-$ (14% of unlabelled CN$^-$ signal) is observed. This is indicative of a small amount of rearrangement or carbon scrambling, however this is a minor process, probably occurring only upon collisional activation of the anion. Conversely, the N^{13}C-C-CN radical anion shows loss of both labelled and unlabelled cyanide radicals in a ratio of almost 1 : 1 as would be anticipated for this labelling configuration. The ratio of the ^{13}CN and CN anions in this spectrum is however not quite unity as would be anticipated, but closer to 0.65. Given the results from the NC-^{13}C-CN labelling configuration, it seems unlikely that rearrangement or carbon scrambling could account for this discrepancy in the N^{13}C-C-CN$^{\cdot-}$ spectrum. More probable is a contribution to the *m/z* 26 peak from fragmentation of a parent ion isobaric with the N^{13}C-C-CN radical anion.[#] The CA spectra seem to indicate that scrambling of the carbons in the NCCCN radical anion is a very minor process and probably does not occur in the absence of collisional activation.[*]

[#] A small loss of hydrogen is observed in the CA spectra of both N^{13}C-C-CN$^{\cdot-}$ and NC-^{13}C-CN$^{\cdot-}$ and seems likely to be from the isobaric [M-H] anion of unlabelled malononitrile (Table 7.4). Although both precursors have an extrememly high carbon-13 incorporation, the ratio of peak abundances corresponding to [M-H]$^-$ and [M-H$_2$]$^{\cdot-}$ in the source of the mass spectrometer is almost 100 : 1. Further, the former ion gives much more intense fragmentations than the latter in both CA and $^-$CR$^+$ spectra. The extent of the isobaric contamination proved difficult to quantify. With the difference in atomic mass between C$_2$^{13}CN$_2$ and C$_3$N$_2$H of only 0.004 a.u., sufficient resolution could not be achieved in order to compare relative peak abundances. Assuming the correct assignment of the impurity the CA, $^-$CR$^+$ and $^-$NR$^+$ spectra for pure malononitrile [M-H]$^-$ are given as a footnote to Table 7.4. Certainly this data helps to rationalise some of the anomolies observed in the spectra of the labelled NCCCN radical anions. For example, In the CA spectrum of the N^{13}C-C-CN radical anion it is probable that the [M-H] anion of unlabelled malononitrile contributes to the intensity of *m/z* 26 but not *m/z* 27 (see Table 7.4) hence creating a spurious ratio for the formation of the labelled and unlabelled cyanide anions.

[*] The metastable ion spectrum (ie. the MIKE spectrum run in the absence of collision gas) of the malononitrile [M-H$_2$] radical anion shows no fragmentation.

Table 7.4 NR, CR and CA spectra for the two labelled configurations of NCCCN radical anions.

Precursor Ion	Spectrum type	Fragmentations mass/charge ratio (relative intensity)[†‡]
NC-C-^{13}CN	$^-$CR$^+$	65(100), 64(7), 53(2)[a], 52(0)[a], 51(22), 50(4), 39(28), 38(21), 27(3), 26(4), 25(2), 24(2), 14(0), 13(0.5), 12(1)
NC-C-^{13}CN	$^-$NR$^+$	65(100), 64(7), 53(22), 52(13), 51(35), 50(6), 39(78), 38(55), 27(13), 26(20), 25(15), 24(9), 14(0), 13(2), 12(4)
NC-C-^{13}CN	CA	65, 64(10), 51(29), 39(14), 38(12), 27(65), 26(100)
NC-^{13}C-CN	$^-$CR$^+$	65(100), 64(5), 53(1)[a], 52(0)[a], 51(33), 50(4), 39(58), 38(24), 27(1), 26(6), 25(3), 24(1), 14(0.5), 13(1), 12(1)
NC-^{13}C-CN	$^-$NR$^+$	65(100), 64(17), 53(15), 52(9), 51(27), 50(6), 39(79), 38(64), 27(16), 26(26), 25(13), 24(9), 14(2), 13(2), 12(5)
NC-^{13}C-CN	CA	65, 64 (13), 51(15), 39(30), 38(3), 27(14), 26(100)

† For CR and NR intensity is given as a percentage of the parent ion, whilst for CA spectra the value given is as a pecentage of the base peak.
‡ The masses which appear underlined in the table are the result of isobaric interference most probably from [NC-CH$_2$-CN - H]$^-$ (i) CA (negative ion): 65, 64 (73), 51(63), 50(31), 39(98), 38(41), 26(100). (ii) $^-$CR$^+$: 65(100), 64(30), 53(1), 51(11), 50(5), 39(8), 38(20), 27(1), 26(3), 25(2), 24(1). (iii) $^-$NR$^+$: 65(100), 64(39), 53(1), 51(9), 50(6), 39(9), 38(27), 27(1), 26(2), 25(1), 24(1).
a The peak abundances corresponding to losses of carbon-12 and carbon-13 in the $^-$CR$^+$ spectra should not be used as evidence for the presence or absence of scrambling. These signals are only slightly above the noise level of the spectra and as such a satisfactory relative ratio of intensities could not be established.

If the carbons of the NCCCN radical anion are not scrambling then the question remains as to whether this process is occurring for neutral NCCCN, the NCCCN cation or both. It is possible that rearrangement of the neutral, such as cyano-isocyano isomerisation (Scheme 7.9, b) may be a process related to scrambling of the carbons. That is, scrambling of the carbons may accompany isomerisation. This connection had been established by theoretical calculations described in a subsequent section on pp 182. Hence the observation of statistical losses of carbon-12 and carbon-13 in the $^-$NR$^+$ spectra of both labelled NCCCN radical anions favours isomerisation of the neutral rather than its direct fragmentation (Scheme 7.9, b and a respectively). The possibility of facile scrambling of the carbons occurring at the cation stage and preceding fragmentation cannot be excluded. The $^-$CR$^+$ spectrum of N^{13}C-C-CN$^{•-}$ shows formation of the ^{13}CN cation at *m/z* 27 whilst this peak is

174

absent in the corresponding spectrum of NC-^{13}C-CN$^{\cdot-}$. This would suggest little carbon scrambling of the NCCCN cation. However the NC-^{13}C-CN$^{\cdot-}$ spectrum does show a peak at *m/z* 38 corresponding to loss of labelled cyanide radical. It is unclear as to whether this points to some rearrangement of the cation or simply losses from an isobaric impurity.[#] Whilst both these explanations can account for the appearance of *m/z* 38 in the $^{-}$CR^{+} spectrum of NC-^{13}C-CN$^{\cdot-}$, neither can explain the increased abundance of this peak in the $^{-}$NR^{+} spectrum. The ratio of *m/z* 38 to *m/z* 39 in the $^{-}$CR^{+} spectrum is approximately 0.4 while in the corresponding $^{-}$NR^{+} spectrum it is approaching unity (Table 7.4). This can only be rationalised in terms of rearrangement or scrambling of the carbons in neutral C_3N_2.

To summarise the experimental observations: (i) both the $^{-}$NR^{+} and $^{+}$NR^{+} spectra of NCCCN ions show a pronounced loss of carbon to form a peak at *m/z* 52 which is only a very minor process in the $^{-}$CR^{+} and the positive ion CA spectra. (ii) In both NR spectra the peak corresponding to loss of carbon is comparable in abundance to that of loss of nitrogen, and (iii) the loss of carbon seems to be accompanied by a scrambling of the carbons at the neutral stage of the experiment. These observations support the conclusion that the initially formed NCCCN neutral isomerises to NCCNC with accompanying scrambling of the carbons. It is then the cyanoisocyano carbene which is reionised to the corresponding cation and fragments to give comparable losses of carbon and nitrogen in both $^{-}$NR^{+} and $^{+}$NR^{+} spectra (Scheme 7.9, b). Theoretical calculations presented in the subsequent section support this conclusion, showing that if sufficient energy is present in the neutral for isomerisation to occur then energy barriers to carbon scrambling can also be overcome.

Two further experiments may well reinforce this conclusion. Firstly, in order to further establish that scrambling of the carbons is a neutral process, measurement of the $^{-}$NR^{-} spectrum of NC-^{13}C-CN$^{\cdot-}$ may prove definitive. We have demonstrated that the NCCCN radical anion undergoes only minimal carbon scrambling. Therefore an increase in the abundance of the peak corresponding to the ^{13}CN anion in the $^{-}$NR^{-} spectrum of

---

[#] The $^{-}$CR^{+} spectrum of the [M-H] anion of malononitrile shows a pronounced peak at *m/z* 38 (Table 7.4).

NC-^{13}C-CN$^{\cdot-}$ can only be attributed to scrambling of the carbons in the intermediate neutral. Unfortunately, attempts to measure these $^{-}$NR^{-} spectra failed due to the relatively weak fragmentation of the NCCCN anion and hence no useful data could be collected.[#] Secondly, the two mechanistic possibilities for carbon loss in the $^{-}$NR^{+} and the $^{+}$NR^{+} spectra could be differentiated by measuring a NR/CA spectrum. This experiment requires at least a three sector facility[*] and involves (i) carrying out the NR experiment between the first two sectors, (ii) mass selecting the recovery ion with the second sector and (iii) collisionally activating this ion between the second and third sectors. If the loss of carbon is not observed in the $^{-}$NR^{+}/CA spectrum of NCCCN$^{\cdot-}$ (or the $^{+}$NR^{+}/CA spectrum of NCCCN$^{\cdot+}$) it could be concluded this process is the result of fragmentation of the neutral (Scheme 7.9, a). If however the loss of carbon is present, then isomerisation of the neutral (Scheme 7.9, b) would be the more likely mechanism.

3. *Theoretical predictions of NCCCN structure and energetics*

The success of the B3LYP density functional method for accurate prediction of the structure of the NCN nitrene suggests it is appropriate for use with the higher NCCCN homologue. Calculation at this level predicts a linear $^{3}\Sigma_g^{-}$ ground state for neutral NCCCN (Figure 7.4, a) consistent with the available experimental data[229] but in contrast to early low-level theoretical studies which favour a bent C_{2v} structure.[238] A bent C_{2v} structure is predicted for the excited singlet $^{1}A_1$ electronic state (Figure 7.4, b).

[#] This experiment was attempted using O_2 and benzene in adjacent collision cells. Whilst a weak recovery signal was detected, sufficient intensity could not be achieved to observe negative ion fragments. It is possible that the use of mercury vapour or some alkali earth metal vapour as the reionisation gas may increase the number of reionised negative ions and consequently allow the observation of fragments. Currently such facilities are not available in the Adelaide group.

[*] Such facilities are not yet available in the Adelaide group. It is hoped that future collaborations may allow the $^{-}$NR^{+}/CA and $^{+}$NR^{+}/CA spectra of the NCCCN negative and positive ions to be measured.
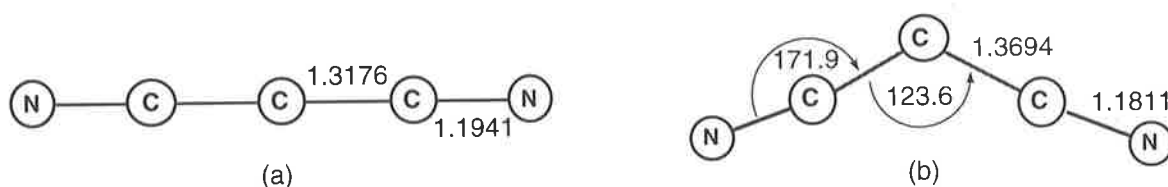
Figure 7.4 *Structures of neutral NCCCN (a)* $^3\Sigma_g^-$ *ground state and (b)* $^1A_1$ *excited state. Calculated at the B3LYP/6-31+G(d) level of theory.*
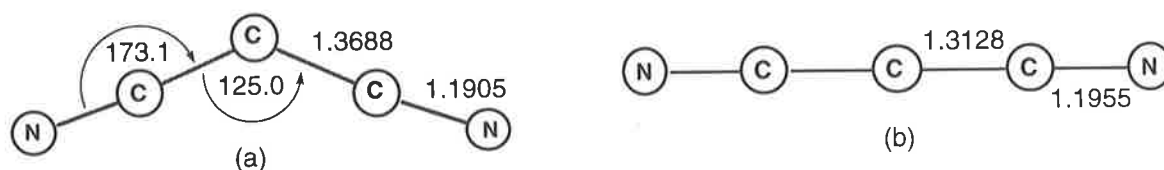

Figure 7.5 *Structures of NCCCN ions, (a)* $^2B_2$ *ground state anion and (b)* $^2\Pi_u$ *ground state cation. Calculated at the B3LYP/6-31+G(d) level of theory.*

The contracted C-C bonds in the triplet ground state [r(C-C) = 1.3176 Å] are between triple and double bond in character. This suggests that in valence bond terms this species is considered as a hybrid of a pure cumulenic nitrene and a cyano-acetylene nitrene. Both cumulenic and acetylenic structures would account for the predicted linear geometry of this diradical. The two unpaired electrons can be considered to occupy two orthogonal Π orbitals giving rise to the $^3\Sigma_g^-$ term. By contrast the bent C_{2v} structure of the singlet is that of a pure disubstituted-carbene.
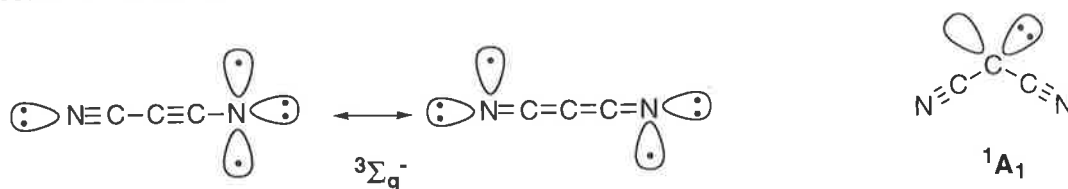
There are no data either experimental or theoretical pertaining to the structures of the anionic and cationic NCCCN radicals. The geometries predicted using the same protocol as for the neutral species are given in Figure 7.5. It is interesting to note the structural similarities between (i) the NCCCN radical cation and the triplet neutral and (ii) the NCCCN radical anion and the singlet neutral. In valence bond terms the charged species may be considered by simply adding or removing an electron from the HOMO of the neutral counterpart.

$^2\Pi_u$ $^2B_1$
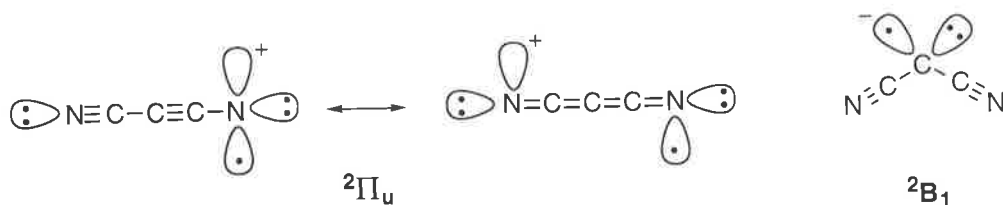
These geometric similarities must also be considered in the context of the various NRMS experiments discussed in the preceding section. For example, in the $^-NR^+$ experiment previously described, Franck-Condon factors for the anion-singlet neutral transition should be more favourable than those governing the anion-triplet neutral transition. It would be anticipated therefore, that the singlet neutral should be predominantly formed in this instance. Conversely, in the $^+NR^+$ experiment the ground state triplet neutral is more likely to form. This allows for the possibility that the loss of carbon observed in both NRMS spectra, may arise from the unimolecular reactions of both the singlet and the triplet neutrals. However the negative or positive precursor ions are not energetically cold: as such, it is unlikely that the neutrals in each experiment will be purely of one spin state or the other. It is most probable that both are formed with a preference for the species of greatest structural similarity to the precursor ion. Therefore, one may conclude that the loss of carbon could be occurring from unimolecular behaviour on one or both of the NCCCN neutral potential surfaces.

Table 7.5 Thermochemical properties for NCCCN calculated at different levels of theory. The geometries of the various species are given in Figures 7.4 and 7.5 while the electronic energies from which these properties are derived are listed in Table 7.6.

Level of theory	Electron affinity (eV)	Ionisation Potential (eV)	Singlet-Triplet splitting (eV)[a]
B3LYP/6-31+G(d)	3.07	14.02	0.78
RCCSD(T)/aug-cc-pVDZ// B3LYP/6-31+G(d)	3.11	13.78	0.46
RCCSD(T)/aug-cc-pVTZ// B3LYP/6-31+G(d)	3.20	14.02	0.47

[a] The energy separation between the triplet ground state and the excited singlet electronic state.

The energies of the various charge and spin states of NCCCN have also been calculated using the density functional approach and also at the more comprehensive RCCSD(T) level. The results are given in Table 7.5 which shows the calculated electron affinities, ionisation

potentials and singlet-triplet splittings (data from which these properties are calculated is given in Table 7.6). The electron affinity of NCCCN is notably more than 3 eV. Perhaps this is not surprising considering the electron affinity of the cyanide radical is also extremely large [EA(CN) = 3.8620 ± 0.0050 eV].[249] The singlet electronic state of neutral NCCCN is calculated to be only 0.46 eV above the triplet ground state. This singlet-triplet splitting is substantially smaller than that observed for the smaller NCN homologue suggesting the excited NCCCN singlet $^1A_1$ state should be detectable by photoelectron spectroscopy.[246] Unfortunately there exists no experimental data for comparison with these theoretical thermochemical predictions. The success of this theoretical protocol in predicting structural and energetic properties of the NCN system together with the coherence of the results for this system across two theoretical methods and three basis sets adds validity to the data presented.

Table 7.6 The results of theoretical calculations for anion, neutral and cation charge states of NCCCN. The geomtries are calculated at the B3LYP/6-31+G(d) level of theory and are given in Figures 7.4 and 7.5 with high level single point energies calculated at the RCCSD(T)/aug-cc-pVDZ and RCCSD(T)/aug-cc-pVTZ levels.

NCCCN Species	Electronic State	Electronic Energy (Hartrees)	Zero-point Energy (Hartrees)[†]	Relative Energy (kcal mol^{-1})[‡]
NCCCN$^{\cdot-}$	$^2B_1$	-223.79962[a]	0.01912[a]	0.0
		-223.23528[b]		0.0
		-223.41429[c]		0.0
NCCCN	$^3\Sigma_g^-$	-223.68708	0.01934	70.8
		-223.12093		71.6
		-223.29674		73.9
NCCCN	$^1A_1$	-223.65783	0.01885	88.8
		-223.10339		82.3
		-223.27897		84.8
NCCCN$^{\cdot+}$	$^2\Pi_u$	-223.28532	0.02010	323.3
		-222.72938		318.1
		-222.89994		323.4

[a] Calculated using B3LYP/6-31+G(d)//B3LYP/6-31+G(d)
[b] Calculated using RCCSD(T)/aug-cc-pVDZ//B3LYP/6-31+G(d)
[c] Calculated using RCCSD(T)/aug-cc-pVTZ//B3LYP/6-31+G(d)
[†] ZPE uncorrected
[‡] Energy given relative to the NCCCN radical anion. The relative energy includes ZPE corrected by 0.9804.[91]

4. Rearrangement reactions of neutral NCCCN

Isonitrile-nitrile rearrangements have been known for more than 100 years.[250,251] Theoretical and experimental studies have been carried out on this isomerisation reaction.[252,253] It is generally accepted that the free energy difference between nitriles and isonitriles is approximately 15 kcal mol^{-1} in favour of the nitriles for a wide variety of substituents. Further, the barrier to this rearrangement is of the order of 30-45 kcal mol^{-1}. By way of example, *p* -tolyl isocyanide rearranges to *p* -toluonitrile in the gas phase at 180-220°C a calculated activation of ca. 33.8 kcal mol^{-1} (Scheme 7.11).[254] By contrast, the reverse nitrile-isonitrile rearrangement, has a larger activation barrier and produces a less thermodynamically stable species. Examples of this scenario are rare.[255]

Scheme 7.11
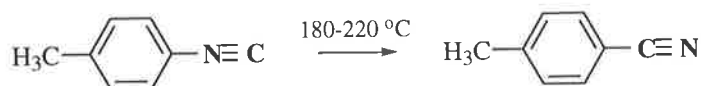
Such a cyano-isocyano rearrangement occurring in neutral NCCCN has been suggested as a possible explanation for the loss of carbon observed in the NRMS spectra (Scheme 7.9, b). The energetics of this process have been investigated by the B3LYP/6-31+G(d) theoretical method. The success of this method for prediction of structure and energy of the NCN and NCCCN systems has already been discussed. It is therefore utilised here for calculation of the relative energies of isomeric C_3N_2 species and the activation barriers connecting them.

Table 7.7 Energies and relative energies of the various singlet neutral C_3N_2 isomers. Also some pertinent transitions states are included. These are calculated at the B3LYP/6-31+G(d)//B3LYP/6-31+G(d) level of theory. The geometries of transition states and reactive intermediates are given as appendices to this Chapter (Table 7.9).

C_3N_2 Species	Electronic State	Electronic Energy (Hartrees)	Zero-point Energy (Hartrees)[†]	Relative Energy (kcal mol^{-1})[‡]
1 [NCCCN]	$^1A_1$	-223.65783	0.01885	0.0
TS1/2	singlet	-223.56382	0.01688	57.8
2 [(NCC)CN]	$^1A'$	-223.64491	0.01964	8.6
TS2/3	singlet	-223.58223	0.01638	45.9
3 [CNCCN]	$^1A'$	-223.63286	0.01842	15.4
TS3/4	singlet	-223.53633	0.01613	74.6
4 [CN(CCN)]	$^1A'$	-223.61706	0.01930	25.9
TS4/5	singlet	-223.54882	0.01607	66.7
5 [CNCNC]	$^1A_1$	-223.61338	0.01792	27.3
TS3/3	singlet	-223.57234	0.01634	52.1
TS4/4	singlet	-223.51852	0.01489	85.0
^1C + NCCN	singlet	-223.44712	0.01652	130.8

[†] ZPE uncorrected

[‡] Relative energy includes ZPE corrected by 0.9804.[91]

5. Isomerisation on the C_3N_2 singlet potential surface

The singlet cyano-isocyano carbene (**3**, CNCCN) is found to be a stable minimum some 15 kcal mol^{-1} more energetic than singlet NCCCN (**1**, Table 7.7). The difference in energy is in good agreement with the general cyano-isocyano trend outlined earlier. The geometry of CNCCN is a bent C_S configuration similar to that for singlet NCCCN and characteristic of a disubstituted carbene. Rearrangement of NCCCN to CNCCN is found to occur through the intermediacy of a cyclic species (NCC)CN (**2**) with the activation energies for the ring closing and ring opening steps of this reaction determined to be 57.8 and 37.3 kcal mol^{-1} respectively (Figure 7.6). Conversely, the reverse reaction (ie. isocyano-cyano) has an activation energy of ca. 42 kcal mol^{-1} in good agreement with the experimental determinations for similar isomerisations (ca. 38 kcal mol^{-1}, *cf.* Scheme 7.11).
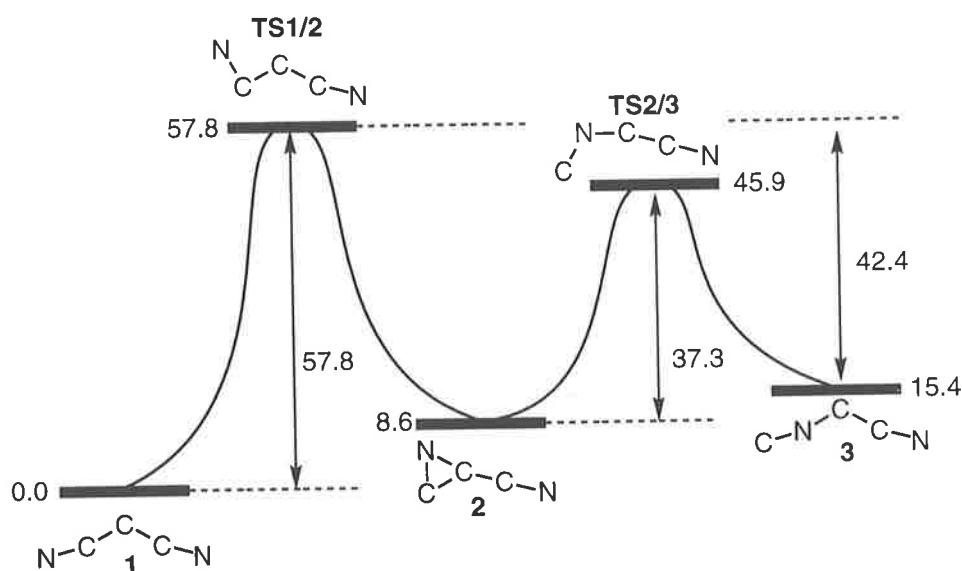
Figure 7.6 *The reaction coordinate diagram for the cyano-isocyano rearrangement of singlet neutral dicyanocarbene 1 to singlet neutral cyano-isocyano carbene 3. All energies are reported in kcal mol^{-1} and given relative to NCCCN with exception of activation energies which are indicated by vertical arrows.*

Should this rearrangement occur, the nascent cyano-isocyano carbene (**3**) would have sufficient energy to overcome the barrier to carbon scrambling. This can occur through the rhombic transition state **TS3/3** which is found to exist some 52 kcal mol^{-1} above the NCCCN singlet global minimum (Table 7.7). Scheme 7.12 shows schematically how this symmetric saddle point can produce scrambling of the central and isocyano carbon atoms.

Scheme 7.12
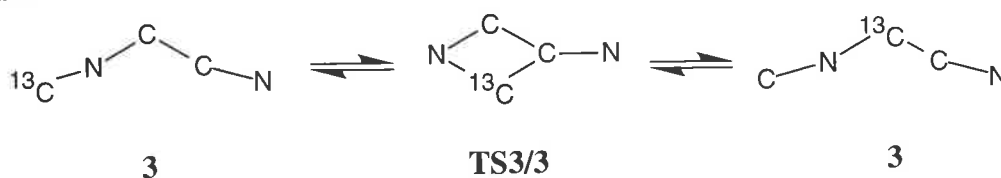
Further rearrangement of CNCCN (**3**) to the diisocyano carbene CNCNC (**5**) is also possible. A similar stepwise mechanism has been found which brings about this rearrangement (Figure 7.7). The energetics are slightly more demanding for the diisocyano species. This carbene is found to be 27 kcal mol^{-1} less stable than the dicyanocarbene with the activation barriers to its formation some 75 and 67 kcal mol^{-1} above the singlet NCCCN global minimum. It is interesting to note the continuation of the energy trend with CNCNC

(5) less stable than CNCCN (3) by almost 15 kcal mol^{-1} whilst CNCCN (3) is less stable

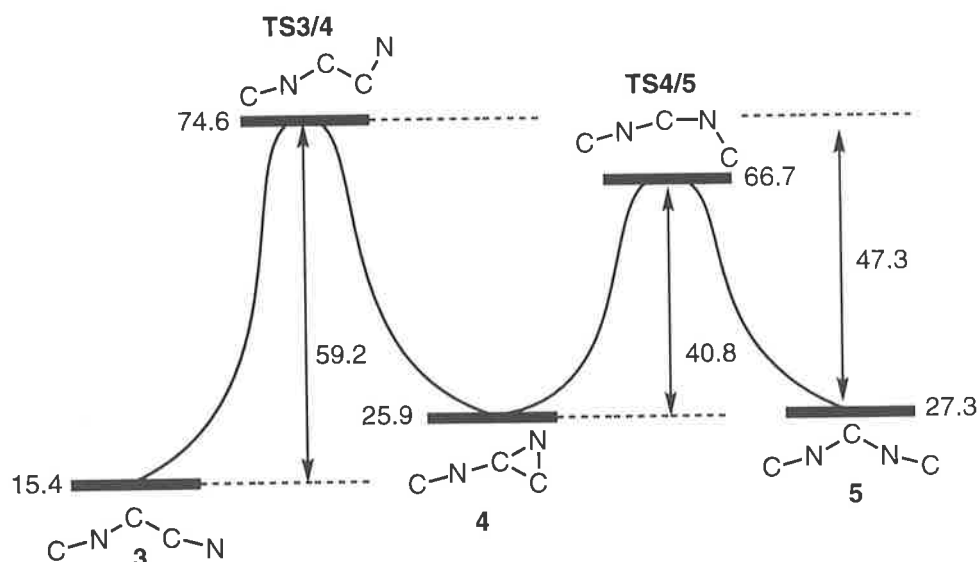than NCCCN (1) by a similar magnitude (Table 7.7).

Figure 7.7 *The reaction coordinate diagram for the cyano-isocyano rearrangement of singlet neutral isocyanocyano carbene 3 to diisocyanocarbene 5. All energies are reported in kcal mol^{-1} and given relative to NCCCN with exception of activation energies which are indicated by vertical arrows.*

Carbon scrambling can also occur for the diisocyanocarbene *via* a similar type of rhombic transition state as that described previously (Scheme 7.13). The activation barrier to this scrambling is however quite demanding, some 58 kcal mol^{-1} above the CNCNC carbene and 85 kcal mol^{-1} above the singlet NCCCN minimum (Table 7.7).

Scheme 7.13
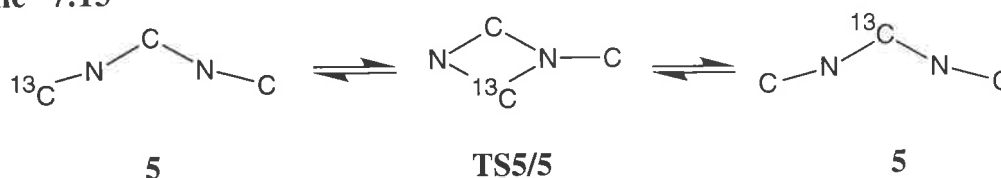
6. *Isomerisation on the C$_3$N$_2$ triplet potential surface*

The triplet potential surface also warrants some investigation. The relative energies of triplet C$_3$N$_2$ isomers are given in Table 7.8. The triplet isocyanocarbenes, CNCCN (3) and CNCNC (5) are substantially less stable than the triplet NCCCN minimum by 26 and 51

kcal mol^{-1}, respectively. Consequently rearrangement processes of the type described for the singlet surface will be substantially more endothermic. Further to this, triplet intermediates such as the cyclic species (NCC)CN (**2**) are also unstable, some 55 kcal mol^{-1} above the global minimum. It would seem from these data that isomerisation of the triplet NCCCN nitrene is extremely unlikely on energetic grounds and hence transition states connecting these minima have not been calculated.

Table 7.8 Energies and relative energies of some of the triplet neutral C_3N_2 isomers. These are calculated at the B3LYP/6-31+G(d)//B3LYP/6-31+G(d) level of theory. The geometries of these species are given as appendices to this Chapter (Table 7.10).

C_3N_2 Species	Electronic State	Electronic Energy (Hartrees)	Zero-point Energy (Hartrees)[†]	Relative Energy (kcal mol^{-1})[‡]
1 [NCCCN]	$^3\Sigma_g^-$	-223.68708	0.01934	0.0
2 [(NCC)CN]	triplet	-223.59678	0.01728	55.4
3 [CNCCN]	$^3A''$	-223.64415	0.01793	26.0
5 [CNCNC]	$^3A''$	-223.60491	0.01802	50.7
^3C + NCCN	singlet	-223.51343	0.01652	107.2

[†] ZPE uncorrected

[‡] Relative energy includes ZPE corrected by 0.9804.[91]

7. *Fragmentation of neutral NCCCN*

Fragmentation of neutral NCCCN (singlet or triplet) has been suggested as a possible alternative explanation for the loss of carbon observed in the NRMS spectra (Scheme 7.9, a). If this process is occurring then several questions must be addressed: (i) which carbon is lost, (ii) what is the mechanism for this fragmentation and (iii) what are the energy requirements? Attempts to find a transition state for carbon loss from singlet and triplet NCCCN species failed and hence the first two questions cannot be addressed directly. It is however possible to examine the overall energetics of this unimolecular reaction if we compare the energy of neutral C_3N_2 species with the most stable possible fragmentation products. These were found to be atomic carbon and cyanogen (N≡CC≡N). The energy of these fragments separated at infinity are tabulated for comparison with singlet and triplet C_3N_2 species in Tables 7.7 and 7.8 respectively. It is clear from these data that this is not an energetically favourable process. Loss of carbon and formation of cyanogen is exothermic by approximately 130 kcal mol^{-1} on the singlet potential surface and almost 110 kcal mol^{-1}

on the triplet. Even without the consideration of the thermochemical barriers to these reactions the energy requirements are much greater than for the rearrangement processes outlined in the previous section.

(IV) SUMMARY

The NRMS experiments carried out in this study, including those with carbon-13 labelling, point to a unimolecular rearrangement of some of the transient NCCCN neutral to NCCNC.[*] It seems likely that reionisation of the latter species to the corresponding cation and subsequent fragmentation accounts for the pronounced loss of carbon in the NR spectra. The possibility of fragmentation of the transient neutral cannot however be rigorously excluded and further experimental investigations have been suggested, namely $^-$NR$^-$ and NR/CA experiments, which should prove conclusive. The theoretical part of this work demonstrates a possible reaction pathway for cyano-isocyano isomerisation for at least the singlet neutral C_3N_2 surface. The energy demands for this process are high (nearly 60 kcal mol^{-1}) and it is unclear whether such energies would be attainable by a neutral species in an NRMS experiment.[#] It has been shown however that if the energy barrier to isomerisation can be surmounted then the system will possess sufficient internal energy to undergo carbon scrambling.
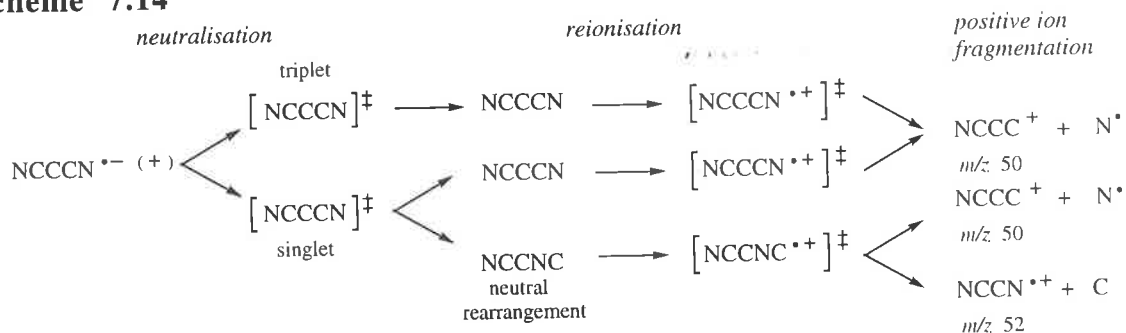
The weight of evidence suggests the following scenario: (i) both $^-$NR$^+$ and $^+$NR$^+$ experiments generate singlet and triplet NCCCN species. (ii) It is likely that a greater

---

[*] In principle, further isomerisation to the CNCNC is also possible however the larger energy requirement suggests that it is less likely than formation of the NCCNC.

[#] In Chapter 4 we have demonstrated that theoretically C_2CHC_2 requires only 22 kcal mol^{-1} to rearrange to the more stable C_4CH configuration. However the experimental evidence suggests that this process does not occur during the NR experiment. By contrast, in this Chapter the experimental and theoretical evidence points to the operation of a neutral rearrangement during the NR experiment which requires activation of nearly 60 kcal mol^{-1}. Why should a unimolecular reaction, with a calculated activation barrier of 60 kcal mol^{-1}, proceed when it has been shown that a process requiring only 22 kcal mol^{-1} does not? It must be remembered, that the activation barrier to a given chemical reaction is not the only property of the system which determines the efficiency of the process. The pre-Arrhenius (or frequency) factor must also be considered when estimating the rate of chemical reaction (Chapter 2, pp 36). This parameter and consequently the reaction rate is not simply derived for a rearrangement occurring during an NRMS experiment because the amount of energy imparted to the system is so ambiguous (Chapter 1, pp 15). The two molecules in question (NCCCN and C_2CHC_2), and indeed their respective rearrangement reactions are completely different. It would therefore be anticipated that the respective frequency factors and consequently the respective reaction rates would vary substantially.

proportion of singlet NCCCN is produced in the $^-$NR$^+$ experiment and conversely more triplet in the $^+$NR$^+$ experiment due to Franck-Condon factors. (iii) The singlet species undergoes some isomerisation to give singlet NCCNC with concomitant scrambling of the carbons, whilst the triplet is unlikely to rearrange under the reaction conditions. (iv) The mixture of singlet and triplet NCCCN and singlet NCCNC forms the bulk of the neutral beam in the NR experiments and upon reionisation these species fragment sequentially from the termini giving loss of nitrogen to produce NCCC$^+$ and loss of carbon to give NCCN$^{\cdot+}$. This is outlined in Scheme 7.14.

Scheme 7.14

neutralisation   *reionisation*   *positive ion fragmentation*

NCCCN$^{\cdot-}$ $^{(+)}$

triplet

$[$NCCCN$]^{\ddagger}$ $\longrightarrow$ NCCCN $\longrightarrow$ $[$NCCCN$^{\cdot+}]^{\ddagger}$

$[$NCCCN$]^{\ddagger}$

singlet

NCCCN $\longrightarrow$ $[$NCCCN$^{\cdot+}]^{\ddagger}$

NCCNC $\longrightarrow$ $[$NCCNC$^{\cdot+}]^{\ddagger}$

neutral rearrangement

NCCC$^+$ + N$^{\cdot}$
m/z 50

NCCC$^+$ + N$^{\cdot}$
m/z 50

NCCN$^{\cdot+}$ + C
m/z 52

(V) EXPERIMENTAL SECTION

A. Mass Spectrometric Methods

CA, CR and NR spectra were measured using a two-sector reversed geometry VG ZAB 2HF spectrometer. This instrument is described in detail in Chapter 1. The typical experimental conditions and procedures are similar to those discussed in previous chapters.[#] Those routines unique to this study are outlined below.

Samples were introduced into the source *via* a heated septum inlet, with solid samples dissolved in a small amount of methanol. This was done to produce a measured pressure of 5×10^{-6} Torr inside the source housing. EI produced positive ions under these conditions whilst negative ions were obtained in the presence of N_2O at an operating pressure inside the source housing of ca. 5×10^{-5} Torr, and thus an estimated pressure inside the ion source of close to 0.1 Torr. N_2O was used as (i) an electron moderating agent for electron attachment and (ii) as a NICI reagent, generating $O^{\cdot-}$ as the primary reactant ion. $^-NR^+$ and $^-CR^+$ spectra of the anions were measured under typical O_2/O_2 conditions. Neutralisation of the positive ions ($^+NR^+$) in the first collision cell was achieved by collision with benzene at a typical pressure of 5.5×10^{-6} Torr. This reduces the main beam to 70% of its initial intensity, producing conditions slightly greater than a single collision senario.[38] Residual ions were removed using the deflector electrode, with neutrals passing into the second cell where they were reionised to the cation by collision with dioxygen (5×10^{-6} Torr, single collision conditions). The corresponding CA spectra were obtained under the same conditions except that the deflector electrode is grounded. Although this increases the likelihood of double collisions in the CA experiment, it allows some comparison between $^+NR^+$ and positive CA spectra. All spectra were repeated a minimum of three times in order to establish their reproducibility. The $^-NIDD^+$ spectrum of $NCCCN^{\cdot-}$ is produced by the normalisation of the peak intensities for $^-NR^+$ and $^-CR^+$ spectra, followed by the subtraction of the $^-CR^+$ from the $^-NR^+$ data[*] according to Equation 7.1.[66]
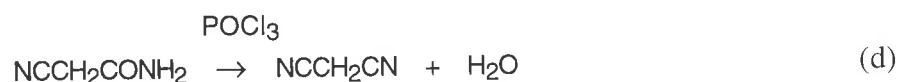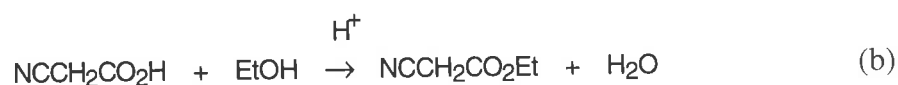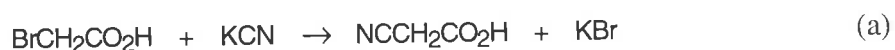

[#] See Chapter 4, pp 85.
[*] A discussion of the NIDD method and its application appears in Chapter 1, pp 20.

Equation 7.1

$$I_i(NIDD) = [I_i(NR)/\Sigma_i I_i(NR)] - [I_i(CR)/\Sigma_i I_i(CR)]$$

B. Syntheses of Precursor Molecules

Tetracyanoethylene oxide, malononitrile and cyanamide are all commercially available materials purchased from the Aldrich Chemical Company and used without further purification. ^{13}C-labelling of malononitrile at the cyano (N^{13}CCH$_2$CN) and methylene (NC^{13}CH$_2$CN) positions was carried out by the procedure of Cheung and Gray,[256] with ^{13}C > 99% in both cases. The synthetic scheme is outlined in Scheme 7.15 with Br^{13}CH$_2$CO$_2$H giving NC^{13}CH$_2$CN whilst K^{13}CN is used to produce N^{13}CCH$_2$CN.

Scheme 7.15

$$BrCH_2CO_2H + KCN \rightarrow NCCH_2CO_2H + KBr \qquad (a)$$

$$NCCH_2CO_2H + EtOH \xrightarrow{H^+} NCCH_2CO_2Et + H_2O \qquad (b)$$

$$NCCH_2CO_2Et + NH_{3(aq)} \rightarrow NCCH_2CONH_2 + EtOH \qquad (c)$$

$$NCCH_2CONH_2 \xrightarrow{POCl_3} NCCH_2CN + H_2O \qquad (d)$$

C. Computational Methods

Theoretical protocols utilised in this study are very similar to those outlined in preceding Chapters. Briefly however, geometry optimisations were carried out with the Becke 3LYP method[88,89] using the 6-31+G(d) basis within the GAUSSIAN 94 suite of programs.[92] Stationary points were characterised as either minima (no imaginary frequencies) or transition states (one imaginary frequency) by calculation of the frequencies using analytical gradient procedures. The minima connected by a given transition structure were confirmed by intrinsic reaction coordinate (IRC) calculations. The calculated frequencies were also used to determine the zero-point vibrational energies which were then scaled[91] by 0.9804 and used as a zero-point energy correction for the electronic energies calculated at this and

higher levels of theory. More accurate energies for the B3LYP geometries were determined with the RCCSD(T) method,[176-181] using the Dunning aug-cc-pVDZ and aug-cc-pVTZ basis sets,[95,96] within the MOLPRO package.[94] Calculations involving GAUSSIAN 94 geometry optimisation were carried out using the Power Challenge Super Computer at the South Australian Super Computing Centre (Adelaide). MOLPRO 97.4 single point energy calculations were carried out with the Power Challenge Super Computer at the Australian National University Super Computing Facility (Canberra).

(VI) APPENDICES

Table 7.9 Geometries of minima and transition states on the singlet C_3N_2 potential surface. Calculated at the B3LYP/6-31+G(d). All bond lengths given in angstroms and all angles in degrees.

TS1/2 (C_1)

bond	N_1-C_2	1.2249
length	C_2-C_3	1.5303
	N_1-C_3	1.7370
	C_3-C_4	1.3736
	C_4-N_5	1.1781
angle	N_1-C_2-C_3	76.8
	C_2-C_3-C_4	108.5
	C_3-C_4-N_5	174.9
dihedral	N_1-C_2-C_3-C_4	139.1
angle	C_2-C_3-C_4-N_5	174.5

2 (C_s) $^1A'$

bond	N_1-C_2	1.3946
length	C_2-C_3	1.4192
	N_1-C_3	1.3084
	C_3-C_4	1.3975
	C_4-N_5	1.1657
angle	N_1-C_2-C_3	55.4
	C_2-C_3-C_4	158.0
	C_3-C_4-N_5	177.9
dihedral	N_1-C_2-C_3-C_4	180.0
angle	C_2-C_3-C_4-N_5	0.0

TS2/3 (C_1)

bond	C_1-N_2	1.2306
length	N_2-C_3	1.4348
	C_3-C_4	1.4181
	C_4-N_5	1.1774
angle	C_1-N_2-C_3	101.8
	N_2-C_3-C_4	121.7
	C_3-C_4-N_5	162.5
dihedral	C_1-N_2-C_3-C_4	15.8
angle	N_2-C_3-C_4-N_5	170.4

3 (C_s) $^1A'$

bond	C_1-N_2	1.2035
length	N_2-C_3	1.3169
	C_3-C_4	1.4046
	C_4-N_5	1.1738
angle	C_1-N_2-C_3	170.3
	N_2-C_3-C_4	116.8
	C_3-C_4-N_5	169.2
dihedral	C_1-N_2-C_3-C_4	180.0
angle	N_2-C_3-C_4-N_5	180.0

TS3/4 (C_1)

bond	C_1-N_2	1.1997
length	N_2-C_3	1.3199
	C_3-C_4	1.4580
	C_3-N_5	1.7084
	C_4-N_5	1.2198
angle	C_1-N_2-C_3	172.5
	N_2-C_3-C_4	115.7
	C_3-C_4-N_5	78.7
dihedral	C_1-N_2-C_3-C_4	-141.6
angle	N_2-C_3-C_4-N_5	135.2

4 (C_s) $^1A'$

bond	C_1-N_2	1.1889
length	N_2-C_3	1.3281
	C_3-C_4	1.4117
	C_3-N_5	1.3013
	C_4-N_5	1.4042
angle	C_1-N_2-C_3	177.1
	N_2-C_3-C_4	158.1
	N_2-C_3-N_5	139.7
dihedral	C_1-N_2-C_3-C_4	0.0
angle	C_1-N_2-C_3-N_5	180.0
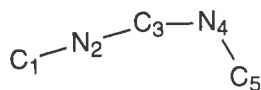
$$C_1 - N_2 - C_3 - N_4$$
$$|$$
$$C_5$$

TS4/5 (C$_1$)
bond   C$_1$-N$_2$ 1.2041
length   N$_2$-C$_3$ 1.3114
         C$_3$-N$_4$ 1.4349
         N$_4$-C$_5$ 1.2508
         C$_3$-C$_5$ 1.7602
angle   C$_1$-N$_2$-C$_3$ 168.3
         N$_2$-C$_3$-N$_4$ 143.4
         C$_3$-N$_4$-C$_5$ 81.6
dihedral   C$_1$-N$_2$-C$_3$-N$_4$ 178.2
angle   N$_2$-C$_3$-N$_4$-C$_5$ 0.2
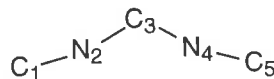
$$C_1 - N_2 - C_3 - N_4 - C_5$$

5 (C$_{2v}$) ^{1}A'
bond   C$_1$-N$_2$ 1.1970
length   N$_2$-C$_3$ 1.3422
         C$_3$-N$_4$ 1.3422
         N$_4$-C$_5$ 1.1970
angle   C$_1$-N$_2$-C$_3$ 167.5
         N$_2$-C$_3$-N$_4$ 112.3
         C$_3$-N$_4$-C$_5$ 167.5
dihedral   C$_1$-N$_2$-C$_3$-N$_4$ 180.0
angle   N$_2$-C$_3$-N$_4$-C$_5$ 180.0

$$N_1 \genfrac{}{}{0pt}{}{C_2}{C_3} C_4 - N_5$$
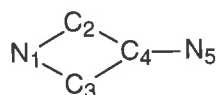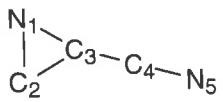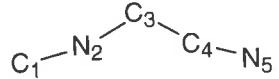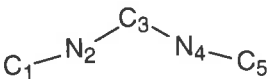
TS3/3 (C$_{2v}$)
bond   N$_1$-C$_2$ 1.3327
length   N$_1$-C$_3$ 1.3327
         C$_2$-C$_4$ 1.6073
         C$_3$-C$_4$ 1.6073
         C$_4$-N$_5$ 1.1836
angle   N$_1$-C$_2$-C$_4$ 107.6
         N$_1$-C$_3$-C$_4$ 107.6
         C$_2$-C$_4$-N$_5$ 147.7
dihedral   N$_1$-C$_2$-C$_4$-C$_3$ 0.0
angle   N$_1$-C$_2$-C$_4$-N$_5$ 180.0

$$C_1 - N_2 \genfrac{}{}{0pt}{}{C_3}{C_4} N_5$$
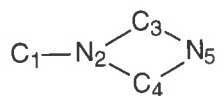
TS5/5 (C$_1$)
bond   C$_1$-N$_2$ 1.1983
length   N$_2$-C$_3$ 1.7460
         N$_2$-C$_4$ 1.7460
         C$_3$-N$_4$ 1.3167
         C$_4$-N$_5$ 1.3167
angle   C$_1$-N$_2$-C$_3$ 146.0
         C$_1$-N$_2$-C$_4$ 146.0
         N$_2$-C$_3$-N$_5$ 98.2
dihedral   C$_1$-N$_2$-C$_3$-C$_4$ 171.1
angle   C$_1$-N$_2$-C$_3$-N$_5$ 163.1

Table 7.10 Geometries of minima on the triplet C_3N_2 potential surface. Calculated at the B3LYP/6-31+G(d). All bond lengths given in angstroms and all angles in degrees.

2 (C_1) triplet

bond	N_1-C_2	1.2497
length	C_2-C_3	1.4214
	N_1-C_3	1.5713
	C_3-C_4	1.3450
	C_4-N_5	1.1956
angle	N_1-C_2-C_3	71.7
	C_2-C_3-C_4	155.1
	C_3-C_4-N_5	174.3
dihedral	N_1-C_2-C_3-C_4	111.9
angle	C_2-C_3-C_4-N_5	150.5

3 (C_s) $^3A''$

bond	C_1-N_2	1.2071
length	N_2-C_3	1.2796
	C_3-C_4	1.3274
	C_4-N_5	1.1928
angle	C_1-N_2-C_3	174.9
	N_2-C_3-C_4	151.7
	C_3-C_4-N_5	174.2
dihedral	C_1-N_2-C_3-C_4	180.0
angle	N_2-C_3-C_4-N_5	180.0

5 (C_{2v}) $^3A''$

bond	C_1-N_2	1.2043
length	N_2-C_3	1.2985
	C_3-N_4	1.2985
	N_4-C_5	1.2043
angle	C_1-N_2-C_3	171.9
	N_2-C_3-N_4	134.9
	C_3-N_4-C_5	171.9
dihedral	C_1-N_2-C_3-N_4	180.0
angle	N_2-C_3-N_4-C_5	180.0

# Chapter 8: Summary and Conclusions

(I) THEORETICAL CALCULATIONS

Theoretical calculations of molecular structure and energy have been carried out for the range of cumulene and heterocumulene systems investigated in Chapters 4-7. Structural prediction using the B3LYP hybrid density functional approach has proved successful. The geometries obtained with this economical method have shown good agreement with more expensive theoretical approaches (Table 5.5, pp 118) and where available, experimental data (Chapter 7, pp 161). Where possible the more comprehensive RCCSD(T) coupled-cluster approach has been utilised, in conjunction with the B3LYP geometries, for the estimation of the thermochemical properties of the species of interest. Model systems for which experimental data is available have been used to test this theoretical protocol. The electron affinities of C_3H, and C_3H_2 calculated at the RCCSD(T)/aug-cc-pVDZ level using B3LYP geometries differ by only ca. 0.1 eV from the reported values (Chapter 4, pp 84 and Chapter 5, pp 116). This places some confidence in the calculated electron affinities for the cumulenes and heterocumulenes discussed in this thesis.

Many of the electron deficient cumulenes and heterocumulenes investigated in this study are predicted to have large electron affinities. Some of the most striking examples are $EA(C_2CHC_2) = 4.54$ eV, $EA(C_4CH_2) = 2.38$ eV, $EA(C_6CH_2) = 2.82$ eV and $EA(NCCCN) = 3.20$ eV. The stability of such anions suggests that they may be present, together with their neutrals, in the interstellar environment. Theoretical calculations have provided support for structural assignments in the gas phase: they have been used to demonstrate the stability of anions and neutrals relative to isomerisation, decomposition and electron detachment processes. Conversely, theoretical prediction of the stability of the C_2CHC_2 anion actually provided the impetus for the experimental investigation which resulted in the generation and characterisation of this ion (Chapter 4, pp 61).

The theoretical calculations presented in this thesis have allowed for comparison of the relative stability of structural isomers on anion, neutral and cation potential surfaces. For the C_5H system (Chapter 4), C_4CH and cyclic isomers HC_2C_3 and C_2C_3H have shown stability on the anion and neutral potential surfaces. This is in line with the previously reported trends for the prototypical C_3H system.[146] For the cumulenes C_nH_2 (where n = 5 and 7) the $C_{n-1}CH_2$ structures have proved to be the most stable radical anions, whilst for the corresponding neutrals HC_nH and some aromatic ring-chain conformations are the most negative in energy (Chapters 5 and 6). These results are consistent with those for the prototypical C_3H_2 system.[132]

The theoretical part of this study has also provided some rationale for the observed stability of some cumulenes possessing the unsaturated C_3-ring system. It has been demonstrated that some substituted derivatives of aromatic cyclopropenylidene (**A**, Scheme 8.1) possess aromaticity resulting in stabilisation of these highly strained geometries. Two stable conformations have been identified. Firstly, where one or both ring hydrogens of **A** are substituted for acetylene or diacetylene functions, producing a structure **B** (where X and Y are -H and/or -C≡CH and/or -C≡CC≡CH). The carbene **B** maintains the 2π-electron population on the C_3-ring and hence the aromaticity and consequent stabilisation. Addition of a further electron to such a molecule will further populate the π-system of the ring and result in loss of aromaticity and destabilisation of the resulting radical anion (*cf.* Chapter 5 and 6). The second possibility, **C** (where X is -H or -C≡CH), possesses two unsubstituted carbons on the C_3-ring. In principle, such a configuration can produce an anion, radical neutral or cation without disrupting the aromaticity of the system (*cf.* Chapter 4). In the cases where such aromatic stabilisation can be invoked the ring chain species are as stable or more stable than their open chain isomers.

Scheme 8.1
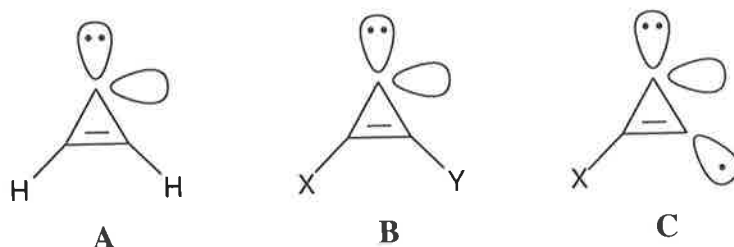
(II) MASS SPECTROMETRIC STUDIES

A range of different ionisation methods have been invoked in this work in order to generate charged analogues of neutral cumulene systems in the gas phase. Closed shell anions have been produced by deprotonation and desilylation under typical NICI conditions whilst radical anions have been generated by reactions of suitable precursors with $O^{\cdot-}$ and $SF_6^{\cdot-}$. Some of the cumulene anions of interest could not be formed by simple ionisation techniques. Consequently, a number of precursors were identified which give rise to these anions *via* unimolecular decomposition involving the loss of neutral fragments. Loss of closed shell fragments from acetylide precursors give the C_4CH and C_2CHC_2 anions, while homolytic decomposition has been used to selectively generate isomeric C_5H_2 and C_7H_2 radical anions. The selectivity of such methodologies is demonstrated by the range of anions produced, many of which had not previously been identified. This work represents the first reported preparation of the gas phase ions, $C_2CHC_2^-$, $C_4CH_2^{\cdot-}$, $HC_5H^{\cdot-}$, $C_2CHC_2H^{\cdot-}$, $C_6CH_2^{\cdot-}$, $HC_2C(C_2)C_2H^{\cdot-}$ and $C_2CH_2C_4^{\cdot-}$. Although most of these anions are predicted by theory to be reasonably stable, species such as $C_2CH_2C_4^{\cdot-}$ have also been prepared. $C_2CH_2C_4^{\cdot-}$ is calculated to be substantially more positive in energy than other C_7H_2 anions but it has been successfully prepared in the gas phase and does not appear to rearrange to any of the more stable configurations (Chapter 6). This result is significant, as it suggests that provided suitable precursors can be identified, anion analogues of a full range of cumulenes can be prepared by this approach.

Despite the selectivity of the ionisation methods utilised here, it is important to further establish the structure of the resulting ions by alternate means. This is particularly important

because of the number of isomeric anions synthesised and hence differentiation of isomers has been paramount. Generally, negative ion CA mass spectrometry has proved ineffective for this task. The cumulenic anions investigated here have shown little structurally significant fragmentation in their respective CA spectra. The C_7H_2 radical anions proved an exception, producing reasonably intense CA spectra with fragmentation unique to each structural isomer (Chapter 6). CR and NR mass spectra of these cumulenic anions have demonstrated more extensive fragmentations. In general, the CR and NR spectra of isomeric anions have proved distinct (Chapters 4-6) with similar fragmentations but differing peak abundances. In some cases, the nature of the fragmentation can be attributed directly to the ion structure. For example, the CR and NR spectra of the C_4CH_2 radical anion show peaks corresponding to losses of C_n (n = 1-3). In contrast, the comparable spectra of $HC_5H^{\cdot-}$ show a lower abundance of such peaks but exhibit larger peaks corresponding to loss of C_nH fragments (Figure 5.2, pp 101). CR and NR spectra do not always differentiate isomers, with the spectra of C_2CHC_2H similar to those of C_4CH_2. In such cases much of the structural ambiguity may be removed by the use of appropriate deuterium labelling.

Neutralisation reionisation mass spectrometry has allowed the investigation of the stability of neutral cumulenes on the microsecond timescale. All hydrocarbon cumulenes investigated by this methodology were shown to survive the NR experiment. The stability of these neutrals was assessed by comparison of the $^-NR^+$ and $^-CR^+$ spectra for a given anion precursor. Such experiments allowed the confirmation of theoretical predictions for the stability of C_4CH, C_2CHC_2, C_4CH_2, HC_5H, C_2CHC_2H, C_6CH_2, $HC_2C(C_2)C_2H$ and $C_2CH_2C_4$. This work represents the first reported experimental observation of many of these transient species. It is interesting to note that cumulenes such as C_2CHC_2, which is predicted by theory to reside in a reasonably shallow minimum (the barrier for isomerisation to C_4CH is calculated to be only ca. 22 kcal mol^{-1}) shows no evidence of isomerisation during the NR experiment (Chapter 4, pp 81). This suggests that NR may be used to synthesise a full range of transient cumulene neutrals in the gas phase, even those which may appear predisposed to unimolecular reaction. Some caution must be exercised however, as

rearrangements have been identified which occur on the NR timescale. Investigation of the NCCCN system has revealed one such example (Chapter 7). Comparison of the $^-NR^+$ and $^-CR^+$ spectra of the NCCCN radical anion point to at least partial isomerisation of neutral NCCCN to NCCNC between the neutralisation and reionisation events. Other evidence also supports this proposal, including theoretical calculations which present a possible reaction pathway.

Overall, the combination of NICI and NRMS methods used in this work has demonstrated the ability to investigate the stability of a range of cumulene systems. The protocols established here for the generation of anionic analogues of cumulenes may in the future be used in conjunction with spectroscopic methods, such as photoelectron spectroscopy, to give further thermochemical insight into the neutral systems. Such data may help build the picture of the chemistry of the interstellar and circumstellar environments.

(III) POTENTIAL INTERSTELLAR MOLECULES?

Linear species such as C_4CH and C_3CH_2 are known interstellar molecules (Chapter 3, pp 41). In this study we have examined a range of structurally more complex derivatives, both structural isomers (eg. C_2CHC_2) and higher homologues (eg. C_4CH_2 and C_6CH_2). The stability of these species has been demonstrated in the laboratory by NRMS experiments and is supported by theoretical calculations. It seems probable that unsaturated hydrocarbons of this type may participate in the chemistry of interstellar and circumstellar gas clouds. From a practical point of view detection of complex cumulenes may be difficult by radioastronomical techniques (Chapter 3, pp 40). In contrast, linear species presented in this thesis, such as C_4CH_2 and C_6CH_2 represent prime candidates for detection because of their simple structures and large dipole moments (5.8 and 8.1 Debye respectively).[193,209]

In addition to the neutral cumulenes, the possibility of anionic cumulenes as interstellar species may also be considered. Currently no anions have been detected in interstellar or circumstellar gas clouds but nevertheless the possibility exists (Chapter 3, pp 43).[118,119]

Many of the cumulenes generated in this study have been calculated to have large electron affinities thus increasing the likelihood of electron attachment. Perhaps if some of these hydrocarbons are detected in interstellar or circumstellar clouds then their corresponding anions may also be located in these environments.

References

1   Dempster, A. J. *Phys. Rev.* **1918**, *18*, 415.

2   Chapman, J. R. *Practical Organic Mass Spectrometry*, 2nd ed.; John Wiley & Sons: Chinchester, **1993**.

3   Rose, M. E.; Johnstone, R. A. W. *Mass Spectrometry for Chemists and Biochemists*; Cambridge University Press: Cambridge, **1982**.

4   Pellizzari, E. D. *J. Chromatogr.* **1974**, *98*, 323.

5   Budzikiewicz, H. *Angew. Chem., Int. Ed. Engl.* **1981**, *20*, 624.

6   Dillard, J. G. *Chem. Rev.* **1973**, *73*, 589.

7   Harrison, A. G. *Chemical Ionization Mass Spectrometry*; CRC Press: Boca Raton, **1983**.

8   Froelicher, S. W.; Freiser, B. S.; Squires, R. R. *J. Am. Chem. Soc.* **1986**, *108*, 2853.

9   Graul, S. T.; Squires, R. R. *J. Am. Chem. Soc.* **1988**, *110*, 607.

10   DePuy, C. H.; Bierbaum, V. M.; Flippin, L. A.; Grabowski, J. J.; King, G. K.; Schmitt, R. J.; Sullivan, S. A. *J. Am. Chem. Soc.* **1980**, *102*, 5012.

11   Klass, G.; Trenerry, C.; Sheldon, J. C.; Bowie, J. H. *Aust. J. Chem.* **1981**, *34*, 519.

12   DePuy, C. H.; Bierbaum, V. M.; Damrauer, R.; Soderquist, J. A. *J. Am. Chem. Soc.* **1985**, *107*, 3385.

13   Born, M.; Ingemann, S.; Nibbering, N. M. M. *Mass Spectrom. Rev.* **1997**, *16*, 181.

14   Bowie, J. H. *Mass Spectrom. Rev.* **1990**, *9*, 349.

15   Bowie, J. H. The Fragmentations of (M-H)$^-$ Ions Derived from Organic Compounds. In *Experimental Mass Spectrometry*; Russell, D. H., Ed.; Plenum Press: New York, **1994**.

16   Eichinger, P. C. H.; Bowie, J. H. *J. Org. Chem.* **1986**, *51*, 5078.

17   Dua, S.; Blanksby, S. J.; Bowie, J. H. *manuscript in preparation* **1999**.

18   Chantry, P. J. *J. Chem. Phys.* **1969**, *51*, 3369.

19   Chantry, P. J. *J. Chem. Phys.* **1969**, *51*, 3380.

20   Dawson, J. H. J.; Jennings, K. R. *J. Chem. Soc. Faraday Trans. 2* **1976**, *72*, 700.

21   Lee, J.; Grabowski, J. J. *Chem. Rev.* **1992**, *92*, 1611.

22   Goode, G. C.; Jennings, K. R. *Adv. Mass Spectrom.* **1974**, *6*, 797.

23   Nibbering, N. M. M. *Recl. Trav. Chim. Pays-Bas.* **1981**, *100*, 297.

24   McDonald, R. N.; Chowdhury, A. K.; Sester, D. W. *J. Am. Chem. Soc.* **1980**, *102*, 6491.

25   Schalley, C. A.; Blanksby, S. J.; Harvey, J. N.; Schröder, D.; Zummack, W.; Bowie, J. H.; Schwarz, H. *Eur. J. Org. Chem.* **1998**, 987.

26   Wenthold, P. G.; Hu, J.; Squires, R. R. *J. Am. Chem. Soc.* **1994**, *116*, 6961.

27   Wenthold, P. G.; Hu, J.; Squires, R. R. *J. Am. Chem. Soc.* **1996**, *118*, 11865.

28   Yates, B. F.; Bouma, W. J.; Radom, L. *J. Am. Chem. Soc.* **1984**, *106*, 5805.

29   Beynon, J. H.; Caprioli, R. M.; Ast, T. *Org. Mass Spectrom.* **1971**, *5*, 229.

30   Johnson, E. G.; Nier, A. O. *Phys. Rev.* **1953**, *91*, 10.

31   Beynon, J. H.; Cooks, R. G.; Amy, J. W.; Baitinger, W. E.; Ridley, T. Y. *Anal. Chem.* **1973**, *45*, 1023A.

32   Cooks, R. G.; Beynon, J. H.; Caprioli, R. M.; Lester, G. R. *Metastable Ions*; Elsevier: Amsterdam, **1973**.

33   Haddon, W. F.; McLafferty, F. W. *J. Am. Chem. Soc.* **1968**, *90*, 4745.

34   Kim, M. S.; McLafferty, F. W. *J. Am. Chem. Soc.* **1978**, *100*, 3279.

35   Wysocki, V. H.; Kenttämaa, H. I.; Cooks, R. G. *Int. J. Mass Spectrom. Ion Processes* **1987**, *75*, 181.

36   Todd, P. J.; McLafferty, F. W. Collisionally Activated Dissociation of High Kinetic Energy Ions. In *Tandem Mass Spectrometry*; McLafferty, F. W., Ed.; John Wiley & Sons: New York, **1983**; pp 149.

37   Laramée, J. A.; Cameron, D.; Cooks, R. G. *J. Am. Chem. Soc.* **1981**, *103*, 12.

38   Holmes, J. L. *Org. Mass Spectrom.* **1985**, *20*, 169.

39   Bowie, J. H.; Blumenthal, T. *J. Am. Chem. Soc.* **1975**, *97*, 2959.

40   Bowie, J. H.; Blumenthal, T. *Aust. J. Chem.* **1976**, *29*, 115.

41   Bursey, M. *Mass Spectrom. Rev.* **1990**, *9*, 555.

42   Howe, I.; Bowie, J. H.; Szulejko, J. E.; Beynon, J. H. *J. Chem. Soc. Chem. Commun.* **1979**, 983.

43   Szulejko, J. E.; Bowie, J. H.; Howe, I.; Beynon, J. H. *Int. J. Mass Spectrom. Ion Phys.* **1980**, *34*, 99.

44   DeLange, W.; Nibbering, N. M. M. *Int. J. Mass Spectrom. Ion. Processes* **1986**, *68*, 111.

45   Bowie, J. H.; White, P. Y. *Aust. J. Chem.* **1978**, *31*, 1511.

46   Burgers, P. C.; Holmes, J. L.; Mommers, A. A.; Szulejko, J. E. *J. Am. Chem. Soc.* **1984**, *106*, 521.

47   Bursey, M. M.; Hass, J. R.; Harvan, D. J.; Parker, C. E. *J. Am. Chem. Soc.* **1979**, *101*, 5485.

48   Keough, T.; Beynon, J. H.; Cooks, R. G. *J. Am. Chem. Soc.* **1973**, *95*, 1695.

49   Terlouw, J. K.; Schwarz, H. *Ang. Chem. Int. Ed. Engl.* **1987**, *26*, 805.

50   McLafferty, F. W. *Science* **1990**, *247*, 925.

51   Zagorevskii, D. V.; Holmes, J. H. *Mass Spectrom. Rev.* **1994**, *13*, 133.

52   Goldberg, N.; Schwarz, H. *Acc. Chem. Res.* **1994**, *27*, 347.

53   McLafferty, F. W.; Todd, P. J.; McGilvery, D. C.; Baldwin, M. A. *J. Am. Chem. Soc.* **1980**, *102*, 3360.

54   McMahon, A. W.; Chowdhury, S. K.; Harrison, A. G. *Org. Mass Spectrom.* **1989**, *24*, 620.

55   Villeneuve, S.; Burgers, P. C. *Org. Mass Sepctrom.* **1986**, *21*, 733.

56   Danis, P. O.; Feng, R.; McLafferty, F. W. *Anal. Chem.* **1986**, *56*, 348.

57   Danis, P. O.; Feng, R.; McLafferty, F. W. *Anal. Chem.* **1986**, *58*, 355.

58   Lorquet, J. C.; Leyh-Nihaut, B.; McLafferty, F. W. *Int. J. Mass Spectrom. Ion Processes* **1990**, *100*, 465.

59   Nguyen, V. G.; Turecek, F. *J. Mass Spectrom.* **1996**, *31*, 842.

60   Schalley, C. A.; Hornung, G.; Schröder, D.; Schwarz, H. *Chem. Soc. Rev.* **1998**, 27, 91.

61   Wesdemiotis, C.; Leyh, B.; Fura, A.; McLafferty, F. W. *J. Am. Chem. Soc.* **1990**, *112*, 8655.

62   Goldberg, N.; Iraqi, M.; Schwarz, H. *Chem. Ber.* **1993**, *126*, 2353.

63   Schröder, D.; Heinemann, C.; Schwarz, H.; Harvey, J. N.; Dua, S.; Blanksby, S. J.; Bowie, J. H. *Chem. Eur. J.* **1998**, *4*, 2550.

64   Feng, R.; Wesdemiotis, C.; Baldwin, M. A.; McLafferty, F. W. *Int. J. Mass Spectrom. Ion Processes* **1988**, *86*, 95.

65   Schalley, C.; Schröder, D.; Schwarz, H. *Int. J. Mass Spectrom. Ion Processes* **1996**, *153*, 173.

66   Schalley, C. A.; Hornung, G.; Schröder, D.; Schwarz, H. *Int. J. Mass Spectrom. Ion Processes* **1998**, *172*, 181.

67   Barton, D. H. R.; Beaton, J. M.; Geller, L. E.; Pechet, M. M. *J. Am. Chem. Soc.* **1961**, *83*, 4076.

68   Hornung, G.; Schalley, C. A.; Dieterle, M.; Schröder, D.; Schwarz, H. *Chem. Eur. J.* **1997**, *3*, 1866.

69   Longevialle, P. *Mass Spectrom. Rev.* **1992**, *11*, 157.

70   Waugh, R. J.; Hayes, R. N.; Eichinger, P. C. H.; Downard, K. M.; Bowie, J. H. *J. Am. Chem. Soc.* **1990**, *112*, 2537.

71   Eichinger, P. C. H.; Bowie, J. H. *J. Chem. Soc. Perkin Trans. II* **1988**, 497.

72   McLafferty, F. W. Decompositions and Rearrangements of Organic Ions. In *Mass Spectrometry of Organic Ions*; McLafferty, F. W., Ed.; Academic Press: New York, **1963**; pp 309.

73   Budzikiewicz, H.; Djerassi, C.; Williams, D. H. *Mass Spectrometry of Organic Compounds*; Holden-Day: San Francisco, **1967**.

74   Williams, D. H.; Howe, I. *Principles of Organic Mass Spectrometry*; McGraw Hill: London, **1972**.

75   Williams, D. H.; Fleming, I. *Spectroscopic Methods in Organic Chemistry*, 4th ed.; McGraw-Hill: London, **1989**.

76   Levine, I. N. *Quantum Chemistry*, 4th ed.; Prentice Hall: London, **1991**.

77   Atkins, P. W. *Molecular Quantum Mechanics*, 2nd ed.; Oxford University Press: New York, **1983**.

78   Foresman, J. B.; Frisch, Æ. *Exploring Chemistry with Electronic Structure Methods*, 2nd ed.; Gaussian, Inc.: Pittsburgh, **1993**.

79   Born, M.; Oppenheimer, J. R. *Ann. Phys.* **1927**, *84*, 457.

80   Bartlett, R. J. *J. Phys. Chem.* **1989**, *93*, 1697.

81   Noga, J.; Bartlett, R. J. *J. Chem. Phys.* **1987**, *86*, 7041.

82   Parr, R. G.; Yang, W. *Density-Functional Theory of Atoms and Molecules*; Oxford University Press: New York, **1989**.

83   Hohenberg, P.; Kohn, W. *Phys. Rev.* **1964**, *B136*, 864.

84   Kohn, W.; Sham, L. *Phys. Rev.* **1965**, *A140*, 1133.

85   Becke, A. D. *Phys. Rev. A* **1988**, *38*, 3098.

86   Perdew, J. P. *Phys. Rev. B* **1986**, *36*, 8822.

87   Lee, C.; Yang, W.; Parr, R. G. *Phys. Rev. B* **1988**, *37*, 785.

88   Becke, A. D. *J. Phys. Chem.* **1993**, *98*, 5648.

89   Stevens, P. J.; Devlin, F. J.; Chablowski, C. F.; Frisch, M. J. *J. Phys. Chem.* **1994**, *98*, 11623.

90   Andzelm, J.; Wimmer, E. *J. Chem. Phys.* **1992**, *96*, 1280.

91   Wong, M. W. *Chem. Phys. Lett.* **1996**, *256*, 391.

92   Frisch, M. J.; Trucks, G. W.; Schlegel, H. B.; Gill, P. M. W.; Johnson, B. G.; Robb, M. A.; Cheeseman, J. R.; Keith, T.; Peterson, G. A.; Montgomery, J. A.; Raghavachari, K.; Al-Laham, M. A.; Zakrzewski, V. G.; Ortiz, J. V.; Foresman, J. B.; Peng, C. Y.; Ayala, P. Y.; Chen, W.; Wong, M. W.; Andres, J. L.; Replogle, E. S.; Gomperts, R.; Martin, R. L.; Fox, D. J.; Binkley, J. S.; Defrees, D. J.; Baker, J.; Stewart, J. P.; Head-Gordon, M.; Gonzales, C.; Pople, J. A. GAUSSIAN94; Revision B 3 ed.; GAUSSIAN Inc.: Pittsburgh PA, **1995**.

93   Plattner, D. A.; Houk, K. N. *J. Am. Chem. Soc.* **1995**, *117*, 4405.

94   Werner, H.-J.; Knowles, P. J.; Almlöf, J.; Amos, R. D.; Deegan, M. J. O.; Elbert, S. T.; Hampel, C.; Meyer, W.; Peterson, K.; Pitzer, R.; Stone, A. J.; Taylor, P. R.; Lindh, R. MOLPRO; 97.4 ed., **1997**.

95   Dunning Jr., T. H. *J. Chem. Phys.* **1989**, *90*, 1007.

96   Woon, D. E.; Dunning, J., T.H. *J. Chem. Phys.* **1993**, *98*, 1358.

97   Kendall, R. A.; Dunning Jr., T. H.; Harrison, R. J. *J. Chem. Phys.* **1993**, *96*, 6796.

98   Gonzalez, C.; Schlegel, H. B. *J. Chem. Phys.* **1989**, *90*, 2154.

99   Atkins, P. W. *Physical Chemistry*, 4th ed.; Oxford University Press: Oxford, **1990**.

100   Gilbert, R. G.; Smith, S. C. *Theory of Unimolecular and Recombination Reactions*; Blackwell Scientific Publications: Oxford, **1990**.

101   Thaddeus, P.; Gottlieb, C. A.; Mollaaghababa, R.; Vrtilek, J. M. *J. Chem. Soc. Faraday Trans.* **1993**, *89*, 2125.

102   Smith, D.; Spanel, P. *Mass Spectrom. Rev.* **1995**, *14*, 255.

103   Turner, B. E.; Zuirys, L. M. Interstellar Molecules and Astrochemistry. In *Galactic and Extragalactic Radio Astronomy*; 2nd ed.; Verschuur, G. L., Kellermann, K. I., Eds.; Springer-Verlag:, **1988**.

104   Omont, A. "Polyynes and Polycyclic Aromatic Molecules in C-rich Circumstellar Envelopes"; Molecules in the Stellar Environment, **1993**, Copenhagen, Denmark.

105   Bieging, J. H.; Tafalla, M. *Astron. J.* **1993**, *105*, 576.

106   Lequeux, J.; Roueff, E. *Phys. Rep.* **1991**, *200*, 241.

107   Pauzat, F.; Ellinger, Y.; McLean, A. D. *Astrophys. J.* **1991**, *369*, L13.

108   McCarthy, M. C.; Travers, M. J.; Kovács, A.; Chen, W.; Novick, S. E.; Gottlieb, C. A.; Thaddeus, P. *Science* **1997**, *275*, 518.

109   Leach, S. *Planet Space Sci.* **1995**, *43*, 1153.

110   Linnartz, H.; Motylewski, T.; Maier, J. P. *J. Chem. Phys.* **1998**, *109*, 3819.

111   Bettens, R. P. A.; Lee, H.-H.; Herbst, E. *Astrophys. J.* **1995**, *443*, 664.

112   Smith, I. W. M. *Int. J. Mass Spectrom. Ion Processes* **1995**, *149/150*, 231.

113 Kaiser, R. I.; Lee, Y. T.; Suits, A. G. *J. Chem. Phys.* **1995**, *103*, 10395.

114 Kaiser, R. I.; Oschenfeld, C.; Head-Gordon, M.; Lee, Y. T.; Suits, A. G. *J. Chem. Phys.* **1997**, *106*, 1729.

115 Herbst, E. *Nature* **1981**, *289*, 656.

116 Omont, A. *Astron. Astrophys.* **1986**, *164*, 159.

117 Lepp, S.; Dalgarno, A. *Astrophys. J.* **1988**, *324*, 553.

118 Bettens, R. P. A.; Herbst, E. *Astrophys. J.* **1996**, *468*, 686.

119 Petrie, S. *Mon. Not. R. Astron. Soc.* **1996**, *281*, 137.

120 Petrie, S.; Herbst, E. *Astrophys. J.* **1997**, *491*, 210.

121 Travers, M. J.; McCarthy, M. C.; Gottlieb, C. A.; Thaddeus, P. *Astrophys. J.* **1996**, *465*, L77.

122 McCarthy, M. C.; Travers, M. J.; Kovács, A.; Gottlieb, C. A.; Thaddeus, P. *Astron. Astrophys.* **1996**, *309*, L31.

123 Gottlieb, C. A.; McCarthy, M. C.; Travers, M. J.; Grabow, J.-U.; Thaddeus, P. *J. Chem. Phys.* **1998**, *109*, 5433.

124 Skell, P. S.; Klebe, J. *J. Am. Chem. Soc.* **1960**, *82*, 247.

125 Reisenauer, H. P.; Maier, G.; Reimann, A.; Hoffmann, R. W. *Angew. Chem.* **1984**, *96*, 596.

126 Maier, G.; Reisenauer, H. P.; Schwab, W.; Carsky, P.; Hess, B. A.; Schaad, L. J. *J. Am. Chem. Soc.* **1987**, *109*, 5183.

127 Dawson, J. H. J.; Kaandorp, T. A. M.; Nibbering, N. M. M. *Org. Mass Spectrom.* **1977**, *12*, 330.

128 Oakes, J. M.; Ellison, G. B. *Tetrahedron* **1986**, *42*, 6263.

129 Hehre, W. J.; Pople, J. A.; Lathan, W. A.; Radom, L.; Wasserman, E.; Wasserman, Z. R. *J. Am. Chem. Soc.* **1976**, *98*, 4381.

130 Seburg, R. A.; Patterson, E. V.; Stanton, J. F.; McMahon, R. J. *J. Am. Chem. Soc.* **1997**, *119*, 5847.

131 Mebel, A. M.; Jackson, W. M.; Chang, A. H. H.; Lin, S. H. *J. Am. Chem. Soc.* **1998**, *120*, 5751.

132   Ikuta, S. *J. Chem. Phys.* **1997**, *107*, 4579.

133   Robinson, M. S.; Polak, M. K.; Bierbaum, V. M.; DePuy, C. H.; Lineberger, W. C. *J. Am. Chem. Soc.* **1995**, *117*, 6766.

134   Smith, D.; Adams, N. G. *Int. J. Mass Spectrom. Ion Processes* **1987**, *76*, 307.

135   Wong, M. W.; Radom, L. *Org. Mass Spectrom.* **1989**, *24*, 539.

136   Prodnuk, S. D.; DePuy, C. H.; Bierbaum, V. M. *Int. J. Mass Spectrom. Ion Processes* **1990**, *100*, 693.

137   Prodnuk, S. D.; Gronert, S.; Bierbaum, V. M.; DePuy, C. H. *Org. Mass Spectrom.* **1992**, *27*, 416.

138   McEwan, M. J.; McConnell, C. L.; Freeman, C. G.; Anicich, V. G. *J. Phys. Chem.* **1994**, *98*, 5068.

139   Wong, M. W.; Radom, L. *J. Am. Chem. Soc.* **1993**, *115*, 1507.

140   Clauberg, H.; Minsek, D. W.; Chen, P. *J. Am. Chem. Soc.* **1992**, *114*, 99.

141   Chyall, L. J.; Squires, R. R. *Int. J. Mass Spectrom. Ion Phys.* **1995**, *149/150*, 257.

142   Bofill, J. M.; Farras, J.; Olivella, S.; Sole, A.; Vilarrasa, J. *J. Am. Chem. Soc.* **1988**, *110*, 1694.

143   Dua, S.; Bowie, J. H.; Sheldon, J. C. *J. Chem. Soc. Perkin Trans. 2* **1994**, 543.

144   Woon, D. E. *Chem. Phys. Lett.* **1995**, *244*, 45.

145   Aoki, K.; Hashimoto, K.; Ikuta, S.; Nomura, O. *Chem. Phys. Lett.* **1995**, *242*, 527.

146   Ikuta, S. *J. Chem. Phys.* **1997**, *106*, 4536.

147   Raksit, A. B.; Bohme, D. K. *Int. J. Mass Spectrom. Ion Processes* **1983/1984**, *55*, 69.

148   Bohme, D.; Raksit, A. B.; Fox, A. *J. Am. Chem. Soc.* **1983**, *105*, 5481.

149   Raksit, A. B.; Bohme, D. K. *Int. J. Mass Spectrom. Ion Physics* **1983**, *49*, 275.

150   Bohme, D. K.; Wodek, S.; Williams, L.; Forte, L.; Fox, A. *J. Chem. Phys.* **1987**, *87*, 6934.

151   Dheandhanoo, S.; Forte, L.; Fox, A.; Bohme, D. K. *Can. J. Chem.* **1986**, *64*, 641.

152   Dua, S.; Sheldon, J. C.; Bowie, J. H. *J. Chem. Soc. Chem. Commun.* **1995**, 1067.

153   Goldberg, N.; Sülzle, D.; Schwarz, H. *Chem. Phys. Lett.* **1993**, *213*, 593.

154   Sülzle, D.; Schwarz, H. *Chem. Phys. Lett.* **1989**, *156*, 397.

155   Natterer, J.; Koch, W.; Schröder, D.; Goldberg, N.; Schwarz, H. *Chem. Phys. Lett.* **1994**, *229*, 429.

156   Taylor, T. R.; Cangshan, X.; Neumark, D. M. *J. Chem. Phys.* **1998**, *108*, 10018.

157   Tucker, K. D.; Kutner, M. L.; Thaddeus, P. *Astrophys. J.* **1974**, *193*, L115.

158   Sastry, K. V. L. N.; Helminger, P.; Charo, A.; Herbst, E.; Lucia, F. C. D. *Astrophys. J.* **1981**, *251*, L119.

159   Guélin, M.; Green, S.; Thaddeus, P. *Astrophys. J.* **1978**, *224*, L27.

160   Gottlieb, C. A.; Gottlieb, E. W.; Thaddeus, P.; Kawamura, H. *Astrophys. J.* **1983**, *275*, 916.

161   Thaddeus, P.; Gottlieb, C. A.; Hjalmarson, Å.; Johansson, L. E. B.; Irvine, W. M.; Friberg, P.; Linke, R. A. *Astrophys. J.* **1985**, *294*, L49.

162   Gottlieb, C. A.; Vrtilek, J. M.; Gottlieb, E. W.; Thaddeus, P.; Hjalmarson, Å. *Astrophys. J.* **1985**, *294*, L55.

163   Cernicharo, J.; Kahane, C.; Gómez-González, J.; Guélin, M. *Astron. Astrophys.* **1986**, *164*, L1.

164   Gottlieb, C. A.; Gottlieb, E. W.; Thaddeus, P. *Astron. Astrophys.* **1986**, *164*, L5.

165   Cooper, D. L.; Murphy, S. C. *Astrophys. J.* **1988**, *333*, 482.

166   Natterer, J.; Koch, W. *Mol. Phys.* **1995**, *84*, 691.

167   Yamamoto, S.; Saito, S.; Ohishi, M.; Suzuki, H.; Ishikawa, S.-I.; Kaifu, N.; Mukakami, A. *Astrophys. J.* **1987**, *322*, L55.

168   Kaiser, R. I.; Oschenfled, C.; Head-Gordon, M.; Lee, Y. T.; Suits, A. G. *Science* **1996**, *274*, 1508.

169   Jiang, Q.; Rittby, C. M. L.; Graham, W. R. M. *J. Chem. Phys.* **1993**, *99*, 3194.

170   Stanton, J. F. *Chem. Phys. Lett.* **1995**, *237*, 20.

171 Raghavachari, K.; Whiteside, R. A.; Pople, J. A.; Schleyer, P. v. R. *J. Am. Chem. Soc.* **1981**, *103*, 5649.

172 Oschenfeld, C.; Kaiser, R. I.; Lee, Y. T.; Suits, A. G.; Head-Gordon, M. *J. Chem. Phys.* **1997**, *106*, 4141.

173 Crawford, T. D.; Stanton, J. F.; Saeh, J. C.; Schaefer III, H. F. *J. Am. Chem. Soc.* **1999**, in press.

174 Bohme, D. K.; Wodek, S.; Williams, L.; Forte, L.; Fox, A. *J. Chem. Phys.* **1987**, *87*, 6934.

175 Blanksby, S. J.; Dua, S.; Bowie, J. H.; Sheldon, J. C. *Chem. Commun.* **1997**, 1833.

176 Cizek, J. *Adv. Chem. Phys.* **1969**, *14*, 35.

177 Pople, J. A.; Krishnan, R.; Schlegel, H. B.; Binkley, J. S. *Int. J. Quantum Chem.* **1978**, *XIV*, 545.

178 Hampel, C.; Peterson, K.; Werner, H.-J. *Chem. Phys. Lett.* **1992**, *190*, 1.

179 Watts, J. D.; Gauss, J.; Bartlett, R. J. J. *J. Chem. Phys.* **1993**, *98*, 8718.

180 Knowles, P. J.; Hampel, C.; Werner, H.-J. *J. Chem. Phys.* **1993**, *99*, 5219.

181 Deegan, M. J. O.; Knowles, P. J. *Chem. Phys. Lett.* **1994**, *227*, 321.

182 Terlouw, J. K.; Burgers, P. C.; Holmes, J. L. *Org. Mass Spectrom.* **1979**, *14*, 307.

183 Holmes, J. L. *Org. Mass Spectrom.* **1985**, *20*, 169.

184 Holmes, A. B.; Jennings-White, C. L. D.; Schulthess, A. H. *J. Chem. Soc. Chem. Commun.* **1979**, 840.

185 Brandsma, L. *Preparative Acetylenic Chemistry*, 2nd ed.; Elsvevier: Amsterdam, **1988**.

186 Jones, E. R. H.; Lee, H. H.; Whiting, M. C. *J. Chem. Soc.* **1956**, 4765.

187 Jones, E. R. H.; Skatteböl, L.; Whiting, M. C. *J. Chem. Soc.* **1960**, 3483.

188 Hauptmann, H. *Tetrahedron Lett.* **1974**, *40*, 3587.

189 Vogel, A. I. *Practical Organic Chemistry*, 3rd ed.; Longmans, Green and Co. Ltd.: London, **1958**.

190   Carlson, C. G.; Hall, J. E.; Huang, Y. Y.; Kotila, S.; Rauk, A.; Tavares, D. F. *Can. J. Chem.* **1987**, *65*, 2461.

191   Thaddeus, P.; Vrtilek, J. M.; Gottlieb, C. A. *Astrophys. J.* **1985**, *299*, L63.

192   Seburg, R. A.; DePinto, J. T.; Patterson, E. V.; McMahon, R. J. *J. Am. Chem. Soc.* **1995**, *117*, 835.

193   Seburg, R. A.; McMahon, R. J.; Stanton, J. F.; Gauss, J. *J. Am. Chem. Soc.* **1997**, *119*, 10838.

194   Fulara, J.; Freivogel, P.; Forney, D.; Maier, J. P. *J. Chem. Phys.* **1995**, *103*, 8805.

195   Fan, Q.; Pfeiffer, G. V. *Chem. Phys. Lett.* **1989**, *162*, 472.

196   Parent, D. C. *J. Am. Chem. Soc.* **1990**, *112*, 5966.

197   Schulz, P. A.; Mead, R. D.; Jones, P. L.; Lineberger, W. C. *J. Chem. Phys.* **1982**, *77*, 1153.

198   Coles, B. F.; Walton, D. R. M. *Synthesis* **1975**, *6*, 390.

199   Jones, G. E.; Holmes, A. B. *Tetrahedron Lett.* **1982**, *23*, 3203.

200   Brandsma, L. Ethynylation and Alkynylation of Carbonyl Groups. In *Preparative Acetylenic Chemistry*; Elsvevier: Amsterdam, **1988**; pp 81.

201   Landini, D.; Montanari, F.; Rolla, F. *Synthesis* **1979**, 134.

202   Piancatelli, G.; Scettri, A.; D'auria, M. *Synthesis* **1982**, 245.

203   Woon, D. E.; Dunning, J., T.H. *J. Chem. Phys.* **1993**, *99*, 3730.

204   Kawaguchi, K.; Kasai, Y.; Ishikawa, S.; Kaifu, N. *Publ. Astron. Soc. Jpn.* **1995**, *43*, 853.

205   Bell, M. B.; Avery, L. W.; Watson, J. K. G. *Astrophys. J. Supp. Series* **1993**, *86*, 211.

206   Herbst, E.; Leung, C. M. *Astrophys. J. Supp. Series* **1989**, *69*, 271.

207   Maluendes, S. A.; McLean, A. D. *Chem. Phys. Lett.* **1992**, *200*, 511.

208   Aoki, K.; Ikuta, S. *J. Mol. Struct. (Theochem)* **1994**, *310*, 229.

209   McCarthy, M. C.; Travers, M. J.; Gottlieb, C. A.; Thaddeus, P. *Astrophys. J.* **1997**, *483*, L139.

210   Blanksby, S.; Dua, S.; Bowie, J. H.; Schröder, D.; Schwarz, H. *J. Phys. Chem. A* **1998**, *102*, 9949.

211   Blanksby, S. J.; Dua, S.; Bowie, J. H. *Chem. Commun.* **1998**, 1767.

212   Albert, A. H.; Wynberg, H. *J. Chem. Soc. Chem. Commun.* **1988**, 748.

213   Olah, G. A.; Krishnamurti, R.; Prakash, G. K. S. *J. Org. Chem.* **1990**, *55*, 6061.

214   Brown, R. D.; Eastwood, F. W.; Elmes, P. S.; Godfrey, P. *J. Am. Chem. Soc.* **1983**, *105*, 6496.

215   Brown, R. D.; Pullin, D. E.; Rice, E. H. N.; Rodler, M. *J. Am. Chem. Soc.* **1985**, *107*, 7877.

216   Hirahara, Y.; Ohshima, Y.; Endo, Y. *J. Chem. Phys.* **1994**, *101*, 7342.

217   Kasai, Y.; Sumiyoshi, Y.; Endo, Y.; Kawaguchi, K. *Astrophys. J.* **1997**, *477*, L65.

218   Kappe, T.; Ziegler, E. *Angew. Chem., Int. Ed. Engl.* **1974**, *13*, 491.

219   Muedas, C. A.; Sülzle, D.; Schwarz, H. *Int. J. Mass Spectrom. Ion Processes* **1992**, *113*, R17.

220   Flammang, R.; Laurent, S.; Flammang-Barbieux, M.; Wentrup, C. *Org. Mass Spectrom.* **1993**, *28*, 1161.

221   Flammang, R.; Van Haverbeke, Y.; Wong, M. W.; Rühmann, A.; Wentrup, C. *J. Phys. Chem.* **1994**, *98*, 4814.

222   Wentrup, C.; Kappe, O.; Wong, M. W. *Pure Appl. Chem.* **1995**, *67*, 749.

223   Cairns, T. L.; Carboni, R. A.; Coffman, D. D.; Engelhart, V. A.; Heckert, R. E.; Little, E. L.; McGeer, E. G.; McKusick, B. C.; Middleton, W. J.; Scribner, R. M.; Theobald, C. W.; Winberg, H. E. *J. Am. Chem. Soc.* **1958**, *80*, 2775.

224   Swenson, J. S.; Renaud, D. J. *J. Am. Chem. Soc.* **1965**, *87*, 1394.

225   Boldt, P.; Schulz, L. *Tetrahedron Lett.* **1967**, 4351.

226   Hartzler, H. D. Radicals with Cyano Groups. In *The Chemistry of the Cyano Group*; Rappoport, Z., Ed.; Interscience: London, **1970**; pp 671.

227   Ciganek, E. *J. Am. Chem. Soc.* **1965**, *87*, 652.

228   Ciganek, E. *J. Am. Chem. Soc.* **1966**, *88*, 1979.

229   Wasserman, E.; Barash, L.; Yager, W. A. *J. Am. Chem. Soc.* **1965**, *87*, 2076.

230   Ciganek, E.; Krespan, C. G. *J. Org. Chem.* **1968**, *33*, 541.

231   Anastassiou, A. G.; Simmons, H. E. *J. Am. Chem. Soc.* **1967**, *89*, 3177.

232   Anastassiou, A. G. *J. Am. Chem. Soc.* **1967**, *89*, 3184.

233   Smith, W. M.; Leroi, G. E. *Spectrochim. Acta* **1969**, *25A*, 1917.

234   Dunkin, I. R.; McCluskey, A. *Spectrochim. Acta.* **1994**, *50A*, 209.

235   Jennings, K. R.; Linnett, J. W. *Trans. Faraday Soc.* **1960**, *56*, 1737.

236   Smith, G. P.; Copeland, R. A.; Crosley, D. R. *J. Chem. Phys.* **1989**, *91*, 1987.

237   McNaughton, D.; Metha, G. F.; Tay, R. *Chem. Phys.* **1995**, *198*, 107.

238   Lucchese, R. R.; Schaefer III, H. F. *J. Am. Chem. Soc.* **1977**, *99*, 13.

239   Baird, N. C.; Taylor, K. F. *J. Am. Chem. Soc.* **1978**, *100*, 1333.

240   Mueller, P. H.; Rondan, N. G.; Houk, K. N.; Harrison, J. F.; Hooper, D.; Willen,
       B. H.; Liebman, J. F. *J. Am. Chem. Soc.* **1981**, *103*, 5049.

241   Martin, J. M. L.; Taylor, P. R.; François, J. P.; Gijbels, R. *Chem. Phys. Lett.*
       1994, *226*, 475.

242   Herzberg, G.; Travis, D. N. *Can. J. Phys.* **1964**, *42*, 1658.

243   Beaton, S. A.; Ito, Y.; Brown, J. M. *J. Mol. Spectrosc.* **1996**, *178*, 99.

244   Dawson, J. H. J.; Nibbering, N. M. M. *Int. J. Mass Spectrom. Ion Phys.* **1980**,
       33, 3.

245   Kroeker, R. L.; Kass, S. R. *J. Am. Chem. Soc.* **1990**, *112*, 9024.

246   Clifford, E. P.; Wenthold, P. G.; Lineberger, W. C.; Petersson, G. A.; Ellison, G.
       B. *J. Phys. Chem. A* **1997**, *101*, 4338.

247   Dua, S.; Blanksby, S. J.; Bowie, J. H. *manuscript in preparation* **1999**.

248   Petrellis, P. C.; Dietrich, H.; Meyer, E.; Griffin, G. W. *J. Am. Chem. Soc.* **1967**,
       89, 1967.

249   Bradforth, S. E.; Kim, E. H.; Arnold, D. W.; Neumark, D. M. *J. Chem. Phys.*
       1993, *98*, 800.

250   Gautier, A. *Ann. Chim. (Paris) Ser. 4.* **1869**, *17*, 215.

251   Casanova, J. J. Rearrangement Reactions Involving the Cyano Group. In *The Chemistry of the Cyano Group*; Rappoport, Z., Ed.; Interscience: London, **1970**; pp 885.

252   Saxe, P.; Yamaguchi, Y.; Pulay, P.; Schaefer III, H. F. *J. Am. Chem. Soc.* **1980**, *102*, 3718.

253   Meier, M.; Müller, B.; Rüchardt, C. *J. Org. Chem.* **1987**, *52*, 648.

254   Kohlmaier, G.; Rabinovitch, B. S. *J. Phys. Chem.* **1959**, *63*, 1793.

255   Booth, M. R.; Frankiss, S. G. *J. Chem. Soc. Chem. Commun.* **1968**, 1347.

256   Cheung, H. T. A.; Gray, P. G. *J. Labelled Compd. Radiopharm.* **1983**, *XXI*, 471.

Published Papers

"Generation of Two Isomers of C_5H From the Corresponding Anions. A Theoretically Motivated Mass Spectrometric Study."
Blanksby, S.J.; Dua, S.; Bowie, J.H. *J. Phys. Chem A* **1999**, in press.
(reprint unavaiable at time of publication of thesis)

"Gas Phase Syntheses of Three Isomeric C_5H_2 Radical Anions and Their Elusive Neutrals. A Combined Experimental and Theoretical Study"
Blanksby, S.J.; Dua, S.; Bowie, J.H.; Schröder, D.; Schwarz, H. *J. Phys. Chem. A* **1998**, *102*, 9949.

"Ethylene Dionen (OCCO): An Intrinsically Unstable Molecule"
Schröder, D.; Heinemann, C.; Schwarz, H.; Harvey, J.N.; Sulzle, D.; Dua, S.; Blanksby S.J.; Bowie, J.H. *Chem. -Eur. J.* **1998**, *4*, 2550.

"A Combined Neutralization-Reionization Mass Spectrometric and Theoretical Study of Oxyallyl and Other Elusive [C_3,H_4,O] Neutrals."
Schalley, C.A.; Blanksby, S.; Harvey, J.N.; Schröder, D.; Zummack, W.; Bowie, J.H. Schwarz, H. *Eur. J. Org. Chem.* **1998**, *6*, 987.

"The Sytheses of $C_6CH_2^{-\cdot}$ and the Corresponding Carbenoid Cumulene C_6CH_2 in the Gas Phase."
Dua, S.; Blanksby, S.J.; Bowie, J.H. *Chem Commun.* **1998**, 1767.

"The collision induced loss of carbon monoxide from deprotonated benzyl benzoate in the gas phase. An anionic 1,2-Wittig type rearrangement"
Chia, C.S.B.; Taylor, M.S.; Dua, S.; Blanksby, S.J.; Bowie, J.H. *J.Chem. Soc., Perkin Trans. 2*, **1998**, 1435.

"The Synthesis and Structure of the Symmetrical Isomer of C$_5$H$^-$."

Blanksby, S.J.; Dua, S.; Bowie, J.H.; Sheldon, J.C. *Chem. Commun.* **1997**, *19*, 1833.

"Competitive Charge-Remote and Anion-Induced Fragmentations of the Non-8-enoate Anion. A Charge-Remote Reaction Which Co-occurs with Hydrogen Scrambling."

Dua, S.; Bowie, J.H.; Cerda, B.A.; Wesdemiotis, C.; Raftery, M.J.; Kelly. J.F.; Taylor, M.S.; Blanksby, S.J.; Buntine, M.A. *J. Chem. Soc. Perkin Trans. 2* **1997**, *4*, 695.

"Anionic Migration in Aromatic Systems Effected by Collisional Activation. Unusual Fragmentations of Deprotonated Anilides Containing Methoxyl and Ethoxyl Substituents."

Blanksby, S.J.; Dua, S.; Hevko, J.M.; Christie, H.; Bowie, J.H. *Eur. Mass Spectrom.* **1996**, *2*, 33.

"Anionic Migration Reactions In Aromatic Systems Effected by Collisional Activation. Deprotonated Anilides Containing Methoxycarbonyl Substituents."

Blanksby, S.J.; Dua, S.; Christie, H.; Bowie, J.H. *Rapid Commun. Mass Spectrom.* **1996**, *10*, 478.

"Unusual Cross-Ring S$_N$2 Reactions of [M-H]$^-$ Ions of Methoxyacetanilides."

Blanksby, S.J.; Dua, S.; Bowie, J.H. *Rapid Commun. Mass Spectrom.* **1996**, *9*, 177.

Blanksby, S.J., Dua, S., Bowie, J.H., Schroder, D. & Schwarz, H. (1998) Gas-phase synthesis of three isomeric C5H2 radical anions and their elusive neutrals. A joint experimental and theoretical study.
Journal of Physical Chemistry A, v. 102(48), pp. 9949-9956

The syntheses of $C_6CH_2^{\cdot-}$ and the corresponding carbenoid cumulene C_6CH_2 in the gas phase

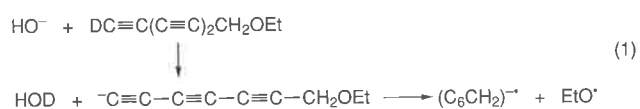Suresh Dua, Stephen J. Blanksby and John H. Bowie†

Department of Chemistry, The University of Adelaide, South Australia, 5005, Australia

The ion $(C_6CH_2)^{\cdot-}$ is formed in the gas phase by the process $-C{\equiv}C-C{\equiv}C-C{\equiv}C-CH_2OEt \rightarrow (C_6CH_2)^{\cdot-} + EtO^{\cdot}$, and charge stripping of the product radical anion yields the carbenoid neutral C_6CH_2; this can be either a singlet (the ground state), which is best represented as the carbene $:C{=}C{=}C{=}C{=}C{=}C{=}CH_2$, or a triplet; the adiabatic electron affinity and the dipole moment of the carbenoid neutral are calculated to be 2.82 eV and 7.33 D respectively.

Small cumulenes have been detected in circumstellar gas and dust envelopes which surround red giant stars, in particular, the bright carbon-rich star IRC-10216.[1–3] These include C_n ($n = 3$ and 5), C_nH ($n = 2$–8) and C_nH_2 ($n = 2$–4 and 6), with neutrals where n is even generally being more abundant than those where n is odd.[1–5] The high electron affinities of these neutrals suggests the possibility that the corresponding anions may co-occur with the neutrals in circumstellar envelopes.[6–8] We have reported the syntheses of a number of these anions in the source of a VG ZAB 2HF mass spectrometer [e.g. C_5H^{-} [8] and three isomers of $C_5H_2^{\cdot-}$[9]] and have used collision-induced charge stripping of the anions to effect the syntheses of the appropriate neutrals.[9] Both C_5CH_2 and C_6CH have already been detected in circumstellar envelopes,[3] and it has been suggested that C_6CH_2 should also be present,[10] and that it should be an excellent candidate for detection because of its large dipole moment [calculated to be 7.33 D (Table 1)].[5] The proposed pathways via which such hydrocarbons can form in the interstellar environment have been reviewed.[11]

We describe the synthesis and structures of both $(C_6CH_2)^{\cdot-}$ and the corresponding carbenoid cumulene neutral.

The radical anion of C_6CH_2 was synthesised in the source of the ZAB 2HF mass spectrometer as summarised in sequence (1). The reaction between HO^- and DC_6CH_2OEt‡ yields the

$$HO^- + DC{\equiv}C(C{\equiv}C)_2CH_2OEt$$
$$\downarrow \qquad\qquad\qquad\qquad\qquad (1)$$
$$HOD + {}^-C{\equiv}C-C{\equiv}C-C{\equiv}C-CH_2OEt \longrightarrow (C_6CH_2)^{-\cdot} + EtO^{\cdot}$$

anion $^-C_6CH_2OEt$ which undergoes facile loss of $EtO^{\cdot}$ to yield $(C_6CH_2)^{\cdot-}$. Source formed $(C_6CH_2)^{\cdot-}$ ions are then fired through a collision cell containing O_2 (at 2×10^{-7} Torr; 1 Torr = ca. 133 Pa) to produce a beam of neutral C_6CH_2 which then proceeds into a second collison containing O_2 (at 2×10^{-7} Torr) which effects ionisation of the neutral to form a decomposing C_6CH_2 radical cation. The resultant neutralisation reionisation spectrum of $(C_6CH_2)^{\cdot-}$ ($^-NR^+$)[16] is shown in Fig. 1. The observation of a pronounced recovery signal (at m/z 86) in the spectrum indicates that the neutral has a lifetime of at least 10^{-6} s, and the similarities between the $^-NR^+$ spectrum and the corresponding charge reversal (CR) spectrum of $C_6CH_2^{\cdot-}$ (listed in the caption to Fig. 1) suggests that the neutral formed has the same connectivity as the radical anion.[17]

Ab initio calculations for both the neutral and radical anion were carried out at the RCCSD(T)/aug-cc-VDZ//B3LYP/6-31G* level of theory using GAUSSIAN94[19] and MOLPRO 96.4.[20] Details are summarised in Table 1. The radical anion and both the singlet and triplet neutrals are best represented as
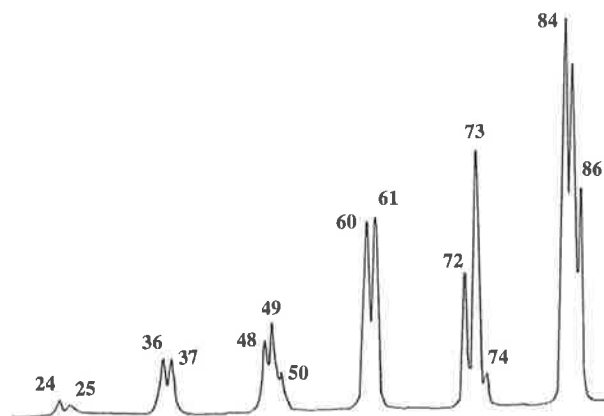

Fig. 1 Neutralisation reionisation ($^-NR^+$) mass spectrum of $C_6CH_2^{\cdot-}$. VG ZAB 2HF mass spectrometer. O_2 in both collision cells (measured pressure outside cells = 2×10^{-7} Torr). CR spectrum of $C_6CH_2^{\cdot-}$ (O_2 in the first collision cell, measured pressure outside cell -2×10^{-7} Torr) as follows [m/z (relative abundance)]: 86(49%), 85(88), 84(100), 74(4), 73(57), 72(13), 62(3), 61(43), 60(29), 50(3), 49(19), 48(9), 37(15), 36(9), 25(1), 24(0.5).

Table 1 *Ab initio* calculations for anions and neutrals

$$C^1-C^2-C^3-C^4-C^5-C^6-C^7\begin{smallmatrix} \\ H^8 \\ \diagup \\ \diagdown \\ H^9 \end{smallmatrix}$$

	Anion	Neutral (singlet)	Neutral (triplet)
State	$(^2B_1)$	$(^1A_1)$	$(^3A_2)$
Symmetry	C_{2v}	C_{2v}	C_{2v}
Energy (hartrees)[a]	−266.969928	−266.866186	−266.833462
Rel. energy (kJ mol−1)	0	272	358
Adiabatic electron affinity (eV)		2.82	
Dipole moment (Debye)	8.10	7.33	6.40
Bond length (Å)[b]			
C^1C^2	1.272	1.289	1.301
C^2C^3	1.334	1.301	1.301
C^3C^4	1.256	1.270	1.274
C^4C^5	1.323	1.293	1.297
C^5C^6	1.261	1.271	1.272
C^6C^7	1.345	1.320	1.329
C^7H^8	1.090	1.090	1.089
C^7H^9	1.090	1.090	1.089
Bond angles (°)[b]			
$C^1C^2C^{3c}$	180.0	180.0	180.0
$C^6C^7H^8$	121.98	121.61	121.16
$C^6H^7H^9$	121.98	121.61	121.16
$H^8C^7H^9$	116.04	116.78	117.67
$C^6C^7H^8H^9$	180.0	180.0	180.0

[a] RCCSD(T)/aug-cc-p VDZ level of theory including zero point vibrational energy [calculated from vibrational frequencies at the B3LYP/6-31G* level of theory, and scaled by 0.9804 (ref. 18)]. [b] B3LYP/6-31G* level of theory. [c] All other angles along the carbon skeleton are also 180.0°.

simple linear cumulenes. The ground state of neutral C_6CH_2 corresponds to the singlet carbenoid cumulene $:C{=}C{=}C{=}C{=}C{=}C{=}CH_2$ (*cf.* ref. 21) which has a calculated dipole moment of 7.33 D. The adiabatic electron affinity of this neutral is estimated to be 2.82 eV; thus we propose that $C_6CH_2{}^{\cdot-}$ as well as the corresponding neutral may be present in the circumstellar environment.

Notes and References

‡ 1-Ethoxy-7-deuteriohepta-2,4,6-triyne was formed by desilyation of the corresponding trimethylsilyl triyne with MeOD/DO$^-$ (*cf.* ref. 12). The trimethylsilyl triyne was prepared by coupling between TMS–C≡C–C≡C–Li (ref. 13) and Br–C≡C–CH$_2$OEt (ref. 14) using CuBr as catalyst (ref. 15).

1 H. Olofsson, in *Molecules in the Stellar Environment, Lecture Notes in Physics*, ed. O. G. Jorgenson, Springer, Heidelberg, 1994, pp. 114–133, and refs. cited therein.
2 P. F. Bernath, K. H. Hinkle and J. J. Keady, *Science*, 1989, **244**, 562; K. H. Hinkle, in *Molecules in the Stellar Environment, Lecture Notes in Physics*, ed. O. G. Jorgensen, Springer, Heidelberg, 1994, pp. 99–114, and refs. cited therein.
3 A. Omont, in *Molecules in the Stellar Environment, Lecture Notes in Physics*, ed. O. G. Jorgenson, Springer, Heidelberg, 1994, pp. 135–138, and refs. cited therein.
4 M. J. Travers, M. C. McCarthy, C. A. Gottlieb and P. Thaddeus, *Astrophys. J.*, 1996, **465**, L77.
5 Cited as unpublished work in, M. C. McCarthy, M. J. Travers, A. Korvacs, W. Chen, S. E. Novick, C. A. Gottlieb and P. Thaddeus, *Science*, 1997, **275**, 518.
6 J. Natterer, W. Koch, D. Schröder, N. Goldberg and H. Schwarz, *Chem. Phys. Lett.*, 1994, **229**, 429.
7 S. Petrie, *Mon. Not. R. Astron. Soc.*, 1996, **281**, 137.
8 S. J. Blanksby, S. Dua, J. H. Bowie and J. C. Sheldon, *Chem. Commun.*, 1997, 1833.
9 S. J. Blanksby, S. Dua, J. H. Bowie, D. Schröder and H. Schwarz, submitted for publication in *J. Phys. Chem.*
10 M. C. McCarthy, M. J. Travers, C. A. Gottlieb and P. Thaddeus, *Astrophys. J.*, 1997, **483**, L139.
11 D. Smith and P. Spanel, *Mass Spectrom. Rev.*, 1995, **14**, 255.
12 B. N. Ghose, *Synth. React. Inorg. Metal-Org. Chem.*, 1994, **24**, 29.
13 A. B. Holmes, C. L. D. Jennings-White, A. H. Shulthess, B. Akinde and D. R. M. Walton, *J. Chem. Soc., Chem. Commun.*, 1979, 840.
14 C. Cai and A. Vasella, *Helv. Chim. Acta*, 1995, **78**, 2053.
15 J. Miller and G. Zweifel, *Synthesis*, 1983, 128.
16 For an account of neutralisation/reionisation of negative ions, and definitions of nomenclature, see N. Goldberg and H. Schwarz, *Acc. Chem. Res.*, 1994, **27**, 347.
17 For an account of the application of the comparison of $^-$NR$^+$ and CR spectra of an anion, see C. A. Schalley, G. Hornung, D. Schröder and H. Schwarz, *Chem. Soc. Rev.*, 1998, **27**, 91.
18 M. W. Wong, *Chem. Phys. Lett.*, 1996, **256**, 391.
19 GAUSSIAN94, Revision C3, M. J. Frish, G. W. Trucks, H. B. Schlegel, P. M. W. Gill, B. G. Johnson, M. A. Robb, J. R. Cheeseman, T. Keith, G. A. Petersson, J. A. Montgomery, K. Raghavavhari, M. A. Al-Latham, V. G. Zakrzewski, J. V. Ortiz, J. B. Foresman, J. Cioslowski, B. B. Stefanov, A. Nanayakkara, M. Challacombe, C. Y. Peng, P. V. Ayala, W. Chen, M. W. Wong, J. L. Andres, E. S. Replogle, R. Gomperts, R. L. Martin, D. J. Fox, J. S. Binkley, D. J. Defrees, J. Baker, J. P. Stewart, M. Head-Gordon, C. Gonzalez and J. A. Pople, Gaussian Inc., Pittsburgh, PA, 1995.
20 H.-J. Werner, P. J. Knowles, R. D. Amos, M. J. O. Deegan, S. T. Elbert, C. Hampel, C. Meyer, K. Peterson, R. Pitzer, A. J. Stone and R. Lindh, MOLPRO 96.4.
21 K. Aoki and S. Ikuta, *J. Mol. Struc.*, 1994, **310**, 229.

The collision induced loss of carbon monoxide from deprotonated benzyl benzoate in the gas phase. An anionic 1,2-Wittig type rearrangement

C. S. Brian Chia, Mark S. Taylor, Suresh Dua, Stephen J. Blanksby and John H. Bowie

Department of Chemistry, The University of Adelaide, South Australia, 5005

The ion $PhCO_2-^-CHPh$, upon collision activation, undergoes competitive losses of CO and CO_2 of which the former process produces the base peak of the spectrum. Product ion and substituent effect (Hammett) studies indicate that $PhCO_2-^-CHPh$ cyclises to a deprotonated hydroxydiphenyloxirane which ring opens to $PhCOCH(O^-)Ph$. This anion then undergoes an anionic 1,2-Wittig type rearrangement {through $[PhCO^-(PhCHO)]$} to form Ph_2CHO^- and CO. The mechanism of the 1,2-rearrangement has been probed by an *ab initio* study [at MP4(SDTQ)/6-31++G(d,p) level] of the model system $HCOCH_2O^- \longrightarrow MeO^- + CO$. The analogous system RCO_2-^-CHPh (R = alkyl) similarly loses CO, and the migratory aptitudes of the alkyl R groups in this reaction are $Bu^t > Me > Et \sim Pr^i$). This trend correlates with the order of anion basicities (*i.e.* the order of ΔG°_{acid} values of RH), supporting the operation of an anion migration process. The loss of CO_2 from $PhCO_2-^-CHPh$ yields Ph_2CH^- as the anionic product: several mechanistic scenarios are possible, one of which involves an initial *ipso* nucleophilic substitution.

Introduction

As part of a study of the gas phase Cannizzaro reaction, we reported that deprotonated benzyl benzoate, upon collisional activation, eliminates carbon monoxide to form deprotonated diphenylmethanol.[1] This must involve some form of re-arrangement.[c,f,2] There are a number of possible mechanistic scenarios which need to be considered: these are summarised in Schemes 1 and 2. Both pathways shown in Scheme 1 involve
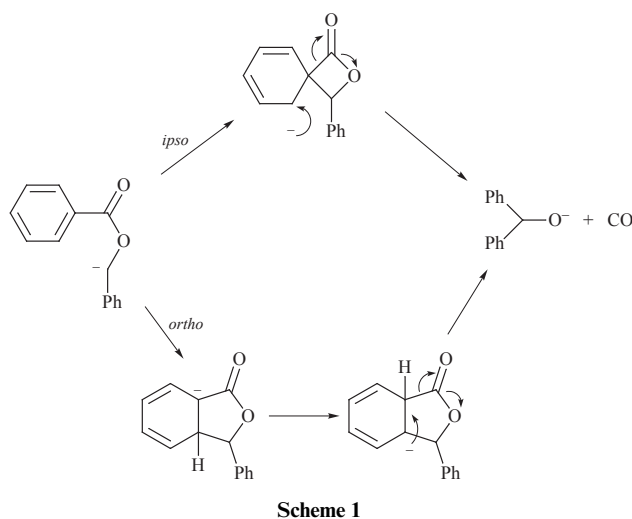
Scheme 1

initial nucleophilic attack of the benzylic anion to a phenyl ring. In contrast, both mechanisms shown in Scheme 2 involve a 'Wittig' type 1,2-migration (where Ph migration and CO elision are synchronous) in the last step, but they differ in the way the key 'Wittig' precursor species is formed.

This paper provides experimental evidence which suggests that the cyclisation–'Wittig' rearrangement best accounts for the loss of CO from $PhCO_2-^-CHPh$.

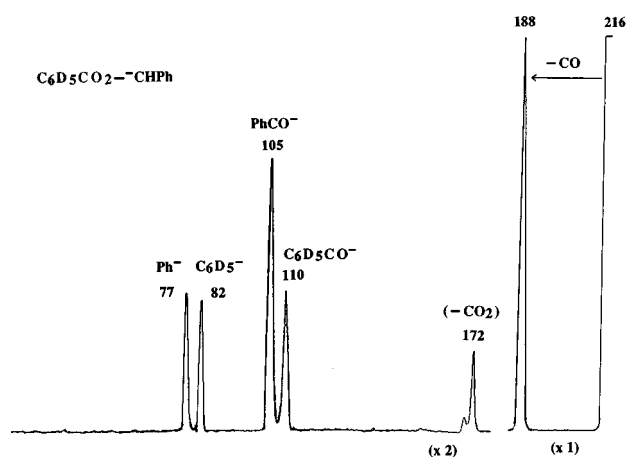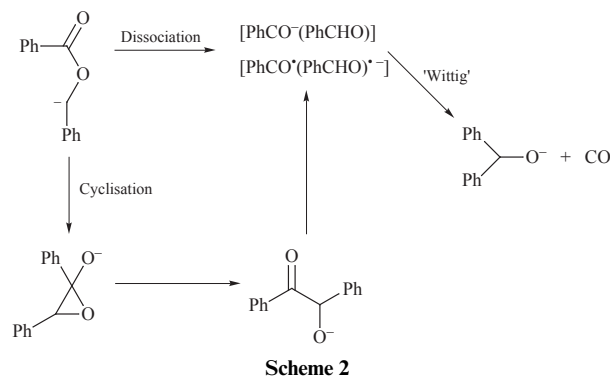## Results and discussion

The reaction between DO^- and $PhCO_2CD_2Ph$ gives an

Fig. 1 CID mass spectrum (MS–MS) of $C_6D_5CO_2-^-CHPh$. VG ZAB 2HF mass spectrometer. For details see Experimental section.

Scheme 2

$(M - D)^-$ ion exclusively, while the analogous reaction between HO^- and $C_6D_5CO_2CH_2Ph$ yields only an $(M - H)^-$ ion. The collisional activation tandem mass spectrum (CID MS–MS) of the latter parent anion is recorded in Fig. 1. In addition to the pronounced loss of CO, there is also a rearrangement peak corresponding to loss of CO_2. We will discuss each of these rearrangements seriatim.

Table 1 Mass spectra of $Ar^1CO_2^-$ $^-CHAr^2$

Substituents			Relative intensity						
Ar^1	Ar^2	σ value	$[(M-H)^- - CO]$	Ar^1CO^-	$[(M-H)^- - Ar^1CHO]$	$[(M-H)^- - CO_2)]$	Ar^{1-}	Ar^{2-}	$[(M-H)^- - Me^\bullet]$
p-MeO	H	−0.28	100	60	19	28	5	1	68
H	H[b]	0	100	33[a]	17[a]	8	6[b]	6[b]	
m-MeO	H	+0.10	100	35	15	25	6	2	60
p-F	H	+0.15	100	34	13	20	10	4	
m-F	H	+0.35	100	6	12	35	8	1	
m-CN	H	+0.61	100	4	6	20	18		
p-CN	H	+0.65	100	4		35	20		
H	p-MeO	−0.28	100	33	54	32	5	15	38
H	H[b]	0	100	33[a]	17[a]	8	6[b]	6[b]	
H	m-MeO	+0.10	100	11	23	17	4	14	26
H	p-F	+0.15	100	4	18	32	4	18	
H	m-F	+0.35	100	2	11	28	3	12	
H	m-CN	+0.61	100	1	7	24		22	
H	p-CN	+0.65	100	0.5	10	35		28	

[a] From Fig. 1. [b] $Ar^1 = Ar^2 = Ph$.
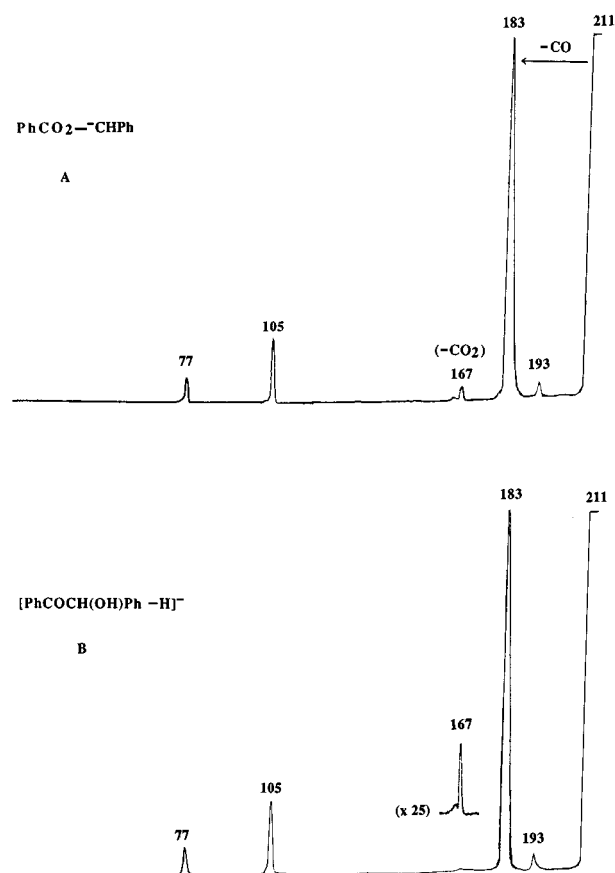
Fig. 2 CID mass spectra of (A) $PhCO_2^-$ ^-CHPh, and (B) $[PhCO-CH(OH)Ph - H]^-$. Peak widths at half height (A) −CO (31.7 ± 0.3); −CO$_2$ (35.4); (B) −CO (31.7), −CO$_2$ (23.5 ± 0.3 V).

(A) The loss of carbon monoxide from deprotonated benzyl benzoates

The mechanisms to be considered for the loss of CO are summarised in Schemes 1 and 2. The simplest way to commence this investigation is to consider the cyclisation–'Wittig' mechanism shown in Scheme 2: initial cyclisation through a deprotonated hydroxyoxirane system has ample precedent in the literature.[3–5] If the loss of CO follows the conversion of the parent anion $PhCO_2^-CHPh$ to $PhCOCH(O^-)Ph$, the spectra of both species should exhibit $[(M - H)^- - CO]$ ions and the peak widths at half height of these ions should be the same in the two spectra. The two mass spectra are shown, for comparison, in Fig. 2. The two spectra are similar, in particular, the peak widths at half height of the two $[(M - H)^- - CO]^-$ peaks are the same within experimental error (see legend to Fig. 2). The only difference noted in the two spectra concerns the $[(M - H)^- - CO_2]$ peaks. This peak is of smaller abundance in the spectrum of $[PhCOCH(OH)Ph - H]^-$ and the widths at half height of the peaks in the two spectra are significantly different (see legend to Fig. 2). This suggests that the losses of CO are arising *via* intermediates common to both $PhCO_2^-$ ^-CHPh and $[PhCOCH(OH)Ph - H]^-$, but that the situation concerning the losses of CO_2 from the two parent ions is more complex.

The experimental evidence outlined above suggests that the loss of CO from deprotonated benzyl benzoate is occurring *via* the cyclisation–'Wittig' process summarised in Scheme 2. Let us now investigate whether there is any evidence which favours (or disfavours) either of the *ipso* or *ortho* nucleophilic substitution mechanisms shown in Scheme 1. Such gas-phase rearrangements are not uncommon and examples have been reported before (*cf.* the *ipso* Smiles rearrangement and the competing *ortho* rearrangement[6,7]). We have investigated these aspects using a Hammett type substituent effect study. Different *meta* and *para* substituents were placed on each of the phenyl rings of the benzyl benzoate and the abundances of ions $[(M - H) - CO]^-$ were monitored as a function of the electronic nature (the Hammett σ value) of the substituent. It is necessary to be wary using Hammett studies in the gas phase, since there is often no inbuilt standard (or standard fragmentation) with which to compare the reaction under investigation. The following Hammett study is used only to indicate general trends. The abundance ratios of the major fragment ions in the spectra of a variety of ions of the general formula Ar^1-CO_2^- $^-CHAr^2$, together with known Hammett σ values[8] of the substituents used in this study, are summarised in Table 1.

A comparison of the abundances of $[(M - H) - CO]^-$ ions with those of either the Ar^1CO^- or $[(M - H) - Ar^1CHO]^-$ fragment ion (see Table 1), shows that the abundance of the rearrangement ion increases with an increase in σ (with an increase in electron withdrawing character) of the substituent on either ring. Consider now the *ipso* and *ortho* nucleophilic cyclisation mechanisms summarised in Scheme 1. In both cases, (i) if the ring cyclisation (the first step) is rate determining for the loss of CO from $Ar^1CO_2^-$ $^-CHAr^2$, then a higher value of σ^1 and a lower value of σ^2 will accelerate the ring cyclisation (*i.e.* increasing electron withdrawing character on Ar^1 will enhance the electrophilicity at the carbon to which the nucleophile approaches, and increasing electron introducing character on Ar^2 will enhance the nucleophilicity of the attacking carbanion). Consider next, the second step (the 1,2-H transfer) of the *ortho* cyclisation mechanism (Scheme 1). Such a concerted

1,2-H transfer through a proton bound transition state is forbidden by the Woodward Hoffman rules: it has an activation barrier in the vicinity of 200 kJ mol^{-1} [9–11] and there are no recorded examples in the condensed phase of 1,2-H migration along a carbon side chain *via* carbanions.[12] However, if a 1,2-H transfer does operate, this step is likely to be rate determining. In such a situation, a lower value of σ^1 (*i.e.* making the reacting carbanion more basic) will increase the rate, and although the effect of σ^2 should be small, an increase in σ^2 will make the H of the breaking C–H bond more acidic, and marginally increase the rate. The final possibility is that where the final steps of both the *ipso* and *ortho* mechanistic proposals are rate determining (Scheme 1). A decrease in σ^1 will increase the electron density on the initial carbanion site thus increasing the rate, while an increase in σ^2 will stabilise the product alkoxide anion, thus effectively reducing the barrier to the transition state. None of the considered scenarios correlate with the experimental observation (that the abundance of the rearrangement ion is greater with a high value of σ^1 and a low value of σ^2). Thus we may eliminate the mechanistic scenarios proposed in Scheme 1, and return to the consideration of a 1,2-'Wittig' type mechanism.

The classical 1,2-Wittig rearrangement in solution is usually represented as shown in Scheme 3 (R is generally an alkyl

Scheme 3
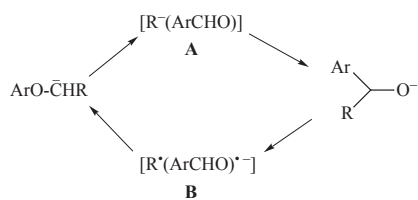
group). The reaction is reported to be stepwise with the second step being rate determining.[13] There has been debate as to whether the intermediate is anion–neutral **A** or radical–radical anion **B**, but since the rates follow the migratory aptitudes of radicals in some cases, the radical–radical anion mechanism has been preferred.[14] However, the radical mechanism is not universally accepted.[15] The 1,2-Wittig reaction also occurs in the gas phase,[16,17] and an *ab initio* study of a model system

($^-$CH$_2$OMe $\longrightarrow$ EtO$^-$), suggests an anionic pathway in which there is no discrete intermediate.[18]

We know that the initial reaction pathway proceeds *via* an oxirane cyclisation–ring opening in the case of PhCO$_2$–$^-$CHPh (see Scheme 2): it is the mechanism of the phenyl migration which needs to be established. Thus we have carried out *ab initio* calculations [at MP4(SDTQ)/6-31++G(d,p) level][19] for the model system HCOCH$_2$O$^-$ (*i.e.* HCOCH$_2$O$^-$ $\longrightarrow$ MeO$^-$ + CO). There are two anion rearrangement channels; no evidence is found for any reaction involving radical migration (*i.e.* both RHF and UHF calculations on the two intermediates shown in Fig. 3 give identical anionic structures). The first rearrangement channel is an unfavourable concerted reaction with a barrier of 310 kJ mol^{-1}. The geometry of the transition state is shown in Table 2. The second rearrangement pathway is the stepwise process summarised in Fig. 3, with details recorded in Table 2. There are a number of equilibrating cluster ions (separated in energy by less than 5 kJ mol^{-1}) on a plateau close in energy to the initial transition state. Two of these are shown in Fig. 3. The equilibrating clusters may undergo two reactions. The first is the dissociation process yielding HCO$^-$ and CH$_2$O (endothermic by 202 kJ mol^{-1}). The second process is the rearrangement. Once the second complex is formed, the system may proceed to the rearrangement products (MeO$^-$ and CO). The rearrangement process is inefficient because the reaction channel is narrow [*i.e.* the frequency factor (the pre Arrhenius A factor) is low], because reversion to reactant is more favourable than conversion to products across the flat energy plateau. The consequence of this is that the migration (second) step shown in Fig. 3 is likely to be rate determining.

The PhCO$_2$–$^-$CHPh system is too large for us to compute at an appropriate level using *ab initio* calculations, thus we have constructed a reaction coordinate diagram using Benson's rules[20] and known electron affinities[21] to estimate the energies of all stable species, and have used the results of the *ab initio* calculation on the model system as a guide to the barrier heights of the phenyl migration steps. These data are summarised in Fig. 4.

Let us now revisit the results of the Hammett study. Although it now seems likely that the final migration step is rate determining, let us consider the expected substituent effects for each of
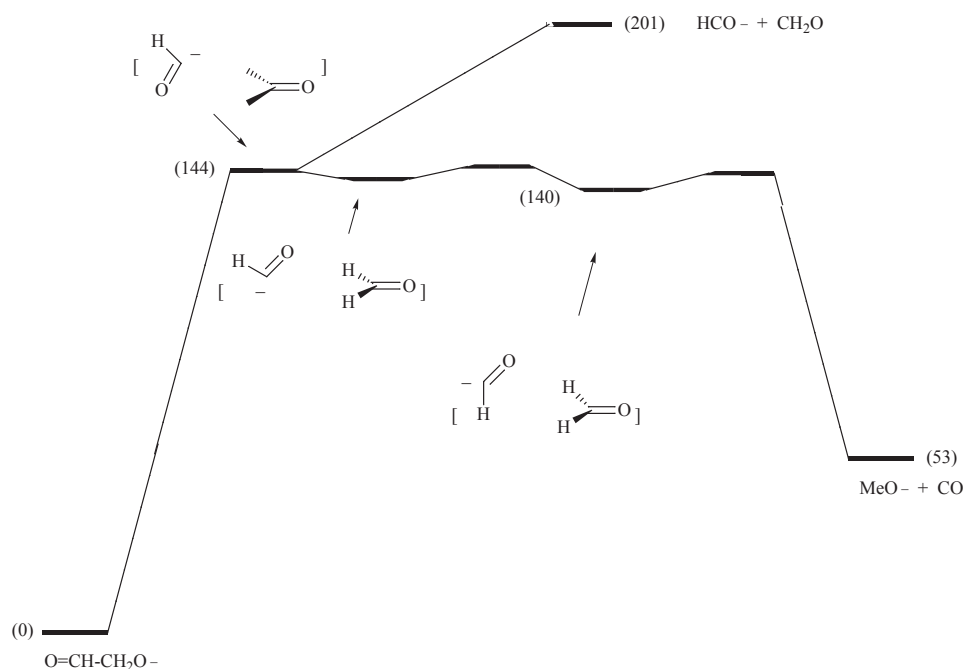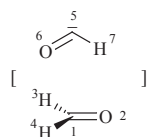

Fig. 3 Reaction coordinate energy diagram of the reactions O=CH–CH$_2$O$^-$ $\longrightarrow$ HCO$^-$ + CH$_2$O and O=CH–CH$_2$O$^-$ $\longrightarrow$ MeO$^-$ + CO. Gaussian 94. Geometries optimised at MP2(full)/6-31++G(d,p). Energies optimised at MP4(SDTQ)/6-31++G(d,p)//MP2(full)/6-31++G(d,p) level [zero point energy corrected (scaled 0.9)]. C–C distances as follows: transition state (2.842 Å), association complex 1 (2.960 Å), and association complex 2 (2.962 Å). For full data concerning energies and geometries see Table 2.

Table 2 Energies and geometries of transition states and intermediates shown in Fig. 3[a]
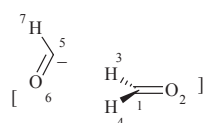
Reactant [O=CHCH$_2$O$^-$ (anti form)]:	−227.833 563 8 hartrees,	0 kJ mol^{-1}
Product (MeO$^-$ + CO):	−227.813 419 5,	+52.9
Product (HCO$^-$ + CH$_2$O):	−227.756 706 8,	+201.8

Transition state concerted

−227.833 563 8 hartrees	C$_1$O$_2$	1.308 Å	O$_2$C$_1$H$_3$(H$_4$)	119.54°
+309.6 kJ mol^{-1}	C$_1$H$_3$(H$_4$)	1.116	H$_3$C$_1$H$_4$	110.32
	C$_5$O$_6$	1.217	O$_6$C$_5$H$_7$	164.82
	C$_1$C$_5$	2.023	O$_6$C$_1$H$_3$(H$_4$)	76.45
	C$_1$O$_6$	2.661	O$_2$C$_1$H$_7$	86.48

Transition state stepwise

−227.778 559 5 hartrees	C$_1$O$_2$	1.238 Å	O$_2$C$_1$H$_3$(H$_4$)	122.55°
+144.41 kJ mol^{-1}	C$_1$H$_3$(H$_4$)	1.090	H$_3$C$_1$H$_4$	114.87
	C$_5$O$_6$	1.258	O$_6$C$_5$H$_7$	109.87
	C$_5$H$_7$	1.168	C$_5$C$_1$H$_3$(H$_4$)	62.62
	C$_1$C$_5$	2.842	C$_5$C$_1$O$_2$	150.17
	O$_6$H$_3$(H$_4$)	2.517		

Association complex 1
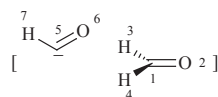
−227.778 660 5 hartrees	C$_1$O$_2$	1.236 Å	O$_2$C$_1$H$_3$(H$_4$)	122.41°
+144.15 kJ mol^{-1}	C$_1$H$_3$(H$_4$)	1.092	H$_3$C$_1$H$_4$	115.02
	C$_5$O$_6$	1.261	O$_6$C$_5$H$_7$	109.17
	C$_5$H$_7$	1.163	H$_3$(H$_4$)C$_1$C$_5$	62.50
			C$_5$C$_1$O$_2$	153.13
			O$_6$C$_1$O$_2$	128.18

Association complex 2

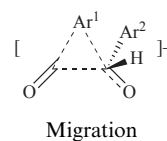| −227.780 315 5 hartrees | C$_1$O$_2$ | 1.238 Å | O$_2$C$_1$H$_3$(H$_4$) | 122.14° |
+139.80 kJ mol^{-1}	C$_1$H$_3$(H$_4$)	1.092	H$_3$C$_1$H$_4$	114.97
	C$_5$O$_6$	1.253	O$_6$C$_5$H$_7$	109.14
	C$_5$H$_7$	1.198	H$_3$(H$_4$)C$_1$H$_7$	58.73
	C$_1$O$_6$	2.344	C$_1$O$_6$C$_5$	107.15
	C$_1$C$_5$	2.964	C$_5$C$_1$O$_2$	147.18
	C$_1$H$_7$	2.582		

[a] Gaussian 94.[19] Geometries at MP2(full)/6-31++G(d,p). Energies at MP4 (SDTQ)6-31++G(d,p)//MP2(full)6-31++G(d,p), corrected for zero point energy (scaled 0.9).

the four steps shown in Fig. 4. Experimentally, we have determined that increasing the electron withdrawing effect of substituents on either Ar^1 or Ar^2 increases the abundance of the [(M − H) − CO]$^-$ ion (*i.e.* a larger *k* value with a high σ^1 and a low σ^2).

If step 1 is rate determining, the rate will increase with increasing σ^1 (increases the electrophilicity of the carbonyl carbon), and decreasing σ^2 (increases the nucleophilicity of the attacking carbanion). If step 2 is rate determining the rate will increase with decreasing σ^1 and increasing σ^2. If the dissociative step (step 3) of the 1,2-rearrangement is rate determining, the rate will increase with increasing σ^1 and decreasing σ^2. None of these scenarios conform to the experimental results.

Table 3 Mass spectra of RCO$_2$−$^-$CDPh

R	[(M − H)$^-$ − CO]	RCO$^-$	−RCO^{2}D	−RCO$_2$H	Ph$^-$	[(M − H)$^-$ − R$^{\bullet}$]
	Relative intensity					
Me	100	14	74	24	32	8
Et	14	14	100	75	71	12
Pr^i	15	17	49	18	23	100
Bu^t	25	1.5	10	5	26	100

Migration

Migration step 4 may be represented as shown above. The expected electronic effects are as follows: (a) electron withdrawing effects (large σ^2) will assist the attack of the nucleophile at the carbonyl group of Ar^{2}CHO, and (b) there are two opposing substituent effects of Ar^1: *viz.* (i) electron withdrawing effects (large σ^1) will aid the dissociation of Ar^1−CO$^-$ to Ar^{1-} and CO, and (ii) electron introducing effects (small σ^1) will aid the attack of the nucleophilic Ar^{1-} at the carbonyl group of Ar^{2}CHO. The only scenario which conforms to the experimental results of the Hammett study (*i.e.* the rate increasing with increasing σ^1 and increasing σ^2) is that step 4 is rate determining with (a) and (b, i) being the major features affecting the rate. Thus the electronic effect of the substituent on the dissociation of Ar^{1}CO$^-$ to Ar^{1-} is more important than its effect on the nucleophilicity of Ar^{1-}.

Finally, we need to consider the possibility that the migration step is a radical reaction (*cf*. Scheme 3). There are several possible stepwise pathways and a concerted route to consider [from Ar^{1}COCH(O$^-$)Ar^2] but they all have one feature in common. If the migration of Ar$^{1\bullet}$ to $^{\bullet}$CH(Ar^2)(O$^-$) to yield Ar^{1}Ar^{2}CHO$^-$ is rate determining, the rate must increase with decreasing σ^1 and increasing σ^2. This is not in accord with experimental data. In addition, radical reactions are generally much less influenced by electronic effects than are ionic processes:[22] the substituent effects shown in Table 1 for loss of CO are pronounced.

We conclude that (a) the formation of Ph$_2$CHO$^-$ and CO from PhCO$_2$−$^-$CHPh occurs by the complex sequence shown in Fig. 4, (b) phenyl migration step 4 is rate determining and (c) there are two major factors influencing the rate of the phenyl rearrangement step, *viz.* the low probability of phenyl migration in comparison to (i) the back reaction, and (ii) the competing cleavage reaction (*i.e.* that yielding PhCO$^-$ + PhCHO).

(B) The loss of carbon monoxide from RCO$_2$−$^-$CHPh (R = alkyl)

We have described above (i) how there has been debate concerning whether the 1,2-Wittig rearrangement is a radical or anionic reaction, and (ii) that the loss of CO from PhCO$_2$−$^-$CHPh is best represented in terms of an anionic 1,2-Wittig type mechanism. What we wish to do now is to study a cognate system in which there is a reasonable possibility that the rearrangement step could involve a radical rather than an anion migration. To this end we have made a series of compounds RCO$_2$CD$_2$Ph [R = alkyl (Me, Et, Pr^i and Bu^t)]. Should the (M − D)$^-$ ions of these compounds lose CO, it is possible that the rearrangement may involve radical migration, since [RCO$^{\bullet}$ (PhCDO)$^{\bullet-}$] might partake in the reaction {*i.e.* in the case of [MeCO$^{\bullet}$ (PhCHO)$^{\bullet-}$], the electron affinities of MeCO$^{\bullet}$[23] and PhCHO[24] are both close to 42 kJ mol^{-1}}.

The mass spectrum of the (M − D)$^-$ ion from MeCO$_2$CD$_2$Ph is shown in Fig. 5, while the major fragmentations of all four of the (M − D)$^-$ ions are summarised in Table 3. The spectra show both [(M − H)$^-$ − CO] and RCO$^-$ ions (see Table 3
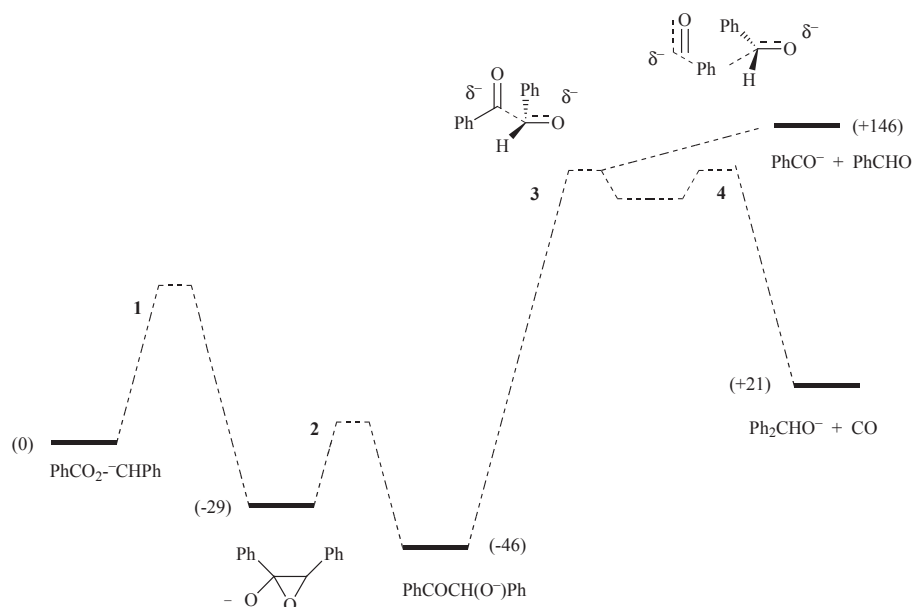
Fig. 4 Reaction coordinate energy diagram of the system PhCO$_2$– $^-$CHPh $\longrightarrow$ (Ph)$_2$CHO$^-$ + CO. Energies calculated using Benson's rules[20] and estimated electron affinities.[21] Transition state energies for the final rearrangement reaction are those computed for Fig. 3.
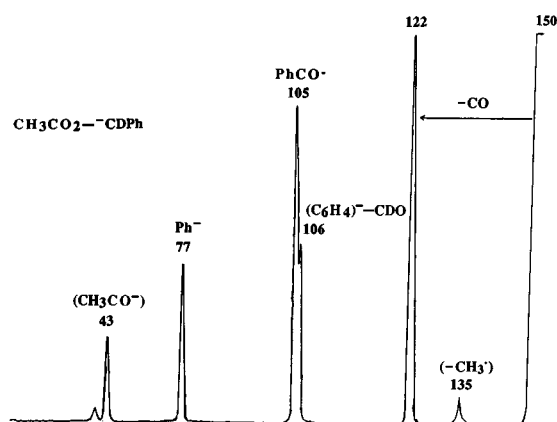

Fig. 5 CID mass spectrum (MS–MS) of (CH$_3$CO$_2$CD$_2$Ph − D)$^-$. VG 2HF mass spectrometer. For experimental details see Experimental section.

and Fig. 5, and *cf.* Fig. 4) and a comparison of the relative abundances of these peaks in the four spectra should give a qualitative indication of the relative probabilities of the rearrangement reactions in the four systems, *i.e.* the migratory trend of the alkyl groups. If it is a radical reaction, the migratory aptitudes should be Bu^r$^\bullet$ > Pr^i$^\bullet$ > Et$^\bullet$ > Me$^\bullet$.$^{cf.14}$ If the reaction is anionic, the gas-phase anion migratory aptitude should follow the ΔG°_{acid} value for the process RH $\longrightarrow$ R$^-$ + H$^+$ (the smaller the value, the higher the migratory aptitude). The ΔG°_{acid} values are as follows: CH$_4$ (1709 kJ mol^{-1}),[25] C$_2$H$_6$ (1724),[26] Me$_2$CH$_2$ (1722)[26] and Me$_3$CH (1701 kJ mol^{-1}).[26] Thus the theoretical thermodynamic gas-phase anion migration trend should be Bu^r$^-$ > Me$^-$ > Pr^i$^-$ > Et$^-$. The data listed in Table 2 show the following trend in migratory aptitude: Bu^r > Me > Et ∼ Pr^i, these data are thus consistent with an anion reaction.

(C) The loss of CO$_2$ from PhCO$_2$– $^-$CHPh

The spectra of both PhCO$_2$– $^-$CHPh and [PhCOCH(OH)-Ph − H]$^-$ show loss of CO$_2$, the peak widths of these product peaks are different (see legend to Fig. 2), and the product peak is of smaller abundance in the spectrum of [PhCO-CH(OH)Ph − H]$^-$. The Hammett study (see Table 1) does not indicate any particular trend, unlike the situation pertaining to the loss of CO. The CO$_2$ yields product ions in both spectra

which show the characteristic fragmentations of the diphenyl-methyl anion.[27]

There are two plausible mechanisms for the loss of CO$_2$ from PhCO$_2$– $^-$CHPh: these are summarised in Scheme 4, together with estimated $\Delta_f H^\circ$ values for reactant, intermediates and products. The first possibility involves phenyl migration within the oxirane species **C** to form the diphenylacetate anion which then decarboxylates to form the diphenylmethyl anion. The second process is an *ipso* nucleophilic substitution to give **D** which then loses CO$_2$. Loss of carbon dioxide from PhCO-CH(O$^-$)Ph occurs specifically through **C**, since the [(M − H) − CO$_2$] peaks in the spectra of Ph$_2$CHCO$_2$$^-$ and [PhCOCH-(OH)Ph − H]$^-$ have the same width at half height (23.5 ± 0.3 V) {the [(M − H) − CO$_2$]$^-$ ion produces the only major daughter peak in the spectrum of Ph$_2$CHCO$_2$$^-$}. The peak width of the [(M − H) − CO$_2$]$^-$ peak from PhCO$_2$– $^-$CHPh (35.4 ± 0.3 V) is appreciably different from the widths of the corresponding peaks from [PhCOCH(OH)Ph]$^-$ and Ph$_2$CHCO$_2$$^-$ (both 23.5 ± 0.3 V). Thus the mechanism of CO$_2$ loss from PhCO$_2$– $^-$CHPh cannot occur exclusively *via* **C**. We propose that either the loss of CO$_2$ occurs (i) exclusively by an *ipso* mechanism through **D** (see Scheme 4), or (ii) the competitive pathways shown in Scheme 4 are both operative.

Scheme 4

Conclusions

Deprotonated benzyl benzoate undergoes competitive rearrangement reactions resulting in the losses of CO and CO_2. The rearrangement pathways are summarised in Scheme 2 and Scheme 4. Cyclisation of $PhCO_2^-{}^-CHPh$ yields an energised deprotonated diphenylhydroxyoxirane which undergoes ring opening to form deprotonated deoxybenzoin which then dissociates via an anionic 1,2-Wittig type rearrangement to yield the diphenylmethoxide anion and carbon monoxide (Scheme 2). The loss of CO_2 from $PhCO_2^-{}^-CHPh$ is more complex: this may occur exclusively by an *ipso* arrangement through **D**, or by two competitive losses through **C** and **D** (Scheme 4).

Experimental

Mass spectrometric methods

Collisional activation (CID) mass spectra (MS–MS) were determined with a VG ZAB 2HF mass spectrometer.[28] Full operating details have been reported.[29] Specific details were as follows: the chemical ionisation slit was used in the chemical ionisation source, the ionising energy was 70 eV, the ion source temperature was 100 °C, and the accelerating voltage was 7 kV. The liquid samples were introduced through the septum inlet with no heating [measured pressure of sample 1×10^{-6} Torr (1 Torr = 133.322 Pa)]. Solid samples were introduced via the direct probe with no heating. Deprotonation was effected for unlabelled compounds using HO^- (from H_2O: measured pressure 1×10^{-5} Torr). In the case of deuterated derivatives, DO^- (from D_2O) was used as the base. The estimated source pressure was 10^{-1} Torr. CID MS–MS data were obtained by selecting the particular anion under study with the magnetic sector, passing it through the collision cell, and using the electric sector to separate and monitor the product ions. Argon was used as collision gas in the second collision cell (measured pressure, outside the cell, 2×10^{-7} Torr), giving a 10% reduction in the main beam, equivalent to single collision conditions. Peak width measurements were performed with the instrument in MS–MS mode using the electric sector to scan the peak under study. The peak width (at half height), quoted in V, is a mean of ten individual experiments (the main beam peak width at half height under the instrumental conditions used was 6 V).

Ab initio calculations on stable anions for the model system $HCOCH_2O^- \longrightarrow MeO^- + CO$ were carried out using Gaussian 94.[19] Geometries were optimised at MP2(full)/6-31++ G(d,p) level while energies were computed at the MP4(SDTQ)/ 6-31++G(d,p)//MP2(full)/6-31++G(d,p) level and corrected for zero point energies (scaled to 0.9). Full procedural details of such calculations have been reported.[30]

Benzyl benzoate, deoxybenzoin and diphenylacetic acid were commercial products.

Benzyl [α,α-²H₂]benzoate. This was made by a standard procedure[31] from [α,α-²H₂]benzyl alcohol and benzoyl chloride. Yield 78%. [²H₂] = 99%.

Benzyl [²H₅]benzoate. This was prepared by a standard procedure[31] from benzyl alcohol and [²H₅]benzoyl chloride. Yield 76%. [²H₅] = 98%.

[*O*-²H]benzoin. This was prepared by three exchanges with MeOD at room temperature. [²H] = 90%.

Compounds $PhCO_2CH_2C_6H_4R$. These were prepared by the following reported methods: R = 4-F,[32] 3-MeO,[33] 4-MeO,[34] 3-CN[32] and 4-CN.[32]

3-Fluorobenzyl benzoate. This was made by a standard method[32] from 3-fluorobenzyl alcohol and benzoyl chloride. Colourless liquid (bp 135–136 °C/0.5 mmHg). Yield 56%. Found, C, 73.04; H, 4.82. $C_{14}H_{11}O_2F$ requires C, 72.83; H, 4.65%. λ_{max}/nm (log ε, EtOH), 206, 230 (3.87, 3.90); ν_{max}/cm^{-1} 1720; δ_H(200 MHz) 5.35 (s, 2H), 7.20–8.11 (m, 9H); m/z 230 (M$^{\cdot+}$, 15%), 109 ($FC_6H_4CH_2^+$, 43), 105 ($PhCO^+$, 100), 77 (Ph$^+$, 22).

Compounds $RC_6H_4CO_2CH_2Ph$. These were prepared by the following reported methods: R = 4-F,[35] 3-MeO,[36] 4-MeO[37] and 4-CN.[38]

Benzyl 3-fluorobenzoate. This was made by a standard method[35] from 3-fluorobenzoyl chloride and benzyl alcohol. Colourless liquid (bp 122–123 °C/0.5 mmHg). Yield 84%. Found, C, 72.97; H, 4.66. $C_{14}H_{11}O_2F$ requires C, 72.83; H, 4.65%. λ_{max}/nm (log ε, EtOH), 206, 237 (3.88, 3.85); ν_{max}/cm^{-1} 1720; δ_H(CDCl$_3$, 200 MHz), 5.37 (s, 2H), 7.2–7.9 (m, 9H); m/z 230 (M$^{\cdot+}$, 30%), 123 ($FC_6H_4CO^+$, 100), 95 ($FC_6H_4^+$, 36).

Benzyl 3-cyanobenzoate. This was made by a standard procedure[38] from 3-cyanobenzoyl chloride and benzyl alcohol. White crystals, mp 39–40 °C (from dichloromethane). Yield 82%. Found, C, 75.94; H, 4.67. $C_{15}H_{11}NO_2$ requires 75.64; H, 4.41%. λ_{max}/nm (log ε, EtOH), 210, 230 (4.23, 3.74); ν_{max}/cm^{-1} 2250, 1730; δ_H(CDCl$_3$, 200 MHz), 5.40 (s, 2H), 7.4–8.4 (m, 9H); m/z 237 (M$^{\cdot+}$, 87%), 130 (NC-$C_6H_4CO^+$, 77), 102 (NC-$C_6H_4^+$, 34), 91 ($C_7H_7^+$, 100).

[²H₂] Compounds RCO_2CD_2Ph (R = Me, Et, Pr^i and Bu^t. These compounds were made in 80–90% yield, by the standard reaction[39] from the appropriate acid chloride and [α,α-²H₂]- benzyl alcohol. All products were distilled *in vacuo* and [²H₂] = 99% in all cases. The purity of products was checked by ¹H NMR and positive ion MS.

Acknowledgements

References

1 J. C. Sheldon, J. H. Bowie, S. Dua, J. D. Smith and R. A. J. O'Hair, *J. Org. Chem.*, 1997, **62**, 3931.
2 S. Dua, P. C. H. Eichinger, G. W. Adams and J. H. Bowie, *Int. J. Mass Spectrom. Ion Processes*, 1994, **133**, 1 and references cited therein.
3 S. D. Lee, T. H. Chan and K. S. Kwon, *Tetrahedron Lett.*, 1984, 3399.
4 M. B. Rubin and S. Inbar, *J. Org. Chem.*, 1988, **53**, 3355 and references cited therein.
5 P. C. H. Eichinger, R. N. Hayes and J. H. Bowie, *J. Am. Chem. Soc.*, 1991, **113**, 1949.
6 P. C. H. Eichinger, J. H. Bowie and R. N. Hayes, *J. Am. Chem. Soc.*, 1989, **111**, 4224 and references cited therein.
7 P. C. H. Eichinger and J. H. Bowie, *Org. Mass Spectrom.*, 1992, **27**, 995.
8 F. Ruff and I. G. Csizmadia, *Organic Reactions, Equilibria, Kinetics and Mechanism*, Elsevier, Amsterdam, 1994, p. 164.
9 W.-K. Li, R. Nobes and L. Radom, *THEOCHEM*, 1987, **149**, 67.
10 W. I. Sou and W.-K. Li, *J. Chem. Res. (S)*, 1995, 464.
11 S. Dua, G. W. Adams, J. C. Sheldon and J. H. Bowie, *J. Chem. Soc., Perkin Trans. 2*, 1996, 1251.
12 D. A. Hunter, J. B. Stothers and E. W. Warnhoff, in *Rearrangements in Excited and Ground States*, ed. P. deMayo, Academic Press, New York, 1980, ch. 6.
13 G. Wittig, *Angew. Chem.*, 1954, **66**, 10; H. E. Zimmermann, in *Molecular Rearrangements*, ed. P. deMayo, Interscience, 1963, vol. 1, p. 345; J. E. Baldwin, J. DeBernardis and J. E. Patrick, *Tetrahedron Lett.*, 1970, 353.
14 C. R. Hauser and S. W. Kantor, *J. Am. Chem. Soc.*, 1951, **73**, 1437; J. Cast, T. S. Stevens and J. Holmes, *J. Chem. Soc.*, 1960, 3521; P. T. Lansbury, V. A. Pattison, J. D. Sidler and J. B. Bierber, *J. Am. Chem. Soc.*, 1966, **88**, 78; H. Schafer, U. Schollkopf and D. Walter, *Tetrahedron Lett.*, 1968, 2809; U. Schollkopf, *Angew. Chem., Int. Ed. Engl.*, 1970, **9**, 763.
15 J. F. Garst and C. D. Smith, *J. Am. Chem. Soc.*, 1976, **98**, 1526.
16 P. C. H. Eichinger, J. H. Bowie and T. Blumenthal, *J. Org. Chem.*, 1986, **51**, 5078; P. C. H. Eichinger and J. H. Bowie, *J. Chem. Soc., Perkin Trans. 2*, 1987, 1499; P. C. H. Eichinger and J. H. Bowie, *J. Chem. Soc., Perkin Trans. 2*, 1988, 497; P. C. H. Eichinger and J. H. Bowie, *J. Chem. Soc., Perkin Trans. 2*, 1990, 1763.
17 M. R. Ahmed, G. D. Dahlke and S. R. Kass, *J. Am. Chem. Soc.*, 1996, **118**, 1398.
18 P. Antoniotto and G. Tonachini, *J. Org. Chem.*, 1993, **58**, 3622.

19 Gaussian 94, Revision C3, M. J. Frish, G. W. Trucks, H. B. Schlegel, P. M. W. Gill, B. G. Johnson, M. A. Robb, J. R. Cheeseman, T. Keith, G. A. Petersson, J. A. Montgomery, K. Raghavachari, M. A. Al-Latham, V. G. Zakrzewski, J. V. Ortiz, J. B. Foresman, J. Cioslowski, B. B. Stefanov, A. Nanayakkara, M. Challacombe, C. Y. Peng, P. V. Ayala, W. Chen, M. W. Wong, J. L. Andres, E. S. Replogle, R. Gomperts, R. L. Martin, D. J. Fox, J. S. Binkley, D. J. Defrees, J. Baker, J. P. Stewart, M. Head-Gordon, C. Gonzalez and J. A. Pople, Gaussian Inc., Pittsburgh, PA, 1995.
20 S. W. Benson, *Thermochemical Kinetics*, Wiley, New York, 1968.
21 S. G. Lias, J. E. Bartmess, J. F. Liebman, J. L. Holmes, R. D. Levin and W. G. Mallard, Gas Phase Ion and Neutral Thermochemistry, in *J. Phys. Chem. Ref. Data 17*, 1988, Suppl. 1 (the computer version was used); M. J. Travers and G. B. Ellison, *Experimentally Determined Electron Affinities*, Department of Chemistry, The University of Colorado, Boulder, 1989.
22 F. Ruff and I. G. Csizmadia, *Organic Reactions, Equilibria, Kinetics and Mechanism*, Elsevier, Amsterdam, 1994, pp. 161–210.
23 C. H. DePuy, V. M. Bierbaum, R. Damrauer and J. A. Soderquist, *J. Am. Chem. Soc.*, 1985, **107**, 3385.
24 A. J. Birch, A. L. Hinde and L. Radom, *J. Am. Chem. Soc.*, 1980, **102**, 3370; M. Mishima, C. Huh, H. Nakamura, M. Fujio and Y. Tsuno, *Tetrahedron Lett.*, 1993, 4223.
25 G. B. Ellison, P. C. Engelking and W. C. Lineberger, *J. Am. Chem. Soc.*, 1978, **100**, 2556.
26 C. H. DePuy, V. M. Bierbaum and R. Damrauer, *J. Am. Chem. Soc.*, 1984, **106**, 4051.
27 G. J. Currie, J. H. Bowie, R. A. Massy-Westropp and G. W. Adams, *J. Chem. Soc., Perkin Trans. 2*, 1988, 403.
28 VG Instruments, Wythenshawe, Manchester, UK, Model ZAB 2HF.
29 M. B. Stringer, J. H. Bowie and J. L. Holmes, *J. Am. Chem. Soc.*, 1986, **108**, 3888.
30 S. Dua, M. S. Taylor, M. I. Buntine and J. H. Bowie, *J. Chem. Soc., Perkin Trans. 2*, 1997, 1991.
31 A. I. Vogel, *Textbook of Practical Organic Chemistry*, Longmans, London, 4th edn. 1956, p. 503.
32 Y. Yakawa, Y. Tsono and M. Sawada, *Bull. Chem. Soc. Jpn.*, 1972, **45**, 1198.
33 F. Zymalkowski, T. Schuster and H. Scherer, *Arch Pharm.*, (*Weinhein, Ger.*), 1969, 272.
34 B. Gastambide and J. Blanc, *Bull. Soc. Chim. Fr.*, 1962, **2**, 1071.
35 P. B. Spratt and C. Dorn, *Anal. Chem.*, 1985, **57**, 359.
36 D. L. Corina, J. N. Wright and K. W. Ballard, *Org. Mass Spectrom.*, 1983, **18**, 60.
37 Y. Kita, S. Akai, M. Yamomoto and M. Taniguchi, *Synthesis*, 1989, **4**, 33.
38 A. K. Bose, M. S. Manhas, J. S. Chib, H. P. Chawla and B. Dayal, *J. Org. Chem.*, 1974, **39**, 2877.
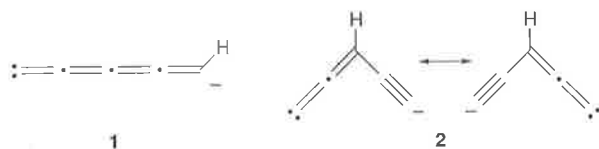39 R. L. Merker and M. J. Scott, *J. Org. Chem.*, 1961, **26**, 5180.

The synthesis and structure of the symmetrical isomer of C_5H^-

Stephen J. Blanksby, Suresh Dua, John H. Bowie* and John C. Sheldon

Department of Chemistry, The University of Adelaide, Adelaide, South Australia 5005, Australia

The ion $(C_2CHC_2)^-$ is formed in the gas phase by the process $^-C\equiv C-CH(OCOR)-C\equiv CD \rightarrow (C_2CHC_2)^- + ({}^\prime RDCO_2{}^\prime)$ [R = H, Me or Et]; the ground state structure is a singlet, with C_{2v} symmetry.

Unusual organic molecules have been detected in circumstellar gas and dust envelopes which surround red giant stars.[1] These include C_3, C_5 and the hydrocarbons C_nH (n = 2–6), which have been identified around the bright carbon-rich star IRC + 10216.[1–3] The high electron affinities of these neutrals suggest the possibility that the corresponding anions may co-occur with the neutrals in circumstellar envelopes,[4,5] and it is of interest in this context that negative ions are present in the coma of comet Halley.[6] We have reported the syntheses of C_3H^-,[7] $C_5^{-\cdot}$,[8] and linear $C_5H^{-\cdot}$[8] (and their conversion through the appropriate neutral to decomposing positive ions) in the ion source of a VG ZAB 2HF mass spectrometer. *Ab initio* calculations [at CISD/6-311G (d,p) level] indicate that linear C_5H^- has both singlet and triplet states, with triplet **1** being the ground state, and that the corresponding neutral has an electron affinity of 2.4 eV.[8]
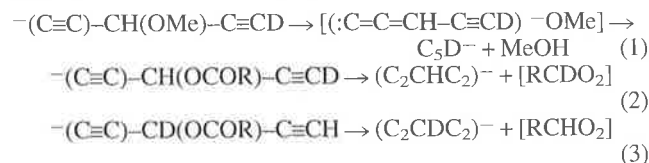

1   **2**

Ab initio calculations [GAUSSIAN 94[9] at CISD/6-311G (d,p) level] indicate further that (i) there is a stable symmetrical isomer $C_2CHC_2^-$, and that this isomer (like linear C_5H^-) also has stable singlet and triplet forms, and (ii) there is no energy and stable species C_3CHC^-. *Ab initio* data for $C_2CHC_2^-$ are summarised in Tables 1 and 2. In this case the singlet is significantly more stable than the triplet. The geometry of the central carbon of the ground-state singlet approximates to trigonal planar (the $C_2-C_3-C_4$ angle is close to 130°), and the C_1-C_2 and C_2-C_3 bonds have significant triple and double bond character respectively (see Table 2). The structure is depicted (in valence bond form) as **2**. Isomer **2** is less stable than isomer **1** by 170 kJ mol^{-1} at the level of theory indicated. The electron affinity of the neutral corresponding to **2** is calculated to be 4.2 eV.

We initially attempted to form the elusive **2** in the ion source of the VG 2HF mass spectrometer by a number of methods related to that shown in eqn. (1):

$$^-(C\equiv C)-CH(OMe)-C\equiv CD \rightarrow [(:C=C=CH-C\equiv CD)~^-OMe] \rightarrow$$
$$C_5D^- + MeOH \quad (1)$$
$$^-(C\equiv C)-CH(OCOR)-C\equiv CD \rightarrow (C_2CHC_2)^- + [RCDO_2] \quad (2)$$
$$^-(C\equiv C)-CD(OCOR)-C\equiv CH \rightarrow (C_2CDC_2)^- + [RCHO_2] \quad (3)$$

unfortunately, the base deprotonates exclusively at the central position to yield linear C_5D^- (*cf.* **1**) rather than remove D^+ to form $C_2CHC_2^-$. However, the energised precursor anions shown in eqns (2) and (3) (R = H, Me, Et) [formed by the reaction of HO^- with $DC\equiv C-CH(OCOR)-C\equiv CD$ and $HC\equiv C-CD(OCOR)-C\equiv CH$] decompose to yield $(C_2CHC_2)^-$ and $(C_2CDC_2)^-$ respectively and exclusively. We are not sure whether this process involves incipient R^- deprotonating at the terminal position (to yield CO_2 and RH as neutral products) or whether the acetylenic H transfers to oxygen to yield RCO_2H as the neutral products.

When source formed $(C_2CHC_2)^-$ ions are fired through a collision cell containing Ar (at 2×10^{-7} Torr; 1 Torr = *ca.* 133 Pa) the resultant tandem negative ion mass spectrum exhibits only loss of H· to form $C_5^{-\cdot}$ (*cf.* ref. 8). Under the same experimental conditions, charge stripping of $(C_2CHC_2)^-$ ions yields energised parent cations C_5H^+, whose resultant spectrum [the charge reversal spectrum[10,11] of $(C_2CHC_2)^-$] is *m/z* (composition relative abundance) 61 (C_5H^+, 35), 60 ($C_5^{+\cdot}$, 100), 49 (C_4H^+, 77), 48 ($C_4^{+\cdot}$, 62), 37 (C_3H^+, 81), 36 ($C_3^{+\cdot}$, 69), 25 (C_2H^+, 4), 24 ($C_2^{+\cdot}$, 21), 12 ($C^{+\cdot}$, 0.2). Although this spectrum shows the same peaks as those observed in the corresponding spectrum of isomer **1** (*cf.* ref. 8), the peak abundances in the two spectra are significantly and reproducibly different. In particular, the abundances of *m/z* 61 (C_5H^+) and 60 ($C_5^{+\cdot}$) are 35 and 100 for **2**, and 100 and 76 for **1**. Since the two charge reversal spectra are different, we conclude that isomers **1** and **2** are stable. However, the data cannot exclude the possibility of

Table 1 *Ab initio* calculations for $C_2CHC_2^{-a}$

State	Singlet	Triplet
Symmetry	C_{2v}	C_{2v}
HF/6-311G (d,p)	−189.74150	−189.67132
Zero point vibrational energy	0.03188	0.02767
Total thermal energy	0.03685	0.03282
CISD/6-311G (d,p)	−190.286804	−190.20186

a Ab initio optimization used the Berny procedure (ref. 12) at HF/6-311G (d,p), GAUSSIAN 94 (ref. 9). The correctness of the geometries was confirmed by the lack of negative analytical computed harmonic vibration frequencies. The post Hartree–Fock energies (CISD) were calculated at the Hartree–Fock geometries. All energies are recorded in hartrees.

Table 2 Bond lengths and angles for $C_2CHC_2^-$ taken from *ab initio* calculations

	Singlet	Triplet
Bond length/Å		
C_1-C_2	1.2425	1.2746
C_2-C_3	1.3679	1.3636
C_3-H	1.0843	1.1048
Bond angle (°)		
C_1-C_2-X	85.3	80.0
$X-C_2-C_3$	90.0	90.0
C_2-C_3-H	115.3	107.2

minor interconversion of **2** to **1** under the experimental conditions.

The neutral analogue of **1** has already been detected in the interstellar environment:[1-3] it would be of interest to search for anions **1**, **2** and the neutral corresponding to **2**.

Footnote and References

* E-mail: jbowie@chemistry.adelaide.edu.au

1 H. Olofsson, *Molecular Abundances in the Envelopes around Evolved Stars*, in *Molecules in the Stellar Environment, Lecture Notes in Physics*, ed. O. G. Jorgenson, Springer, Heidelberg, 1994, pp. 114–133 and references cited therein.
2 P. F. Bernath, K. H. Hinkle and J. J. Keady, *Science*, 1989, **244**, 562; K. H. Hinkle, *Infrared Spectroscopy of Molecules in Circumstellar Envelopes*, in *Molecules in the Stellar Environment, Lecture Notes in Physics*, ed. O. G. Jorgensen, Springer, Heidelberg, 1994, pp. 99–114 and references cited therein.
3 A. Omont, *Polyynes and Polycyclic Aromatic Molecules in C-rich Circumstellar Envelopes*, in *Molecules in the Stellar Environment, Lecture Notes in Physics*. ed. O. G. Jorgenson, Springer, Heidelberg, 1994, pp. 135–148 and references cited therein.
4 J. Natterer, W. Koch, D. Schröder, N. Goldberg and H. Schwarz, *Chem. Phys. Lett.*, 1994, **229**, 429.
5 S. Petrie, *Mon. Not. R. Astron. Soc.*, 1996, **281**, 137.
6 P. Chaizy, H. Rème, J. A. Sauvaud, C. d'Uston, R. P. Lin, D. E. Larson, D. L. Mitchell, K. A. Anderson, C. W. Carlson, A. Korth and D. A. Mendis, *Nature*, 1991, **349**, 393.
7 S. Dua, J. H. Bowie and J. C. Sheldon, *J. Chem. Soc., Perkin Trans. 2*, 1994, 543.
8 S. Dua, J. C. Sheldon and J. H. Bowie, *J. Chem. Soc., Chem. Commun.*, 1995, 1067.
9 GAUSSIAN 94, Revision C3, M. J. Frish, G. W. Trucks, H. B. Schlegel, P. M. W. Gill, B. G. Johnson, M. A. Robb, J. R. Cheeseman, T. Keith, G. A. Petersson, J. A. Montgomery, K. Raghavavhari, M. A. Al-Latham, V. G. Zakrzewski, J. V. Ortiz, J. B. Foresman, J. Cioslowski, B. B. Stefanov, A. Nanayakkara, M. Challacombe, C. Y. Peng, P. V. Ayala, W. Chen, M. W. Wong, J. L. Andres, E. S. Replogle, R. Gomperts, R. L. Martin, D. J. Fox, J. S. Binkley, D. J. Defrees, J. Baker, J. P. Stewart, M. Head-Gordon, C. Gonzalez and J. A. Pople, Gaussian Inc., Pittsburgh, PA, 1995.
10 J. H. Bowie and T. Blumenthal, *J. Am. Chem. Soc.*, 1975, **97**, 2959; J. E. Szulejko, J. H. Bowie, I. Howe and J. H. Beynon, *Int. J. Mass Spectrom. Ion Phys.*, 1980, **13**, 76.
11 R. Clair, J. L. Holmes, A. A. Mommers and P. C. Burgers, *Org. Mass Spectrom.*, 1985, **20**, 207; W. DeLange and N. M. M. Nibbering, *Int. J. Mass Spectrom Ion Processes*, 1986, **68**, 111.
12 C. Peng, P. Y. Ayala, H. B. Schlegel and M. J. Frisch, *J. Comput. Chem.*, 1996, **17**, 49.

Competitive charge-remote and anion-induced fragmentations of the non-8-enoate anion. A charge-remote reaction which co-occurs with hydrogen scrambling

Suresh Dua,[a] **John H. Bowie,**[*,a] **Blas A. Cerda,**[b] **Chrys Wesdemiotis,**[b] **Mark. J. Raftery,**[a] **Julian F. Kelly,**[a] **Mark S. Taylor,**[a] **Stephen J. Blanksby**[a] **and Mark A. Buntine**[a]

[a] *Department of Chemistry, The University of Adelaide, South Australia, 5005, Australia*
[b] *Department of Chemistry, The University of Akron, Akron, Ohio 44325-3601, USA*

The non-8-enoate anion undergoes losses of the elements of C_3H_6, C_4H_8 and C_6H_{12} on collisional activation. The mechanisms of these processes have been elucidated by a combination of product ion and labelling (^2H and ^{13}C) studies, together with a neutralisation reionisation mass spectrometric study. These studies allow the following conclusions to be made. (i) The loss of C_3H_6 involves cyclisation of the enolate anion of non-8-enoic acid to yield the *cyclo*pentyl carboxylate anion and propene. (ii) The loss of 'C_4H_8' is a charge-remote process (one which proceeds remote from the charged centre) which yields the pent-4-enoate anion, butadiene and dihydrogen. This process co-occurs and competes with complex H scrambling. (iii) The major loss of 'C_6H_{12}' occurs primarily by a charge-remote process yielding the acrylate anion, hexa-1,5-diene and dihydrogen, but in this case no H scrambling accompanies the process. (iv) It is argued that the major reason why the two charge-remote processes occur in preference to anion-induced losses of but-1-ene and hex-1-ene from the respective 4- and 2-anions is that although these anions are formed, they have alternative and lower energy fragmentation pathways than those involving the losses of but-1-ene and hex-1-ene; *viz.* the transient 4-anion undergoes facile proton transfer to yield a more stable anion, whereas the 2-(enolate) anion undergoes preferential cyclisation followed by elimination of propene [see (i) above].

Introduction

Collision-induced loss of a neutral from an even-electron negative ion in the gas phase often involves reaction involving the charged centre.[1,2] There are also fragmentations of even-electron anions which are 'charge-remote', *viz.* reactions which occur remote from the charged centre. Amongst the latter are some radical losses which form stabilised radical anions.[3,4] Substantiated reports of charge-remote reactions involving the loss of even-electron neutrals from even-electron anions are not common. The classical charge-remote mechanistic proposal for alkanoate anions is shown in reaction (1). This was first

proposed by Adams and Gross,[5-8] but the mechanism has been questioned.[9-11] Support for the charge-remote mechanism has been provided by Cordero and Wesdemiotis[12] who have used neutralisation reionisation mass spectrometry (NRMS) to identify butene as a neutral product of the reaction shown in reaction (1). This charge-remote process has a large activation barrier; estimates range from *ca.* 200 kJ mol^{-1} (experimental[5-8]) to 385 kJ mol^{-1} (computational[13]).

This paper reports the fragmentations of the non-8-enoate anion, *i.e.* a system similar to the alkanoate shown in reaction (1), except that it has double bond functionality at the opposite end of the molecule to the carboxylate moiety. We anticipated that collision-induced transfer of a proton from the allylic position to the carboxylate anion would yield an allylic anion, and

that this should result in competition between charge-remote fragmentation of the carboxylate anion, and anion-directed fragmentation from the allylic centre. We will show that both charge-remote and anion induced processes do indeed occur in this system, but not as a consequence of fragmentation of an allylic anion.

Results and discussion

We have described above why we chose to study an enoate anion for this study. The first task is to choose which enoate anion is the most suitable for study. The mass spectra of a number of such anions are listed in Table 1. The spectra of the lower homologues are dominated by loss of carbon dioxide and are not suitable for this study. In contrast, the higher homologues show the type of losses previously noted in the spectra of alkanoate anions,[5-7,12] for example, losses of the elements of C_3H_6, C_4H_8 and C_6H_{12}. In principle, these losses could all be charge-remote reactions analogous to that shown in reaction (1), except of course that the neutral products will be a diene and dihydrogen. We have chosen to probe the mechanisms of these processes using the non-8-enoate anion as a suitable example. The investigation uses a combination of product ion, labelling (D and ^{13}C), neutral reionisation mass spectrometry (NRMS) and computational studies.
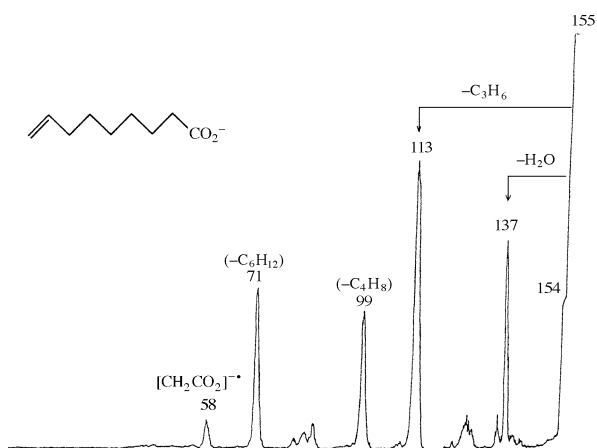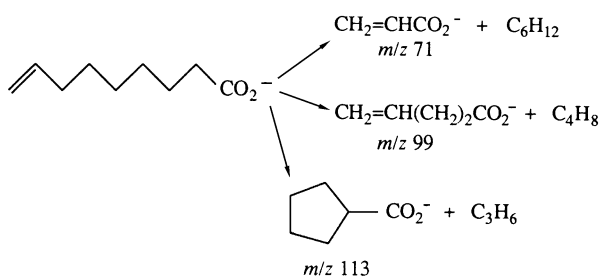
(a) The evidence based on product ion and labelling studies

The collision-induced negative chemical ionisation tandem mass spectrum (MS/MS) of the $(M - D)^-$ ion of CH_2=CH–$(CH_2)_6CO_2D$ is recorded in Fig. 1. The first part of this investigation involves the identification of the structures of the product ions formed following losses of 'C_3H_6', 'C_4H_8' and 'C_6H_{12}'. This was done by comparing (i) MS/MS/MS fragmentation

Table 1 MS/MS data from $CH_2=CH(CH_2)_nCO_2^-$ ions

$CH_2=CH(CH_2)_nCO_2^-$ n	Loss									Formation $^\bullet CH_2CO_2^-$
	H$\cdot$	H$_2$	H$_2$O^a	CO$_2$	C$_3$H$_6$	C$_4$H$_8$	C$_5$H$_{10}$	C$_6$H$_{12}$	C$_8$H$_{16}$	
1	100		3	88						5
2	65	5	10	100						7
3	100	10	34	29	2					10
4	100	15	72			8				1
5	100	20	16		17		5			2
6	54	5	72		100	48	3	56		9
8	22		51		100	39	14	10	10	5

^{a} The loss of H$_2$O is a standard reaction of carboxylate species and proceeds following proton transfer to form the enolate anion.[14] To take a specific example relevant to the enoic acids: $CH_2=CHCH_2CD_2CO_2^-$ loses HOD and D$_2$O in the ratio 2 : 1. The processes are as follows: $CH_2=CHCH_2CD_2$-$CO_2^- \longrightarrow CH_2=CHCH_2{}^-CDCO_2D \longrightarrow [(CH_2=CHCH_2CD=C=O)\,DO^-] \longrightarrow CH_2=CH^-CHCD=C=O + HOD$ and $CH_2=CHCH_2C{\equiv}CO^- + D_2O$.

Fig. 1 The collision-induced negative chemical ionisation tandem mass spectrum (MS/MS) of the $(M - D)^-$ ion of $CH_2=CH(CH_2)_6$-CO_2D. VG ZAB 2HF instrument. For experimental conditions, see Experimental section.
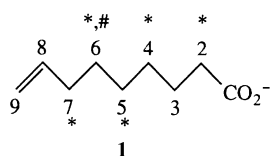
data of each product anion [using an MS 50 TA instrument (through the courtesy of Dr R. N. Hayes and Professor M. L. Gross)] and (ii) MS/MS fragmentation data of source formed product ions (using the VG ZAB 2HF instrument), with the MS/MS data of known ions produced by deprotonation of the appropriate neutral molecules. These data are recorded in Table 2. Results are summarised in Scheme 1. (B^2/E) Linked scans of

Scheme 1

source formed m/z 71, 99 and 113 confirm that each is formed directly from the parent $(M - H)^-$ ion.

The product ions shown in Scheme 1 which result from the losses of 'C$_4$H$_8$' and 'C$_6$H$_{12}$' are those that would be formed from the appropriate charge-remote process [$cf.$ reaction (1)].
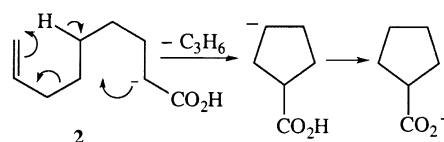

1

However, if the loss of 'C$_3$H$_6$' involves a 'charge-remote' process, the ionic product will be $CH_2=CH(CH_2)_3CO_2^-$. The data in Table 2 identify the product ion as the cyclopentyl carboxylate anion and therefore the loss of C$_3$H$_6$ must involve a cyclisation process.

We now wish to study the losses of 'C$_3$H$_6$', 'C$_4$H$_8$' and 'C$_6$H$_{12}$' in detail, and to assist with this endeavour, we have prepared carboxylate anions from five D$_2$ compounds [those indicated by an * in **1**] and one ^{13}C compound [that depicted by # in **1**]. The MS/MS data derived from all labelled species are recorded in Table 3.

The cyclisation process—loss of C$_3$H$_6$. It has already been shown that the product anion of this process is the cyclopentyl carboxylate anion. The deuterium labelling results indicate that both the hydrogens at the 7 position and one hydrogen at position 5 are lost as part of C$_3$H$_6$. These data may be rationalised as shown in Scheme 2. Transfer of a proton from position 2 to
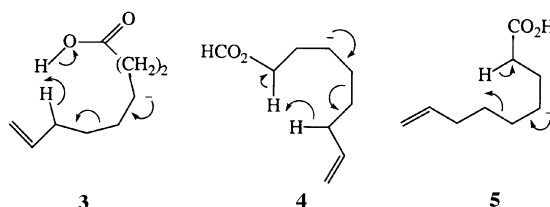

Scheme 2

the carboxylate anion produces the key enolate intermediate (**2**), which undergoes the cyclisation process shown. We have drawn the cyclisation process [see intermediate **2**] in synchronous fashion because of the deuterium labelling results {the alternative stepwise process in which an intermediate [($cyclo$C$_5$H$_9$CO$_2$H)$^-$ $^-$CH$_2$CH=CH$_2$] decomposes to yield $cyclo$-C$_5$H$_9$CO$_2^-$ and CH$_3$CH=CH$_2$, would involve the loss of one H from position 2 (the precursor enolate anion is formed following proton transfer from position 2 to the carboxylate anion centre), not, as observed, from position 5}.

The losses of 'C$_4$H$_8$' and 'C$_6$H$_{12}$'. The two most plausible mechanisms for the loss of 'C$_4$H$_8$' are the charge-remote reaction (2)†

† There are anionic processes like those summarised in formulae (**3**) and (**4**), which would give the same products as those formed by charge-remote process (2). These processes are less favourable on energetic grounds than that shown in reaction (3). In addition, we will show later, that such ionic processes do not occur because the precursor 4-anion preferentially undergoes facile proton transfer to form carboxylate (and enolate) anions.
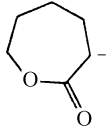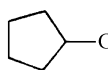
Table 2 MS/MS and MS/MS/MS data for some product ions from the non-8-enoate anion

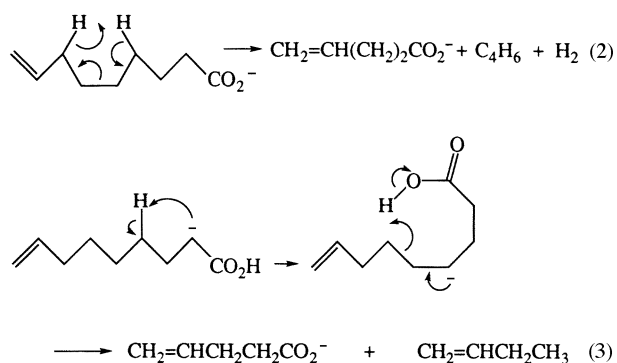| Precursor ion (*m/z*)	Product ion (*m/z*)	Spectrum type	Spectrum [*m/z* (loss) abundance]
$CH_2=CH(CH_2)_6CO_2^-$ (155)	$-C_3H_6$ (113)	MS/MS/MS [a]	111 (H_2) 100, 71 (C_3H_6) 60
$CH_2=CH(CH_2)_3CO_2^-$ (113)		MS/MS	111 (H_2) 100, 71 (C_3H_6) 65, 44 ($C_5H_9^·$) 4
		MS/MS	112 ($H^·$) 100, 111 (H_2) 10, 95 (H_2O) 34, 71 (C_3H_6) 2
			69 (CO_2) 29, 58 ($C_4H_7^·$) 10
$CH_3CH_2CH=CHCH_2CO_2^-$ (113)		MS/MS	112 ($H^·$) 18, 97 (CH_4) 8, 84 ($C_2H_5^·$) 4, 69 (CO_2) 100,
			67 ($CO_2 + H_2$) 4, 58 ($C_4H_7^·$) 2, 53 ($CO_2 + CH_4$) 3, 44 ($C_5H_9^·$) 3
$CH_3(CH_2)_2CH=CHCO_2^-$ (113)		MS/MS	112 ($H^·$) 68, 111 (H_2) 28, 95 (H_2O) 14, 84 ($C_2H_5^·$) 62, 69 (CO_2) 100
(113)		MS/MS	112 ($H^·$) 8, 111 (H_2) 2, 95 (H_2O) 100, 85 (28) 8,
			83 (CH_2O) 64, 71 (C_3H_6) 6, 69 (CO_2) 2, 57 (C_4H_8) 2, 43 (70) 1
--CO_2^- (113)		MS/MS	111 (H_2) 100, 71 (C_3H_6) 72, 44 ($C_5H_9^·$) 5
$CH_2=CH(CH_2)_6CO_2^-$ (155)	$-C_4H_8$ (99)	MS/MS/MS [a]	98 ($H^·$) 70, 81 (H_2O) < 10 [b], 58 ($C_3H_5^·$) < 10 [b], 55 (CO_2) 100
$CH_2=CH(CH_2)_2CO_2^-$ (99)		MS/MS	98 ($H^·$) 65, 97 (H_2) 5, 81 (H_2O) 10, 58 ($C_3H_5^·$) 7, 55 (CO_2) 100
$CH_2=CH(CH_2)_6CO_2^-$ (155)	$-C_6H_{12}$ (71)	MS/MS/MS [a]	70 ($H^·$) 100, 27 (CO_2) 35
$CH_2=CHCO_2^-$ (71)		MS/MS	70 ($H^·$) 100, 44 ($C_2H_3^·$) 4, 27 (CO_2) 29

[a] The MS/MS/MS spectra are weak: peaks < 5% are lost in baseline noise. [b] The spectra are weak—the abundances of these peaks are only approximate.

Table 3 MS/MS data for labelled non-8-enoate anions

Precursor ion (*m/z*)	Spectrum [*m/z* (loss) abundance]
$CH_2=CH(CH_2)_5CD_2CO_2^-$ (157)	156 ($H^·$) 55, 155 ($D^·$) 32, 138/137 [a] (HOD, D_2O) 15, 115 (C_3H_6) 100, 101 (C_4H_8) 30 [b], 102 (C_4H_7D) 25 [b], 72 ($C_6H_{11}D$) 48, 60 ($C_7H_{13}^·$) 22
$CH_2=CH(CH_2)_3CD_2(CH_2)_2CO_2^-$ (157)	156 ($H^·$) 65, 155 ($D^·$) 15, 139 (H_2O) 38, 115 (C_3H_6) 100, 101 (C_4H_8) 15, 100 (C_4H_7D) 30, 71 ($C_6H_{10}D_2$) 45, 58 ($C_7H_{11}D_2^·$) 24
$CH_2=CH(CH_2)_2CD_2(CH_2)_3CO_2^-$ (157)	156 ($H^·$) 70, 139 (H_2O) 28, 114 (C_3H_5D) 100, 101 (C_4H_8) 15, 100 (C_4H_7D) 8, 71 ($C_6H_{10}D_2$) 38, 58 ($C_7H_{11}D_2^·$) 18
$CH_2=CHCH_2CD_2(CH_2)_4CO_2^-$ (157)	156 ($H^·$) 45, 139 (H_2O) 22, 115 (C_3H_6) 100, 101 (C_4H_8) 8 [b], 100 (C_4H_7D) 15 [b], 99 ($C_4H_6D_2$) 25 [b], 71 ($C_6H_{10}D_2$) 52, 58 ($C_7H_{11}D_2^·$) 25
$CH_2=CHCD_2(CH_2)_5CO_2^-$ (157)	156 ($H^·$) 30, 155 ($D^·$) 30, 139 (H_2O) 28, 113 ($C_3H_4D_2$) 100, 100 (C_4H_7D) 15 [b], 99 ($C_4H_6D_2$) 29 [b], 71 ($C_6H_{10}D_2$) 38, 58 ($C_7H_{11}D_2^·$) 18
$CH_2=CHCH_2{}^{13}CH_2(CH_2)_4CO_2^-$ (156)	155 ($H^·$) 50, 138 (H_2O) 15, 114 ($^{12}C_3H_6$) 100, 99 ($^{12}C_3{}^{13}CH_8$) 28, 71 ($^{12}C_5{}^{13}CH_{12}$) 12, 58 ($^{12}C_6{}^{13}CH_{13}^·$) 5

[a] Composite peak not resolved. [b] Peaks not fully resolved.

and the anionic process (3).‡ Deuterium labelling studies should resolve the problem as to which of processes (2) and (3) is operative. In practice, this turns out not to be the case, since the deuterium labelling data [Table 3, and *cf.* **1**] indicate a particularly complex scenario. These data show that hydrogens at positions 2, 4, 5, 6 and 7 have partially scrambled prior to or during the loss of 'C_4H_8'. Hydrogen scrambling in anion systems can, in principle, occur by one of two general processes, *viz.* (i) by specific proton transfer processes occurring to particular anionic sites in the molecule, or (ii) by some type of skeletal rearrangement of the carbon skeleton, or (iii), some combination of both (i) and (ii). The latter scenario is reminiscent of the fragmentations of positively charged long chain carboxylate

‡ An alternative anionic process involves the reaction of the 4-anion shown in (**5**).† This would result in the formation of but-1-ene and the enolate anion of pent-4-enoic acid. We were unable to find a transition state for this reaction using AM1 calculations and have not considered the process further.

$$CH_2=CH(CH_2)_2CO_2^- + C_4H_6 + H_2 \quad (2)$$

$$\longrightarrow CH_2=CHCH_2CH_2CO_2^- \quad + \quad CH_2=CHCH_2CH_3 \quad (3)$$

esters, where both H and C rearrangements abound.[15] We prepared the 6-^{13}C labelled derivative of non-8-enoic acid in order to distinguish between these possibilities. If carbon skeletal rearrangement is occurring in this negative ion system, both '$^{12}C_3{}^{13}CH_8$' and '$^{12}C_4H_8$' will be lost from the 6-^{13}C labelled
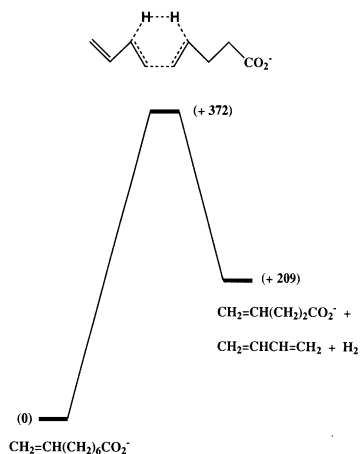
Fig. 2 Semi-empirical AM1 calculations for charge-remote reaction (2). Energy (kJ mol^{-1}) reaction coordinate plot. For computational procedures, see Experimental section.
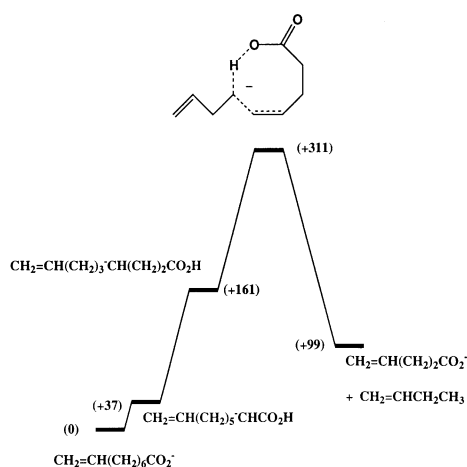

Fig. 3 Semi-empirical AM1 calculations for anionic mechanism reaction (3). Energy (kJ mol^{-1}) reaction coordinate plot.

Fig. 4 $^-$N$_f$R$^+$ spectra of the CID neutrals from (a) the non-8-enoate anion, and (b) the nonanoate anion. VG AutoSpec instrument. For experimental procedures, see Experimental section.

firm the hydrogens involved in the loss of 'C$_6$H$_{12}$'. No detectable hydrogen scrambling competes with this loss.

The evidence to date does not allow us to differentiate between charge-remote and anion-induced mechanisms for 'C$_4$H$_8$' or 'C$_6$H$_{12}$' loss.

(b) The evidence based on neutralisation reionisation mass spectrometry

The charge-remote and anionic processes described above can be differentiated based on the neutral molecules they release. For example, the charge-remote reaction (2) produces butadiene plus dihydrogen, whereas the anionic mechanism reaction (3) yields but-1-ene. Which neutrals are cleaved can be found by a NRMS-type experiment, *i.e.* by post-ionising the neutral CID losses and directly detecting them in the corresponding neutral fragment-reionisation, $^-$N$_f$R$^+$, spectrum.[12,18] That of the non-8-enoate anion is shown in Fig. 4(a).

For the interpretation of this spectrum, it is important to realise that all neutrals eliminated from the collisionally-activated non-8-enoate precursor anion (see Fig. 1) are post-ionised simultaneously. Each of the neutrals produces several ions upon collision-induced dissociative ionisation (CIDI),[19] the resulting $^-$N$_f$R$^+$ spectrum arising by superimposition of the individual CIDI spectra.[18] Because of this convolution, spectral interpretation and structural assignments are substantially facilitated if the $^-$N$_f$R$^+$ spectrum of the unknown [Fig. 4(a)] is compared against the collisional ionisation spectra of relevant reference molecules. An alkene and an alkadiene [Figs. 5(a) and 5(b)] as well as the neutral losses from the saturated nonanoate anion [see Fig. 4(b)] were chosen as the pertinent references in this case and will be discussed first.

Collisional ionisation spectra of hex-1-ene and hexa-1,5-diene. Depending on the decomposition mechanisms of the non-8-enoate anion (see above), the major neutral CID fragments are either alkenes or alkadienes. The types of ions formed upon collisional ionisation of these neutrals can be found by

parent anion. The (M − H)$^-$ ion from 6-^{13}C-non-8-enoic acid shows exclusive loss of '^{12}C$_3$^{13}CH$_8$': no carbon scrambling precedes or accompanies this or any other fragmentation (see Table 3).

Since we cannot distinguish between reactions (2) and (3) by deuterium labelling, perhaps computational studies may assist. We are not in a position to do high level *ab initio* calculations with systems of such complexity, but estimates of the reaction coordinate profiles for reactions (2) and (3) have been made using semi-empirical calculations (at AM1 level) using GAUSSIAN 94[16] and GAMESS-US[17] (see Experimental section for full details of the procedures used), and these are summarised in Figs. 2 and 3. The data shown in Figs. 2 and 3 should only be used qualitatively, but they do indicate (i), that both processes are energetically unfavourable with high activation barriers [an earlier AM1 calculation of the activation energy of a charge-remote reaction of an alkanoate anion gave a value of 385 kJ mol^{-1} (*cf.* the value in Fig. 2 of 372 kJ mol^{-1}), even though the value was nominally reduced using an experimental correction[13]], and (ii) the anionic process has the lower barrier to the transition state, it is less endothermic overall, but it is the more complex in terms of the number of steps involved. It would be unwise using these data, to propose which of reactions (2) or (3) is the more kinetically favoured.

Turning now to the loss of 'C$_6$H$_{12}$': this process could occur by either the charge-remote reaction (4) or from the enolate anion as shown in reaction (5). Since the same hydrogens are eliminated in both processes, deuterium labelling will not distinguish between the two possibilities. The data in Table 3 con-
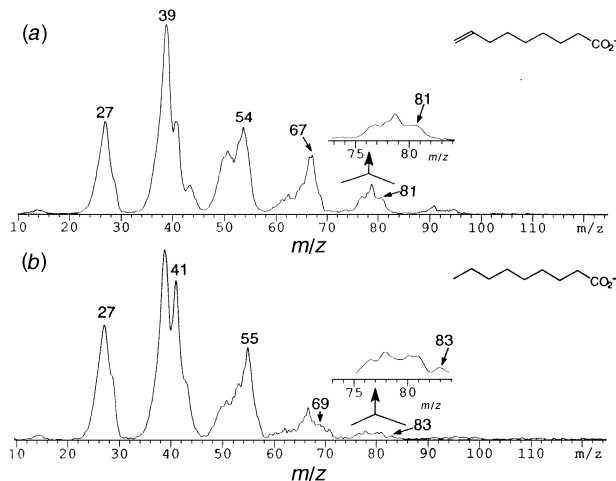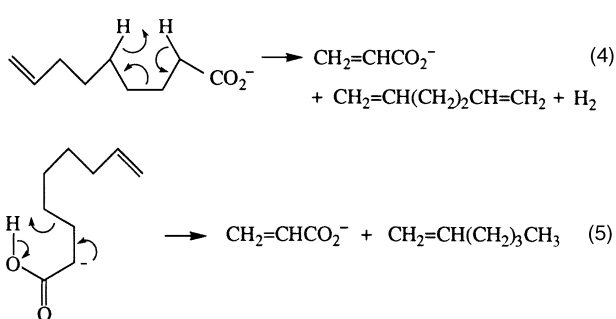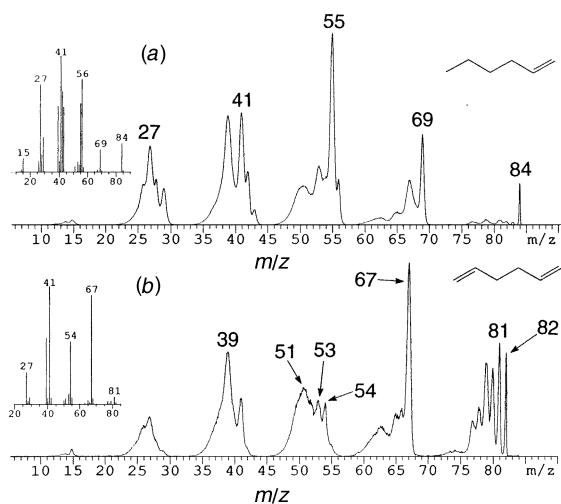
Fig. 5 $^+NR^+$ spectra of the molecular cations from (a) hex-1-ene and (b) hexa-1,5-diene. VG AutoSpec instrument.
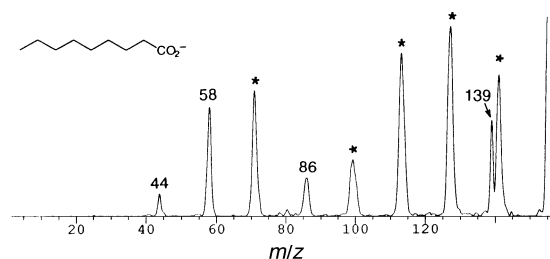

Fig. 6 The CID mass spectrum of the nonanoate anion. VG AutoSpec instrument.

neutralisation-reionisation ($^+NR^+$) of their molecular ions. $^+NR^+$ experiments were conducted with hexa-1,5-diene and hex-1-ene, the larger neutral fragments generated by reactions (4) and (5). Owing to the high kinetic energy, and hence superior transmission and reionisation efficiencies of large neutrals, such moieties generally provide dominant contributions to N_fR spectra.[18]

The $^+NR^+$ spectrum of ionised hex-1-ene [Fig. 5(a)] contains a prominent alkenyl ion series, viz. $C_nH_{2n-1}^+$ (m/z 27, 41, 55, 69). These ions, which also appear in the EI spectrum of hex-1-ene [inset in Fig. 5(a)],[20] are diagnostic for alkenes.[21] The given alkenyl ions are less important or even absent in the $^+NR^+$ spectrum of ionised hexa-1,5-diene [Fig. 5(b)]. Instead, this spectrum includes a sizeable $C_nH_{2n-3}^+$ series (m/z 39, 53, 67, 81) and other highly unsaturated ions, consistent with the higher degree of unsaturation in the diene.[21] Highly unsaturated fragments also dominate the EI spectrum of hexa-1,5-diene[20] [see inset in Fig. 5(b)]. It can be seen from Fig. 5, that alkenes and alkadienes can be distinguished from a consideration of their collisional ionisation products. It should be noted that the relative fragment ion abundances in $^+NR^+$ and EI spectra differ: this is a consequence of the different internal energy distributions deposited in parent ions by neutralisation-reionisation compared with electron ionisation.[22] Thus collisional ionisation reference spectra are most suitable for comparisons with N_fR data.

CID neutrals from the nonanoate anion. The majority of the fragment ions generated upon CID of the $(M - H)^-$ ion from the saturated nonanoic acid correspond to nominal C_nH_{2n+2} losses (marked by an * in Fig. 6). The only important fragments which do not belong to this series are those at m/z 139 (H_2O loss), 86 ($C_5H_{11}^•$ loss), 58 ($C_7H_{15}^•$ loss) and 44 ($C_8H_{17}^•$ loss). Overall, the C_nH_{2n+2} losses make up the largest fraction of the neutral CID fragments and should therefore be the principle contributor of the ions observed in the $^-N_fR^+$ spectrum [Fig. 4(b)]. The latter contains a relatively abundant alkenyl series

$C_nH_{2n-1}^+$ (m/z 27, 41, 55, 69 and 83), but much less (if any) alkyl ions $C_nH_{2n+1}^+$ (m/z 29, 43, 57, 71 and 85). These spectral characteristics reveal that the formal C_nH_{2n+2} losses cannot be alkanes or alkyl radicals plus $H^•$, because such species would have produced considerable $C_nH_{2n+1}^+$ after reionisation.[12] As discussed in the foregoing section for hex-1-ene, alkenyl ions are diagnostic of alkenes.[12,21] Thus the $^-N_fR^+$ data indicate that the major neutrals eliminated from the nonanoate anion are $C_nH_{2n} + H_2$, in agreement with the charge-remote fragmentation depicted in reaction (1). Parallel conclusions were reached from the $^-N_fR^+$ data of other saturated fatty acids.[12]

The relative intensities in the reference $^+NR^+$ spectrum of hex-1-ene and the $^-N_fR^+$ spectrum of nonanoate [Figs. 5(a) and 4(b)] do not match. This is because the latter also contains contributions from other smaller alkenes as well as from other CID neutrals (see below). Also, alkenes formed by charge-remote fragmentations are energised because of the large reverse activation energy associated with such processes (cf. Fig. 2). This explains why $C_2H_{<2n-1}^+$ fragments, which lie higher in energy than $C_2H_{2n-1}^{+23}$ are more dominant in the $^-N_fR^+$ spectrum [Fig. 4(b)] than in the reference $^+NR^+$ spectrum [Fig. 5(a)]. For the same reason, alkene molecular ions ($C_nH_{2n}^{•+}$) have a lower relative abundance in the $^-N_fR^+$ spectrum than in reference $^+NR^+$ spectra. For example, compare m/z 84 ($C_6H_{12}^{•+}$) in Figs. 4(b) and 5(a) (the peak height of $C_6H_{12}^{•+}$ is artifically enhanced in the reference $^+NR^+$ spectrum owing to the small peak width of precursor ions, which are not subject to kinetic energy release. In contrast, the $C_6H_{12}^{•+}$ peak in the $^-N_fR^+$ spectrum is much wider because it originates from the larger nonanoate ion, and through a process of large reverse activation energy that leads to substantial kinetic energy release).

Three nominal radical losses are observed, namely the losses of $C_5H_{11}^•$, $C_7H_{11}^•$ and $C_8H_{17}^•$ (see Fig. 6). Reionised $C_5H_{11}^•$ yields a detectable $C_5H_{11}^+$ ion (m/z 71), whereas only a trace of $C_7H_{15}^+$ (m/z 99) is formed, and there is no $C_8H_{17}^+$ (m/z 113) above noise level. It is possible that the larger radicals decompose more extensively upon post-ionisation. More likely, the CID ions of m/z 58 and 44 are not formed in one step by elimination of $C_7H_{15}^•$ or $C_8H_{17}^•$ respectively, but originate by consecutive processes, e.g. from m/z 86 by losses of C_2H_4 or C_3H_6.

CID neutrals from the non-8-enoate anion. Comparison of the $^-N_fR^+$ spectra of the non-8-enoate and nonanoate anions [Figs. 4(a) and 4(b)] shows that the former contains more unsaturated product ions. Fig. 4(a) includes dominant peaks at m/z 54, 67 and 81 but barely any heavier ions within the corresponding peak groups. These products (several of which belong to the $C_nH_{2n-3}^+$ series) also appear in the $^+NR^+$ spectrum of hexa-1,5-diene [Fig. 5(b)] and are characteristic for alkadienes. The small relative abundances of m/z 55, 69 and 83 [see insets in Fig. 4(a)], which are indicative of alkenes [see previous section and Fig. 5(a)], further attests that these alkenes are not an important component in the neutral loss mixture released from the non-8-enoate anion.

The sizeable m/z 54 signal ($C_4H_6^{•+}$) in Fig. 4(a) is due to the elimination of butadiene, consistent with the operation of charge-remote reaction (2). Similarly, the negligible relative intensities of m/z 55 and 56 ($C_4H_7^+$ and $C_4H_8^{•+}$) indicate the loss of but-1-ene (C_4H_8) from the non-8-enoate anion to be an unfavourable process.

The abundant peak corresponding to m/z 81 ($C_6H_9^+$) in Fig. 4(a), shows a small shoulder corresponding to m/z 82 ($C_6H_{10}^{•+}$). The presence of these two products confirms that C_6H_{10} is eliminated from the non-8-enoate anion, supporting the operation of charge-remote process **5**. That the neutral is hexa-1,5-diene is confirmed by the reference collisional ionisation spectrum shown in Fig. 5(b). All ions present in the reference spectrum are seen in the $^-N_fR^+$ spectrum of non-8-enoate [Fig. 4(a)]. The abundance ratio of m/z 54 : 67 is larger in the $^-N_fR^+$ than the $^+NR^+$ spectrum, because the former includes a contribution from C_4H_6 loss [reaction (2)]. As explained earlier, the large

reverse activation energy of charge-remote reactions supplies excess energy to the neutral products, promoting extensive fragmentation upon reionisation and reducing peak resolution [*cf.* Figs. 4(*a*) and 5(*b*)].

The alkenyl ions $C_6H_{11}^+$ and $C_6H_{12}^{\cdot+}$ (*m/z* 83 and 84) are of very small abundance in the $^-N_fR^+$ spectrum of the non-8-enoate anion [Fig. 4(*a*)]. The nonanoate anion loses hexene, and its $^-N_fR^+$ spectrum [Fig. 4(*b*)] shows a small peak correspondng to $C_6H_{11}^+$. Based on the relative ratios of *m/z* 83 : 81 in Figs. 4(*a*) and 4(*b*), we conclude that the loss of hex-1-ene from the non-8-enoate anion is, at best, a minor process compared with that resulting in loss of hexa-1,5-diene.

Thus $^-N_fR^+$ data are consistent with (i) charge-remote process (2) operating to the exclusion of anionic process (3), and (ii) the operation of charge-remote process (4) with the possibility of a minor contribution from anionic process (5).

Summary and conclusions

The above study shows that competitive charge-remote and anion-induced processes occur following collisional activation of the non-8-enoate anion.

In summary:

(i) The loss of C_3H_6 is a reaction of the enolate anion (formed following proton transfer to the carboxylate centre), which effects cyclisation to yield the cyclopentyl carboxylate anion and propene. Hydrogen scrambling does not accompany this process.

(ii) The loss of 'C_4H_8' is a charge-remote process resulting in the formation of the pent-4-enoate anion together with butadiene and dihydrogen. This reaction co-occurs with extensive proton transfer processes occurring between various carbanions on the carbon skeleton.

(iii) The major process producing overall loss of 'C_6H_{12}' is a charge-remote reaction which yields the acrylate anion together with hexa-1,5-diene and dihydrogen. A minor accompanying anionic process may involve loss of hex-1-ene. No detectable hydrogen scrambling accompanies this (these) process(es).

In conclusion:

(*a*) the observation of a charge-remote fragmentation $[-(C_4H_6 + H_2)]$ co-occurring with anionic proton scrambling processes is unique in negative ion chemistry. The fact that charge-remote reaction (2) occurs in preference to the anionic process may be rationalised as follows. The 4-carbanion, whose formation is inferred from deuterium labelling data, rearranges by facile proton transfer (to form either or both of the stable enolate or carboxylate anions) in preference to the reaction shown in reaction (3) (there is ample precedent for unstable carbanions undergoing proton transfer to form more stable anions[24]). We have tested whether such a process is feasible by the use of AM 1 semiempirical calculations. When the 4-carbanion (see Fig. 3) achieves the conformation shown in (**6**),

6
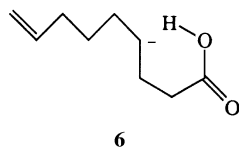
proton transfer to form the non-8-enoate anion is immediate: no stable hydrogen bonded intermediate is formed during this process.

(*b*) The situation concerning loss of 'C_6H_{12}' is arguably even more complex. NRMS data are consistent with the charge-remote reaction (4) being predominant, and the lack of competitive hydrogen scrambling in this instance implies that the process must have a lower activation barrier than that of the corresponding reaction (2). Further, anionic reaction (5) must have a lower activation barrier than that of the corresponding

reaction (3), since the enolate anion precursor [in reaction (5)] is some 130 kJ mol^{-1} more negative in energy than that shown for the precursor 4-anion [in reaction (3)] (see Fig. 3). This leads to the final question: why then does not anionic reaction (5) occur to the exclusion of charge-remote reaction (4)? The answer must be that the enolate anion preferentially undergoes the cyclisation process already described (see Scheme 2) rather than reaction (5).

Experimental

Mass spectrometric methods

Collisional activation (CID) mass spectra (MS/MS) were determined with a VG ZAB 2HF mass spectrometer.[25] Full operating details have been reported.[26] Specific details are as follows: the chemical ionisation slit was used in the chemical ionisation source, the ionising energy was 70 eV, the ion source temperature was 100 °C, and the accelerating voltage was 7 kV. Non-8-enoic acid was introduced into the source *via* the direct probe with no heating [measured pressure of sample 1×10^{-6} Torr (1 Torr = 133.322 Pa)]. Deprotonation was effected using HO$^-$ (from H_2O) or DO$^-$ (from D_2O) for deuterium-labelled derivatives. The measured pressure of H_2O or D_2O was 1×10^{-5} Torr. The estimated source pressure was 10^{-1} Torr. Argon was used in the second collision cell (measured pressure, outside the cell, 2×10^{-7} Torr), giving a 10% reduction in the main beam, equivalent to single collision conditions.

MS/MS/MS tandem mass spectra were measured (through the courtesy of Professor M. L. Gross and Dr R. N. Hayes) with an MS TA 50 mass spectrometer as described previously.[27] The pressure of He collision gas in both collision cells was 1×10^{-6} Torr, producing a reduction in the main beam of 30%.

The NRMS-type experiments were conducted with an E_1BE_2 tandem mass spectrometer (VG AutoSpec at Akron) that has previously been described.[28] This instrument houses two collision cells (C-1 and C-2) and an intermediate deflector in the interface region between E_1B and E_2. The carboxylate anions $(M − H)^-$ from nonanoic acid and non-8-enoic acid were formed by FAB ionisation, using a 20 keV Cs^+ ion gun and triethanolamine as the matrix. The $(M − H)^-$ precursor anions were accelerated to 8 keV, selected by E_1B and dissociated with He in C-1. CID coproduces ionic and neutral fragments. After exiting C-1, the ionic fragments and any undissociated $(M − H)^-$ ions were deflected from the beam path, and the remaining neutral losses were post-ionised in C-2 by collision-induced dissociative ionisation with O_2.[19] The newly formed cations were mass-analysed by E_2 and recorded in the neutral fragment-reionisation, $^-N_fR^+$, spectrum.[12,28] The superscripts besides N and R in the N_fR notation designate the charge of the precursor ion (from which the neutrals are eliminated) and the charges of the ultimate product ions (to which the neutrals are reionised), respectively.[18] Neutralisation-reionisation ($^+NR^+$) spectra of the molecular cations of hex-1-ene and hexa-1,5-diene were measured similarly by replacing He in C-1 (which causes CID) with trimethylamine (which causes charge exchange neutralisation).[18] In these experiments, molecular cations were generated by electron impact, and were accelerated to the kinetic energy with which hex-1-ene and hexa-1,5-diene would be eliminated from 8 keV nonanoate and 8 keV non-8-enoate, respectively (4.2 to 4.3 keV).

Syntheses of unlabelled and labelled precursor molecules

Hex-1-ene, hexa-1,5-diene, but-3-enoic acid, nonanoic acid and ε-caprolactam were commercial products. The following compounds were made by reported procedures: pent-4-enoic acid,[29] hex-5-enoic acid,[30] hept-6-enoic acid,[29] oct-7-enoic acid,[29] non-8-enoic acid[31] and cyclopentane carboxylic acid.[32]

2,2-[²H₂]pent-4-enoic acid. This was prepared as for the unlabelled analogue,[29] except that hydrolysis of the precursor

ester was carried out with NaOD and the final acidification by D_2SO_4 in D_2O. Overall yield 75%, $D_2 = 90\%$.

2,2-[$^2H_2$]Non-8-enoic acid. Non-8-enoic acid[33] (0.5 g) was heated under reflux in MeOD–MeONa [Na (0.2 g) in MeOD (5 cm³)] for 15 h. After being cooled to 25 °C, the solvent was removed *in vacuo*, the residue dissolved in water (5 cm³), cooled (0 °C), acidified to pH 1 with aqueous hydrogen chloride (10%), and extracted with diethyl ether (5 cm³). Removal of the solvent gave the desired product (95% yield; $D_1 = 10$, $D_2 = 90\%$).

4,4-[$^2H_2$]Non-8-enoic acid. Diethyl succinate was reduced[34] with lithium aluminium deuteride in refluxing tetrahydrofuran to yield 1,1,4,4-[$^2H_4$]butane-1,4-diol (yield 85%), which was tosylated[35] with tosyl chloride§ (1 equiv.) in anhydrous pyridine to yield a mixture of mono- and di-tosylated 1,1,4,4-[$^2H_4$]butane-1,4-diol. The mono-tosylated product was obtained in 60% yield following column chromatography [on silica eluting with diethyl ether–hexane (1.5 : 8.5)]. The mono-tosylate was coupled[36] with pent-4-ene magnesium bromide to yield 4,4-[$^2H_2$]non-8-enol (yield 72%) which was oxidised[37] with chromium trioxide to give the desired 4,4-[$^2H_2$]non-8-enoic acid (overall yield 55%; $D_2 = 99\%$).

5,5-[$^2H_2$]Non-8-enoic acid. This was synthesised by a similar methodology as that used above for 4,4-[$^2H_2$]non-8-enoic acid. Glutaric anhydride was reduced with lithium aluminium deuteride to obtain 1,1,5,5-[$^2H_4$]pentane-1,5-diol. Overall yield of 5,5-[$^2H_2$]non-8-enoic acid, 45%; $D_2 = 99\%$.

6,6-[$^2H_2$]Non-8-enoic acid. This was prepared by first coupling[38] 4,4-[$^2H_2$]-4-bromobut-1-ene[39] with 5-magnesium bromide pentanol tetrahydropyranyl ether[38] to obtain 6,6-[$^2H_2$]non-8-enol tetrahydropyranyl ether in 67% yield. 6,6-[$^2H_2$]Non-8-enol was formed following deprotection of the tetrahydropyranyl ether with acid,[40] and then oxidised[37] to give 6,6-[$^2H_2$]non-8-enoic acid in 50% yield ($D_2 = 99\%$).

7,7-[$^2H_2$]Non-8-enoic acid. This was synthesised using a similar methodology as that used for 4,4-[$^2H_2$]non-8-enoic acid. 1,1,7,7-[$^2H_4$]Heptane-1,7-diol was prepared by reduction of dimethyl pimelate with lithium aluminium deuteride.[34] Overall yield of 7,7-[$^2H_2$]non-8-enoic acid, 55% ($D_2 = 99\%$).

6-^{13}C-Non-8-enoic acid. The reaction[41] between allyl bromide (1.2 g) and Cu^{13}CN (1.1 g, $^{13}C = 99\%$)[42] gave allyl (^{13}C cyanide) in 70% yield. The allyl (^{13}C cyanide) was hydrolysed[43] to the labelled vinyl acetic acid (65% yield), which was reduced[34] with lithium aluminium hydride in refluxing tetrahydrofuran to form 1-^{13}C-but-3-en-1-ol in 78% yield. The alcohol was tosylated[44] with tosyl chloride. The tosylate was purified by column chromatography over silica in diethyl ether–hexane (1.5 : 8.5), coupled[36] with 5-magnesium bromide pentanol tetrahydropyranyl ether[38] to yield 6-^{13}C-non-8-enol tetrahydropyranyl ether, which was then deprotected to give the alcohol[39] and then oxidised[37] to 6-^{13}C-non-8-enoic acid (overall yield from 1-^{13}C-but-3-en-1-ol, 40%: $^{13}C = 99\%$).

Computational methods

Semi-empirical molecular orbital calculations using the AM1 model Hamiltonian[45] were performed with the GAUSSIAN 94[16] and GAMESS-US[17] systems of programs. Calculations were performed on a variety of computational platforms, including DECStation 5000/25 and Silicon Graphics Indigo² xZ workstations, as well as Thinking Machines CM-5 and Silicon Grapics Power Challenge supercomputers.

Optimised molecular geometries were characterised as local minima or transitions states by subsequent vibrational frequency calculations. Molecular geometries representing local minima possess all positive vibrational frequencies; transition states are identified as possessing one (only) imaginary frequency as well as one (only) negative eigenvalue of the Hessian matrix. The zero-point energy for each structure was also obtained from the frequency calculations. Calculated zero-point energies tend to overestimate actual energies by up to *ca.* 15% and are therefore scaled by 0.89.[46] The reaction barriers were determined by comparing zero point-corrected energies of the appropriate local minima and transition state. Intrinsic reaction coordinate (IRC) calculations from the transition state were undertaken to confirm that the calculated transition state geometry does indeed connect the relevant local minima on the overall reaction potential energy surface.

The following computational protocol was employed in this study. Optimised geometries for reactants and products were determined using GAUSSIAN 94. The molecular geometry of the transition state linking local minima on the reaction potential energy surface (Fig. 3) were then determined using the Linear Synchronous Transit (LST) approach.[47] The structure resulting from an LST calculation was subsequently used as input for a saddle point geometry optimisation using GAMESS. The saddle point geometry determined from the GAMESS calculation was then input, along with the reactant and product geometric specifications, into a QST3 transition state optimisation using GAUSSIAN 94. QST3 Transition state optimisations employ the Synchronous Transit-Guided Quasi-Newton (STQN) method developed by Schlegel and co-workers.[48] Finally, IRC calculations were used to confirm that computed transition state geometries do connect the reactants and products of interest.

References

1 J. H. Bowie, *Mass Spectrom. Rev.*, 1990, **9**, 349.
2 J. H. Bowie, in *Experimental Mass Spectrometry*, ed. D. H. Russell, Plenum Press, New York and London, 1994, pp. 1–38.
3 P. C. H. Eichinger and J. H. Bowie, *Int. J. Mass Spectrom. Ion Processes*, 1991, **110**, 123.
4 S. Dua, J. H. Bowie and J. C. Sheldon, *J. Chem. Soc., Perkin Trans. 2*, 1994, 543.
5 J. Adams and M. L. Gross, *J. Am. Chem. Soc.*, 1986, **108**, 6915.
6 J. Adams and M. L. Gross, *J. Am. Chem. Soc.*, 1989, **111**, 435, and references cited therein.
7 J. Adams, *Mass Spectrom. Rev.*, 1990, **9**, 141.
8 M. L. Gross, *Int. J. Mass Spectrom. Ion Processes*, 1992, **118/119**, 137.
9 V. H. Wysocki, M. H. Bier and R. G. Cooks, *Org. Mass Spectrom.*, 1988, **23**, 627.
10 V. H. Wysocki, M. M. Ross, S. R. Horning and R.G. Cooks, *Rapid Commun. Mass Spectrom.*, 1988, **2**, 214.
11 V. H. Wysocki and M. M. Ross, *Int. J. Mass Spectrom. Ion Processes*, 1991, **104**, 179.
12 M. M. Cordero and C. Wesdemiotis, *Anal. Chem.*, 1994, **66**, 861.
13 M. M. Siegel and N. B. Colthup, *Appl. Spectrosc.*, 1988, **42**, 1214.
14 K. M. Downard, J. C. Sheldon, J. H. Bowie, D. E. Lewis and R. N. Hayes, *J. Am. Chem. Soc.*, 1989, **111**, 8112, and references cited therein.
15 W. Sonneveld, D. Van der Steen and H. J. J. Pabon, *Recl. Trav. Chim., Pays-Bas*, 1968, **87**, 1110; Ng. Dinh-Nguhen, *Arkiv. Kemi*, 1968, **28**, 289.
16 Gaussian 94, Revision C.3, M. J. Frisch, G. W. Trucks, H. B. Schlegel, P. M. W. Gill, B. G. Johnson, M. A. Robb, J. R. Cheesman, T. Keith, G. A. Petersson, J. A. Montgomery, K. Raghavachari, M. A. Al-Latham, V. G. Zakrzewski, J. V. Ortiz, J. B. Foresman, J. Cioslowski, B. B. Stefanov, A. Nanayakkara, M. Challacombe, C. Y. Peng, P. V. Ayala, W. Chen, M. W. Wong, J. L. Andres, E. S. Replogle, R. Gomperts, R. L. Martin, D. J. Fox, J. S. Binkley, D. J. Defrees, J. Baker, J. P. Stewart, M. Head-Gordon, C. Gonzalez and J. A. Pople, Gaussian Inc., Pittsburgh, PA, 1995.

§ Tosyl chloride = 4-methylphenylsulfonyl chloride.

17 M. W. Schmidt, K. K. Baldridge, J. A. Boatz, S. T. Elbert, M. S. Gordon, J. H. Jensen, S. Koseki, N. Matsunaga, K. A. Nguyen, S. Su, T. L. Windus, M. Depuis and J. A. Montgomery, *J. Comput. Chem.*, 1993, **14**, 1347.

18 M. J. Polce, S. Beranova, M. J. Nold and C. Wesdemiotis, *J. Mass Spectrom.*, 1996, **31**, 1073.

19 P. C. Burgers, J. L. Holmes, A. A. Mommers, J. E. Szulejko and J. K. Terlouw, *Org. Mass Spectrom.*, 1984, **19**, 422.

20 F. W. McLafferty and D. B. Stauffer, *Wiley/NBS Registry of Mass Spectral Data*, 1989, Wiley, New York.

21 F. W. McLafferty and F. Turecek, *Interpretation of Mass Spectra*, University Science Books, Mill Valley, CA, 4th edn., 1993.

22 S. Beranova and C. Wesdemiotis, *J. Am. Soc. Mass Spectrom.*, 1994, **5**, 1093.

23 S. G. Lias, J. E. Bartmess, J. F. Liebman, J. L. Holmes, R. D. Levin and W. G. Mallard, *Gas Phase Ion and Neutral Thermochemistry*, *J. Phys. Chem. Ref. Data 17*, 1988, Suppl. 1. The computer-based version was used.

24 S. T. Graul and R. R. Squires, *J. Am. Chem. Soc.*, 1990, **112**, 2506 and references cited therein; K. M. Downard, R. N. Hayes and J. H. Bowie, *J. Chem. Soc.*, *Perkin Trans. 2*, 1992, 1815.

25 J. K. Terlouw, P. C. Burgers and H. Hommes, *Org. Mass Spectrom.*, 1979, **14**, 307.

26 G. W. Adams, J. H. Bowie and R. N. Hayes, *J. Chem. Soc.*, *Perkin Trans. 2*, 1991, 689.

27 D. J. Burinsky, R. G. Cooks, E. K. Chess and M. L. Gross, *Anal. Chem.*, 1982, **54**, 295; M. L. Gross, E. K. Chess, P. A. Lyon, F. W. Crow, S. Evans and H. Tudge, *Int. J. Mass Spectrom. Ion Phys.*, 1982, **42**, 574.

28 M. J. Polce, M. M. Cordero, C. Wesdemiotis and P. A. Bott, *Int. J. Mass Spectrom. Ion Processes*, 1992, **113**, 35.

29 R. P. Linstead and H. N. Rydon, *J. Chem. Soc.*, 1933, 580.

30 R. P. Linstead and H. N. Rydon, *J. Chem. Soc.*, 1934, 1995.

31 H. Stetter and W. Dierichs, *Chem. Ber.*, 1952, **85**, 1061.

32 D. W. Gohen and W. R. Vaughan, *Org. Syn. Coll. Vol. 4*, 1963, 594.

33 T. H. Chan and D. Stossel, *J. Org. Chem.*, 1986, **51**, 2423.

34 A. Burger, L. Turnbull and J. G. Dinwiddie, *J. Am. Chem. Soc.*, 1950, **72**, 5512.

35 A. I. Vogel, *Textbook of Practical Organic Chemistry*, Longman and Green Pty Ltd., 4th edn., 1978, p. 1103.

36 G. Fouquet and M. Schlosser, *Angew Chem.*, *Int. Ed. Engl.*, 1974, **13**, 82.

37 E. J. Eisenbraun, *Org. Syn. Coll. Vol. 5*, 1973, 310.

38 J. H. Babler and B. J. Invergo, *J. Org. Chem.*, 1979, **44**, 3723.

39 A. Padwa, W. F. Rieker and R. J. Rosenthal, *J. Org. Chem.*, 1984, **49**, 1353.

40 E. J. Corey, H. Niwa and J. Knolle, *J. Am. Chem. Soc.*, 1978, **100**, 1942.

41 J. V. Supniewski and P. L. Salzberg, *Org. Syn. Coll. Vol. 3*, 1955, 851.

42 H. J. Barber, *J. Chem. Soc.*, 1943, 79.

43 E. Reitz, *Org. Syn. Coll. Vol. 3*, 1955, 851.

44 L. Brandsma and H. D. Verkrnijsse, *Synthesis of Ethylenes, Allenes and Cumulenes*, Elsevier, New York, 1981, p. 223.

45 M. J. S. Dewar, E. G. Zoebisch and E. F. Healy, *J. Am. Chem. Soc.*, 1985, **107**, 3902.

46 W. Hehre, L. Radom, P. v. R. Schleyer and J. A. Pople, Ab Initio *Molecular Orbital Theory*, Wiley, New York, 1986.

47 T. A. Halgren and W. N. Lipscomb, *Chem. Phys. Lett.*, 1977, **49**, 225.

48 C. Peng and H. B. Schlegel, *Israel J. Chem.*, 1993, **33**, 449.

Anionic migration in aromatic systems effected by collisional activation. Unusual fragmentations of deprotonated anilides containing methoxyl and ethoxyl substituents

Stephen J. Blanksby, Suresh Dua, John M. Hevko, Hamish Christie and John H. Bowie

Department of Chemistry, The University of Adelaide, South Australia, 5005, Australia.

Long-range cross-ring reactions occur when $(M - H)^-$ ions of methoxy- and ethoxy-C_6H_4–^-NCOR (R = H, CH_3, C_6H_5 and CH_3O) are subjected to collisional activation. These reactions are generally minor processes: a particular example is the cross-ring elimination p-C_2H_5O–C_6H_4–$^-NCOCH_3 \rightarrow [CH_3^-$ (p-C_2H_5O–C_6H_4–NCO)] $\rightarrow p$-(^-O)–C_6H_4–NCO + C_2H_4 + CH_4. Major processes of these $(M - H)^-$ ions involve (i) losses of radicals to form stabilised radical anions, e.g. (a) loss of a ring $H^\bullet$ or (b) $CH_3^\bullet$ (or $C_2H_5^\bullet$) from the alkoxy group, and (ii) proximity effects when the two substituents are *ortho*, e.g. loss of CH_3OH from o-CH_3O–C_6H_4–^-NCHO yields deprotonated benzoxazole. Another fragmentation of an arylmethoxyl anion involves loss of CH_2O. It is proposed that losses of CH_2O are initiated by anionic centres but the actual mechanisms in the cases studied depend upon the substitution pattern of the methoxyanilide: o- and p-methoxyanilides may undergo *ipso* proton transfer/elimination reactions, whereas the *m*-analogues undergo proton transfer reactions to yield an o-CH_3O substituted aryl carbanion followed by proton transfer from CH_3O to the carbanion site with concomitant loss of CH_2O.

Introduction

The general fragmentation pathways of even-electron organic anions have been reviewed.[1] The major fragmentations often proceed via an anion–neutral complex with the complex either falling apart to give the anion and the neutral; alternatively, the anion effects some reaction within the complex, viz. deprotonation, elimination, an S_N2 reaction etc., resulting in elimination of a neutral. One of the interesting features of such reactions is how far the anion is free to move within the ion complex. There are examples where anions are free to move within the complex and effect reaction at more than one centre: the classical example involves the loss of H_2 from the $[M - H]^-$ ion of cyclohexanone to yield the two products shown in Sequences **1** and **2**.[2] In contrast, there are many examples where the incipient anion is not mobile, but reacts solely at an adjacent position. A particular example is shown in Sequence **3**.[3]

We have reported an anionic migration reaction where an incipient anion may move either around, or across, an aromatic ring to induce an internal S_N2 reaction.[4] The overall process is shown in Scheme 1 and involves the loss of the elements of CH_3CD_3 when R = CD_3. The product anion is formed by two competitive pathways. The first is a stepwise process, involving loss of first $CH_3^\bullet$ and then $CD_3^\bullet$. The second is synchronous, and is rationalised in terms of an incipient CD_3^- ion moving to effect an S_N2 reaction at the carbon of the OCH_3 group resulting in elimination of CH_3CD_3 (the alternative process where CH_3^- undergoes an S_N2 process at the carbon of the CD_3 group is energetically unlikely in comparison).

The present paper extends the work described above. The incipient anion is formed in the same way from the precursor anion Ar–^-NCOR through complex [(ArNCO) R^-].[†] The aims of the present work are (i) to investigate

---

[†]*A reviewer has asked whether the parent anions fragment spontaneously as well as following collision activation, and whether ion complexes are formed in these processes. To take the particular example shown in Scheme 1: the process does occur in the absence of gas in the collision cell, but collision activation significantly increases the peak abundance (this is generally true for other processes described in this paper). If a potential of 1000 V is applied to the collision cell (argon pressure in cell, 2×10^{-7} Torr), the ratio of fragmentation within the collision cell to that outside the cell is 3 : 1 for the process shown in Scheme 1. The intermediacy of ion complexes is proposed for some (but not all) of the processes described in this paper when this aids the mechanistic rationale. In the absence of potential surface data for the reactions, such proposals, although plausible, are speculative.*
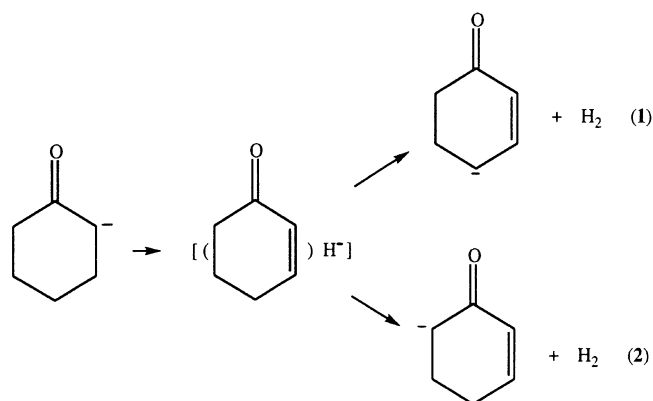
Sequence 1 and 2.

Sequence 3.

the effective migratory aptitude and reactivity of a number of incipient anions, i.e. $R = H$, CH_3, C_6H_5 and CH_3O. We examine the reactions of these anions with o-, m- and p-OCH_3 substituents (cf Reference 4) and $R = CH_3$ and C_6H_5 with o-, m- and p-OC_2H_5.

Experimental section

HO[-] NICI MS/MS data were obtained with a reverse sector VG ZAB 2HF instrument.[5] Full details of the operation of the instrument have been given previously.[6,7] Specific details were as follows: the chemical ionisation slit was used in the ion source, the ionising energy was 70 eV, the ion source temperature was 150°C, and the accelerating voltage 7 kV. All samples were introduced into the ion source using the direct probe which was not heated. The source pressure of sample was typically 5×10^{-7} Torr. Deprotonation was effected by HO[-] (from H_2O, source pressure 1×10^{-5} Torr). The total estimated source pressure was 10^{-1} Torr. The $(M - H)^-$ ion was focussed using the magnet, fired through the second collision cell which contained argon [measured pressure outside the cell, 2×10^{-7} Torr (giving a 10% reduction in the ion beam signal, equivalent to single collision conditions)], and the mass spectrum was obtained by scanning the electric sector.

All unlabelled compounds (listed in Tables 1 and 2) are known[8] and were prepared by conversion of the appropriate substituted aniline to the amide.[8]
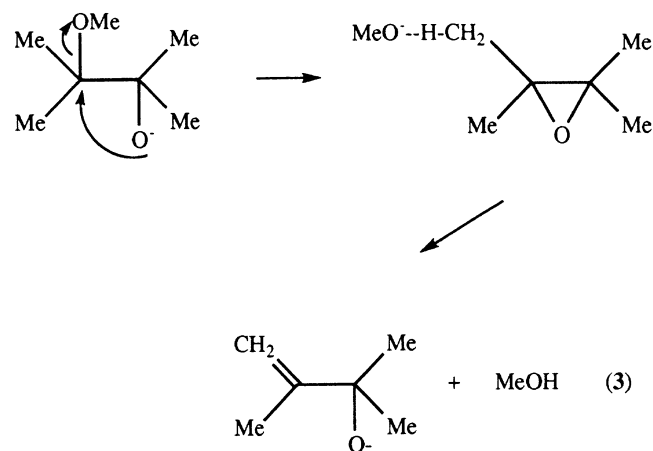
Labelled compounds

o-(D₃-methoxy)formanilide

Reduction of o-nitro-D$_3$-anisole $(D_3 > 99\%)$[9] with aqueous titanous chloride[10] gave o-D$_3$-anisidine (yield 50%, $D_3 > 99\%$) which was formylated[11] with formic acid to give o-(D$_3$-methoxy)formanilide (overall yield 35%, $D_3 > 99\%$).

o-Methoxyform-D-anilide

o-Anisidine hydrochloride (0.75 g) and formic D acid potassium salt (1.0 g, $D_1 = 99\%$) were heated at 120°C for one hour. The cooled mixture was extracted with diethyl ether (3×10 cm^3), the combined ethereal extract washed with aqueous sodium hydroxide (saturated 10 cm^3) and dried (anhydrous $MgSO_4$). Evaporation of the solvent gave o-methoxyform-D-anilide (yield 83%, $D_1 = 99\%$).

p-(D₅-Ethoxy)acetanilide

Prepared by a reported procedure.[12] ($D_5 = 99\%$).

p-(D₃-Methoxy)phenyl methyl carbamate

p-D$_3$-Anisidine[9,10] (see above) was allowed to react with methylchloroformate in acetone[11] to yield p-(methoxy-D$_3$) phenyl methyl carbamate (yield 75%, $D_3 = 99\%$).

p-Methoxy(3,5-D₂-phenyl) methyl carbamate

3,5-D$_2$-4-Anisidine ($D_1 = 45$, $D_2 = 55$),[13] on treatment with methyl chloroformate in acetone,[11] gave p-methoxy(3,5-D$_2$-phenyl) methyl carbamate (yield 70%, $D_1 = 45$, $D_2 = 55\%$).

Results and discussion

Before commencing a discussion of the reactivity of the studied systems, we wish to address the problem of whether the formal intermediate in these reactions corresponds to $[(ArNCO) R^-]$ or $[(ArNCO)^{-\bullet} R^\bullet]$. There has been debate about this type of situation, particularly where the neutral ether has a significantly higher electron affinity than $R^\bullet$, or when R^- is unbound in the free state (i.e. where the electron affinity of $R^\bullet$ is negative) (cf Reference 14). We are currently looking at theoretical potential surfaces of particular reactions (e.g. the Wittig rearrangement, which in principle could be either a radical or anionic 1,2 rearrangement[15]) to study this problem. Our view at this time is that it is not important (for subsequent reactions) which of the two extreme possibilities (i.e. the neutral–anion complex or the radical anion–radical complex) is the more stable, because in principle, reaction via either $R^\bullet$ or R^- may occur within a complex

which may have both anionic and radical character. It is the physical barrier(s) for the next stage(s) of the reaction together with the probability of that process, which will determine whether R^- or $R^\bullet$ is involved in that reaction. In support of this contention, there are certain fragmentations of anions which may be rationalised by competitive processes involving both $R^\bullet$ and R^-. One example is the general scenario for [(neutral) CH_3O^-] complexes which may competitively decompose to (i) form CH_3O^-, eliminate CH_3OH (CH_3O^- deprotonates the neutral), eliminate CH_2O (H^- transfer to the neutral from CH_3O^-), and (ii) lose $CH_3O^\bullet$.[16] Thus, for simplicity, we depict the intermediates in the following discussion as neutral/anion complexes: this should not be taken to mean that they cannot also have radical anion/radical character. There are reactions described in this paper which are clearly reactions of R^- and others which involve loss of $R^\bullet$.

"Long range" S_N2 reactions of anisole derivatives

The first question that we wish to answer is whether the S_N2 process shown in Scheme 1 (already noted[4] for $R = CH_3$) occurs when $R = H$, C_6H_5 and CH_3O, and if so, how is this dependent on the nature of R. The spectra of the deprotonated forms of o, m and p formamide, benzamide and methyl carbamate derivatives of anisole are recorded in Table 1. Deprotonation is effected at the NH moiety,[4] and when $R = C_6H_5$ and CH_3O, losses of $C_6H_5CH_3$ and CH_3OCH_3 are noted (Table 1). Linked B^2/E scans of source formed product ions m/z 134 show, in each case, that the product ion originates competitively (i) directly from the $(M - H)^-$ parent and (ii) by the process $[(M - H)^- - CH_3^\bullet] - R^\bullet$. MS/MS data for source formed m/z 134 ions identify them as the appropriate o, m or p-OCN–C_6H_4–O^- species (cf Reference 4). When $R = H$, the corresponding S_N2 loss should result in the loss of methane. Methane elimination is observed for the *or-*
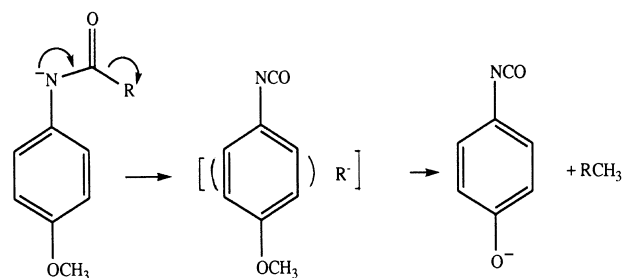
Scheme 1.

tho isomer, but not for either the *meta* or *para* isomers. However, this is not an S_N2 process as evidenced by the spectra of the two deuterium labelled derivatives shown in Figure 1: a ring H together with the CH_3 group from CH_3O are eliminated in this process. A possible rationale is shown in Scheme 2.

We conclude that "long-range cross-ring" S_N2 processes (cf. Scheme 1) occur almost equally when $R = CH_3$, C_6H_5 and CH_3O. However, these are minor processes compared with other fragmentations listed in Table 1 and illustrated in Figure 1. The S_N2 process does not occur when $R = H$.

The "long range" elimination process of phenetoles

If the methoxy group shown in Scheme 1 is replaced by an ethoxyl group the possibility of a cross-ring elimination reaction (E_2 or possibly E_{1cb}) must be considered. This is shown in Scheme 3. We chose $R = CH_3$ and C_6H_5 for this part of the investigation and the spectra of the appropriate $(M - H)^-$ ions are recorded in Table 2 and Figure 2.

When $R = CH_3$ or C_6H_5 for o-, m- or p-substituted phenetoles, the respective losses for the elimination processes (shown, for example, for p-isomers in Scheme 3)

Table 1. Mass spectra of anisole derivatives.

Precursor	H$^\bullet$	H$_2$	CH$_3^\bullet$	CH$_4$	CO	CH$_2$O	CH$_3$OH	(CH$_3^\bullet$ + CO)	CH$_3$OCH$_3$	C$_6$H$_5$CH$_3$	(CH$_3$OH + CH$_2$O)	NCO$^-$	CH$_3$O$^-$	CN$^-$
						Loss							Formation	
o-$^-$NCHO	100		15	5	2	3	22	7				1	1	1
m-$^-$NCHO	100		10			3								
p-$^-$NCHO	100	10	35			5								
o-$^-$NCOC$_6$H$_5$	100	2	8			0.3	3			1				
m-$^-$NCOC$_6$H$_5$	100	2	6			3				8				
p-$^-$NCOC$_6$H$_5$	100		20			7				3				
o-$^-$NCO$_2$CH$_3$	100		2				25		5		4	1	10	
m-$^-$NCO$_2$CH$_3$	100		5				20		3		6	2	3	
p-$^-$NCO$_2$CH$_3$	100	2	30				52		8		20	2	4	
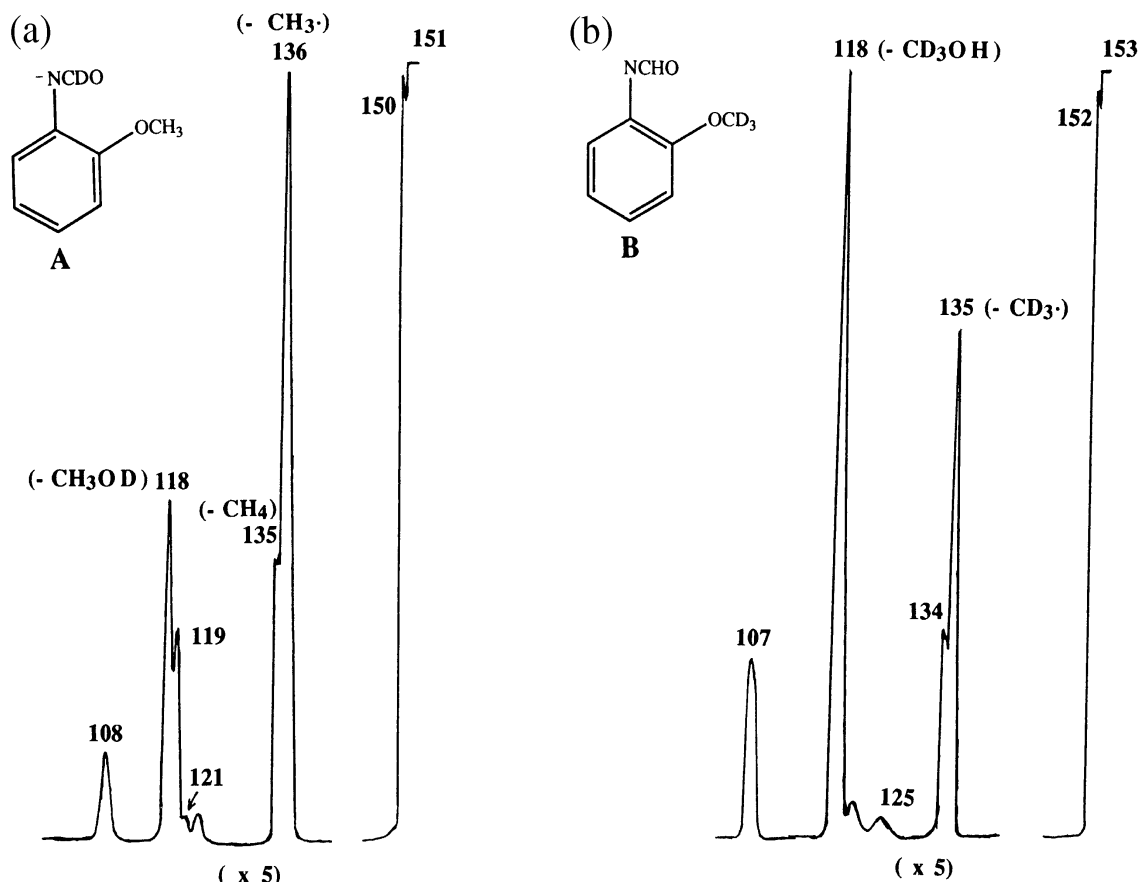
Figure 1. MS/MS data for (a) o-CH$_3$O–C$_6$H$_4$–$^-$NCDO, and (b) o-CD$_3$O–C$_6$H$_4$–$^-$NCHO. ZAB 2HF instrument. For experimental details see Experimental section.
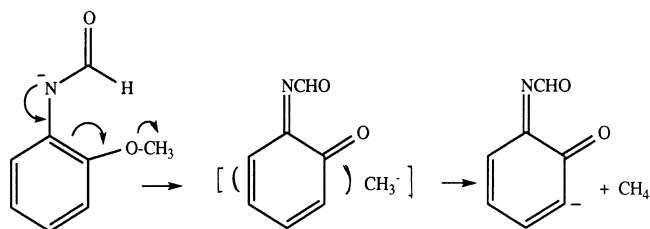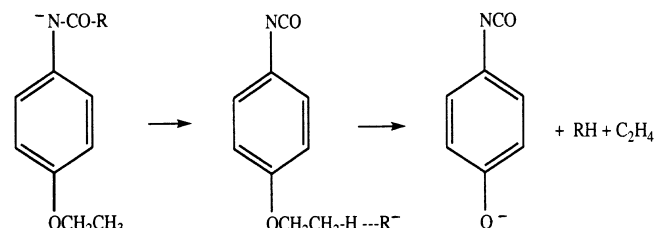
Scheme 2.

Scheme 3.

are $CH_4 + C_2H_4$ ("C_3H_8") and $C_6H_6 + C_2H_4$ ("C_8H_{10}"). The product ions for these processes are again o-, m- or p-OCN–C$_6$H$_4$–O$^-$, identified by comparison of the spectra of source formed m/z 134 ions with those of the spectra of the product ions formed as follows: i.e. HO$^-$ + o-, m- or p-OCN–C$_6$H$_4$–OCH$_3$ → o-, m- or p-OCN–C$_6$H$_4$–O$^-$ + CH$_3$OH (cf Reference 4). In addition, B^2/E linked scans of source formed m/z 134 ions confirm that these ions are formed both directly from the (M – H)$^-$ ions (Scheme 3) and also by the stepwise process [(M – H)$^-$ – C$_2$H$_5^\bullet$ – R$^\bullet$], an exactly analogous scenario to that pertaining to the S$_N$2 reaction of the anisoles.

There is a problem when R = CH$_3$, in that loss of 44 Da from the (M – H)$^-$ ion could either be "C$_3$H$_8$" or CH$_3$CHO (see later for a discussion of the latter process), and the

available evidence cannot exclude the possibility of minor loss of CH$_3$CHO accompanying loss of "C$_3$H$_8$". Thus, we made the OC$_2$D$_5$ derivative of the p-isomer and its spectrum (Figure 2) shows loss of 49 Da (i.e. loss of "C$_3$H$_3$D$_5$").

We chose to study the labelled p-isomer for an additional reason. Of the three isomers, the elimination process should be the least favourable for the $para$ isomer, since the incipient methyl anion has to move furthest in this case. If the elimination mechanism shown in Scheme 3 is operative, either of the steps (i.e. the formation of incipient R$^-$ or the second step which involves R$^-$ deprotonating at the β position) could, in principle, be rate determining. If the second step is rate determining there should be a pronounced deuterium kinetic isotope effect

Table 2. Mass spectra of phenetole derivatives.

Precursor ion	Loss								Formation	
	H$^{\bullet}$	CH$_4$	C$_2$H$_5$$^{\bullet}$	C$_3$H$_8$	CH$_3$CHO	C$_2$H$_5$OH	(C$_2$H$_5$$^{\bullet}$ + CH$_2$O)	"C$_6$H$_5$C$_2$H$_5$"	C$_2$H$_5$O$^-$	NCO$^-$
o-$^-$NCOCH$_3$	70		100	22[a]	22[a]		27			
m-$^-$NCOCH$_3$	80	21	100	34[a]	34[a]		10			
p-$^-$NCOCH$_3$	85	8	100	48[a]	48[a]				1	0.1
o-$^-$NCOC$_6$H$_5$	100		8			3		1		
m-$^-$NCOC$_6$H$_5$	100		10					1		
p-$^-$NCOC$_6$H$_5$	100		40					2		0.2

[a]C$_3$H$_8$ and CH$_3$CHO are both 44 Da.

(when OC$_2$H$_5$ is replaced by OC$_2$D$_5$), and observation of such an effect would provide strong evidence in favour of the operation of an elimination reaction. It must be stressed that it is necessary to be cautious in using inter-molecular isotope effects in gas-phase studies [i.e. comparing the relative extents of losses of "C$_3$H$_8$" (from the unlabelled parent) with "C$_3$H$_3$D$_5$" (from the labelled parent)] because (i) there is no identical internal standard which is common to both spectra, (ii) there may be an isotope effect operating for the formation of the parent ion[17] and (iii) there is a problem in this case since the processes under study compete with the stepwise processes (C$_2$H$_5$$^{\bullet}$ + CH$_3$$^{\bullet}$) and (C$_2D_5$$^{\bullet}$ + CH$_3$$^{\bullet}$), and there could be a secondary deuterium isotope effect operational for the losses of C$_2$H$_5$$^{\bullet}$ and C$_2$D$_5$$^{\bullet}$. However, secondary deuterium isotope effects operating for collision-induced radical losses from anions are small: those reported to date are less than 1.5.[18]
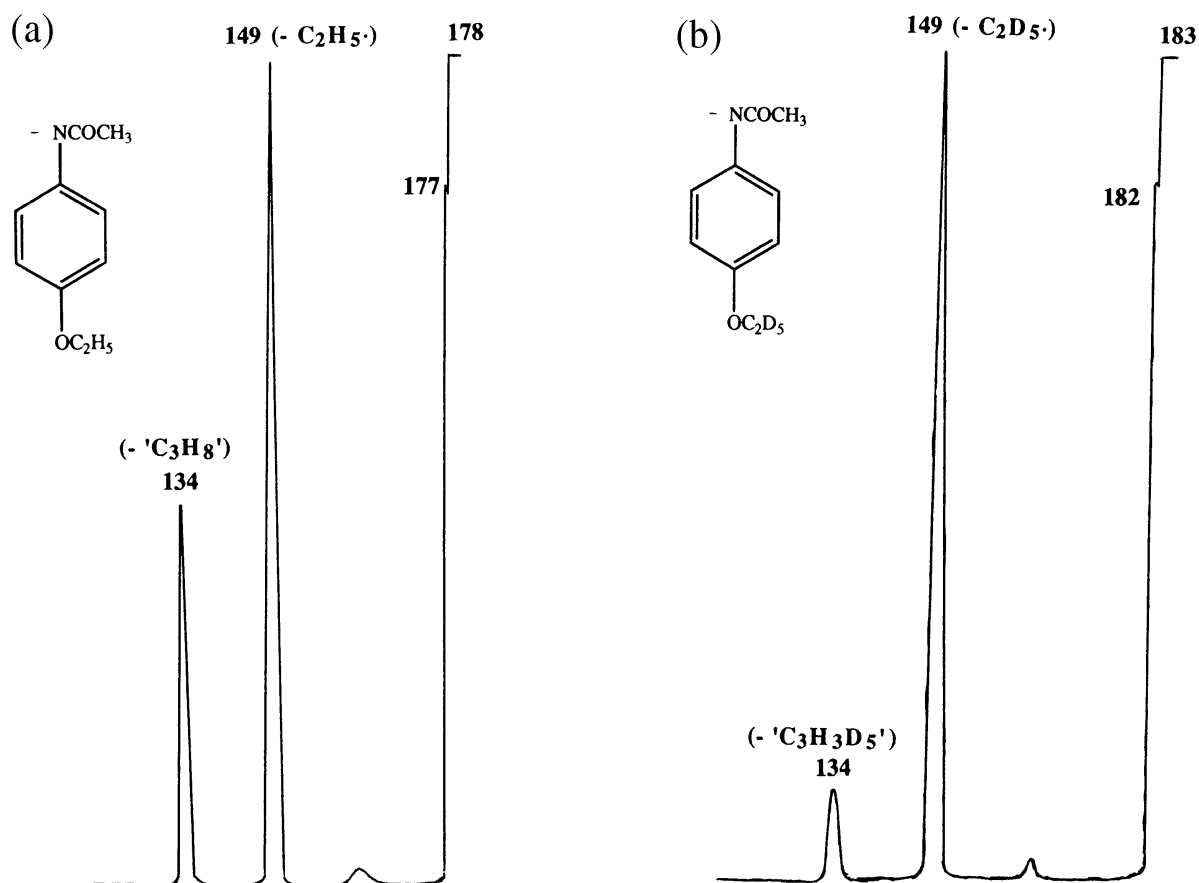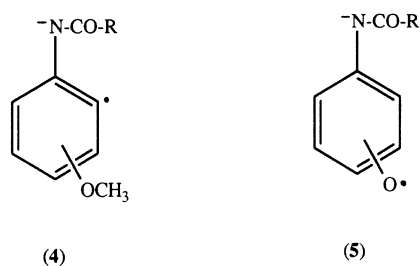

Figure 2. MS/MS data for (a) p-C$_2$H$_5$O–C$_6$H$_4$–$^-$NCOCH$_3$ and (b) p-C$_2$D$_5$–C$_6$H$_4$–$^-$NCOCH$_3$. ZAB 2HF instrument.

(4)   (5)

The two spectra compared in Figure 2 were measured using identical instrumental conditions, and it can be seen that the abundance ratio of m/z 134 to that of the $[(M – H)^- – C_2H_5^\bullet]$ ion [Figure 2(a)] is more than three times that of m/z 134 to the $[(M – H)^- – C_2D_5^\bullet]$ of Figure 2(b). In qualitative terms, this isotope effect is significantly larger than any expected secondary deuterium isotope effect for the competitive stepwise process. This result adds credence to the mechanistic scenario outlined in Scheme 3.

Radical losses and unusual neutral losses from anisoles and phenetoles

The major processes observed in the spectra listed in Tables 1 and 2 involve radical losses to form stable radical anions. A major fragmentation of all $(M – H)^-$ ions involves loss of H$^\bullet$ from the aromatic ring, to produce, for

example, **4**. A major cleavage noted in all spectra involves loss of the alkyl radical from the alkoxy group to yield radical anion **5**.

The loss of the elements of methanol (or ethanol) from $(M – H)^-$ ions occur in a number of the spectra listed in Tables 1 and 2. In the case of the methyl carbamates, the reaction is straightforward: the incipient methoxyl anion, produced from the carbamate, deprotonates the aromatic ring (see later). But the losses of methanol from the $(M – H)^-$ ions of the *ortho* compounds, for which labelling data are shown in Figures 1 and 3, are most unusual and require explanation.

Let us consider the case shown in Figure 1 first. Three possible mechanistic scenarios are shown in Sequences **6** to **8** (Scheme 4). The first two mechanisms are initiated by a hydride ion; Sequence **6** is a deprotonation/elimination, while Sequence **7** results in the formation of a methoxide anion complex following an *ipso* nucleophilic substitution. Sequence **8** involves liberation of a methoxide complex following *ipso* cyclisation via the carbonyl oxygen. The spectra of two labelled derivatives are shown in Figure 1. Figure 1(b) shows loss of "CD$_3$OH", while Figure 1(a) shows losses of "CH$_3$OH" and "CH$_3$OD" in the ratio 1 : 2. Comparison of the ratios of the losses of labelled and unlabelled CH$_3^\bullet$ to "CH$_3$OH" in the spectra of the labelled and unlabelled compounds (Table 1 and Figure 1) indicates no significant deuterium
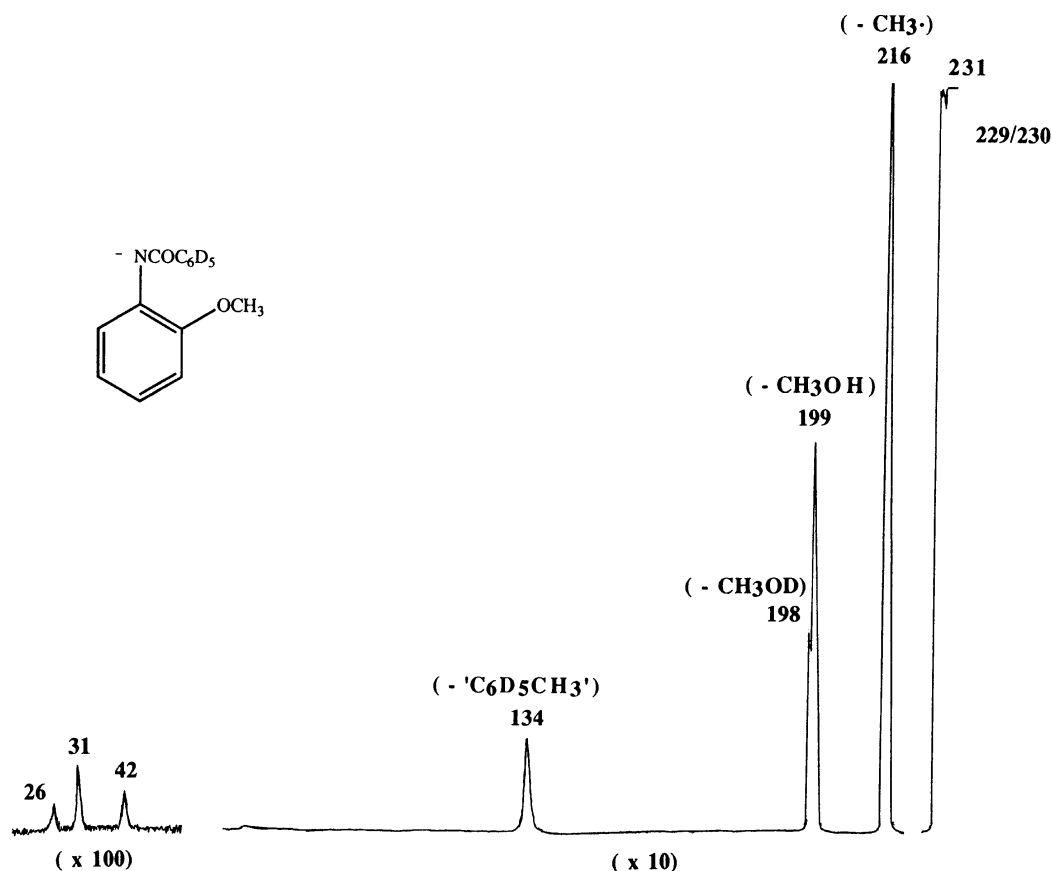

Figure 3. MS/MS data for o-CH$_3$O–C$_6$H$_4$–$^-$NCOC$_6$D$_5$. VG ZAB 2HF instrument.

Table 3. Collisional activation and charge reversal MS/MS data for the [(M – H)⁻ – CH₃OH)] ion from *o*-CH₃O–C₆H₄–NHCHO and the (M – H)⁻ ions from phenylisocyanate and benzoxazole.

Precursor ion	Spectrum type	Spectrum CA [*m/z* (loss) relative abundance] CR [*m/z* (relative abundance)]
[(M – H)– – CH₃OH] from *o*-CH₃O–C₆H₄–NHCHO	CA[a]	117 (H•) 100, 90 (CO) 20[b] and 89 (CHO•) 20[b]
	CR[c]	102 (45), 90 (100), 89 (50), 76 (30), 75 (32), 74 (30), 63 (58), 62 (40), 61 (20), 50 (30), 39 (5)
(M – H)⁻ ion from C₆H₅NCO	CA	117 (H•) 100, 90 (CO) 5
	CR	102 (18), 90 (100), 89 (34), 76 (46), 75 (49), 74 (42), 63 (47), 62 (39), 61 (20), 50 (39), 39 (4)
(M – H)⁻ ion from benzoxazole	CA	117 (H•) 100, 90 (CO) 15[b] and 89 (CHO•) 22[b]
	CR	102 (40), 90 (100), 89 (48), 76 (35), 75 (32), 74 (21), 63 (58), 62 (42), 61 (22), 50 (34), 39 (5)

[a]weak spectrum.

[b]unresolved peaks.

[c]charge reversal (positive ion) spectrum (cf. Reference 19).

isotope effect in the loss of "CH₃OH" compared with "CD₃OH" but an isotope effect of at least three is involved with the comparative losses of "CH₃OH" and "CH₃OD". Thus the –⁻N–CO–H hydrogen is involved in the rate determining step of the reaction. The mechanism shown in Sequence **6** does not accord with the labelling data. Sequences **7** and **8** do fit the labelling data, provided (i) in the case of Sequence **7**, the methoxide anion deprotonates preferentially (but not exclusively) at the position

from which it was liberated and (ii) for Sequence **8**, the methoxide anion deprotonates preferentially (but not exclusively) at the 2-position of the benzoxazole ring. In order to differentiate between these two possibilities, we have compared the MS/MS data for source formed *m/z* 118 (from the *o*-⁻NCHO substituted anisole) with the analogous data for deprotonated phenylisocyanate and benzoxazole. The collisional activation and charge reversal spectra listed in Table 3 are consistent with the prod-
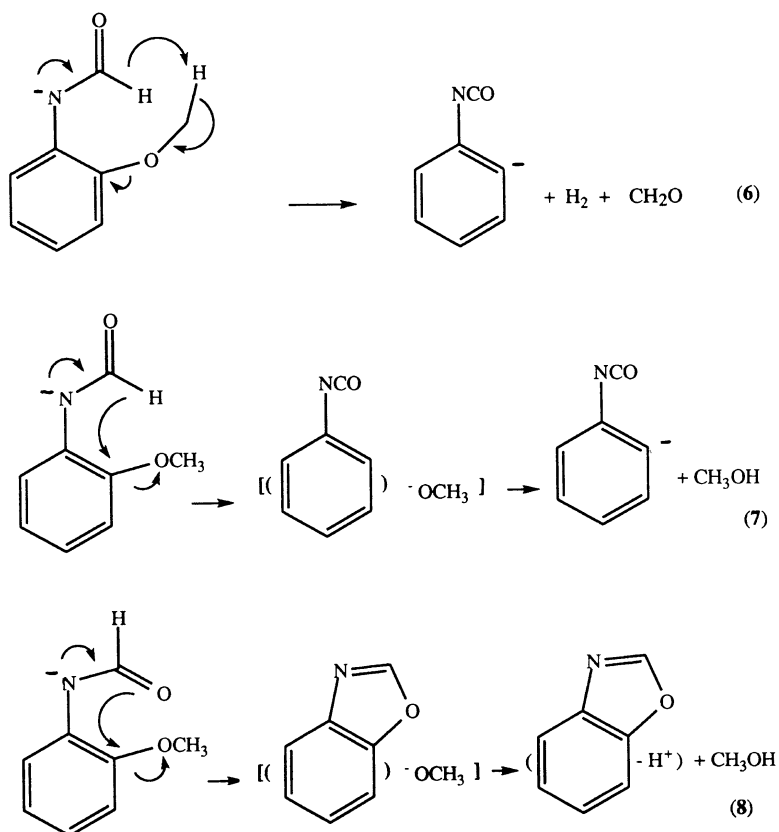
Scheme 4.

uct ion being deprotonated benzoxazole: thus the process is that shown in Sequence **8**.

Loss of the elements of CH_3OH also occurs from $o\text{-}CH_3O\text{-}C_6H_4\text{-}{}^-NCOC_6H_5$ (Table 1), but the spectrum (Figure 3) of $o\text{-}CH_3O\text{-}C_6H_4\text{-}{}^-NCOC_6D_5$ shows that the extra H originates from either aromatic ring. If these losses are analogous to that shown in Sequence **8** (Scheme 4), the product ions from the unlabelled analogue will be deprotonated 2-phenylbenzoxazoles. The mass spectrum of product ion m/z 194 from the unlabelled $(M - H)^-$ ion is too weak for a meaningful comparison with that of deprotonated 2-phenylbenzoxazole, thus we are unable to confirm this proposal in this case.

The loss of formaldehyde from anisole derivatives

There are two characteristic fragmentations of deprotonated anisoles; (i) the loss of a methyl radical (see **5** above) and (ii) the loss of formaldehyde. The loss of formaldehyde has been reported previously.[20,21] The observation[20,21] that ring deprotonated anisole undergoes partial ring *ortho* H/methyl H interchange is of particular relevance, suggesting that proton transfer from CH_3 to the anionic centre on the aromatic ring precedes or accompanies loss of CH_2O. Examination of Table 1 indicates that loss of formaldehyde occurs (i) from parent anions when R = H, OCH_3 and C_6H_5 [the corresponding loss of acetal-

Table 4. Labelling data for the loss of formaldehyde.

Precursor ion	Loss
$o\text{-}CH_3O\text{-}C_6H_4\text{-}{}^-NCDO$	CH_2O
$o\text{-}CD_3O\text{-}C_6H_4\text{-}{}^-NCHO$	CD_2O
$o\text{-}CH_3O\text{-}C_6H_4\text{-}{}^-NCOCD_3$	CH_2O
$m\text{-}CH_3O\text{-}C_6H_4\text{-}{}^-NCOCD_3$	CH_2O / $CHDO$ (1 : 1)
$p\text{-}CH_3O\text{-}C_6H_4\text{-}{}^-NCOCD_3$	CH_2O
$p\text{-}CD_3O\text{-}C_6H_4\text{-}{}^-NCO_2CH_3$ (**A**)	CD_2O
$4\text{-}CH_3O\text{-}[C_6(2,6)H_2(3,5)D_2]\text{--}{}^-NCO_2CH_3$ (**B**)	CH_2O
$[\textbf{A} - CH_3OH]^-$	$CHDO$ / CD_2O (2 : 3)
$[\textbf{B} - CH_3OD]^-$	CH_2O / $CHDO$ (2 : 1)

dehyde occurs from phenetole anions when R = C_6H_5 (see Table 2)], and (ii) from $[(M - H)^- - CH_3OH]$ ions when R = OCH_3. In many of the cases just mentioned, the charge is localised on nitrogen, and, at least initially, remote from the fragmenting site. What then is (are) the mechanism(s) of the losses of CH_2O in these cases?

The losses of CH_2O and labelled analogues are summarised in Table 4 for all of the deuterated anisoles
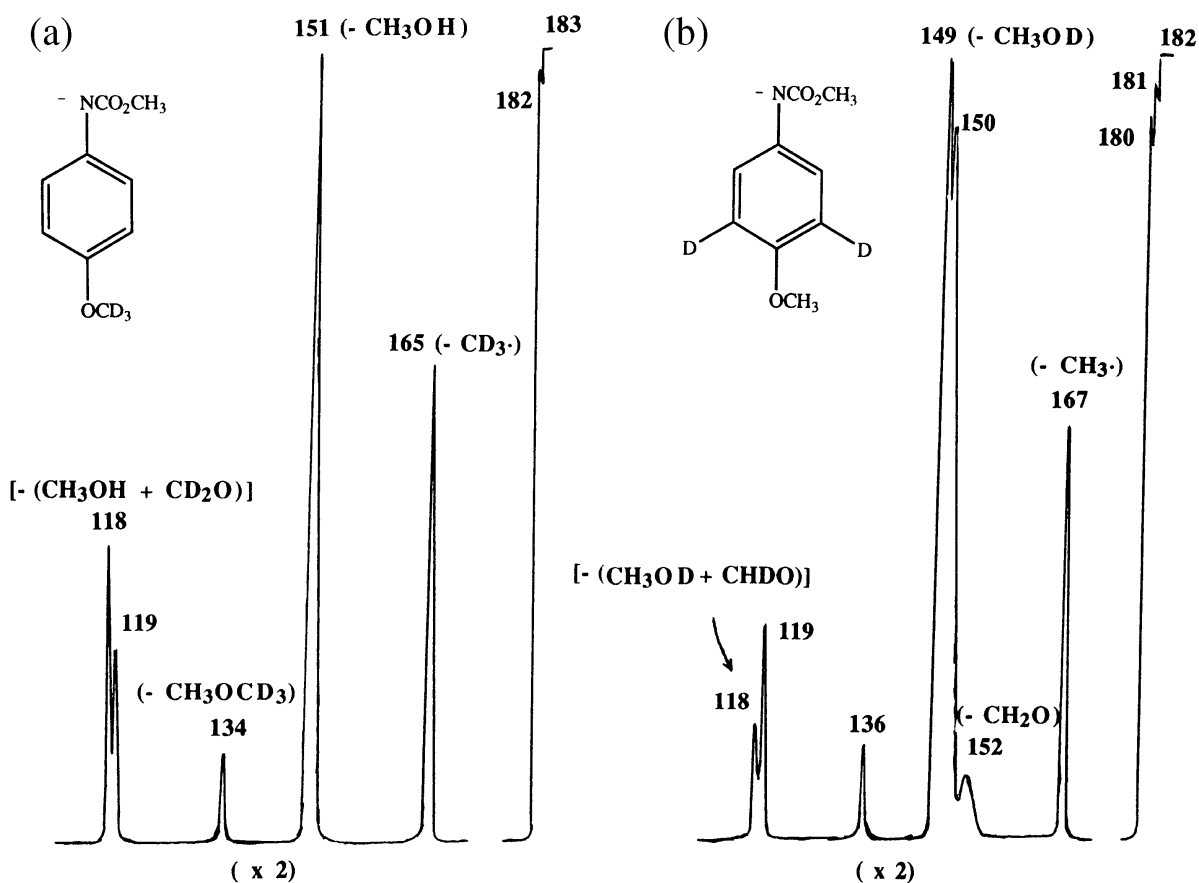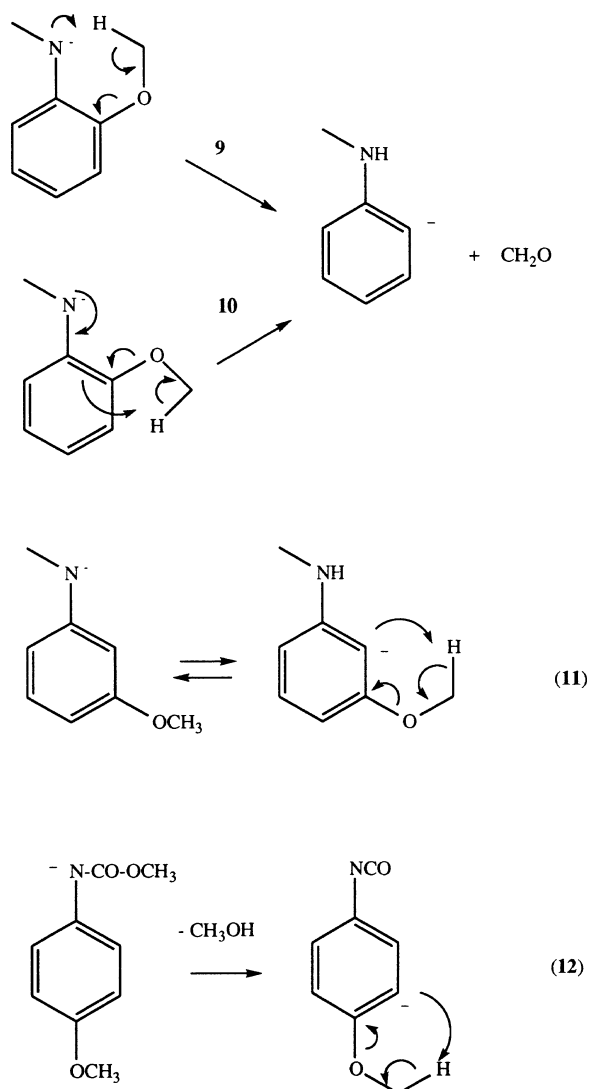

Figure 4. MS/MS data for (a) $p\text{-}CD_3O\text{-}C_6H_4\text{-}{}^-NCO_2CH_3$, and (b) $4\text{-}CH_3O\text{-}[C_6(2,6)H_2(3,5)D_2]\text{-}{}^-NCO_2CH_3$. VG ZAB 2HF instrument.

Scheme 5.

considered in both this and the earlier study.[4] When R = D or CD$_3$, formaldehyde is eliminated from the *ortho* position without any accompanying H scrambling. In the one *meta* compound studied (R = CD$_3$) both CH$_2$O and CHDO are eliminated demanding complex H scrambling accompanying or preceding loss of the neutrals. For the *para* compound where R = CD$_3$, specific CH$_2$O loss is observed. Finally, the spectra of two labelled *para* carbamate derivatives (Figure 4) show two losses of CH$_2$O, viz. (i) from the (M – H)$^-$ ion (this loss occurs without H scrambling), and (ii) from the [(M – H)$^-$ – MeOH] ion. In the latter case, MeO$^-$ deprotonates at both the *ortho* and *meta* positions, and following loss of MeOH, partial ring H/OCH$_3$ hydrogen scrambling precedes or accompanies the loss of CH$_2$O.

We propose that all of the losses of formaldehyde are initiated from anionic centres. The following mechanistic scenarios are proposed. The loss of formaldehyde from *ortho* systems may occur either by the proton transfer/elimination process shown in Sequence **9** (Scheme 5)

or by internal *ipso* proton transfer/elimination shown in Sequence **10**. The loss of formaldehyde from the *p*-substituted species could occur by an *ipso* process analogous to that shown in **10**. Loss of formaldehyde from *meta* systems must be initiated by *ortho* proton transfer to N (see **11**) (and in the case of *o*-methoxyacetanilide systems, Ar–$^-$NCOCH$_3$/ArNHCOCH$_2$$^-$ equilibration competes with the CH$_3$O hydrogen/*ortho* ring hydrogen equilibration). The final case involves loss of CH$_2$O from the [(M – H)$^-$ – CH$_3$OH] ion from the *p*-substituted carbamate: this is shown in Sequence **12**. We propose that this loss of CH$_2$O involves the ion formed by deprotonation at the *meta* position, then CH$_3$O hydrogen/ring H scrambling (via the two equivalent *meta* positions) co-occurs with elimination of formaldehyde.

All of these losses of CH$_2$O have significant activation barriers. Take as an illustration the carbamate example (Sequence **12**): for CH$_3$O$^-$ to deprotonate the aryl ring requires some 80 kJ mol^{-1}, and for an aryl anion to deprotonate the CH$_3$O group, at least 40 kJ mol^{-1} [estimated from ΔG^0_{acid} values; CH$_3$OH = 1565 kJ mol^{-1}, (CH$_3$)$_2$O = 1665 kJ mol^{-1} and aryl H, about 1630 kJ mol^{-1}].[22]

In conclusion, the major collision-induced fragmentation processes of the alkoxyl substituted anilide anions described in this report involve the losses of radicals from alkoxyl groups to form stable radical anions. Competing with these processes are (i) specific *ortho* effects, and (ii) a number of reactions where the parent Ar–$^-$N–CO–R ions liberate R$^-$ through ion complexes [(ArNCO) R$^-$] and the incipient R$^-$ species is able to effect a number of "long-range cross-ring" reactions including deprotonation, S$_N$2 displacement at OCH$_3$ and elimination reactions at OC$_2$H$_5$ substituents.

Acknowledgement

References

1. J.H. Bowie, *Mass Spectrom. Rev.* **9,** 349 (1990).
2. M.J. Raftery and J.H. Bowie, *Int. J. Mass Spectrom. Ion Processes* **79,** 267 (1987).
3. S. Dua, R.B. Whait, M.J. Alexander, R.N. Hayes, A.T. Leberdev, P.C.H. Eichinger and J.H. Bowie, *J. Am. Chem. Soc.* **115,** 5709 (1993).
4. S.J. Blanksby, S. Dua and J.H. Bowie, *Rapid Commun. Mass Spectrom.* **9,** 177 (1995).
5. VG Instruments, Wythenshawe, Manchester, M23 9LE, UK, model ZAB 2HF.
6. M.B. Stringer, D.J. Underwood, J.H. Bowie, J.L. Holmes, A.A. Mommers and J.E. Szulejko, *Can. J. Chem.* **64,** 764 (1986), and references cited therein.
7. M. Eckersley, J.H. Bowie and R.N. Hayes, *Org. Mass Spectrom.* **24,** 597 (1989).

8. A.I. Vogel, *Textbook of Practical Organic Chemistry*, 4th Edition. Longman and Green Pty Ltd, pp. 1129–1131 (1978).

9. R.A. Mackenzie, C.J. Moody and C.W. Rees, *Tetrahedron* **42,** 3259 (1986).

10. T.L. Ho and C.M. Wong, *Synthesis* 45 (1974).

11. E.J. Corey, M.G. Bock, A.V. Ramarao, D. Floyd and B. Lipshultz, *Tetrahedron Letters* 1052 (1978).

12. K.K. Chan and K.S. Pang, *J. Labelled Compds. Radiopharm.* **19,** 321 (1982).

13. T. Suchiero, S. Masuda, R. Nakausa, M. Taguchi, A. Mori, A. Koike and M. Date, *Bull. Chim. Soc. Japan* **60,** 3321 (1987).

14. W. Tumas, R.F. Foster, M.J. Pellerite and J.I. Brauman, *J. Am. Chem. Soc.* **105,** 7464 (1983); W. Tumas, R.F. Foster and J.I. Brauman, *J. Am. Chem. Soc.* **106,** 4053 (1984); K.A. Sammes and J.I. Brauman, *J. Phys. Chem.*, in press.

15. P.C.H. Eichinger, J.H. Bowie and T. Blumenthal, *J. Org. Chem.* **51,** 5078 (1986).

16. S. Dua, J.H. Bowie and J.C. Sheldon, *J. Chem. Soc. Perkin Trans. 2* 543 (1994).

17. P.J. Derrick, *Mass Spectrom. Rev.* **2,** 285 (1983), and references cited therein; P.J. Derrick and K.F. Donchi, in *Comprehensive Chemical Kinetics*, Ed by C.H. Bamford and C.F.H. Tipper. Suppl. Vol. 1, Elsevier, Amsterdam (1983).

18. J.H. Bowie and B. Nussey, *J. Chem. Soc. Chem. Commun.* 17 (1970); R.N. Hayes and J.H. Bowie, *Org. Mass Spectrom.* **21,** 425 (1986).

19. J.H. Bowie and T. Blumenthal, *J. Am. Chem. Soc.* **97,** 2957 (1975); J.E. Szulejko, J.H. Bowie, I. Howe and J.H. Beynon, *Int. J. Mass Spectrom. Ion Phys.* **13,** 76 (1980).

20. T.C. Kleingeld and N.M.M. Nibbering, *Tetrahedron* **39,** 4193 (1983).

21. P.C.H. Eichinger, J.H. Bowie and R.N. Hayes, *Aust. J. Chem.* **42,** 865 (1989).

22. S.G. Lias, J.E. Bartmess, J.F. Liebman, J.L. Holmes, R.D. Levin and W.G. Mallard, "Gas Phase Ion and Neutral Thermochemistry," *J. Phys. Chem. Ref. Data* *17*, Suppl. 1 (1988): the computer version was used.

Blanksby, S.J., Dua, S., Christie, H. & Bowie, J.H. (1996) Anionic migration reactions in aromatic systems effected by collisional activation. Deprotonated anilides containing methoxycarbonyl substituents.
Rapid Communications in Mass Spectrometry, v. 10(4), pp. 478-480

Addressing Referee Concerns

This thesis entitled "Gas Phase Synthesis of Interstellar Cumulenes. Mass Spectrometric and Theoretical Studies." has been reviewed by two referees who are internationally recognised in the field of mass spectrometry. While one of the referees has praised the research presented here-in and stated that it is worthy of special commendation, the other has leveled some criticisms. It is worthwhile to point out that the analyses which the latter referee has questioned, form the basis of two papers which have been accepted for publication in the Journal of Physical Chemistry ("Generation of Two Isomers of C_5H From the Corresponding Anions. A Theoretically Motivated Mass Spectrometric Study." Blanksby, S.J.; Dua, S.; Bowie, J.H. *J. Phys. Chem. A* **1999**, *in press*. "Gas Phase Syntheses of Three Isomeric C_5H_2 Radical Anions and Their Elusive Neutrals. A Combined Experimental and Theoretical Study." Blanksby, S.J.; Dua, S.; Bowie, J.H.; Schröder, D.; Schwarz, H. *J. Phys. Chem. A* **1998**, *102* , 9949.). Nevertheless, we will explicitly counter these criticisms in the following discussion.

The second referee has made several comments regarding the CR and NR spectra discussed in this thesis. He has criticised the use of these spectra for the structural assignment of hydrocarbon anions and in particular their use in differentiating isomeric species. The spectra presented in Chapters 4 and 5 are singled out, with doubts raised over the characterisation of the C_5H and C_5H_2 anions. These concerns are addressed here along with some of the other, less fundamental criticisms.

In Chapter 4 two CR spectra are presented corresponding to independently synthesised C_5H connectivities (Figure 4.5, pp 80). The first and most obvious difference between these spectra is the relative abundance of peaks corresponding to loss of hydrogen radical (*m/z* 60) compared to the abundance of the parent ions (*m/z* 61). It has been rightly pointed out by the

1

reviewer that this dramatic contrast in intensities may be the result of different internal energy distributions within a common C_5H species. Under NICI conditions two different reactions leading to the same anion may produce this species with differing amounts of internal energy depending on the thermochemistry of the respective processes. In this respect, it is significant to note that C_4CH/D anions formed from the precursors $^-C\equiv CC\equiv CCH_2OCH_3$ and $^-C\equiv CCH(OCH_3)C\equiv CD$ (as outlined on pp 76 and 78 respectively) yield CR spectra with directly comparable peak abundances. This is observed, despite the likely difference in their internal energy content, arising from the thermochemistry of their respective formation reactions. Similarly, C_2CHC_2 anions formed from three different anion precursors, namely $^-C\equiv CCH(OCOR)C\equiv CH$ (where R = H, CH_3 and CH_2CH_3 respectively), all give identical CR spectra (as described on pp 78 and 79). The reproducibility of the CR spectra over a range of precursors (including isotopomers) strongly suggests two isomeric C_5H anions rather than simply different internal energies of a single anion structure.

It has further been suggested, that some of the fragmentations observed in the CR spectra of the C_5H isomers cannot arise from simple cleavages of the proposed ion skeleton. For example, the CR spectrum of the C_2CHC_2 anion (pp 80) shows loss of CH, C_2H and C_3 which cannot occur by simple single cleavages from the parent system. It should be noted here that these systems are highly unsaturated and hence it seems likely that all cleavages will be extremely high energy processes. To support this intuitive assessment thermochemical data has been collected from various sources and augmented with some calculated energies to give estimated heats of formation for the various fragmentation channels (Tables 9.1 and 9.2). Although these values, in many cases, include approximations and are intended simply as a guide it is immediately apparent from these data that all decomposition pathways are highly endothermic. Even the most accessible channel lies some 156 kcal mol^{-1} above the estimated heat of formation of the C_4CH^+ ground state. It is therefore quite probable that rearrangement

processes occur below the dissociation threshold and hence it is not surprising that some "less-than-simple" cleavages are observed in these spectra. Consideration of the relative thermochemistry of the two C_5H cation isomers in the context of the energy requirements for the various fragmentations is also useful. According to the calculations presented in this thesis (pp 69) the ground state $C_2CHC_2^+$ cation is expected to be some 80 kcal mol^{-1} less stable than C_4CH^+ and hence much more likely to access the dissociative exit channels in a vertical CR experiment. This is consistent with the experimental observations, with the peaks corresponding to fragment ions much more abundant in the CR spectrum of $C_2CHC_2^-$ than that of C_4CH^- (pp 80).

Table 9.1 Estimated heats of formation for the various fragmentation channels for cations of the form C_5H^+. These values are generated from the estimated heats of formation collated in Table 9.2.

m/z	Fragment (ions and neutrals)	$\Delta H_{f,298}$ (kcal mol^{-1})
61	C_4CH^+	385
60	$C_5^{\cdot+} + H^{\cdot}$	569
49	$C_3CH^+ + C$	541
48	$C_4^{\cdot+} + CH^{\cdot}$	663
37	$C_2CH^+ + C_2$	583
36	$C_3^{\cdot+} + CCH^{\cdot}$	628
25	$CCH^+ + C_3$	597
24	$C_2^{\cdot+} + CC_2H^{\cdot}$	637

It has been suggested that the doubly charged C_5H^{++} ions may prove more structurally diagnostic. Neither the CR nor the NR spectra of the two C_5H anions show peaks corresponding to doubly charged species (pp 80 and 82) suggesting that these are not formed under typical collision conditions. While it is possible that such ions could be observed under multiple collision conditions the anticipated yields would be extremely low and no pertinent information could be expected from such low intensity signals.

Table 9.2 The measured and estimated heats of formation of C_5H^+ ions and their possible charged and neutral fragments. The source of the data are expressed in the third column.

Fragment (ions and neutrals)	$\Delta H_{f,298}$ (kcal mol^{-1})	Source of data
C_4CH^+	385	(IE = 8.18 eV) Theory[a]
C_4CH^-	196	(BDE[C_5-H]=90 kcal mol^{-1})[b]
$C_2CHC_2^+$	465	Rel. Energies[a]
$C_2CHC_2^-$	244	Rel. Energies[a]
$C_5^{·+}$	517	(IE = 12.26 eV) NIST[c]
C_5	234	NIST
C_3CH^+	370	(IE = 9.39 eV) Theory[b]
C_3CH^-	154	(BDE[C_4-H]=130 kcal mol^{-1})[d]
$C_4^{·+}$	521	(IE = 12.54 eV) NIST
C_4	232	NIST
C_2CH^+	383	(PA[C_3] =184 kcal mol^{-1})[e]
C_2CH^-	174	(IE = 9.07 eV) Theory[b]
$C_3^{·+}$	495	(IE = 12.97 eV) NIST
C_3	196	NIST
CCH^+	401	(IE = 11.6 eV) NIST
CCH^-	133	NIST
$C_2^{·+}$	463	(IE = 11.4 eV) NIST
C_2	200	NIST
$C^{·+}$	432	NIST
C	171	NIST
CH^-	142	NIST
H^-	52	NIST

[a] Relative energies taken from calculated values given on pp 69 and 70.
[b] Estimated from energies calculated at the B3LYP/6-31G* level of theory.
[c] Thermochemical data taken from NIST online database http://webbook.nist.gov/
[d] Theoretical prediction of C-H bond dissociation energy in C_4H.[166]
[e] Proton affinity of C_3 bracketed in a flowing afterglow study.[149]

In Chapter 5 three radical anion isomers of the form C_5H_2 are discussed and their CR and NR data are presented. While the spectra of the C_4CH_2 and HC_5H isomers show distinctive and structurally indicative fragmentations (pp 98 and 101), the third species C_2CHC_2H shows fragments and fragment intensities quite similar to those of C_4CH_2. This problem is highlighted in the discussion (pp 100) and it has been addressed by means of isotopic labelling. The isotopomers $C_2CH(D)C_2D(H)$ were independently synthesised in the gas phase (pp 96) and the CR and NR spectra of these ions are listed in Table 5.1 (pp 99). These spectra

clearly demonstrate the inequivalence of the two hydrogens within this ion structure and thus distinguish it from the other two C_5H_2 connectivities discussed (pp 100).

The reviewer has suggested the examination of C_5H_n cations (where n = 1 and 2) formed from EI of suitable precursors. Indeed, there are examples of the formation of such ions in the literature[174, 151] and these are discussed in the introduction to Chapter 4 (pp 64). The problem with such experiments is the structural ambiguity inherent in formation of hydrocarbon cations by EI. Cations of the form C_5H and C_5H_2 have been previously investigated, however in these cases the structures have been assigned simply on the basis of theoretical predictions for the lowest energy configurations.[174, 151] Despite these problems we did conduct some cation experiments but they are not outlined in this thesis because of the inconclusive nature of the results. Briefly, EI on pentadiyne yields abundant peaks corresponding to C_5H and C_5H_2 cations (*m/z* 62 and 61 respectively) amongst others. Fragmentations observed from these ions in both CA and NR experiments however show no clear structural trends and as nothing can be inferred about the structure based on the precursor these data did not prove informative.

It has nowhere been claimed that the CR and NR spectra of the various C_5H_n isomers alone provide indisputable proof of the absolute connectivities of these ions. However careful comparison of these data has been shown to (i) support structural assignments, (ii) distinguish structural isomers and (iii), when used inconjunction with a carefully selected precursor and isotopic labelling data, confirm ion structure.